NATIONAL RESEARCH COUNCIL OF ITALY

ADVISORY COMMITTEE
ON TECHNICAL RECOMMENDATIONS FOR CONSTRUCTION

Guide for the Probabilistic Assessment of the Seismic Safety of Existing Buildings

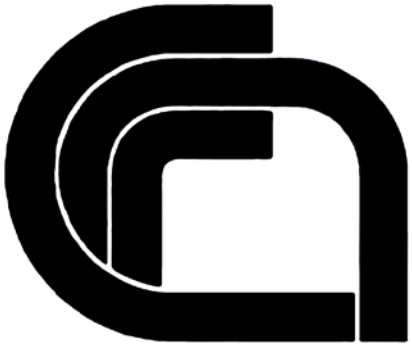

CNR-DT 212/2013

CNR-DT 212/2013

INDEX

1 Introduction

The structure of the current technical regulations for the seismic assessment of existing buildings, at (Italian) national level (NTC2008) and at international level (Eurocode 8 Part 3), is as follows:

- a variable number of limit states that are of interest is established;
- a value of seismic intensity is associated with each limit state, characterized in probabilistic terms by the value of its average return period;
- indications are provided regarding the achievement of a discrete number of pre-determined knowledge levels, each of which is associated with a global factor, to be used in a manner analogous to that of the usual partial factors;
- methods of analysis are indicated with their respective scope of applicability;
- the mechanisms to be verified are indicated and their respective capacity models are provided.

The verification procedure ends with the determination of the ratio between the seismic intensity that produces each limit state and the corresponding design intensity. The checks are fulfilled if this ratio is equal or larger to one.

The limit of the above procedure is that at its end the actual level of protection of the structure, measured in terms of probability of exceeding each of the considered limit states, is unknown.
In fact, the only element described in the probabilistic terms is the design seismic action, while in reality, in the evaluation problem, i.e. in the determination of the probability of exceeding the different limit states, several other sources of uncertainty come into play that are not explicitly modelled. In particular:

a) an unambiguous definition of the limit states, in particular of the ultimate ones that involve widespread global damage, which are difficult to formulate, and the resulting subjectivity of the choice introducing an element of uncertainty in the outcome of the assessment;
b) a complete knowledge of an existing building, which is not actually achievable, requires the structural engineer to make up for the lack of information with his own experience, by making assumptions on the structural layout. This is a further element of subjectivity that introduces uncertainty in the outcome of the assessment;
c) even with the same acquired information and the same assumptions on the structural layout, the choice of modelling and of the method for the analysis reflects substantially the experience and the professional qualities of the structural engineer, besides the computational tools at his disposal. This is a further, and very important element, that differentiates between the outcomes of an assessment;
d) the current state of knowledge about the ultimate capacities of structural components that were not designed accounting for seismic action is still quite incomplete, especially with reference to behaviour just before the collapse, and available capacity models are characterized by considerable dispersion. Furthermore, for each mechanism there are generally available alternative models built on comparable empirical bases. The choice of one or the other, as well as the introduction of the uncertainty on the corresponding model influences the variability of the outcome of the verification.

It follows from the foregoing considerations that the development of technical standards on the assessment of existing existing structures should set itself as its central objective the development of procedures that are appropriate to assess the reflection on the end result of all the uncertainties entering in the verification process, in terms of the probability of exceeding each of the limit states. The procedures that are presented in this Guide are intended to attain the indicated objective. They have been drafted with the intention of requiring only a basic knowledge of reliability theory. On the contrary, as far as the modelling and the analysis of the structural response are concerned, since the limit states having the greatest interest are characterized by high levels of structural damage, even close to collapse, the application of the Guide requires the simulation of nonlinear behaviour of RC elements and of masonry, which presupposes theoretical knowledge and experience in the use of appropriate computer codes. In this regard the Guide reflects the state of the art in the subject of modelling the behaviour of structural elements that do not satisfy the recent seismic standards, subject to cyclic deformations of such magnitude as to lead them close to collapse. Since the state of the art in the field is undergoing an active phase of development, the achievement of significant progress will be transferred in future updates to this Guide.

This Guide provides an approach of higher level than that required by current legislation, and it is to be expected that they will be resorted to in cases of particular economic and/or social significance. It is also expected and hoped that the concepts and the procedures that are contained in them can be of help in future revisions of the current standards.

The document consists of:

- a general section, (chapter 2) containing aspects of the assessment procedures that are common to the different construction types, and in particular masonry and reinforced concrete buildings.
- two sections that provide specific elements regarding masonry buildings (chapter 3) and buildings in reinforced concrete (chapter 4).
- an appendix (App. A) with comments on various sections of the preceeding chapters.
- two appendices (B and C) that include two complete applications on a masonry and a reinforced concrete building, respectively.

2. General aspects

2.1 Performance requirements

In the context of this Guide the seismic safety assessment of an existing building consists in the quantification of the average annual frequency of λ_{SL} exceeding one or more limit states (LS), defined in §2.1.1, and the comparison of this value with the minimum reliability requirements indicated in §2.1.2.
The safety assessment with respect to the limit state of collapse is always required.

2.1.1 Definition of Limit States

Limit states are identified with reference to the performance of the building as a whole, including structural elements, non-structural elements and installations. The limit states considered are:

- Damage Limit State (SLD): the building maintains the integrity of the structural elements (negligible structural damage that does not require repairs) and remains usable even in the presence of light damage to non-structural elements.
- Severe Damage Limit State (SLS)[1]: the building undergoes damages and collapses of non-structural components and installations, and damages to structural components that are associated with a significant loss of stiffness with regard to horizontal actions; the building however retains a part of the strength and stiffness against vertical action and a margin of safety against collapse due to lateral seismic action; this state defines the limit beyond which the extent of damage is such as to render repairs an uneconomic option.
- Limit State for the Prevention of Collapse (SLC): the structural components of the building suffer very serious damage while still maintaining a residual capacity to support vertical loads. The residual safety with respect to horizontal actions is negligible.

2.1.2 Minimum reliability requirements

The structures to which this Guide refers are distinguished according to the significance of the socio-economic consequences of the violation of the limit states in four classes:

- Class I: Buildings with only occasional presence of people.
- Class II: Buildings whose use regularly entails the presence of crowds, with no environmentally hazardous contents and without any essential public and social functions.
- Class III: Buildings whose use envisages significant crowding.
- Class IV: Buildings with important public or strategic functions, even with regard to the management of civil protection in the event of a disaster.

With reference to the four classes and the three limit states introduced in §2.1.1, Table 2.1 provides the maximum thresholds of the average frequency of their exceedance.

[1] This Guide does not provide specific guidelines for the Limit State for the safeguard of Human Life (LSHL) that is considered by the *NTC* 2008. The safety of human life is protected by the control of the Limit State for Collapse (LSC), which in the case of existing buildings is preferable for the reasons that are detailed in Annex A2.

Table 2.1 Minimum reliability requirements (maximum values of λ_{SL}, multiplied by 10^3) depending on the class of construction[2].

Limit State	Class I	Class II	Class III	Class IV
SLD	64.0	45.0	30.0	22.0
SLS	6.8	4.7	3.2	2.4
SLC	3.3	2.3	1.5	1.2

2.2 Seismic action

In the context of this Guide the reference basis for the definition of seismic action is represented by the ensamble of elastic response spectrum for the nine average return periods that are provided by NTC2008. The ordinates of these spectra represent the median value of ordinates obtained by taking into account the epistemic uncertainties related to the analysis of the seismic hazard of each site. For the purpose of determining the average annual frequency of exceeding a limit state λ_{SL} (§2.6.1), these uncertainties are further considered through a modification of the curve of the seismic hazard at the site as indicated in §2.2.1.

2.2.1 Derivation of the hazard curve

The seismic hazard curve of a site, $\lambda_S(s)$, provides the average annual frequency of exceedance of the value s is exceeded by a representative local seismic intensity S.
In this Guide the reference structural model for the determination of the response is three-dimensional and is therefore subject simultaneously to three orthogonal components of the seismic motion (in buildings it is normally acceptable to disregard the vertical component). The seismic intensity S is normally expressed in terms of the spectral acceleration at the fundamental period of the structure under consideration, the maximum of the two horizontal components[3].
The median hazard curve is obtained in discrete terms from the nine median response spectra given in NTC2008:

$$\lambda_S(s_i) = \frac{1}{T_{R,i}} \quad s_i = S(T_{R,i}) \quad i = 1,\ldots,9 \tag{2.1}$$

where $S(T_{R,i})$ is the value of the intensity S at the i-th average return period $T_{R,i}$, with reference to the soil category A of NTC2008 and Eurocode 8.
To calculate λ_{SL} (§2.6.1) reference is made to the average hazard curve $\overline{\lambda}_S$ which is obtained by multiplying the mean curve λ_S by the amplifying factor:

$$\overline{\lambda}_S(s) = \lambda_S(s)\exp\left(\frac{1}{2}\beta_H^2\right) \tag{2.2}$$

The term β_H can be estimated with the formula:

$$\beta_H = \frac{\ln S_{84\%} - \ln S_{16\%}}{2} \tag{2.3}$$

[2] The values presented in Table 2.1 correspond approximately to the inverse of the average return period characterizing the seismic action for the verification of the corresponding state limits in NTC2008, multiplied by the amplifying factor 2.25, which takes account of the randomness both in the response and in the capacity of the structure.
[3] The use of the maximum spectral acceleration between the two horizontal components is necessary to maintain consistency in the integral of the following Eq. (2.12), since hazard data in NTC2008 used in Eq.(2.1) are derived with reference to this measure of intensity.

where the fractiles at 16% and at 84% of the seismic intensity *S*, that vary as a function of the average annual frequency λ_S, can be evaluated in the neighborhood of an estimate of λ_{SL} obtained using the median hazard curve λ_S.

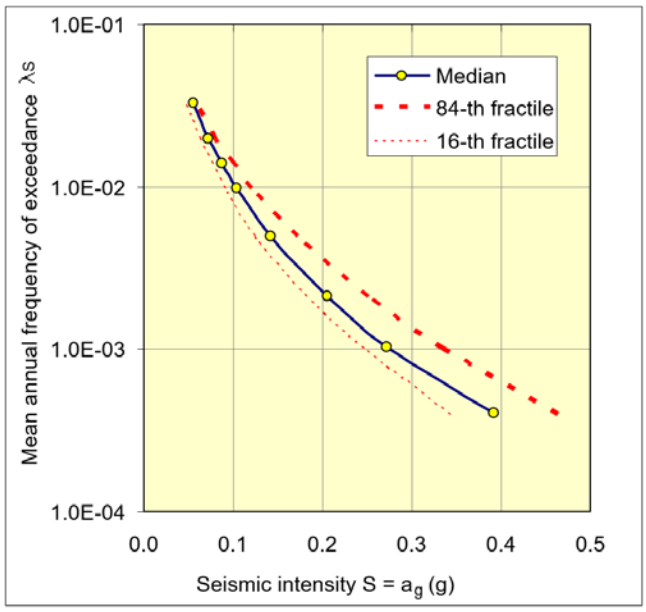

Fig. 2-1 Example of fractile hazard curves (50%, 16% and 84%) for peak ground acceleration ag. [Source: Project DPC-INGV S2].

2.2.2 Time histories of seismic motion

For the purpose of determining the fragility curve of the structure (§2.6.1) it is necessary to use a set of (generally triplets but more often couples of) time-histories of ground acceleration, whose characteristics are compatible with the seismogenic mechanisms that influence the seismicity of the site under consideration[4].

Use can be made of natural records or time histories obtained from models that reproduce the fault mechanism and the propagation of the motion at that specific site, provided they are able to reproduce the variability of the spectral ordinates of the natural motions.

In the event that use is made of recorded accelerograms, one criterion for the selection of recordings is to rely on the results of the breakdown, usually called disaggregation, of seismic hazard for the site in question. This technique provides the range of values of magnitude M and distance R (and of the number ε of standard deviations with respect to the average of the attenuation law used in the hazard analysis) representing events that contribute most to the value of the average frequency λ_S of exeeding[5] the intensity $S = s$. The recordings will be selected preferably within the range M-R pro-

[4] It is not necessary to have a close compatibilty with the standard iso-probable spectrum. This would actually provide an estimate in excess of the average annual rate λ_{SL}: this spectrum in fact represents an "envelope" of the effects of all possible events to the site (see also §A.4).

[5] Strictly speaking, to maintain consistency in the integral in the following Eq. (2.12), the disaggregation should be that of the frequency of occurrence of the value S=s and not of its exceedance. The most widely diffused codes for the calculation of the hazard nonetheless carry out the disaggregation of the frequency of exceedance. Generally, however, the two disaggregations provide similar results so that this latter can be used in approximation.

vided by the disaggregation[6], for a value of intensity with an average annual rate comprised between approximately 1/500 and 1/1000.
In the absence of specific data for the site under consideration and in view of the range of magnitude values that are characteristic of regions with medium and high seismicity, the choice of the accelerograms may fall on records obtained on soils of category A or B (NTC2008, EC8), in the range of M between 5.5 and 6.5, and for epicentral distances up to 30 km.
For sites that are located in the vicinity of known active faults it is necessary to assess the probability of occurrence of impulsive motions and take them into account in the selection of signals for structural analysis (see §**A.4**).
For sites that belong to soil categories C or lower, for which a selective amplification of the motion on the surface is envisaged, the acceleration time-histories previously selected or generated with reference to conditions of hard ground, must be modified by means of local seismic response analysis. This analysis can be conducted with equivalent linear methods only for those stratigraphic profiles where even at higher intensities significant levels of plastic deformation are not expected[7]. The uncertainty associated with mechanical properties of the local stratigraphy must be taken into account. For this purpose the parameters of the site response model (stiffness, resistance, etc.) can be modelled with continuous random variables (§2.3.2) and a different sample of these variables can be associated with each selected record. This procedure is analogous and congruent to what is indicated in the following with reference to the uncertainties in the structure (see, for example, §2.6.2), so that the motion on the surface obtained using a soil sample is associated with a sample of the characteristics of the structure.
In case modelling with degrading components (see §2.4) is adopted, the duration of the time histories presents a significant correlation with the level of damage caused. In this case, in principle, it would be necessary to select time histories with a duration compatible with the distribution of the duration conditioned to the level of intensity chosen for the selection of the records. In the absence of this information it is necessary to verify that the chosen time histories will cover in an approximately uniform manner an interval of "significant" length $D_{5\text{-}95}$[8] between 4 s and 10 s.
The minimum number of time histories to be used is equal to 20.

2.3 Knowledge of the structure

The evaluation process begins with the acquisition of a first level of knowledge of the geometric characteristics of the structural system which is responsible for the seismic resistance, including the non-structural parts that can have significant influence on the response. The purpose of this first activity is that of enabling the establishment of a *preliminary model* to be used to perform sensitivity analyses on the values of mechan-

[6] In principle, there may be multiple intervals in the range M-R that contribute in a way comparable to λ_S, for example, a source that generates events with high magnitude at a greater distance, and a source that is characterized by events of lower intensity at shorter distances. In these instances the selection must reflect both intervals.
[7] Two out of the three analytical methods proposed in this Guide are based on an incremental dynamic analysis in which the signals are scaled linearly (in intensity) even at very high levels, until the collapse of the structure is reached. At these levels, particularly for stratigraphic profiles characterized by poor mechanical characteristics, the magnitue of the anticipated deformations is important. In these conditions the equivalent linear methods suffer from known limitations in terms of the reliability of the response, and non-linear methods are therefore preferable.
[8] The significant duration $D_{5\text{-}95}$ is defined as the difference between the time instants t_{95} and t_5 in which the signal strength reaches respectively 95% and 5% of total power.

ical parameters, on geometric parameters and on modelling assumptions for the structural response. The results are useful in order to draw up a plan for the surveys and tests to complement the information already available.
The preliminary analysis also aims to highlight the main features of the seismic response of the structure, in particular the degree of uniformity of the deformations and of their order of magnitude, in addition to the static regime under vertical loads. This information provides further indications on the elements on which to concentrate investigations and tests.
Specific guidelines on modelling procedures for the preliminary analysis are given in §3.1.2 and §4.1.2 for masonry and for reinforced concrete buildings, respectively.

2.3.1 Elements of knowledge

Aspects of knowledge that are necessary for the assessment refer to the following issues:

- Geometry of the structural system
- Construction details
- Mechanical properties of materials

Elements of knowledge may come from:

- A historical-critical analysis aimed at reconstructing the initial construction process and the subsequent modifications that were made over time, as well the significant events that may have influenced the building.
- Design documents regarding the implementation of the project and subsequent modifications.
- A geometric-structural survey with reference to the overall geometry of the structure as well as of structural elements, including the state and nature of possible contacts with adjoining structures, quality and state of conservation of materials and components.
- Experimental investigations, to be justified by type and quantity on the basis of their actual use in the analysis, designed to complete the information concerning the mechanical properties of the materials.

Specific guidelines regarding the type of investigations and tests to be performed are given in §3.1.3 and §4.1.3, for masonry and for reinforced concrete, respectively.

2.3.2 Modelling of uncertainties

With regard to the knowledge of the structure, one must distinguish between:

- Factors which may be considered known in *deterministic* terms, i.e. with a negligible margin of uncertainty, in absolute terms or due to their negligible influence on the response. For these factors, a single value for all the analyses is adopted.
- Factors affected by uncertainties of a *random* type, generally associated with the inherent variability of the properties of the structure. These factors are modelled using random variables, as described in §2.3.2.1.
- Factors affected by uncertainties of an *epistemic* type, associated with lack of knowledge of the structure or of the mechanical behaviour of its component elements. These factors can be modelled in some cases by means of continuous random variables, as described in §2.3.2.1 (when the lack of knowledge concerns the quantification of the value of a parameter of a model), or by us-

ing the technique of the logic tree, as indicated in §2.3.2.2 (when lack of knowledge requires consideration of alternative models).

2.3.2.1 Uncertainties modelled by random variables

Uncertainties modelled by means of continuous random variables, characterized by a probability density function *f(x)* or by the corresponding cumulative distribution function *F(x)*, in the problem of the evaluation of the average annual frequency λ_{SL}, include:

- The mechanical properties of materials (for example, compression or shear strength of masonry, compression strength of concrete, yield strength of steel, etc). These quantities are defined positive and for them the lognormal distribution can be adopted.
- The measure of seismic intensity *S* of the site. This random variable is specified in terms of the seismic hazard function $\lambda_S(s)$.
- Error terms of capacity models (resistance, deformability) of the structural elements. The distribution of these properties depends on the model and is specified in the relevant sections for various construction materials (see §3.4 and §4.4).

The inherent variability of seismic motion for a given intensity *S* is modelled implicitly by means of a sample of its "values" represented by the full set of motions selected for the analysis of the structure (§2.2.2).

The definition of the lognormal[9] probability distribution of the random variables used to describe the properties of materials requires the definition of two parameters:

- *Mean*. For buildings in reinforced concrete, an *a priori* estimate of this parameter can be established on the basis of the design documentation (specifications of materials in the calculations and/or test certificates), where available, updated as necessary by means of the Bayes procedure based on the results of experimental tests (destructive tests for strength values) of proven reliability. In the absence of original documentation, a sufficient number of tests must be carried out in order to obtain a firm estimate of this parameter. For masonry buildings, an *a priori* estimate may be obtained based on literature data, referring to buildings of the same period and type, or on values indicated in §3.1.3.2.
- *Standard deviation*. For buildings in reinforced concrete, an *a priori* estimate of this parameter, representative of the variability of mechanical properties within a single structure, can be established based on of literature data, referring to buildings of the same period and type, or on values given in §4.1.3 and updated as necessary by means of the Bayes procedure based on the results of experimental tests (destructive tests for strength values). For masonry buildings, an estimate *a priori* can be obtained on the basis of literature data referring to buildings of the same period and type, or on the values indicated in §3.1.3.2.

[9] Lognormal distribution has now become customary to represent quantities that are considered positive such as the properties of materials. It is worth mentioning that this distribution is not the only alternative and that also the Gamma (very similar to a lognormal for parameter values between 2 and 4) or the Beta are used.

2.3.2.2 Uncertainties of epistemic type that can be modelled by the use of the logic tree technique

These uncertainties are linked to an imperfect knowledge of the structure (for example, the actual effectiveness of the anchorage between the walls, the capacity of the floors to distribute the forces among the walls, or the variability of the different typology of walls for masonry constructions, or amounts or detailing of the reinforcement, or dimensions of the structural components for reinforced concrete buildings), the quantitative definition of the limit state, the choice between different capacity models, the use of different models and methods for the determination of the seismic response, etc.[10]

These uncertainties are modelled as discrete random variables, characterized by their mass probability functions $p(x_i)$.

In the context of this Guide, the effect of uncertainties of this type is evaluated by means of the technique of the logic tree, in which each of the combinations of the values of the variables is represented by a branch. Assuming statistical independence between variables, the probability associated with each branch is obtained as a product of the probabilities of the values of the variables in the branch. The calculation of the average frequency of exceeding the limit state λ_{SL} must be repeated for all the branches of the tree in accordance with one of the methods in §2.6. The final result of the evaluation consists in the weighted average with the probability of the corrresponding branches (Fig. 2-2) of the values of λ_{SL} obtained for each branch.

The selection of epistemic variables that are strictly necessary and of the corresponding alternative options represents a critical element to contain the onus of the evaluation of λ_{SL}. To this end it is particularly useful to have a sensitivity analysis performed in the preliminary stage that is subsequently updated and integrated as a result of further fact-finding surveys.

Specific indications are given in §3.1 and §3.1, for masonry and reinforced concrete buildings, respectively.

[10] It is to be noted that any response model is still unavoidably characterized by simplifying hypotheses that lead to an estimate that is still affected by uncertainty. This problem is not solved with the use of multiple models using the technique of the logic tree. To date, this uncertainty is not quantified by the majority of the response models available (quantification requires an extended comparison between calculated and experimental answers). If it were systematically quantified, the model could be eliminated from logic tree and the corrresponding error term should be included among the uncertainties modelled using random variables in §2.3.2.1. At the moment this type of mdel uncertainty can be reduced to insignificant levels on the overall risk measure only through systematic recourse to state-of-the-art methods and models.

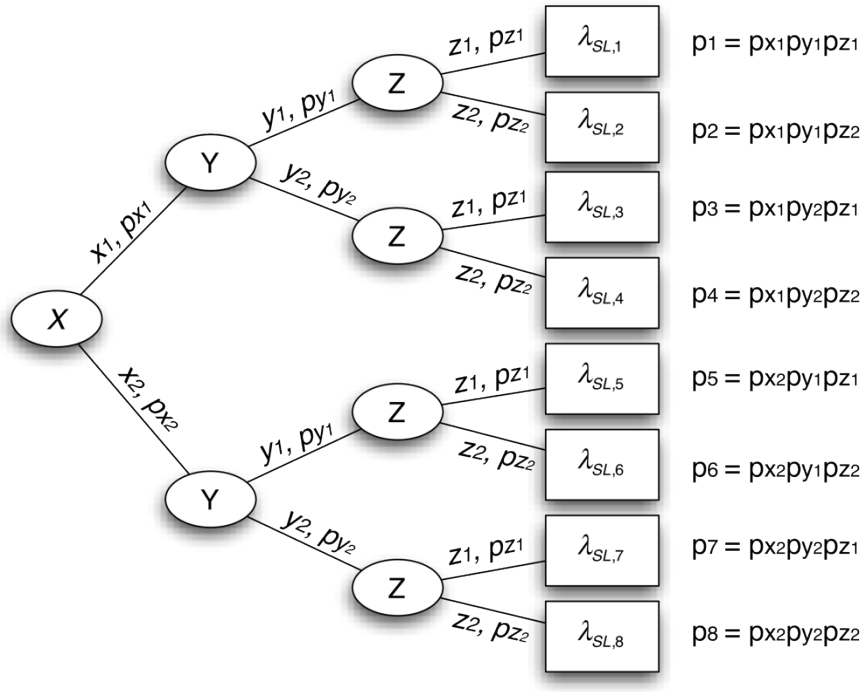

Fig. 2-2 Logic tree for three variables X, Y and Z each with two values.

2.4 Modelling and structural analysis

In this Guide the verification methods (§2.6) require the implementation of non-linear analyses of the response of the structure.

The non-linearities to be included in the modelling are of both mechanical and geometrical type (this latter when significant[11]).

Global response modelling of a building can be done by using frame models, which constitute the practice for buildings in reinforced concrete but also allow the representation of masonry buildings by means of the "equivalent frame" approach, which identifies columns (masonry piers) and beams (spandrels). For composite buildings of masonry and reinforced concrete the adoption of an equivalent frame model is therefore a natural extension of the above-mentioned approaches.

Different modelling criteria, such as macro-element methods or finite elements approaches, by which the continuum is discretized into two-dimensional or solid elements, may also be adopted. These latter models have the potential of providing very accurate results but their use is sometimes hampered by significant computational costs.

For the modelling of the mechanical non-linearity of the elements, constitutive laws may be adopted at the material or section/element level having a stable hysteretic behaviour (with or without cyclic degradation of stiffness but *without* strength degradation), hereinafter referred to as "without degradation", or constitutive laws *with* degradation also of strength, referred to hereinafter as "with degradation".

[11] In general the geometrical non-linearity can be significant for RC frame structures in the stage of large deformations and not significant for masonry structures.

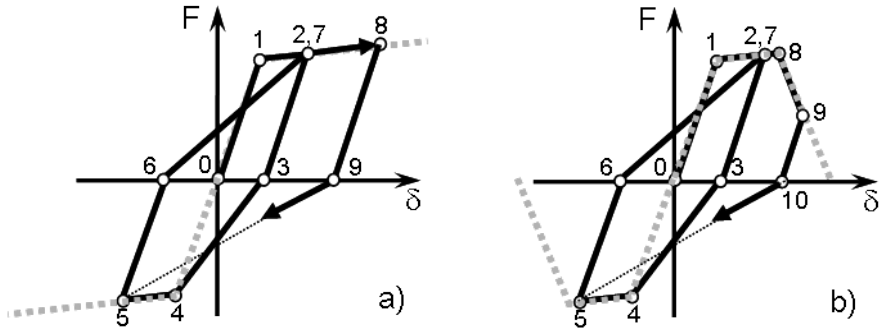

Fig. 2-3 Constitutive laws: a) with stiffness degradation but without degradation of strength, b) with of degradation of stiffness and strength. The curve with degradation in the figure shows only one component of the degradation, that due to negative stiffness in the monotonic load curve (*backbone*). Actually both the strength, and the unloading and reloading stiffnesses will degrade due to the effects of the cyclic dissipation of energy (cyclic degradation). Models are available that describe both forms of degradation (§4.3.1.5).

The two choices are not equivalent in terms of accuracy of the assessment: the choice of laws without degradation leads to a poor approximation for advanced limit states, i.e. severe damage and "near collapse", in which degradation plays a fundamental role. For reinforced concrete, for example, experimental tests on elements not designed according to modern criteria for seismic protection (capacity design) show how degradation commences already with element ductility at very low levels ($\mu = 2$). The response determined with models without degradation acquires therefore a conventional character after the attainment (verifiable only in retrospect) of the deformation threshold at which the degradation of the first element of the structure would start. The choice of the type of constitutive law is also reflected in the procedures for the identification of the limit state of collapse (§2.5.3).
Detailed indications on modelling procedures to be adopted for structural elements are given in §3.2 and §4.2 for masonry and reinforced concrete construction, respectively. In the case of masonry buildings it is also necessary to model and verify the possible local mechanisms, typically associated with the out-of-plane response of portions of the wall. Specific indications are given in §3.2.2.
The analysis of the seismic response can be performed by means of a static non-linear analysis (§2.4.1) or a dynamic non-linear analysis (§2.4.2).

2.4.1 Non-linear static analysis

As is widely known, there are several variants of this method of analysis which differ essentially by the load pattern used, whether invariant or varying depending on the level of inelasticity reached, and by consideration of a single or multiple modes of vibration for the determination of the response.
The scope of each method depends on the dynamic properties of the structure. In the simplest case of structures whose response is predominantly dominated by a single mode of vibration and the elastic demand is sufficiently uniform, the analysis can be performed with an invariant distribution of forces, proportional to the product of the mass matrix times the modal vector.
In general terms, the analysis consists in the application to the model of the structure, on which the gravitational loads have previously been applied, of one or more distributions of horizontal forces increasing up to attainment of collapse conditions. For each distribution of horizontal forces the result of the process is summarized in a global curve that links the shear force at the base to the displacement of a controlled

degree of freedom (the curve is actually transformed through expressions that depend on the modal form and on the distribution of masses in the structure, in order to define the response of an equivalent single degree-of-freedom oscillator, this latter curve is called in literature "capacity curve"). Each point of each capacity curve is associated with a deformed configuration of the structure.
For each value of seismic intensity *S*, the demand of the global displacement (i.e., of the control degree of freedom) is obtained from a response spectrum (inelastic, overdamped elastic, etc.). When multiple modes contribute to the dynamic response of the structure, the demand of the global displacement must be calculated for each capacity curve, and the local responses for any given intensity *S* must be combined by an appropriate modal combination rule before proceeding to the calculation of the value of the limit state variable (§2.5) (method of "multi-modal pushover analysis").

2.4.1.1 Determination of the constitutive relationship of the equivalent oscillator

As anticipated, for the purpose of determining the seismic response of a structure, the results of the non-linear static analysis are used to define the constitutive non-linear relationship of one or more simple oscillators, called "equivalent oscillators", which will be used in Metdods B and C to be subsequently introduced (§2.6.1).
For each of the two orthogonal directions in plan, the monotonic envelope of the equivalent oscillator is obtained by approximating with a multi-linear curve the overall curve of the structure. As shown in Fig. 2-4, in general it will be necessary to perform two analyses by pushing in the opposite directions to account for dissymmetries in the behaviour of the building. In the case that use is made of a method with an invariant load distribution it is also necessary to verifiy the approximate matching between the initial modal deformation and the deformation in a state close to the collapse, and if necessary to repeat the analysis for a different initial distribution (for example, for a distribution that is proportional to the masses in case the formation of a weak storey is identified).

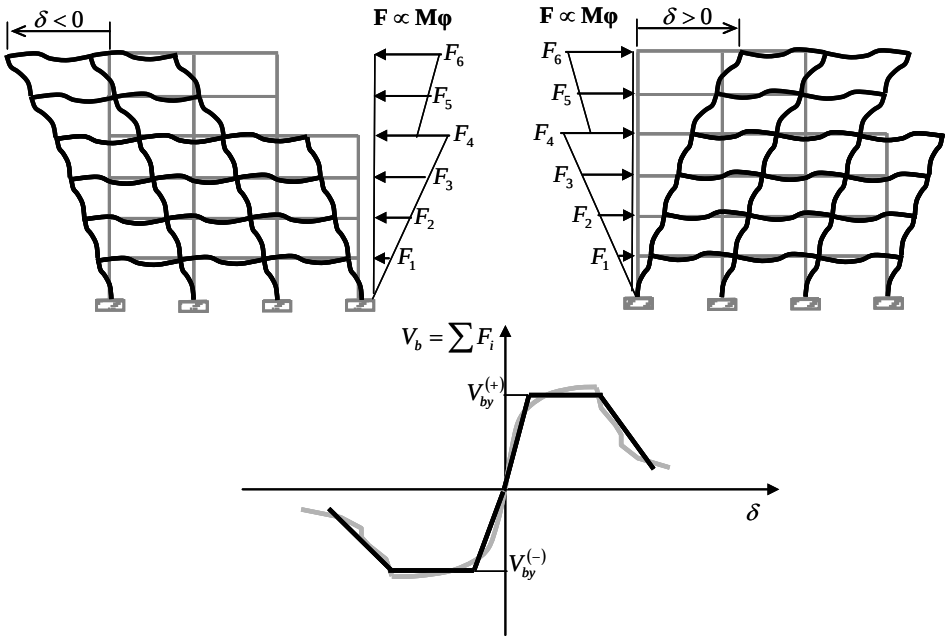

Fig. 2-4 Determination of the monotonic envelope of the constitutive relationship of the equivalent oscillator in the case of non-symmetrical behaviour and modelling with laws characterized by degradation.

The characteristics of the capacity curve depend on modelling choices, as illustrated in Fig. 2-5 that shows three relationships between base shear and displacement at the top for: (a) constitutive non-linear laws without degradation and absence of geometric non-linearity, (b) constitutive laws without degradation and presence of geometric non-linearity, (c) constitutive laws with degradation and geometric non-linearity. The curve of type (a) exhibits a post-elastic behaviour that is perfectly plastic or hardening. Curves of type (b) and (c) exhibit a post-elastic behaviour characterized by negative stiffness and possibly ending with zero shear at the base.

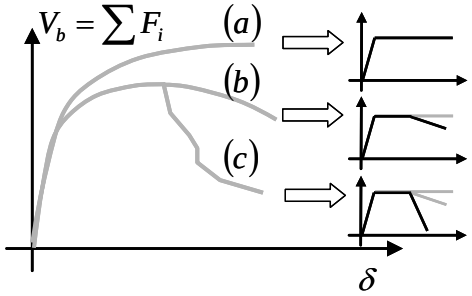

Fig. 2-5 Effect of modelling on the relationship between base shear and top displacement, and qualitative laws of the equivalent oscillator.

The monotonic envelope of the equivalent oscillator will be bi-, tri- or quadri-linear, depending on the model used in the determination of the response.
If the analysis of the equivalent oscillator under to seismic action is carried out with a dynamic method (as in the following Method B, §2.6.3) it is necessary to complete the definition of the constitutive law with an hysteretic rule governing the unloading-reloading curve of the oscillator.

2.4.2 Non-linear dynamic analysis

Non-linear dynamic analysis in step is carried out by numerically integrating the equations of the motion of the structure subjected to the two orthogonal horizontal components of the seismic motion, specified in terms of time histories of ground acceleration selected as indicated in §2.2.2. The analysis is carried out after the application of the vertical loads.
Unlike non-linear static analysis, for which it is sufficient to have constitutive models able to represent the response under monotonically increasing loads, in the case of dynamic analysis the model must account for the dissipative hysteretic behaviour under cyclic displacements.
The demand D obtained by means of a non-linear dynamic analysis shall be understood as the maximum absolute value attained during the time history of the response:

$$D = \max_t \left| D(t) \right| \tag{2.4}$$

2.5 Quantification of limit states exceedance

Within this Guide the quantitative assessment of attaining or exceeding the limit states, as defined qualitatively in §2.1.1, is carried out in terms of a scalar variable Y that expresses the overall state of the structure, as a function of the state of its component elements. Depending on the limit state considered and the non-linear modelling adopted, the variable Y can be expressed as a function of local ratios between the val-

ues of demand *D* and capacity *C*, or as a function of a global ratios between demand and capacity, or as a function of both, as subsequently indicated in §2.5.1, §2.5.2 e §2.5.3.
For limit states of damage and of severe damage that affect respectively the functionality and the economic feasibility of the repair, the definition of *Y* is flexible and the choice of an appropriate threshold is left to the decision of the owner. For the limit state of collapse, linked to safety, the formulation of *Y* does not leave any room for subjective choices.
Exceeding the limit state is indicated by values $Y > 1$.

2.5.1 Damage limit state (DLS)

The formulation of damage limit state indicates negligible damage to structural elements and slight damage to non-structural elements.
The variable *Y* can be expressed as a function of the local ratios *D/C* such as:

$$Y_{SLD} = \frac{1}{\tau_{SLD}} \max \left[\sum_{i=1}^{n_{st}} w_i I\left(\frac{D_i}{C_{i,SLD}}\right); \sum_{j=1}^{n_{nst}} w_j I\left(\frac{D_j}{C_{j,SLD}}\right) \right] \tag{2.5}$$

where *I(D/C)* is an indicator function with a value of 1 if D/C≥1 and otherwise zero, the weights *w* allow for the importance of the different components to be distinguished, and n_{st} and n_{nst} are the number of structural and non-structural elements considered in the summations. Y_{SLD} reaches the unit value when the "maximum" function reaches the value τ_{SLD}, defined by the owner and representing the maximum permissible cumulative damage for the damage limit state (for example, 5%). This formulation is directly applicable in the case of buildings in reinforced concrete, with values regarding the capacity of structural and non-structural elements provided in §4.4-4.5.
In the case of masonry buildings for the calculation of the limit state variable Y_{SLD} (§3.3.1.1), there is a contribution not only of the relationships *D/C* at local level (§3.4.1) but also at the level of the walls (interstorey drift - §3.4.4) and of global displacement, with appropriately defined capacity. In case where methods are used that resort to the definition of an equivalent oscillator, the variable Y_{SLD} can be expressed simply as a function of the relationship:

$$Y_{SLD} = \frac{\delta}{\delta_{SLD}} \tag{2.6}$$

where: δ is the global displacement demand of the structure and δ_{SLD} is the corresponding capacity, i.e. the global drift at which occurs one of the criteria stated subsequently (§3.3.1.1), including one that stipulates that the maximum percentage of the damage must not exceed a preset value.

2.5.2 Severe damage limit state (SLS)

The formulation of this limit state indicates a structure that is characterized by a state of damage that is so *widespread* as to render repair operations *uneconomic*. The variable *Y* assumes in this case the expression:

$$Y_{SLS} = \frac{1}{\tau_{SLS}} \begin{cases} \alpha_{st} \sum_{i=1}^{n_{st}} w_i c\left(\frac{D_i}{C_{i,SLS}}\right) + (1-\alpha_{st}) \sum_{j=1}^{n_{nst}} w_j c\left(\frac{D_j}{C_{j,SLS}}\right) \\ 1 \quad \text{if} \quad Y_{SLC \geq 1} \end{cases} \tag{2.7}$$

where the coefficient α_{st} expresses the weight of the structural component on the total economic value of the building, depending on its features and on its intended use; the summations extend over sets of structural and non-structural elements; the *conventional repair cost* function $c(D_i/C_i)$, depending on the state of damage *D/C*, assumes a zero value for D_i equivalent to zero and an unit value, corresponding to the replacement cost of the component, for $D_i/C_i \geq 1$, with a linear variation between the two extremes, in the absence of more accurate determinations; the weights *w* permit a differentiation between the importance of the various components; the ratio *D/C* in the summation of the non-structural elements can be expressed in terms either of interstorey drift and/or acceleration.
As in the case of limit damage state, the variable Y_{SLS} reaches the unit value when the weighted sum equals the threshold τ_{SLS}, equivalent to a fraction of the total value of the building, defined by the owner as the threshold beyond which demolition/replacement would be cost effective. Obviously in the case of collapse a value corresponding to the replacement cost of the building would be assigned to the threshold τ_{SLS}.
Capacity values to be adopted for structural and non-structural elements are given in §3.4.2 and §4.4.3-4.5 respectively for masonry buildings and for reinforced concrete.
The expression (2.7) is of direct use for buildings in reinforced concrete. A similar formulation, that does not consider non-structural elements but that distinguishes the different roles of masonry piers and spandrels, is given in §3.3.1.2 for masonry buildings.

2.5.3 Limit state for the prevention of collapse (LSC)

Control procedures for the attainment of the limit state of collapse depend on the choices made during the phase of the modelling of the structure (§2.4).

In case of adoption of modelling with constitutive laws *without degradation* the check whether the limit state is reached/exceeded must be made a posteriori, since this is not detectable in the global response curve in a direct manner.
The variable *Y* assumes in this case the expression:

$$Y_{SLC} = \max_{i=1,N_S} \min_{j \in I_i} \frac{D_j}{C_{j,SLC}} \tag{2.8}$$

where N_s is the number of the distinct sets *I* of elements whose joint collapse causes the global collapse of the structure (defined as "cut sets") and I_i is the i-th set (see §A.5).
As regards buildings in reinforced concrete in general the sets to be considered in the calculation of Y_{SLC} are provided in §4.6.2, with the values of the capacity to be adopted for structural elements indicated in §4.4.4.

In case of adoption of modelling with constitutive laws *with degradation* it is necessary to distinguish the case in which all potential failure mechanisms are included in

the modelling from that in which certain mechanisms are not detectable in the analysis.
In the first case the collapse of the structure, resulting from the local collapses of the structural elements, can be explicitly detected in the global curve of the response and, in dynamic conditions, can be identified with the occurrence of an indefinite increase of the displacements for infinitesimal increments of the intensity of the earthquake: in this condition the shear stress at the base is reduced to negligible levels.
The variable *Y* assumes the expression:

$$Y_{SLC} = (1+\Delta) - \frac{S'}{S'_0} \quad \text{con} \quad \Delta \le \frac{S'}{S'_0} \le 1 \tag{2.9}$$

that for $\Delta = 0$ reaches the unit value when the tangent S' at the curve intensity S – displacement δ vanishes. In order to avoid numerical problems in the simulation of the response in the region of dynamic instability one could as an approximation assign to Δ a small value, for example in the range between 0.05 and 0.10, which is equivalent to associating the collapse to a reduction of S' to a corrresponding fraction of the initial tangent S'_0 instead of zero. The condition on the tangent S' serves to exclude sections of the S-δ curve in which there could be an excessive "hardening" ($S' > (S')_0$) that would lead to negative values of Y_{SLC}, or to an inversion ($S' < 0$) that would correspond to values of $Y_{SLC} > 1$, both cases being not meaningful.
In the most common case in which some mechanisms cannot be detected throughout the analysis, a mixed approach is adopted with the following formulation of the variable limit state:

$$Y_{SLC} = \max\left[(1+\Delta) - \frac{S'}{(S')_0}; \max_{n.m.}\left(\frac{D}{C}\right) \right] \tag{2.10}$$

where the maximum of the local ratio D/C is calculated on collapse mechanisms that are not modelled (n.m.).

Finally, in the case of modelling *with degradation*, it is possible as an alternative to perform the check for the limit state for the prevention of collapse through a multiscale approach that accounts for the state of the structural elements, of the strains in significant macroelements (walls and floors) and of the global response, taking into consideration the deterioration of the structure; these controls are calibrated in such a way as to be representative of the conditions that are mentioned above. In cases where use is made of methods that resort to an equivalent oscillator, the variable Y_{SLC} can be expressed in terms of displacement, by appropriately defining the value of the capacity δ_{SLC} (§3.3.1.3):

$$Y_{SLC} = \frac{\delta}{\delta_{SLC}} \tag{2.11}$$

The values of both the local (member) and of the walls' capacities that are useful for the calculation of δ_{SLC} are given in §3.4.3 and §3.4.4 for masonry buildings.

2.6 Verification methods

2.6.1 Calculation of the average annual frequency of exceeding the limit state

The average annual frequency of exceeding the generic limit state is obtained by maing use of the theorem of total probability, as the sum of products of the probability $p_{SL}(s)$ of exceeding the limit state (Y_{SL}>1) conditional upon the level $S = s$ of the seismic intensity, for the average annual frequency of S in the region of s:

$$\lambda_{SL} = \int_0^{\infty} p_{SL}(s) \cdot \left| \frac{d\overline{\lambda}_S(s)}{ds} \right| ds \cong \sum_{i=1}^{n} p_{SL}(s_i) \left| \Delta \overline{\lambda}_i \right| \tag{2.12}$$

where the sum is extended to a number of points n such as to render the estimate stable[12]. To this end it is possible to fit to the average hazard curve $\overline{\lambda}_S$ defined, as indicated in §2.2.1, in nine points ($S = s_i$, $1/\overline{T}_{Ri}$), a quadratic function in logarithmic space $\overline{\lambda}_S$ -S:

$$\overline{\lambda}_S(s) = k_0 \exp\left(-k_1 \ln S - k_2 \ln^2 S\right) \tag{2.13}$$

The conditional probability of exceeding $p_{SL}(s)$ is called the fragility curve of the structure and is described by the equation:

$$p_{SL}(s) = p\left(Y_{SL} \geq 1 \middle| S = s\right) \therefore = p\left(S_{Y_{SL}=1} \leq s\right) = \Phi\left(\frac{\ln s - \mu_{\ln S_{Y=1}}}{\sigma_{\ln S_{Y=1}}} \right) \tag{2.14}$$

where the parameters to be determined are the average $\mu_{\ln S_{Y=1}}$ and the standard deviation $\sigma_{\ln S_{Y=1}}$ of the logarithm of the intensity $S_{Y=1}$ that induces the attainment of the limit state (Y_{SL} = 1). The standard deviation of the logarithm is often also denoted by the symbol β and is called “dispersion”.

The fragility curve can be evaluated according to one of the three methods that are described later in §2.6.2, §2.6.3 and §2.6.4, that differ both in the method for the determination of the seismic response (demand) as well as for the model used (capacity):

- Method A - §2.6.2: the probabilistic characterization of the limit state variable Y_{SL} is based on a dynamic incremental analysis of a complete model of the building with records selected in accordance with §2.2.2.
- Methods based on the analysis of an equivalent oscillator derived from a static non-linear analysis of the complete model of the building:
  - Method B - §2.6.3: the probabilistic characterization of the limit state variable Y_{SL} is based on the dynamic incremental analysis of the equivalent oscillator with records selected in accordance with §2.2.2.
  - Method C - §2.6.4: the probabilistic characterization of the limit state variable Y_{SL} is based on the use of the median spectrum and of those fractiles at 16% and at 84% of the records selected in accordance with §2.2.2, to obtain the maximum displacement of the equivalent oscillator.

[12] In literature there are available closed form solutions, with varying approximations, of the integral in (2.12).

2.6.2 Method A: incremental dynamic analysis on the complete model

The parameters of the distribution of $S_{Y=1}$ are evaluated by means of the technique known by the name of Incremental Dynamic Analysis (IDA).
The technique involves a non-linear dynamic analysis of the complete model of the structure subjected to each of the seismic motions (pairs or triplets of time histories) selected according to §2.2.2, scaled to increasing levels of intensity.
For each motion and intensity level $S=s$, calculations are made of the value of the variable of limit state Y. The coordinate points (Y, S), define in the response-intensity plane a curve that is called "the IDA curve". The set of curves obtained for the n motions allow the identification of a sample of n values of the random variable $S_{Y=1}$, as shown in Fig. 2-6(a) by the red diamonds, with which to estimate the parameters $\mu_{\ln S_{Y=1}}$ e $\sigma_{\ln S_{Y=1}}$.

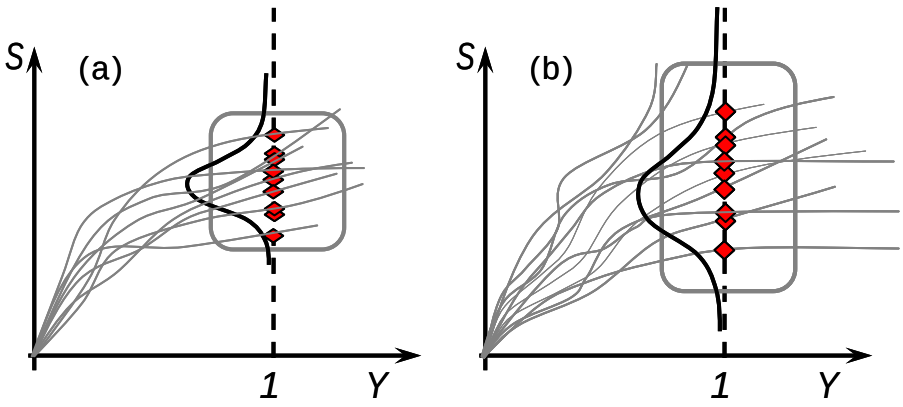

Fig. 2-6 IDA Curves: (a) without randomness of the structure (b) with randomness of the structure.

The effect of the uncertainties modelled with continuous random variables (§2.3.2.1) can be quantified in a simple manner by associating with each of the selected motions of the ground a distinct realization of the random variables, by sampling from their respective probability distributions. The final result, as shown in Fig. 2-6(b), is a bundle of IDA curves, and therefore of values of $S_{Y=1}$,characterized by a greater variability.

2.6.3 Method B: incremental dynamic analysis on the equivalent oscillator

The parameters of the distribution of $S_{Y=1}$ are evaluated by means of the IDA technique, applied in this case to the equivalent oscillator, obtained as shown in §2.4.1.1, subjected to seismic motions selected in accordance with §2.2.2, scaled to rising levels of intensity. It is necessary to consider the simultaneous excitation by the orthogonal components of the seismic motion. A sample application this approach is given in §**C.7.1**.
For each motion and intensity level $S=s$, the maximum value of the displacement δ is converted to the value of the variable of limit state Y, through the relationship δ-Y obtained during the corresponding non-linear static analysis. In the general case of a non-symmetric oscillator it is necessary to register for each level $S = s$ both the maximum displacement $\delta^{(+)}$ as well as the minimum displacement $\delta^{(-)}$, and to allocate to each of them the corrresponding value of the variable limit state Y. The value of Y in the IDA curve of the structure will be $Y = \max (Y^{(+)}, Y^{(-)})$.

The set of IDA curves obtained for the *n* motions allows the identification of a sample of *n* values of the random variable $S_{Y=1}$, as already shown in Fig. 2-6, with which to estimate the parameters $\mu_{\ln S_{Y=1}}$ and $\sigma_{\ln S_{Y=1}}$.

The effect of uncertainties modelled with continuous random variables (§2.3.2.1), can be quantified, as already indicated for Method A, by associating with each of the selected ground motions a separate realization of the random varibales by sampling from their respective probability distributions. Then the static non-linear analysis must be repeated for each of the *n* samples, each of which leading to a separate equivalent oscillator. The final result, also in this case, is a bundle of IDA curves, and therefore of values of $S_{Y=1}$, characterized by a greater variability.

2.6.4 Method C: non-linear static analysis and response surface analysis

The parameters of the distribution of $S_{Y=1}$ are evaluated through the use of non-linear static analysis, with the demand obtained by means of the response spectra of the seismic motions selected according to §2.2.2. It is necessary to consider the simultaneous excitation by the orthogonal components of seismic motion. In many cases, with particular reference to masonry buildings, it is possible to perform separate analyses in the two in-plan directions as indicated in §3.2.1.5. The effect of the uncertainties modelled with continuous random variables (§2.3.2.1) is quantified by means of the use of the technique of response surface.

In this method the factors that contribute towards the total uncertainty are assumed as statistically independent, therefore the parameter $\beta = \sigma_{\ln S_{Y=1}}$ representing both, is given by the following expression:

$$\beta = \sqrt{\beta_S^2 + \beta_C^2} \tag{2.15}$$

where β_S measures the effect on $S_{Y=1}$ of the variability of the seismic demand at a given intensity, due to the difference between the time histories of the motion, evaluated on the median capacity curve (§2.6.4.2), whereas β_C measures the effect on $S_{Y=1}$ of the uncertainty in the capacity curve (§2.6.4.3).

2.6.4.1 Determination of the median of *S* conditioned to *Y*=1

The determination of the mean value $\mu_{\ln S_{Y=1}}$, equal to the logarithm of the median of $S_{Y=1}$, is performed using the median spectrum (50% fractile) of the time histories selected in accordance with §2.2.2 (on the approximate assumption that the median spectrum induces the median response[13]), scaling it up to the value of the intensity *S* such that the *demand* in displacement coincides with the *capacity* corresponding to the considered limit state (§3.4 or §4.4). The curves that represent the relationship between the measure of seismic intensity *S* and the limit state variable Y_{SL} are referred to in this method as ISA curves (Incremental Static Analysis) , in analogy with IDA curves.

The determination of the displacement demand δ can be performed according to two alternative models:

[13] The median capacity curve should be strictly calculated by means of simulation and evaluation of the 50% fractile of the curves obtained for multiple samples of the basic variables. Willing to use a single non-linear static analysis, it is current practice to assume in approximation that the curve obtained by using the average values is the median.

- *Inelastic spectrum method*: this is the method adopted by Eurocode 8 and by NTC 2008 and is easy to implement in the case where for the equivalent oscillator a bilinear law can be assumed; the required displacement depends on the elastic period of the equivalent oscillator (larger than the initial elastic one of the structure, to account for the deterioration of the stiffness during the response phase prior to reaching the maximum strength), and eventually also on the deficit of strength compared to that needed for the structure to remain within the elastic range, in the case of rigid structures ($T<T_C$).
- *Method with overdamped spectra:* in this method it is possible to use a capacity curve of any shape; the required displacement is determined by considering a linear system with secant stiffness and equivalent viscous damping as functions of the ductility, i.e. compatible with the displacement; typically in the elastic phase of the response the damping is set equal to 5% and rises with an increase of the non-linearity (the reduction of spectral ordinates as a function of the damping is operated using the factor η as defined in Eurocode 8 and in NTC 2008).

2.6.4.2 Determination of the uncertainty of the seismic demand β_S

The term β_S is evaluated, in the assumption of a lognormal distribution of $S_{Y=1}$, as a function of the values $S_{Y=1,16\%}$ and $S_{Y=1,84\%}$ calculated, on the median capacity curve, using the response spectra fractiles at 16% and 84% of the time histories selected according to §2.2.2:

$$\beta_S = \frac{\ln S_{Y=1,16\%} - \ln S_{Y=1,84\%}}{2} \tag{2.16}$$

2.6.4.3 Determination of the uncertainty on capacity linked to random variables β_C

The influence on the variable $S_{Y=1}$ of continuous random variables (§2.3.2.1) related to the mechanical and geometrical properties of the structure is estimated through a linear response surface:

$$\ln S_{Y=1} = \alpha_0 + \sum_{k=1}^{N} \alpha_k x_k + \varepsilon \tag{2.17}$$

that expresses the logarithm ln $S_{Y=1}$ in the space of the normalized random variables x_k, defined in such a manner that they are valued ±1 in correspondence to the fractiles at 16% and 84%. In case of variables with normal distribution:

$$x_k = \frac{X_k - \mu_{Xk}}{\sigma_{Xk}} \tag{2.18}$$

where $\mu_{X,k}$ e $\sigma_{X,k}$ are respectively the mean and the standard deviation of the variable X_k. In (2.17) the normal variable ε represents the error term that describes the deviation of the linear response surface from the actual variation of ln $S_{Y=1}$ in the space of the normalized random variables x_k.

The estimate of the N parameters α_k is done by means of a least squares regression on $M = 2^N$ different configurations, generated through a full factorial combination at 2 levels, where the uncertain normalized variables assume a value of +1 or -1. For the generic m-th ($m = 1,\ldots,M$) combination a non-linear static analysis is performed to determine the value of the seismic intensity that leads to the limit state, using the median spectrum used in §2.6.4.1.

Placing the values assigned to the variables x_k for each of the M combinations in the rows of a matrix **Z**, with dimensions $M \times N$, referred to as "matrix for experiments", and the values obtained by $\ln(S_{Y=1,m})$ in a vector **Y**, with dimensions $M \times 1$, the coefficients α_k ($k = 1,\ldots,N$) that multiply the normalized variables are thus obtained by the following vector:

$$\boldsymbol{\alpha} = \left(\mathbf{Z}^T \mathbf{Z}\right)^{-1} \mathbf{Z}^T \mathbf{Y} \tag{2.19}$$

The contribution of the "structural" uncertainty (i.e. of the variability of the capacity curve) to the total variability, in the hypothesis of statistical independence between ε and x_k, is provided by the formula:

$$\beta_C = \sqrt{\sum_{i=1}^{N} \sum_{j=1}^{N} \alpha_i \alpha_j \rho_{x_i x_j} + \sigma_\varepsilon^2} \tag{2.20}$$

where σ_ε is the standard deviation of the residuals and $\rho_{x_i x_j}$ the coefficient of the correlation between x_i and x_j.

3 Masonry buildings

3.1 Knowledge of the structure

The choice of models with which to perform the assessment requires a knowledge of the structure not purely geometrical but including the construction technique and history too. By consideration of construction phases, structural modifications, degree of connection among walls and characteristics of horizontal elements, it is possible to identify the possible local damage mechanisms to be analysed in the assessment of seismic safety. Also the global model assumes choices that require the implementation of diagnostic surveys, both for a proper definition of the geometry and of the links as well as for the assignment of the mechanical properties of materials.

3.1.1 Aspects of knowledge

Elements of knowledge that are necessary for evaluation purposes, referred to in §2.3.1 are:

- Geometry of the structural system
- Construction details
- Mechanical properties of materials

This information can be obtained in an existing masonry building through the following sources:

- Historical-critical analysis
- Geometrical-structural survey
- Structural material survey
- Visual investigations and experimental tests

The historical critical analysis is aimed at an understanding of the system as a whole, composed by its architectural and structural parts, through the knowledge of changes (additions or modifications) that occurred over time with particular reference to those dependent on historical seismic events, useful for the purpose of a proper identification of the resisting system and of its state of stress. Historical documentation (available archive documents, iconographic sources, historical design tables, sketches, etc.) is paramount to the knowledge of the construction phases and of the trasformations that the structure has undergone throughout the time. Particular attention should be paid to the acquisition of information on damage suffered after previous earthquakes and on the following interventions that were carried out.
Geometric-structural survey must be extended both to the overall geometry of the building as well as to that of the construction elements, including relationships with any possible adjoining buildings.
The knowledge of the construction material must allow for the complete identification of the resisting body of the building, also taking into account the quality and the state of conservation of the materials and of their components.

3.1.2 Preliminary analysis

The evaluation of the seismic safety of an existing building requires accurate diagnostic surveys and investigations, which involve a significant cost, within the total amount of the assessment, and an invasive impact on the building, especially in the case of historic buildings. Moreover, the knowledge will never be complete, due to

the huge variety of materials and solutions that can be encountered in a masonry construction, typically not engineered but being the result of empirical construction rules. It is therefore necessary to address the investigations towards elements that mostly influence the response with a view to reducing the uncertainties of the assessment and at the same time avoid unnecessary or insignificant investigations, especially if expensive and invasive. To this end it is appropriate to carry out a sensitivity analysis that would help in the choice of the most suitable model and would identify the geometric and mechanical parameters and the connections upon which the response would mainly depend.

An essential starting point is a minimum basic understanding of the structure, sufficient to allow the definition of a preliminary model. Having identified the parameters X_k (k = 1,N) characterized by a significant uncertainty, it is necessary to estimate a plausible average value m_{Xk} and an interval of confidence, through the measure of deviation s_{Xk}, based on expert judgment and on the possible results of preliminary diagnostic investigations. Reference values for different types of walls are proposed in Table 3.1 (s_{Xk} = 0.5 μ ($e^{\sigma\square\square}$-$e^{-\sigma\square\square}$)), but in the presence of inhomogeneous walls in different parts of the construction and in the absence of reliable experimental data, it is considered advisable to assume a higher value for the variation s_{Xk} than those herein suggested.

The non-linear static analysis performed with the values m_{Xk} constitutes the benchmark for the sensitivity analysis; from the capacity curve and from the median response spectrum of the selected recordings (§2.2.2 and §2.6.4) it is possible to evaluate a central value $\bar{a}$ of peak ground acceleration leading to the limit state of interest.

A series of non-linear static analysis is then performed, assuming for all parameters the average values of these intervals with the exception of one, to which is attributed one of the two extreme values of the range. Having evaluated the corresponding peak ground accelerations, a sensitivity parameter is defined as:

$$\Delta_k^{'} = \frac{a_{k,\max} - a_{k,\min}}{\bar{a}} \tag{3.1}$$

As regards the epistemic uncertainties that cannot be modeled as continuous variables, one proceeds to the definition of discrete epistemic variables (j = 1,…,M), for each of which two or more alternative options (p = 1,…,m_j) are possible. In these cases the sensitivity analysis must be performed by analysing all the possible combinations (branches of the logic tree) and obivously utilizing for the random variables the values m_{Xk}.

In the case where there is only one epistemic variable (j=1) characterized by two alternative options (m_j=2), the sensitivity parameter is defined by the relationship:

$$\Delta_j^{'} = 2\frac{|a_1 - a_2|}{a_1 + a_2} \tag{3.2}$$

where a_1 and a_2 are the ground accelerations leading to the limit state of interest by adopting the two alternative options.

In the case where there are more than two alternative options, the preceding formula can be generalized as follows:

$$\Delta_j^{'} = 2\frac{\max(a_p) - \min(a_p)}{\max(a_p) + \min(a_p)} \qquad p = 1, m_j \tag{3.3}$$

where a_p is the ground acceleration that leads to the limit state of interest in the case where the *p*-th alternative option is considered.
A further generalization is necessary in the case of *M* epistemic variables. The sensitivity parameter of the variable *j* is obtained, having evaluated for each *p*-th option the mean $\mu_{a_p}^j$ of the ground accelerations calculated on the branches of the logic tree characterized by that option, through the relationship:

$$\Delta_j^{'} = 2\frac{\max\left(\mu_{a_p}^j\right) - \min\left(\mu_{a_p}^j\right)}{\max\left(\mu_{a_p}^j\right) + \min\left(\mu_{a_p}^j\right)} \qquad p = 1, m_j \tag{3.4}$$

From an examination of the values $\Delta_k^{'}$, obtained for the *N* continuous random variables, and $\Delta_j^{'}$, relative to the *M* epistemic variables, it is possible to identify the parameters that have the major influence on the response and for which it is necessary to deepen the investigation further, as a result of which it is possible to update the estimate of the parameters, going so far as to define the corresponding probability distribution. Typically the lognormal distribution is the most suitable, while for parameters that are limited within a finite interval the Beta distribution can be used. In the case in which, for the generic parameter X_k, the mean value $m_{x,k}$ is significantly different from that assumed in the preliminary model, it will be necessary to re-run the sensitivity analysis; otherwise the sensitivity parameter can be updated as follows:

$$\Delta_k = \Delta_k^{'}\frac{\sigma_{Xk}}{s_{Xk}} \tag{3.5}$$

where σ_{Xk} represents the estimate of the deviation standard of the variable X_k, evaluated on the basis of diagnostic investigations. In particular, insofar as regards the mechanical properties of the masonry, the execution of diagnostic investigations allows a better classification of the type of walls and eventually an estimate of the average values. Moreover, considering the difficulties to perform a statistically significant number of tests and the limited reliability of in-situ tests, it is not considered justified to assume values of σ_{Xk} that are lower than those obtained from the dispersions σ_{ln} indicated in Table 3.1 ($\sigma_{Xk} = 0.5\, m_{x,k}\, (e^{\sigma\square\square} - e^{-\sigma\square\square})$). Then, based on the new value of the sensitivity parameter Δ_k, one needs to decide whether to consider in the evaluation this parameter as uncertain or to consider it as deterministic.
The variables that result from the sensitivity analysis as significant and for which it is not possible to investigate further, will be considered as uncertain in the safety assessment. For those of random nature, the values previously used are taken as a mean and standard deviation ($\mu_{Xk}=m_{Xk}$, $\sigma_{Xk}=s_{Xk}$). Epistemic ones need the assignment of a subjective probability to alternative hypothesis.
Finally, the variables that influence the response to a negligible extent will not be further investigated; the safety assessment will take the average estimated values, for the random variables, and the model or parameter considered most reliable, for epistemic variables.

3.1.3 Experimental investigations

3.1.3.1 Structural details

Particular attention must be given to the following structural details:

- type of horizontal elements (construction technology, the span direction, stratigraphy of the floor; in the case of vaults, the key profile, the presence of retaining walls or fills)
- systems of vertical connections (stairs), with particular reference to their in-plane stiffness;
- roof system (way in which thrust is eliminated);
- presence of any recesses, cavities, filled gaps in the walls;
- the quality of the connection between vertical walls;
- the quality of the connection between horizontal elements and vertical walls and the possible presence and effectiveness of ring beams or other connecting systems at floors level;
- the presence of structurally effective lintels above openings;
- the presence of structurally effective elements to support possible horizontal thrusts;
- the presence of elements, even non-structural, with high vulnerability;
- the presence of tie rods and their structural efficiency;
- the type of masonry (single or double leaf walls, with or without filling, with or without cross connections, etc.), and its structural details (made of brick or stone, with regular or irregular pattern, etc.);
- type of foundations.

Details regarding these factors allow to reduce the number of variables affected by *epistemic* uncertainty (or limit their range of variability).

3.1.3.2 Mechanical properties of masonry

The mechanical characteristics of materials which are of interest are those related to both deformability and strength, necessary for the modelling of structural behaviour. This aspect, for masonry structures, is strictly related also to the assembling of components (pattern of blocks and joints), in addition to the results of standard mechanical tests. In fact the analysis of the constitutive characteristics of the masonry can be of help in the selection of the appropriate class type for which the reference values of mechanical properties can be assumed, as can be found in literature or in technical standards.

For the stochastic characterization of the mechanical properties of masonry use can be made, as indicated in §2.3.2.1, of a lognormal distribution of probability. Table 3.1 provides reference values for the main types of masonry that can be found in the Italian territory (derived from those proposed in Table C8A.2.1 of Appendix C8A in the Commentary to NTC 2008, Circular No 617, 2 February 2009).

The values proposed in Table 3.1 are representative of basic values for masonry buildings not complying with the rules of good practise (such as, for example, the presence of a good transversal connection or that of a good quality mortar, etc.); the average value may be eventually modified on the basis of the coefficients proposed in Table C8A.2.2 of the above-mentioned Circular, while maintaining the standard deviation unaltered.

The characterization of the mechanical properties should be investigated for at least one wall panel for each masonry type present in the building.

A reliable characterization of the mechanical properties of strength and stiffness is generally achieved by means of experimental tests of a destructive nature (compression, shear-compression, shear-diagonal) which enable a direct characterization. In the identification of possible areas of sacrifice where carrying out a possible destructive test, account can be taken of the indications of historical research and of changes undergone by the structure. Given the destructive nature of the above-mentioned tests, they should only be carried out if justified and warranted by the outcomes of the sensitivity analysis performed earlier. In order to limit the impact of these investigations, the results of experimental tests carried out on masonry buildings with similar characteristics of that under examination and belonging to the same geographical context could be of particular usefulness.

Table 3.1 Reference values for mechanical properties of different masonry types: mean values and standard deviation of the logarithm.

Type of masonry		f_m [N/cm^2]	τ_0 [N/cm^2]	E [MPa]	G [MPa]
Irregular stone masonry	μ	140	2.6	870	290
	σ_{ln}	0.29	0.24	0.21	0.21
Roughly cut stone masonry, having wythes of limited thickness and inner core	μ	250	4.3	1230	410
	σ_{ln}	0.20	0.19	0.17	0.17
Uncut stonework with good texture	μ	320	6.5	1740	580
	σ_{ln}	0.19	0.14	0.14	0.14
Masonry blocks of soft stone	μ	190	3.5	1080	360
	σ_{ln}	0.27	0.20	0.17	0.17
Squared stone masonry	μ	700	10.5	2800	860
	σ_{ln}	0.14	0.14	0.14	0.09
Solid brick masonry and lime mortar	μ	320	7.6	1500	500
	σ_{ln}	0.26	0.21	0.20	0.20
Semisolid brickwork with cement mortar (eg. Double UNI perforations < 40%)	μ	650	28.0	4550	1138
	σ_{ln}	0.24	0.14	0.24	0.24
Semisolid brick blocks (perc. perforations < 45%)	μ	500	35.0	4500	1350
	σ_{ln}	0.20	0.14	0.20	0.20
Masonry made by hollow blocks with vertical dry joints (perc. perforations < 45%)	μ	350	11.5	3150	945
	σ_{ln}	0.14	0.13	0.14	0.14
Masonry blocks of concrete or of expanded clay (perc. perforations between 45% and 65%)	μ	175	11.0	1400	350
	σ_{ln}	0.14	0.14	0.14	0.14
Hollow concrete blocks (perc. perforations < 45%)	μ	370	21.0	2960	740
	σ_{ln}	0.19	0.14	0.19	0.19
f_m: compressive strength of masonry; τ_0: shear strength of masonry; E: modulus of normal elasticity; G: modulus of tangential elasticity					

The number of tests that can be performed on a homogeneous type of masonry will be generally very limited and will not allow a statistical treatment of the results. The interpretation of the results should therefore necessarely consists of a reasoned judgment in which even the use of a single experimental data can be significant.
The systematic use of non-destructive testing or slightly destructive testing (sclerometric hammer test, sonic test, double flat-jack test) is crucial to assess the actual homogeneity of the characteristics of a given masonry type inside the building.

3.2 Modelling criteria

Masonry buildings consist of a construction formed by several masonry walls (i.e. elements having a small thickness compared to the in-plane size of the wall) and possibly by masonry columns, connected by horizontal diaphragm elements (intermediate floors and roof) of different nature and material (vaults, timber or reinforced concrete diaphragms or composed by steel profiles and bricks). This section does not explicit consider other types of existing masonry buildings such as towers, churches, fortifications, city walls, etc..

Wall elements, besides carrying vertical loads, must also withstand horizontal seismic action. The horizontal elements contribute to connect together the vertical elements and, depending on their stiffness, possibly redistribute the seismic actions among the different walls.

The mechanisms of damage observed in masonry buildings can be traced to two categories: mechanisms of the first and of the second modes.

Generally the phenomena of interaction between the two classes of behaviour is neglected.

3.2.1 Global response: continuous structural elements and equivalent frame models

In cases where local mechanisms are prevented, a global behavior develops and the building withstands all the horizontal seismic actions mainly by exploiting the walls strength in their respective planes. The model of the whole building consists of various interconnected walls, linked also through horizontal diaphragms characterized by their in-plane stiffness. The exclusive use of models that consider the infinite stiffness of horizontal diaphragms is only justified when diagnostic investigations actually support this hypothesis. The verification of the building through a separate analysis of each wall becomes necessary when horizontal diaphragms have a really negligible stiffness. These modelling approaches constitute two extreme cases that can be used, in the absence of more accurate and reliable methods, as alternative options for accounting the epistemic uncertainty of the model.

The in-plane modelling of the wall can be carried out with various different non-linear models, as long as they are able to reproduce the degradation of the stiffness, the resistance to horizontal action and its progressive degradation until the collapse stage. For example, it is possible to use finite element methods, discretizing the wall through solid or plane elements with constitutive laws that are able to describe the behaviour of the masonry as an equivalent continuous material (Rots 1991, Lourenco et al. 1995, Lourenco et al. 2006, Calderini and Lagomarsino 2008), or models that discretize the wall through macroelements (panels), that have characteristics equivalent to those of a macro-portion of the wall and are connected between them with springs or with appropriate interfaces (Caliò et al. 2012).

A widely used modelling approach, extensively described below, is that which leads to the identification in the wall of vertical structural elements (piers) and horizontal elements (spandrels), connected through portions of finite size (nodes), assumed to be rigid and resistant (Magenes and Della Fontana 1998, Chen et al. 2008, Belmouden and Lestuzzi 2009, Grande et al. 2011, Lagomarsino et al. 2013). It is in this way that an equivalent frame is constituted (Fig. 3-1).

Marques and Lourenco (2011) have compared the results obtained from different models based on the equivalent frame idealization. The reliability of this modelling approach was also discussed by means of a comparison between the results obtained by finite elements models (Calderini et al. 2012). The equivalent frame approach does not necessarily require the use of dedicated codes but can be implemented on *general*

purpose finite elements codes (Kappos et al. 2002, Salonikos et al. 2003, Pasticier et al. 2008). It can also be noted that such approach is also a viable option for the modelling of mixed masonry-reinforced concrete buildings, as shown in (Cattari and Lagomarsino 2013).

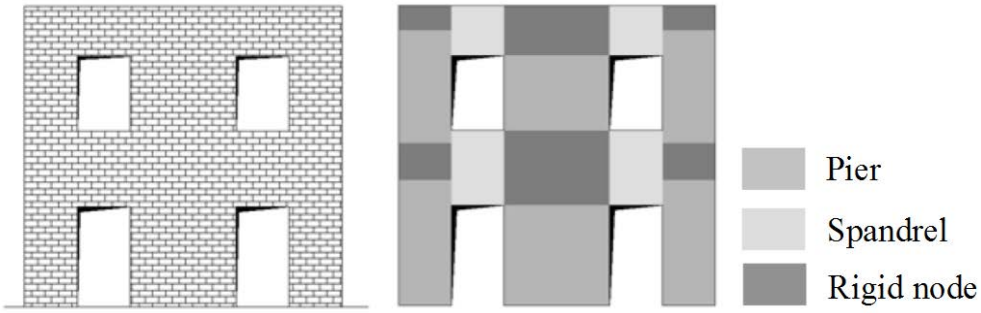

Fig. 3-1 Idealization of a masonry wall into the equivalent frame

The most significant aspect of the finite element modelling, or that with macroelements or based on the equivalent frame approach is that the collapse mechanisms are not predetermined apriori, unlike what happens in the case of two quite simplified models still adopted in practice:

a) Strong spandrels-weak piers: it assumes the spandrels as infinitely rigid and resistant, concentrating the deformation and the damage only in masonry piers;
b) Weak spandrels-strong piers: it assumes the spandrels as nor resistant elements that couple masonry piers only with respect the horizontal displacement.

The first model leads to an overestimation of the stiffness and strength of the structure, with a reduced displacement capacity; the second one to an underestimation of the strength (often of a considerable amount) to a benefit, however, of the displacement capacity. These models can constitute a useful reference in the presence of uncertainties regarding knowledge about the structural details of the building, for the sensitivity analysis or as possible alternatives in the application of the logic tree approach.

The single 2D-walls are then assembled in 3D models. In this regard there are several possible different modelling strategies: a) to consider for each node 6 degrees of freedom (d.o.f.), attributing to the wall a modest amount of out-of-plane stiffness; b) to condense the degrees of freedom, keeping only 3 degrees of freedom for the nodes that belong to a single wall and 5 degrees of freedom for those at the intersection among two or more walls (in this case by virtue of the absence of out-of-plane stiffness of the wall, the rotation around the vertical axis is not taken into account). In the case of an imperfect coupling between the walls, it is possible to couple only some of the degrees of freedom or to include in the model equivalent beam elements of appropriate stiffness.

The horizontal diaphragms are considered as stiffening elements that rule the distribution of seismic actions among the walls. In general the out-of-plane behaviour of the horizontal elements is not explicitly modelled given its small relevance on the global seismic response, and being the out-of-plane response of the walls neglected. The assumption of an infinitely rigid slab in its plane is justified in the case of reinforced concrete diaphragms (even if lightened) or in steel or timber diaphragms, provided they have a top slab of suitable thickness and well connected. In the case of traditional

horizontal elements typical of old masonry buildings (timber diaphragms, covered with timber boards or tiles; steel beams with tiles or small brick vaults; stone or bricks vaults) it is instead necessary to consider in the model their deformability in the horizontal plane, as well as possible limit values of resistance and drift. Expressions for the calculation of the stiffness of different diaphgrams types are provided, for example, in ASCE/SEI 41/06, NZSEE 2006.
In the following paragraphs some criteria are introduced for the resistance of the elements that define the equivalent frame model of a masonry building, that is vertical piers and spandrel beams. The failure criteria of these elements are expressed in terms of generalized forces (N, V, M) and of generalized deformation components (displacement and rotation at the end sections of the element).
In the case of the adoption of continuous models, such as finite elements with discretization through bidimensional or solid elements, the ultimate conditions of the wall result from the integration over proper sections of the local response of the material, described by appropriate constitutive laws, amied to incorporate the degradation of stiffness and strength. The information given later in §3.2.1.1 and §3.2.1.2 is not therefore necessary. Particular attention should be given in this case to the following aspects: i) the dependence of the response from the discretization adopted; ii) the convergence of the solution; iii) the availability of algorithms capable of following the response in the *softening* phase, in the context of a pushover analysis under a controlled load pattern. It is noted that even in the case of an analysis with continuous models it is always necessary to define a posteriori generalized strain quantities, as subsequently explained in §3.3.1, for the quantification of limit states, that requires the assessment of the angular deformation of the panels (*drift*).

3.2.1.1 Models for pier elements

In the equivalent frame model the constitutive formulation of the vertical structural elements (pier) aims to reproduce - through generalized stress and displacement variables at both ends - a complex variety of behaviours, such as for example: shear failure due to diagonal cracking, failure of end sections under normal force and bending, coupling between axial displacement and rotation due to opening of corner joints (uplift), different hysteretic cyclic responses in relation to the type of failure. There are various formulations of macroelements that, on a mechanical or on a phenomenological basis, are capable of representing many of these response phenomena through appropriate internal variables.
The simplest method, which captures most of the aspects above, is that of a non-linear beam, with a constitutive law represented in terms of shear force and drift, whose parameters are defined as follows:

a) the elastic stiffness is that of a shear beam having the same section of the pier (typically using reduced elastic moduli, referred to as “cracked”, to better approximate, with a linear behaviour, the non-linear response of the actual panel until it reaches its strength limit);
b) the shear strength is evaluated by means of appropriate failure criteria depending on the mechanical properties of the masonry, the geometry of the panel and the stress state;
c) the post-peak behaviour is brittle or ductile depending on the failure mode (shear or flexural) and can be modelled with varying levels of detail. The most simple approach considers a horizontal branch with limited ductility, whose extent is defined by a limit value of drift, followed by a sharp reduction to ze-

ro of the resistance; more accurate models can describe the progressive degradation of resistance, for example through a series of discrete descending steps;

d) the hysteretic cyclic response is diversified as a function of the failure mode and of the level of deformation that has been reached.

The failure domain of masonry piers in the N-V plane is provided by the envelope of the two criteria that identify the rupture at the end sections under crushing (due to normal force and bending) and that at the centre of the panel for shear. Several formulations are suggested below, taken from scientific literature and from various standards although it cannot be excluded the use of other criteria as long as they are of proven validity.

With regard to normal force and bending, neglecting the tensile strength of masonry and considering a suitable non-linear distribution of compressive stresses, in the case of a pier with rectangular section the ultimate moment M_{pf} at one end can be calculated as:

$$M_{pf} = 0.5 l^2 t \sigma_0 \left(1 - \frac{\sigma_0}{0.85 f_m}\right) \tag{3.6}$$

where: l and t are the length and the thickness of the pier, respectively; σ_0 is the average normal compressive stress, referred to the total area of the section; f_m is the average compressive strength of the masonry. Given the shear length h', i.e. the distance between the end section and that of the beam with zero moment, the ultimate shear force under normal force and bending is evaluated by:

$$V_{pf} = \frac{M_{pf}}{h'} \tag{3.7}$$

Regarding shear failure, the failure criterion should be differentiated in relation to the masonry type.

In the case of irregular masonry or when, even in the presence of regular texture, the blocks are weaker than the mortar, the response tends to be isotropic and the failure occurs with a diagonal crack upon reaching the limit value of the diagonal tensile strength. The shear strength is given by the formula (Turnšek e Čačovič 1970, Turnšek e Sheppard 1980):

$$V_t = lt \frac{f_t}{b} \sqrt{1 + \frac{\sigma_0}{f_t}} = lt \frac{1.5\tau_0}{b} \sqrt{1 + \frac{\sigma_0}{1.5\tau_0}} \tag{3.8}$$

where: b is a corrective coefficient related to the stress distribution in the section, depending on the slenderness of the panel ($b=h/l$, not exceeding, however, 1.5 and not less than 1, where h is the height of the panel); f_t and τ_0 are, respectively, the diagonal tensile strength and the initial shear strength (f_t =1.5 τ_0). In the case where f_t is derived from diagonal compression tests, the value is assumed to be equal to the diagonal load at failure divided by two times the average section of the tested panel.

In the case of masonry with regular texture, or formed of blocks that are sufficiently regular and with mortar weaker than blocks, the shear failure occurs with stepwise cracks along the joints. This is the case of masonry with solid brickwork and lime mortar, masonry of stone squared blocks, masonry with soft stone blocks with mortar of inferior characteristics; this failure type also occurs in masonry of split stones, provided they have an elongated shape and are well coupled together. The shear strength can be obtained by the formula:

$$V_t = \frac{lt}{b}\left(\tilde{f}_{vm0} + \tilde{\mu}\sigma_0\right) \le V_{t,\lim} \tag{3.9}$$

where: $\tilde{f}_{vm0}$ is the equivalent shear strength of the masonry, related to cohesion of the mortar joint (f_{vm0}) and the texture; $\tilde{\mu}$ is an equivalent friction coefficient, that is function of the friction coefficient on the joint (μ) and of the masonry texture (for masonry with square blocks or solid bricks one would generally assume $\tilde{\mu}$ =0.4; lower values, down to 0.2, are recommended for masonry piers with rough and irregular blocks); $V_{t,lim}$ is related to the failure of blocks (estimated, for example, as a suitable fraction of the compressive strength of the blocks). This criterion is derived from that put forward by Mann and Muller (1980), generalized so as to consider the different geometries of the panels, by means of the coefficient *b*. As an alternative to the conventional limitation $V_{t,lim}$, the failure of the blocks can be explicitly taken into account through the following failure criterion (Mann and Muller 1980):

$$V_{t,\lim} = \frac{lt}{b}\frac{f_{bt}}{2.3}\sqrt{1+\frac{\sigma_0}{f_{bt}}} \tag{3.10}$$

where: f_{bt} is the tensile strength of the block.

The drift of the element can be estimated at the two ends of the panel in terms of chord rotation, through the following expressions (Figure 3-2):

$$\begin{aligned} \theta_i &= \varphi_i - \frac{u_i - u_0}{h'} \\ \theta_j &= \varphi_j - \frac{u_0 - u_j}{h - h'} \end{aligned} \tag{3.11}$$

where: φ_i and φ_j are the rotations at the end section in the nodes *i* and *j*; u_j and u_i are the transversal displacements of the two nodes, respectively; u_0 is the transversal displacement at the contraflexure point; *h* is the height of the element and *h'* the shear length (computed from the *i*-node).

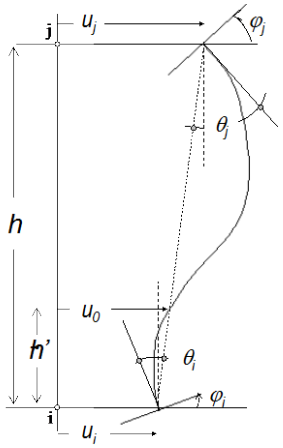

Fig. 3-2. Definition of the terms useful for the calculation of the drift according to (3.10)

As an alternative, formulations may be adopted that consider an average drift of the panel, such as provided by the formula:

$$\theta = \frac{\varphi_i + \varphi_j}{2} + \frac{u_j - u_i}{h} \tag{3.12}$$

In the case of a predominant flexural behaviour and in presence of low normal stress values, the pier behaviour is characterized by a higher ductility, both because the panel is able to withstand higher values of drift as well as because the loss of resistance is minimal and takes place as a result of plasticization localized only in the corners and of the effects of geometric non-linearity.
Instead in the case of a shear failure the behaviour is of the brittle type, with lower values of drift and major drops in the resistance.
In the shear-drift curves (V-θ) it is possible to identify three degrees of damage: severe (3), very severe (4) and collapse (5), indicated by the letters DL3, DL4 and DL5 in Fig. 3-3: these refer to the degrees of damage usually used in modern macroseismic scales (EMS98, Gruntal 1998). Values of drift that correspond to the first two levels of damage are recommended by national and international standards. Damage level 5 corresponds to a condition where the masonry pier also loses the ability to carry the axial load N; once reached this limit, in the equivalent frame models usually the element is transformed into a rod but at this stage the structure must be considered as collapsed.
By way of example, multilinear constitutive models are proposed in the following, represented in a dimensionless form in Fig. 3-3; they are sufficiently accurate for an evaluation of the global response and easy to be implemented in codes based on the equivalent frame approach. Table 3.2 shows indicative ranges for drift values, suggested for the various failure modes. These values, according to the actual state-of-the art, are based, however, on a number of experimental tests that are still insufficient for a complete validation, especially for some masonry types and stress conditions.

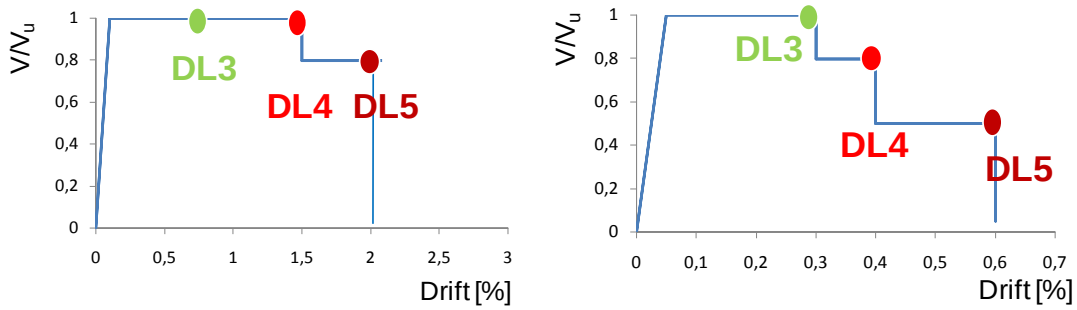

Fig. 3-3. Constitutive shear-drift laws for masonry piers: failure under normal force and bending (left) and shear failure (right).

Table 3.2. Indicative intervals for drift values
and for the residual resistance for the different states of damage.

	Drift (%)			Residual resistance	
damage	3	4	5	3→4	4→5
normal force and bending	0.4 ÷ 0.8	0.8 ÷ 1.2	1.2 ÷ 1.8	1.0	0.8 ÷ 0.9
shear	0.25 ÷ 0.4	0.4 ÷ 0.6	0.6 ÷ 0.9	0.6 ÷ 0.8	0.25 ÷ 0.6

Experimental tests, both in the laboratory as well as in-situ, show that often the two aforementioned failure mechanisms interact, in particular when the difference between the two limit values V_{pf} and V_t is limited (for example, the shear failure in the middle of the panel occurs in the presence of reduced crushed zones at the ends); in those cases also the drift values associated with different levels of damage are intermediate. These mixed failure modes can be considered by defining a constitutive relationship characterized by drift values θ_i, associated with different levels of damage (i=3,5), depending on the ratio V_{pf}/V_t through the following relation:

$$\theta_i = \begin{cases} \theta_{i,pf} & V_{pf}/V_t < 0.95 \\ \theta_{i,pf} - 4\left(\theta_{i,pf} - \theta_{i,t}\right)\left(V_{pf}/V_t - 0.95\right) & 0.95 \le V_{pf}/V_t \le 1.2 \\ \theta_{i,t} & V_{pf}/V_t > 1.2 \end{cases} \qquad (3.13)$$

Residual resistance can be defined in a similar manner in the different parts of the curve.

3.2.1.2 Models for spandrels elements

The behaviour of masonry spandrels was tested in a systematic manner only recently and presents different features from vertical piers for several reasons: 1) the masonry texture is rotated 90° to the axis of the element; 2) at the ends of the spandrel there is an interlocking with the adjacent vertical piers, instead of a continuous joint; 3) normally the spandrel is supported by a lintel (arched, in stone, timber, steel or reinforced concrete), that introduces further resistance; 4) sometimes other elements (tie beams, tie rods) are coupled to the spandrel.

In the absence of specific macroelements, formulated on a mechanical or phenomenological basis, it is possible to use a non-linear beam model, with an appropriate constitutive law in terms of shear force and drift.

The presence of a structurally effective lintel is an essential condition to be able to include the spandrels in the equivalent frame model, as it prevents collapse for vertical loads; its contribution to shear strength and deflection can possibly be explicitly modelled.

The failure criteria that are subsequently proposed, which have no binding nature for the application of assessment methods proposed in this document, refer exclusively to the contribution offered by the masonry part of the spandrel.

For normal force and bending, unlike the case of pier elements, the resistance domain can be calculated by relying on a tensile strength (f_{tf}) that is generated at the section ends as a result of the connection with the portions of the adjacent masonry. The failure mechanisms may involve the crisis by the tensile stresses in the brick ($f_{tf,b}$) or by sliding across the horizontal mortar joints ($f_{tf,g}$). The horizontal tensile strength may be therefore given by the formula (Cattari and Lagomarsino 2008):

$$f_{tf} = \min\left(f_{tf,b}; f_{tf,g}\right) = \min\left(\frac{f_{bt}}{2}; f_{vm0} + \mu\sigma_y\phi\right) \qquad (3.14)$$

where: σ_y is the average normal stress acting on the horizontal mortar joints at the end section (in the absence of more accurate assessments, it may be estimated as a fraction, conservatively assumed equal to 0.5, of the average normal stress σ_0 acting on the adjacent pier elements); f_{vm0} is the cohesion of the mortar joint (that can be conservatively neglected); ϕ is a coefficient accounting for the interlocking (in the case of

walls made of bricks or regular blocks $\phi=a/2b$, where a and b are respectively the width and the height of the block). Having estimated the tensile strength of the spandrel f_{tf}, the resistance M-N domain can be calculated by the conservation of the plane section assumption and an elastic-plastic stress-strain bond with controlled ductility in traction and compression (with regard to compression strength one should use that in the horizontal direction f_{mh}, usually less than that in the vertical direction).
For the shear failure, resistance criteria introduced in §3.2.1.1 may be utilized in relation to the different types of masonry.
The value of the normal force N acting on the spandrel (on which its resistance depends) cannot always be assessed in a reliable manner from the equivalent frame model, for various reasons: a) the presence of rigid diaphragms; b) the way in which the horizontal forces are applied; c) the uncertainty in the modelling of the interaction between the spandrel and other horizontal tensile-resistant elements. Usually the values of N are, however, rather modest. It is therefore appropriate to take into account the contribution to the resistance of the spandrel provided by the acting normal force only if the calculation model provides a reliable estimate, viceversa: 1) in case there are not other coupled tensile-resistant elements, the resistance of the spandrel is evaluated on the assumption that N=0; 2) in case there is a coupled element that is tensile-resistant, the maximum value of the normal stress (N_{max}) that is believed the spandrel can develop will be estimated.
Having reached the limit value of resistance, the spandrels may show a phase of degradation of the resistance (*softening*) even more highly pronounced than that of piers. The type of lintel and the presence of a possible tensile-resistant element coupled to the spandrel determine its greater or lesser ductility (Fig. 3-4). In the case of spandrels supported by a masonry arch, behaviour is very fragile, characterized by a very limited ductility and with residual resistance values that are decidedly modest (Fig. 3-4a); the presence of a tie rod marginally increases the ductility. In the case of lintels made of wood, steel or reinforced concrete, there is a higher ductility prior to the fall in resistance, which turns out to be lower than in the case of the arch (Fig. 3-4b); the presence of another element that is resistant to tension increases the ductility and, if this is a ring beam, it can lead to the hardening of a branch of the response (Fig. 3-4c).
Similarly to the case of piers, it is possible to identify on the drift-shear curve increasing levels of damage severe (3), very severe (4), collapse (5); they can be associated both with the fracture of the masonry portion of the spandrel as well as with the loss of efficiency of the lintel.

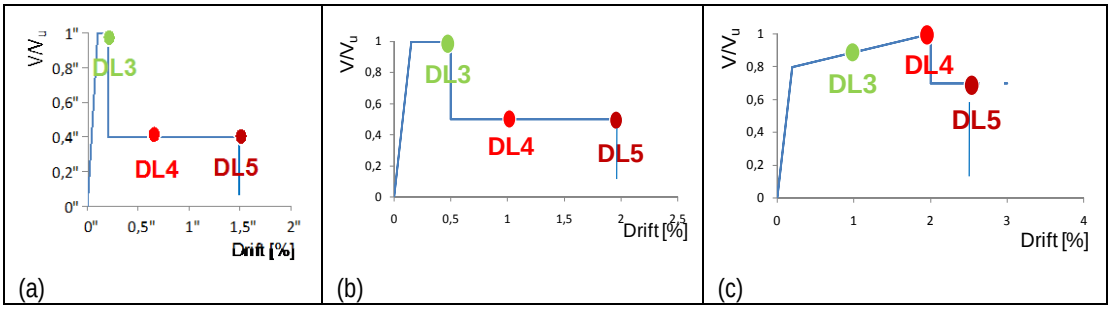

Fig. 3-4. Constitutive drift-shear laws for spandrels supported by: a) a masonry arch; b) a lintel in timber, steel or reinforced concrete; c) a lintel coupled to a tensile-resistant element.

Table 3.3 shows the indicative ranges of the values of drift and of residual resistance. The values of residual strength should be intended as purely indicative: more accurate estimates can be made in specific cases through simplified criteria on mechanical ba-

sis (Beyer 2012). In general, experimental evidence suggests drift values that are significantly higher than those adopted for piers (Beyer and Dazio 2012, Gattesco et al. 2008, Graziotti et al. 2011).

Table 3.3 Indicative ranges of the values of drift and of residual resistance for the various damage levels.

damage	Drift (%)			Residual resistance	
	3	4	5	3→4	4→5
Lintel without tie rod or tie beam	0.40 ÷ 0.60	0.80 ÷ 1.20	1.80 ÷ 2.20	0.40 ÷ 0.60	
Lintel with tie rod or tie beam	0.80 ÷ 1.20	1.60 ÷ 2.00	2.40 ÷ 2.60	1.00	0.60 ÷ 0.80
Arch	0.15 ÷ 0.25	0.45 ÷ 0.75	1.20 ÷ 2.00	0.30 ÷ 0.50	
Arch with Tie rod	0.20 ÷ 0.40	0.50 ÷ 0.80	1.40 ÷ 2.40	1.00	0.40 ÷ 0.60

3.2.1.3 Models for horizontal diaphragms

In the case of high-rise buildings with walls having different stiffness and strength, significant angular deformations may arise in the horizontal diaphragms, such as to produce ductile or brittle failure conditions. In particular this latter case occurs in the presence of horizontal elements of limited thickness. The equivalent frame model can provide a non-linear modelling of horizontal elements with control of their angular deformation in the horizontal plane.
At present the literature is lacking to experimental data on this issue.

3.2.1.4 Tie beams and tie rods

Tie beams and tie rods may be introduced in the equivalent frame model.
The latter have the function of increasing the resistance of the spandrels, thanks to the state of horizontal compression resulting from the initial pre-stress and from a similar increase that occurs as a result of the opening of cracks. This latter effect is not caught by the model in case a non-linear beam element is used for the spandrels which does not consider the coupling between axial and flexural components; in this case the equivalent frame model leads to an underestimation of the actual axial load acting on the spandrel.
Rigorous modelling of tie beams would require the development of coupled spandrel-tie beam characterized by appropriate stiffness and failure criteria; however, literature on this subject is very limited. It is nonetheless possible to add the tie beams to the equivalent frame as non-linear independent beams and simply connected to the same nodes. The deformable portion of the tie beam may be intermediate between the length of the spandrel and the distance between the nodes (some simulations of experimental data have shown that the first solution may provide results that are quite acceptable).

3.2.1.5 Non-linear static analysis

The determination of the seismic response of a masonry building through a non-linear static analysis and the use of response spectra make it possible to assess the attainment of various limit states taking into account the simultaneous presence of the two orthogonal components of motion and of the contribution of different modes of vibration. The procedure that concerns the method C (§2.6.4) makes reference to the global response of the building considering both components of seismic motion.

When referring to ordinary masonry buildings that have sufficiently rigid diaphragms, the number of modes characterized by a significant percentage of participating mass is small. If the number of floors is limited (as frequently happens in masonry buildings) and the building is regular along its height, it is often possible to assume as a reference the response only of the first mode in each direction. Finally, if the construction is regular in plan, the first modes along two orthogonal directions are substantially decoupled (absence of significant torsional effects). In these cases, the verification is reduced to a calculation of the response independently along two orthogonal directions, considering only the excitation that occurs in the direction of the verification. Since equivalent frame models that are usually adopted only consider the response in the plane of the walls, without taking account of interaction with out-of-plane mechanisms, the seismic safety with respect to each limit state is defined by the greatest of the values of the average annual frequency of exceedance λ_{SL} obtained in two directions examined.
In case in a given mode there is the presence of torsional effects, or when the ratio between the coefficients of participation in the orthogonal direction and in that according to which the verification is performed, is, in absolute value, greater than 10%, it is necessary to proceed to the combination of the effects produced by the two components of the seismic motion.
In addition, when the participating mass on the first mode in a given direction does not reach 75% of the total mass, it is necessary to consider the contribution of higher modes by distinguishing between the following cases:

a) If higher modes with significant participating mass, necessary to reach a total of at least 75% of the total mass, have frequencies that are sufficiently close one to each other (for example, a relationship between the minimum and the maximum that is higher than 0.70) and do not present on the individual walls a reversal of the sign of horizontal displacements at the various floors, the distribution of modal forces can be combined with suitable rules (CQC, in the presence of modes with close frequencies, or SRSS), so as to define a distribution of forces with which to perform a single non-linear static analysis. This situation occurs in the presence of flexible diaphragms or in buildings that are extended and articulated in plan, for which the horizontal diaphragms are not stiff enough to ensure a rigid coupling between the different walls.
b) If the higher modes that should be taken into account present on the individual walls an inversion of the sign of horizontal displacements at different levels, it is necessary to perform a non-linear multi-modal static analysis, i.e. to run separate analyses with the distribution of forces corresponding to the differrent vibration modes and then appropriately combine the effects. This is the case of high buildings or buildings that are irregular in height.

In all these cases the definition of the variables Y_{SL} is more complex than subsequently indicated in §3.3.1. In Appendix A.6 there is an outline of the procedures that are to be followed.

3.2.1.6 Damping

Masonry buildings are characterized by a significant cyclic hysteretic dissipation that is added in the non-linear phase to the viscous dissipation that is ever present (usually assumed equivalent to 5%). The simulation of dissipative mechanisms is performed differently depending on the method of assessment that is adopted.
If method A is adopted (§2.6.2), the constitutive laws of the elements (in particular piers and spandrels) must be formulated in a cyclic context in order to be able to eval-

uate the seismic response through an incremental dynamic analysis of the entire building model.
In case that method B (§2.6.3) is adopted, the constitutive hysteretic law of the equivalent oscillator can be derived from cyclic non-linear static analyses (pushover) or on the basis of qualitative considerations related to the dominant mechanisms of damage. The form of cycles in the equivalent system with a single degree of freedom assumes in fact some recurring features:

a) in the case that shear damage mechanisms are prevalent, the capacity curve shows a progressive degradation of the resistance and dissipative cycles that are somewhat wide, consequence to the friction that is generated in the presence of sliding on the joints of mortar;
b) in the presence of flexural damage mechanisms, the capacity curve shows greater ductility and dissipative cycles that are narrower (whose form is referred to as "*a flag*"), close to the behaviour of a non-linear elastic type;
c) in both cases the amount of dissipation increases with the spread of damage in the building, especially when this is localized in the spandrels and the system is such as to involve the large majority of walls.

Finally, if one adopts method C (§2.6.4), in particular by evaluating the displacement demand δ with the spectral method of overdamped responses spectra, it is sufficient to have a law that expresses the damping as a function of the displacement of the equivalent oscillator δ, or of the ductility demand δ/δ_y when the capacity curve is approximated with a multi-linear function (δ_y is the displacement at the end of the equivalent elastic branch). This function can be derived from the results of a pushover cyclic analysis (if available) or through the following relationship:

$$\xi = \xi_v + \xi_i = \begin{cases} \xi_v & \delta \le \delta_y \\ \xi_v + \zeta\left[1 - \left(\frac{\delta_y}{\delta}\right)^{\kappa}\right] & \delta > \delta_y \end{cases} \qquad (3.15)$$

where: ξ_v e ξ_i are respectively the viscous and the hysteretic dampings, ζ is the maximum hysteretic contribution (occurring for very large displacement), that depends on the form of the cycles, and κ is a coefficient that regulates the rate with which the damping grows with the displacement (Table 3.4 proposes possible intervals for the two parameters)

Table 3.4. Reference intervals of ζ and κ for the determination of the hysteretic damping.

	Shear		Flexure with normal force
	(Takeda "wide")	(Takeda "narrow")	("in the shape of a flag")
ζ	0.25 ÷ 0.45	0.15 ÷ 0.35	0.06 ÷ 0.20
κ	0.40 ÷ 0.60	0.50 ÷ 0.80	0.80 ÷ 10

For the application of method C, in the case of use of the overdamped spectra, it is however sufficient to have the definition of the equivalent damping corresponding to each of the three limit states, which can be estimated by cyclic pushover analyses and which need not necessarily follow a trend represented by (3.12).

3.2.2 Local response: models with discrete elements or with macro-blocks

The response mechanisms of the masonry walls under actions outside their plane generally involve a collapse due to loss of equilibrium, that can be described with the kinematics of the masonry blocks that may be considered rigid. The interlocking between the walls and the connections by means of tie rods, tie beams and diaphragms tend to limit the occurrence of these mechanisms to parts of the building. For these reasons they are also called local mechanisms and the mechanical models refer only to the parts of the construction that are affected by the loss of equilibrium.
The identification and analysis of local mechanisms can be performed with models with discrete elements (de Felice and Giannini 2001) or through limit analysis procedures based on linear programming and discretization in rigid blocks (Baggio and Trovalusci 1998, Orduña and Lourenço 2005, Portioli et al. 2013) or in homogeneous equivalent elements (Milani et al. 2013). A simplified approach, adopted in NTC 2008 and described by way of example below, is that of performing a limit analysis on a predefined kinematic mechanism composed by rigid masonry blocks (macro-block model) (Doherty et al. 2012, Lagomarsino 2014, D'Ayala and Speranza 2003, Casapulla and Maione 2011, Vaculik et al. 2012).

3.2.2.1 Limit analysis (non-linear kinematic)

A local mechanism is defined by a set of masonry blocks (assumed to be rigid), connected to each other by means of internal linkages (hinges, connecting rods, etc.) and by connecting elements (rigid, elastic, by friction), that may for example simulate the presence of steel tie rods, beams or interlocking between walls. There are also external linkages, that simulate the connection of the portion of the structure interested by the mechanism with the rest of the construction. All these linkages are such as to constitute a kinematic chain with a single degree of freedom, whose act of motion is described by a virtual infinitesimal displacement or rotation (Lagomarsino, 2013).
The study of the seismic response of the mechanism requires the identification: of the entity and of the point of application of its own weights and of those that are carried by each block or element; of the applied external forces and of the internal ones in the elastic elements or due to friction. A system of horizontal forces is then applied, that is proportional, through a coefficient α, to the weights and is representative of the seismic action. It has to be noted that account should also be taken of all possible weights that do not weigth directly on the blocks but whose inertial seismic action would act on the blocks of the mechanism (for example a diaphragm that affects the kinematic mechanism with only a section of its own weight but, if they are not restrained, would exert a horizontal seismic action that is proportional to the whole mass).
By applying the theorem of virtual work to infinitesimal motion it is possible to calculate the multiplier α_0 that activates the kinematic mechanism.

$$\alpha_0 = \frac{\sum_{k=1}^{N} P_k \delta_{Py,k} - \sum_{k=1}^{m} F_k \delta_{F,k} + L_i}{\sum_{k=1}^{N} (P_k + Q_k) \delta_{PQx,k}} \tag{3.16}$$

where:

N is the number of blocks that constitute the kinematic chain;

m is the number of external forces, assumed as independent of the seismic action, applied to the various blocks;

P_k is the resultant of the weight forces applied at the *k*-th block (the own weight of the block, applied at its centre of gravity, added to the other weights supported by the block);

Q_k is the resultant of the weight forces not imposed on the *k*-th block but whose mass generates on it a seismic horizontal force, which is not transmitted effectively to other parts of the building;

F_k is the generic external force applied to one of the blocks;

$\delta_{Py,k}$ is the virtual vertical displacement of the centre of gravity of the forces due to its own weight and to other supported weights P_k, acting on the *k*-th block, assumed positive if upwards;

$\delta_{F,k}$ is the virtual displacement of the point of application of the external force F_k, projected in the same direction;

$\delta_{PQx,k}$ is the virtual horizontal displacement of the centre of gravity of horizontal forces $\alpha(P_k+Q_k)$ acting on the *k*-th block, taking as positive the direction of the seismic action that activates the mechanism;

L_i is the total work of any internal forces (lengthening of a tie rod, sliding with friction).

The equation (3.16) corresponds to the application of the kinematic theorem of the limit analysis. The resultant multiplier α_0 represents a conservative estimate of the true collapse multiplier: the two multipliers coincide if the chosen mechanism is the correct one.

In the hypothesis that the section of the construction that is represented by the system of blocks behaves effectively as infinitely rigid until the activation of the kinematic mechanism, the multiplier α_0 represents the peak acceleration (in units of *g*) of the structure at the point where the mechanism is linked to the rest of the building (in the case that the mechanism involves an entire wall down to the ground, α_0 corresponds to the peak ground acceleration).

In order to know the displacement capacity of the local mechanism up to the collapse, the horizontal multiplier α can be evaluated not only on the initial configuration but also on varied configurations of the kinematic chain, representative of the evolution of the kinematic mechanism and described by the horizontal movement d_C of the control point of the system, wherever chosen. In the absence of internal resistant forces, that can grow with the increase of the displacement (such as for example the tension of a steel tie rod), the multiplier is progressively reduced up to a configuration for which it becomes zero for a displacement d_{C0} (loss of equilibrium in static conditions).

The curve α–d_C, obtained through a non-linear kinematic analysis, represents the pushover curve of the local mechanism. For its computation it is necessary to consider how the internal and external forces change and whether they persist or not with the evolution of the kinematic mechanism. For example, in a steel tie rod the tension increases until it reaches the yield strength, so this will remain therefore approximately constant until failure (yielding corresponding to a point beyond which it will no longer offer any contribution); the restraint between two walls will contribute with friction forces up to the formation of a gap between the masonry blocks; the diaphragm will transfer forces until the beams will be pulled out of the walls (in case it is considered that such a movement will lead to the collapse, the pushover curve will be set to zero after this condition).

3.2.2.2 Definition of non-linear equivalent oscillator

In order to evaluate the seismic demand of displacement it is necessary to determine, as shown in §2.4.1, the "capacity curve" of the local mechanism, in perfect analogy with what was done for the global response of the building.
The parameters of the pushover curve, defined in the previous paragraph, are transformed in such a way as to obtain the relation acceleration-displacement (*a*-*d*) of an equivalent non-linear system with one degree of freedom:

$$a = \frac{\alpha g}{e^*} \tag{3.17}$$

$$d = d_C \frac{\sum_{k=1}^{N} (P_k + Q_k) \delta_{PQx,k}^2}{\delta_{Cx} \sum_{k=1}^{N} (P_k + Q_k) \delta_{PQx,k}} \tag{3.18}$$

where:
g is the acceleration of gravity;
δ_{Cx} is the virtual horizontal displacement of the point of control;
e^* is the fraction of the participating mass, evaluated based on the virtual displacements relative to the kinematic mechanism starting from the initial configuration as representative of the mode of vibration of the local mechanism:

$$e^* = \frac{\left[\sum_{k=1}^{N} (P_k + Q_k) \delta_{PQx,k}\right]^2}{\left[\sum_{k=1}^{N} (P_k + Q_k)\right]\left[\sum_{k=1}^{N} (P_k + Q_k) \delta_{PQx,k}^2\right]} \tag{3.19}$$

The resulting capacity curve considers the infinitely rigid behaviour of the mechanism until its activation; this is unrealistic because a wall subjected to action outside its plane shows an elastic response, even if often characterized by a low vibration period, before conditions occur that will activate the kinematic mechanism. It is therefore necessary to introduce an initial elastic branch in the capacity curve, by estimating a value of the period T_0 on the basis of simplified models:

$$a = \frac{4\pi^2}{T_0^2} d \tag{3.20}$$

This linear branch defines the capacity curve up to the intersection with the curve defined above, derived starting from the transformation of the pushover curve obtained from a non-linear kinematic analysis.

3.2.2.3 Models for dynamic analysis

In case the evaluation of the seismic safety is carried out through non-linear dynamic analyses (Method A - §2.6.2; Method B - §2.6.3) it is necessary to properly define the cyclic behaviour.
In order to define the behaviour of a non-linear oscillator with one degree of freedom it is necessary to determine the capacity curve by the application of seismic action in both directions. Besides the case of vertical cantilever elements, free to move out of the plane on both sides, or of systems of arches over piers, the local mechanisms are often characterized by an asymmetric behaviour; a façade (or its upper portion) may

in fact tilt towards the outside, but would hardly do so by tilting towards the internal part of the building, because of the presence of load-bearing walls and of horizontal elements that exert one-sided restraint. The collapse mechanism is therefore different in the two directions.
With regard to cyclic behaviour, the mere overturning of rigid blocks gives rise to a non-linear elastic behaviour, in other words by downloading the system returns to the initial configuration without residual displacements and moving along the same curve; in the presence of elastoplastic connection elements (steel tie rods) or restraints with friction the kinematic mechanism presents instead a hysteretic response, that will eventually deteriorate (following the rupture of some element).
The dynamic response of a rigid oscillating block can be studied through the well-known model of Housner (1963) and the conditions for collapse due to overturning, for each time history of acceleration, can be evaluated by means of rocking spectra (Makris and Konstantinidis 2003). The dynamic response of the block, for its rigid-deteriorating features, is dynamically very unstable; dissipation in fact is due solely to the shocks corresponding to the return to the initial configuration, and the response is very sensitive to the single impulse contained in the accelerogram. More in line with the experimental response (De Canio et al. 2012) are the results provided by a non-linear elastic oscillator, characterized by a softening response evaluated by means of a kinematic non-linear analysis and provided with an equivalent viscous damping whose value can be put in relation with the restitution coefficient of the model of Housner (the values typically range from 4% to 8%).
Even though the formulation can be quite complex, rather than resorting to the equivalent oscillator, it is possible to write the equations of the dynamic equilibrium of the kinematic mechanism consisting of several blocks (Clemente 1998); this allows performing the safety assessment through method A (§2.6.2). In this case it is obviously not necessary to define the capacity curve of the system.

3.2.2.4 Spectral displacement demand

In case the evaluation of seismic safety is done by means of the use of the capacity spectrum (Method C - §2.6.4) it is necessary to determine the displacement demand on the capacity curve with the method of the overdamped spectrum (§2.6.4.2). The intersection of the capacity curve with the response spectrum in the ADRS format gives rise to the displacement d_1; the determination of this displacement may require an iterative process since the spectrum must be that which corresponds to the value of the displacement of the mechanism of rigid blocks ξ_m. T_1 is defined as the equivalent period that corresponds to the displacement d_1:

$$T_1 = 2\pi\sqrt{\frac{d_1}{a(T_1)}} \tag{3.21}$$

Since the verification process does not use design response spectra which exhibit rising spectral displacements with the increase of the period, but the spectra of selected real time histories, it is not possible to observe larger displacements for lower equivalent periods. The maximum displacement of the equivalent system with a single degree of freedom is therefore given by (Lagomarsino, 2013):

$$\delta = \max\left[S_{dm}\left(T, \xi_m(T)\right)\right] \qquad T_0 \le T \le T_1 \tag{3.22}$$

where: S_{dm} is the displacement response spectrum of the seismic input to be considered for the verification of the local mechanism.
The method requires therefore the definition of a function providing the equivalent viscous damping or increasing values of the displacement (or of the secant period) and the process is iterative. In general it is possible to assume a constant equivalent viscous damping, that is not dependent on δ; in this case the determination of the maximum demand for displacement is immediate, even in graphic form.

3.2.2.5 Evaluation of the seismic demand at different levels of the building

Seismic safety in respect of local mechanisms requires knowledge of the input at the height where the mechanism takes place. The motion at the base of the building is filtered by the response of the construction, as function of its dynamic characteristics (natural frequencies) and of the heights to which the blocks of the mechanisms are connected to the structure (modal shape).
In case where methods are adopted that are based on the use of an incremental dynamic analysis (Method A - §2.6.2; Method B - §2.6.3) a global model of the construction is available by means of which to evaluate, through a step by step dynamic analysis, the motion at the height of the mechanism (for this purpose one can generally assume an elastic model for the building, possibly defined by reduced mechanical properties to take account of cracking). The time histories selected for the IDA are therefore transformed into appropriate floor time histories to be used according to the procedures and the models described in §3.2.2.3.
In the case where the evaluation of seismic safety is performed by using the capacity spectrum (Method C - §2.6.4) it is necessary to determine the floor acceleration-displacement spectrum. This can be achieved through a simplified formulation from the ordinates of the response spectrum of the time history at the base of the structure corresponding to the natural periods of the building (Lagomarsino, 2014). Since the formulation is simplified, the displacement response spectrum $S_{dm}(T)$ to be used to verify the mechanism is given, for each value of the period T, by the larger between the response spectrum of ground displacement S_d and the estimate obtained by adding the response contributions provided by the r modes of vibration considered to be significant for the response of the local mechanism:

$$S_{dm}(T) = \max\left[\quad S_d(T) \quad ; \quad \sum_{k=1}^{r} S_{dm,k}(T) \quad \right] \tag{3.23}$$

In the choice of modes to be considered, it is necessary to take into account the possible amplifications of the motion at the upper floors of the building, as well as the interaction between the filtered motion and the dynamic characteristics of the mechanism (resistance and displacement capacity).
The contribution to the displacement response spectrum provided by the k-th mode is given by the following formula:

$$S_{dm,k}(T)=\begin{cases} S_d(T_k)\left|\psi_k(z)\right|\gamma_k \dfrac{\left(\dfrac{T}{T_k}\right)^2}{\sqrt{\left(1-\dfrac{T}{T_k}\right)^2+\dfrac{0.05}{\left[\eta(\xi)\eta(\xi_m)\right]^2}\dfrac{T}{T_k}}} & T\le T_k \\ S_d(T_k)\left|\psi_k(z)\right|\gamma_k\eta(\xi)\eta(\xi_m)\dfrac{\left(\dfrac{T}{T_k}\right)^2}{\sqrt{\left(1-\dfrac{T}{T_k}\right)^2+0.05\dfrac{T}{T_k}}} & T_k<T\le 1.9T_k \\ 3.8S_d(T_k)\left|\psi_k(z)\right|\gamma_k\eta(\xi)\eta(\xi_m) & T\ge 1.9T_k \end{cases} \quad (3.24)$$

where:

T is the period for which the spectral ordinate is calculated;

$S_d(T_k)$ is the value of the ordinate of the displacement spectrum of the accelerogram at the ground, with damping at 5%, calculated for the period T_k of the building;

γ_k is the k-th coefficient of modal participation of the building;

$\psi_\kappa(z)$ is the k-th modal form, normalized to 1 at the top of the building;

z is the elevation of the substructure affected by the mechanism under consideration;

ξ is the damping of the building;

ξ_m is the damping of the substructure under consideration;

η is the factor that alters the elastic spectrum for damping coefficients that are different from 5%, using the formula:

$$\eta(\xi)=\sqrt{\frac{10}{5+\xi}} \quad (3.25)$$

The proposed formulation provides excellent results in the case where the response spectrum of the ground accelerogram is quite smooth (similar to the standard ones). In the case of recorded time histories the spectrum is often very irregular around the period T_k; considering the inherent uncertainties in the estimation of the period of the structure it is appropriate to use in (3.22) instead of the value $S_d(T_k)$ a mean value, evaluated in an appropriate neighbourhood of the period T_k.

In the case of verification of local mechanisms in multi-storey residential buildings, it is generally sufficient to consider only the first mode of vibration of the construction. The coefficient of modal partecipation can be approximated by the expression:

$$\gamma_1=\frac{3n}{2n+1} \quad (3.26)$$

where n is the number of floors. For the first spectral form, a power law may be assumed:

$$\psi(z)=\left(\frac{z}{H}\right)^{\kappa} \quad (3.27)$$

where: H is the height of the building, κ is an appropriate coefficient (κ=1 in the case of modal linear form).

3.2.2.6 Critical modelling issues

The reliability of the evaluation in respect of local mechanisms is primarily linked to the correct choice of the kinematic mechanism of collapse; the identification assumes an adequate knowledge of the construction details, an estimate of the efficiency of the linkage elements and the correct interpretation of the cracking pattern (especially if it is of seismic origin).

The modelling of the out of plane response through rigid blocks presupposes that the quality of the masonry is very good. A wall of poor mechanical characteristics will tend to disintegrate before it is articulated in rigid blocks; even in the presence of good masonry properties, if the walls are not effectively linked one to each other transversely, the out-of-plane stability is reduced. This reduction can be accounted for by moving back the point around which the rotation of the block occurs (this corresponds to consider the base section of the wall as plasticized under compression, instead of assuming a rotation at the edge). Neglecting these aspects leads to assessments that are not on the safe side.

Another important aspect is the estimate of the contribution provided by the interlocking between walls. Neglecting this aspect would lead, in many instances, to estimates that are excessively on the safe side. If the interlocking in a corner or in the connection between the façade and an internal wall can be considered as fully effective, a section of the transversal wall would be involved in the out of plane mechanism; the inclination of the splitting that defines this portion depends on the texture of the masonry walls. When the restraint in the corner is not particularly effective though is not negligible, one could introduce an horizontal frictional force on the surfaces of the connecting blocks, evaluating the vertical compression stress (increasing downwards); this contribution remains until the blocks separate.

In flexural mechanisms rotations occur around a vertical axis that involve a frictional resistance that is quantifiable through a torsional moment, whose work can be taken into account in the numerator of (3.14).

In the case of diaphragm resting on a wall (or a section of a wall) that is subject to overturning, if these are not connected at the two ends in such a way as to represent a bond, it is necessary to consider the stabilizing action provided by the only portion of the load that rests on the wall and the seismic one attributable to the whole mass of the diaphragm (in some cases it is possible to rely on a stabilizing contribution that is due to friction on the support at the other end).

3.3 Quantification of limit states

The evaluation of the performance of a masonry building is performed separately with respect to the global and the local behaviour, both because the methods of analysis do not interact as well as because it would be difficult, in a coupled evaluation, to assign a weight to the attainment of limit states that might interest local portions of a very limited extension but, at the same time, are absolutely relevant in some cases.

In this way the result of the verification allows a more aware estimate of the risk, which helps in planning mitigation strategies and addressing possible interventions of seismic strengthening.

3.3.1 Global response

The general guidelines regarding the quantification of the limit state (§2.5) refer to the state of damage of the components of a building. For masonry buildings these elements (piers and spandrels) are defined a-priori, in the case of modelling with equivalent frames, or can be identified a posteriori, when non-linear continuous modelling (finite elements) or macroelements are adopted. The following indications, based on deformation levels that are reached in the elements of the building, can therefore be applied regardless of the modelling approach that is adopted.

Masonry structures are characterized by a configuration that is irregular and complex in many cases; for this reason it is not meaningful to rely on a simple control of the ratio between demand and capacity at the level of the structural elements since: a) for the damage state limit (SLD), the achievement of an important level of deformation in one element might occur when the other elements are very far from this condition; b) for the limit state for the prevention of collapse (SLC) it is difficult to refer to predefined failure mechanisms, in the case of walls that are characterized by an equivalent frame with a complex configuration.

Limit states are therefore defined on the capacity curve through a multi-scale approach that considers: a) the exceedance of a predetermined level of drift in a number of individual elements (piers and spandrels); b) the interstorey drift in single walls or the attainment of predetermined levels of deformation in horizontal elements (if considered flexible); c) the response at global level on the capacity curve (fractions of the maximum resistance of the equivalent oscillator).

In the sections below there is an explanation of the criteria corresponding to these three scales for the three limit states considered in the evaluation of an existing masonry building. In particular, in the case in which method C is used, indications are given for the evaluation of the displacement capacity δ_{SL} relative to each limit state, for using (2.6) and (2.11).

Method A is able to represent the response of buildings, however complex. With regard instead to methods that refer to the conversion into an equivalent oscillator, the verification procedures significantly depend on regularity. For ease of discussion, the specific indications for each limit state contained in the next three paragraphs refer to the case of a regular building, with diaphragms that have adequate stiffness and with a limited number of floors, for which it is assumed that it is possible to carry out a seismic assessment separately in the two directions considering, for each of these, only the first mode and one component of the seismic motion. Appendix A.6 describes the procedures to be adopted in order to consider, for every mode, both components of the seismic input, when the ratio between the participation coefficients in the direction of verification and the orthogonal one is less than 10 (§A.7.1), and to perform a static non-linear multi-modal analysis, when the percentage of the participating mass in the first mode is less than 75% (§A.7.2).

3.3.1.1 Damage limit state (SLD)

The multi-scale approach for the definition of the limit state variable Y_{SLD} in the case of masonry buildings is applied in a different way according to the verification method that is adopted.

In the case where a non-linear dynamic analysis is run on the complete model of the building (Method A), the (2.5) is modified in the following manner:

$$Y_{SLD} = \max\left(Y_{SLD,S}; Y_{SLD,M}; Y_{SLD,G}\right) \tag{3.28}$$

where: $Y_{SLD,S}$ is the limit state variable defined at the level of the structural element, on the basis of the accumulated damage in both piers and spandrels as defined below; $Y_{SLD,M}$ is the maximum value of the relationship *D/C* in terms of drift in one of the macroelements (walls or diaphragms) that compose the building (this control may be considered significant even for damage to non-structural elements); $Y_{SLD,G}$ is the ratio between the maximum displacement of a control degree of freedom over the time history of the dynamic response and the displacement corresponding to the attainment of the maximum resistance on the pushover curve, defined by using the same degree of freedom (assuming the maximum of this ratio, for both signs in the direction considered).

Damage accumulated in the spandrels $\Sigma_{SLD,F}$ is an indicator defined as the percentage of spandrels in the building that reaches the damage level 4:

$$\Sigma_{SLD,F} = \frac{1}{N_F}\sum_{F} H\left(\frac{D_j}{C_j} - 1\right) \tag{3.29}$$

where the summation is extended to all the N_F spandrels of the building and H is the Heaviside step function, that has a value of 0 until the demand D_j in the j-th spandrel, in terms of drift, does not reach the capacity $C_j = \theta_4$.

The cumulative damage in piers $\Sigma_{SLD,M}$ is an indicator defined as a percentage, weighted on relative resisting areas A_j, of the piers of the building that reach the damage level 3:

$$\Sigma_{SLD,M} = \frac{\sum_{M} A_j H\left(\frac{D_j}{C_j} - 1\right)}{\sum_{M} A_j} \tag{3.30}$$

where the summation is extended to all the N_M piers of the building.

Then, the limit state variable at the level of the structural element is defined as follows:

$$Y_{SLD,S} = \frac{1}{\tau_{SLD}} \max\left(\sum_{SLD,F}, \sum_{SLD,M}\right) \tag{3.31}$$

where τ_{SLD} is a threshold, defined by the owner, and representing the maximum accumulated permissible damage for the damage limit state (SLD) (for example, 3%); this makes it possible to avoid that the damage limit state (SLD) is reached when a single element (pier or spandrel) reaches a fixed threshold.

The control at the level of a wall macroelement is performed by considering the inter-storey drift $\Box\theta_{p,l}$, (p = 1,…,N_p – number of walls; l = 1,..,N_l – number of levels) and identifying the maximum value:

$$\theta_P = \max\left|\theta_{p,l}\right| \tag{3.32}$$

Consistent with the definition of the drift in an element (Equation 3.11 in §3.2.1.1), in the presence of deformable spandrels, the inter-storey drift must be calculated by subtracting the contribution due to the average rotation of nodes.

The limit state variable associated to macroelements $Y_{SLD,M}$ is defined by assuming a threshold limit for the inter-storey drift in the walls $\Box\theta_{SLD,M}$ (§3.4.4) and eventually

taking into account, in an analogous manner, of deformations in the plane of the diaphragms (§3.4.5) if considered flexible:

$$Y_{SLD,M} = \max\left(\frac{\theta_P}{\theta_{SLD,M}}; \max_{\text{floors}} \frac{D_i}{C_i}\right) \tag{3.33}$$

In cases where the verification is done by adopting a system equivalent to a single degree of freedom (Methods B and C) it is possible to define directly on the capacity curve the displacement δ_{SLD} to be used to define Y_{SLD} through (2.6):

$$\delta_{SLD} = \min\left(\delta_{SLD,S}; \delta_{SLD,M}; \delta_{SLD,G}\right) \tag{3.34}$$

where: $\delta_{SLD,S}$, $\delta_{SLD,M}$ and $\delta_{SLD,G}$ are the displacements on the capacity curve for which the corresponding limit state variables $Y_{SLD,S}$, $Y_{SLD,M}$ and $Y_{SLD,G}$ reach the unit value.
Drift values in elements, corresponding to the capacity of the damage limit state (SLD) are shown in §3.4.1, whereas the drift limits of macroelements are shown in §3.4.4 and §3.4.5.

3.3.1.2 Severe damage limit state (SLS)

In the case of masonry buildings, reference is made to a formulation that is analogous to that proposed for reinforced concrete buildings, that refers to a variable that measures the diffusion of damage in the construction. This is placed in a direct relationship with the possibility of damage repair.
For a masonry building it is not significant to introduce the damage, and the relative repair cost, of non-structural elements since, unlike reinforced concrete structures, the latter have a marginal effect on cost (the walls being substantially almost all of structural type). It appears instead appropriate to attribute a different weight to damage in masonry piers and in spandrels, being the latter decidedly less structurally significant and easier to be repaired (indeed, spandrels do not support significant vertical loads). Moreover, in the case of piers, it is necessary to attribute a weight that is commensurate with the corresponding resistant area. The equation (2.7) specializes therefore for the case of masonry buildings as follows:

$$Y_{SLS} = \frac{1}{\tau_{SLS}} \begin{cases} \alpha_M \sum_{i=1}^{n_M} w_i c\left(\frac{D_i}{C_{i,SLS}}\right) + (1-\alpha_M) \sum_{j=1}^{n_F} w_j c\left(\frac{D_j}{C_{j,SLS}}\right) \\ 1 \text{ se } Y_{SLC} \geq 1 \end{cases} \tag{3.35}$$

where:

- the coefficient α_M expresses the weight of piers on the overall economic value of structural elements of the building;
- the summations are extended to cover the n_M pier and n_F spandrels.
- the function *conventional repair cost* $c(D_i/C_i)$ is defined in a similar manner to the case of reinforced concrete buildings; the values of C_j for piers and for spandrels are given in §3.4.2.
- the weights w_i associated with the repair cost to piers are equal to $A_i/\Sigma_k A_k$ where A_i is the area resistant to the i-th pier wall;
- the weights w_j associated with the repair costs of spandrels are all equal and equivalent to $1/N_F$.

- Y_{SLC} is the variable that controls the achievement of the limit state for the prevention of collapse, as defined in §2.5.3 and later in §3.3.1.3. This check, which assumes that the limit state for severe damage (SLS) can never follow the limit state for the prevention of collapse (SLC), is necessary since in the case of particular collapse mechanisms (for instance, of a weak storey) the damage does not spread in a significant manner over the building and the cost function (3.32) does not rise above a certain value.

In the following paragraphs, the weighted sum that appears in the equation (3.35) is also indicated as C_G, the conventional global repair cost.
In the case of methods B and C, the displacement δ_{SLS} is defined on the basis of the achievement of the condition Y_{SLS}=1.

3.3.1.3 Limit state for the prevention of collapse (SLC)

Analogously to what introduced for the damage limit state (SLD), the multi-scale approach for the definition of the limit state variable Y_{SLC} is applied in a different manner according to the verification method that is adopted.
In the case where a dynamic non-linear analysis is run on the complete model of the building (method A) Y_{SLC} is computed as:

$$Y_{SLC} = \max\left(Y_{SLC,S}; Y_{SLC,M}; Y_{SLC,G}\right) \tag{3.36}$$

where:

$$Y_{SLC,S} = \frac{1}{\tau_{SLC}} \sum_{SLC,M} \tag{3.37}$$

having defined $\Sigma_{SLC,M}$ through an analogous formula in (3.29) where the capacity for piers is assumed to correspond to the attainment of the damage level 5; τ_{SLC} is a threshold that is defined by the owner and represents the maximum permissible damage for the severe damage limit state (for example 3%)[14].
The limit state variable associated with macroelements $Y_{SLC,M}$ is defined similarly to the case of damage limit state (SLD), assuming a different threshold limit for the inter-storey drift in the walls (§3.4.4) and for deformations in the plane of horizontal elements (§3.4.5):

$$Y_{SLC,M} = \max\left(\frac{\theta_P}{\theta_{SLC,M}}; \max_{\text{floors}} \frac{D_i}{C_i}\right) \tag{3.38}$$

The limit state variable associated with the global response of the building $Y_{SLC,G}$ is the ratio between the maximum displacement of a control degree of freedom on the time history of the dynamic response and the displacement corresponding to a degra-

[14] The equation (3.35) has a structure that is similar to that of the general equation (2.10), with the limit state variable $Y_{SLC,G}$ that corresponds conceptually to the control on the slope of the global curve IDA (the degradation of 40% on the capacity curve corresponds to a condition precedent to the plateau of the IDA curve, which in the equation (2.10) identifies the limit state for the prevention of collapse (SLC) with the reduction of the tangent to the IDA curve to a fraction Δ of the initial tangent), and with the variable relative to single elements, $Y_{SLC,S}$, and to the macro-elements (walls, ceilings), $Y_{SLC,M}$, that correspond to the check of local failure modes that are not reflected in a clear manner on the global response (for example, because of limitations in modelling). The equation (3.36) represents a way to maintain control on any possible local collapses in a more accurate manner than the simple serial undifferentiated approach in relation to the importance of the elements.

dation computed as a percentage of the total base shear of the building equal to 40% (resistance degraded to 60% of the maximum shear capacity).
In the case where the verification is done by adopting an system equivalent to a single degree of freedom (Methods B and C) it is necessary to define directly on the capacity curve the displacement δ_{SLC}:

$$\delta_{SLC} = \min\left(\delta_{SLC,S}; \delta_{SLC,M}; \delta_{SLC,G}\right) \tag{3.39}$$

where: $\delta_{SLC,S}$, $\delta_{SLC,M}$ and $\delta_{SLC,G}$ are the displacements on the capacity curve where the corresponding limit state variables $Y_{SLC,S}$, $Y_{SLC,M}$ and $Y_{SLC,G}$ reach the value equal to 1. The values of drift in elements corresponding to the capacity for the limit state of prevention of collapse (SLC) are given in §3.4.3, whereas the limit drift for macroelements are illustrated in §3.4.4 and §3.4.5.

3.3.2 Local mechanisms

The verification with respect to the different limit states is carried out considering various mechanisms that are assumed as possible, accounting for the geometric and structural characteristics of the building. Each mechanism is modelled separately and leads to an outcome. In the case in which different possible local mechanisms are analyzed for the same macro-element, the outcome of the evaluation will refer to that which will result more vulnerable (in general not identifiable a priori). In the presence of alternative mechanisms, associated with assumptions on the structural or mechanical characteristics where knowledge is incomplete, reference will be made to the use of logic tree technique.
The modelling of the out of plane response of the part of the building that is involved in the local mechanism, constituted by a kinematic mechanism of rigid block, leads to the definition of a capacity curve that is representative of the response of an equivalent single degree of freedom system, obtained through the application of the kinematic theorem of the limit analysis. The capacity curve of the mechanism, according to what appears in §3.2.2.2, consists of two branches: 1) a first elastic branch, directly associated to the equivalent elastic period of the local mechanism under examination; 2) a curve, often linear, obtained by means of a non-linear kinematic analysis. Fig. 3-5 shows two typical capacity curves for a local mechanism involving or not also the presence of a tie-rod.

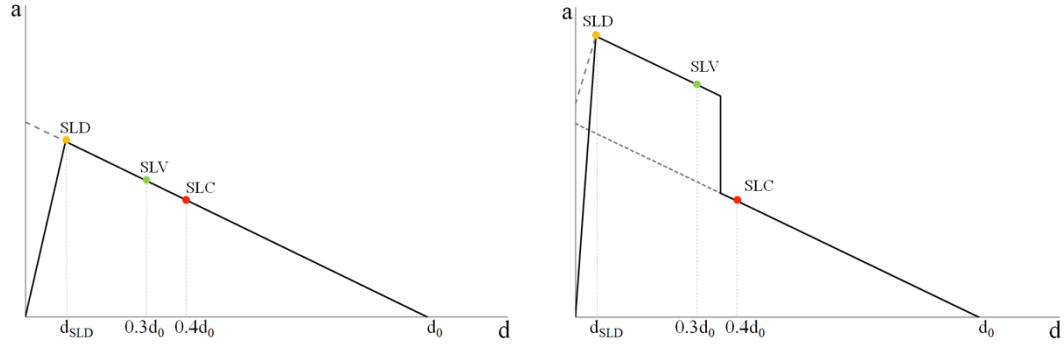

Fig. 3-5. Displacements corresponding to the attainment of various limit states on the capacity curve of local mechanisms: mechanism without resistant elastic-plastic elements (left); mechanism with resistant elastic-plastic elements – tie rods (right).

Displacement values corresponding to the attainment of the various limit states are defined directly on this curve (Lagomarsino, 2013), since any check on the elements that constitute the kinematic mechanism are already considered in the evaluation of the curve (breaking of tie rods, extraction of beams, sliding between blocks, rupture by crushing, etc.).
Having assessed the displacement demand δ, by means of the methods described in §3.2.2, the variable that defines the condition associated to the attainment of the generic limit state is defined by the formula:

$$Y_{SL} = \frac{\delta}{\delta_{SL}} \tag{3.40}$$

The displacement capacities δ_{SL} relative to the various limit states are specified below.

3.3.2.1 Damage limit state (SLD)

The damage limit state (SLD) related to the out of plane response corresponds to the activation of the mechanism, that is to the rotation or the relative sliding of the blocks in correspondence with the kinematic links between them, beyond the limited elastic deformation (if considered). In the building this corresponds generally to the formation of cracks of a small width, without the occurrence of appreciable residual deformations; in the case of free-standing elements (vertical cantilever), the activation of rocking may not produce significant consequences at the end of the seismic shock.
For this reason, for a masonry building, the achievement of the damage limit state (SLD) in local mechanisms can be in most cases considered of a physiological nature, in the sense that forcing to prevent it would require the adoption of strengthening interventions so invasive to be not justified.
When the initial elastic deformation is considered, the intersection point between the elastic branch and the curve obtained by the kinematic analysis defines the displacement to the damage limit state δ_{SLD} (Figure 3. 5, left). In the presence of connecting elements, such as tie rods, the estimated initial elastic period is ambiguous; the displacement δ_{SLD} can be evaluated in correspondence with the attainment of the maximum resistance to the overturning (Figure 3.4, right).

3.3.2.2 Severe damage limit state (SLS)

The out of plane response generally involves limited cracks and residual damage at the end of the seismic shock, that are not particularly significant. It is only when one is very close to the collapse condition, as defined subsequently in §3.3.2.3, that the phenomena of disintegration become appreciable and such as to be representative of severe damage.
For this reason, the limit condition of severe damage limit state (SLS) occurs shoatly before that of the limit state for the prevention of collapse (SLC):

$$\delta_{SLS} = 0.3 d_0 \geq \delta_{SLD} \tag{3.41}$$

where $\square_0$ is the displacement where the capacity curve becomes null.
The lower limit is representative of kinematic mechanisms that are characterized by a limited displacement capacity; in these cases the system is stable in the elastic branch and the attainment of the damage limit state (SLD) coincides with the severe damage limit state (SLS).

3.3.2.3 Limit state for the prevention of collapse (SLC)

The dynamic response of kinematic mechanisms of rigid blocks is characterized by a strong instability, in the sense that, for a given time history, a small increment of acceleration values can lead to a large increase in demand with displacements close or up to the collapse; on the other hand the kinematic mechanism could possibly withstand the application of the same accelerogram, further increased in intensity.
For these reasons, in order to define the displacement values that are compatible with the limit state for the prevention of collapse (SLC), it is necessary to refer to conditions that are sufficiently far from these phenomena. Following the execution of several non-linear dynamic analyses (Lagomarsino 2014), and considering various kinematic mechanisms and accelerograms, it was possible to confirm that the dynamic instabilities do not occur, except in a limited number of cases, until the displacement demand does not reach the value:

$$\delta_{SLC} = 0.4 d_0 \geq \delta_{SLS} \tag{3.42}$$

Figure 3.3 shows, by way of example, displacements that correspond to various limit states for different recurrent situations.
In cases where the evaluation is carried out with incremental dynamic analyses (Method A - §2.6.2; Method B - §2.6.3) the limit state for the prevention of collapse (SLC) can be directly estimated on basis of the value of the seismic action for which there is no convergence (collapse). In order to be on the safe side it may be considered that the limit state for the prevention of collapse (SLC) is reached when the slope of the curve IDA is reduced to a negligible fraction (for example 10%) of the initial slope.

3.4 Capacity of structural elements and macroelements

The following paragraphs provide indications on the deformation capacities to be used for the various limit states, for both single structural elements and macroelements. It is to be noted that the present state of knowledge does not yet allow to provide reliable indications on the uncertainty that is associated with the values indicated and as a result these thresholds cannot be characterized as random variables (cfr. §4.4).

3.4.1 Capacity of structural elements for damage limit state (SLD)

The capacity values of the damage limit state (SLD) of piers and spandrels to be used for the calculation of accumulated damage (3.26) and (3.27), are given in Tables 3.2 and 3.3. They refer to the level of serious damage for piers ($C_j=\theta_3$) and of very serious damage for spandrels ($C_j=\theta_4$). The drift values are obviously differentiated as a function of the failure mechanism and in the case of mixed mechanisms the drift is estimated by means of (3.10). The choice to consider serious or very serious damage levels at the scale of the element, by the definition of a limited damage (SLD) on a global scale, is justified by considering as acceptable these concentrations of damage in few elements.

3.4.2 Capacity of structural elements for severe damage limit state (SLS)

Insofar as piers are concerned, reference is made to a damage level that precedes a serious level ($C_j=0.5\theta_3$), in that it corresponds to a situation where the element is not only in a condition to support the vertical loads but can be conveniently repaired. With regard to spandrels, reference is made instead to a very serious damage level

($C_j=\theta_4$), since the damage of a spandrel has no serious consequences on the stability of the wall and the element can be efficiently reconstructed and coupled to the masonry wall; nevertheless, in the case of spandrels that are supported by an arched masonry lintel, one may also consider a level of serious damage ($C_j=\theta_3$), given the fragility of such collapse mechanism.

3.4.3 Capacity of structural elements for limit state for the prevention of collapse (SLC)

In the case of the limit state for the prevention of collapse, only the capacity of pier masonry walls in controlled since the collapse of a spandrel does not result to be so significant in the context of the evaluation on the global collapse of the building.
The limit state for the prevention of collapse (SLC) is considered to have been reached when even a single pier collapses ($C_j=\theta_5$) because it is no longer in a condition to support the vertical loads and this leads to instability that might to be extended to large portions of the building.
The values that are to be considered are given in Tables 3.2 and 3.3.

3.4.4 Deformation capacity of the wall macroelement

In case of the verification of the damage limit state (SLD) it is necessary to verify that the inter-storey drift does not exceed the value $\theta_{SLD,M}$=0.2%.
In the case of the verification of the limit state for the prevention of collapse (SLC), it is necessary to verify that the inter-storey drift does not exceed the value $\theta_{SLC,M}$=0.6%.

3.4.5 Deformation capacity of the horizontal diaphragm macroelement

In the presence of flexible diaphragms or vaults, if their deformation is modelled by means of elastic elements, it is appropriate to consider for the damage limit state (SLD) thresold reference values of the angular deformation. These must be based on data from literature or derived from laboratory experiments or from numerical analyses. Different values are found varying the different types of diaphragms and in the presence of vaults, in relation to their shape (barrel vaults, pavilion vaults, cross vaults, ribbed vaults), and slenderness (light/thickness ratio). Reference values for some types of diaphragms are proposed for example in ASCE/SEI 41/06.

4 Reinforced concrete buildings

4.1 Knowledge of the structure

4.1.1 Aspects of knowledge

As already indicated in §2.3.1, the aspects of knowledge that are necessary for an evaluation include:

- Geometry of the body of the structure
- Construction details
- Mechanical properties of the materials

These aspects of knowledge are obtained from the following sources:

- A historical-critical analysis.
- Documents of the original design and of possible subsequent interventions (drawings and reinforcement, tests certificates).
- Geometrical-structural relief.
- Experimental surveys and trials.

The first element to be obtained is the geometry of the structural system. In the absence of design documentation that is adequate for the purpose, it is necessary as a preliminary step to carry out a full structural survey.
The next step is the implementation of a preliminary analysis for the purpose and with the procedures shown in §4.1.2. After this analysis, the plan of the experimental investigations is drawn up with the tests to be carried out as specified in §4.1.3, aimed at: a) the verification of the correspondence of the construction with the design plans, where available, or to the acquisition of sufficient data to perform a simulated design of the reinforcement according to the rules that were in force at the time of the construction; b) the knowledge of the properties of the component materials.

4.1.2 Preliminary analysis

The preliminary analysis is designed to determine in an approximate manner the state of the structure and its possible critical areas with a view to directing the investigations, compatible with the needs of the use of the structure, towards the area where they are most relevant to the final judgement.
It is known that a modal analysis with an elastic spectral response on a linear model with ”cracked” stiffness provides in many cases a good approximation the displacement demand even beyond the elastic limit. Such an analysis allows especially:

- the determination of the number of modes that contribute in a significant manner to the response, and therefore to the static non-linear method of analysis that is most appropriate to the verification.
- the identification of the areas (floors, structural elements) that are critical (high *D/C* ratios), on the basis of the yield deformation capacity that is first estimated, where it is more important to check with greater care the construction details and materials. For ductile mechanisms the approximate evaluation of the relationship θ/θ_y is often possible even in the absence of reinforcement details, the yield curvature being proportional to the dimensions of the section (known in good approximation) and to the deformation ε_y of the steel, but only weakly dependent on the amount of reinforcement.

4.1.3 Experimental investigations

4.1.3.1 Structural details

Knowledge of the arrangements of the reinforcement (bends, length of the overlaps and of the anchorage, joints details, etc.) inside every principal element is a matter of considerable importance for the reliability of the outcome of the assessment of a building in reinforced concrete.
In case the original executive drawings (or accounting records) are available, the necessary compatibility checks require the stripping of some of their elements, with the removal of the plaster and of the concrete cover over sufficiently large bands to enable the examination also of the transverse reinforcement[15]. The number of these bands, to be performed in different floors, and especially in areas identified on the basis of the preliminary analysis, is linked to the degree of compliance that is found between original design and actual implementation.
In the case of incomplete or missing executive drawings, the number of bands should be such as to allow the reconstruction of the criteria followed in the design of the structure, criteria that is to be adopted in a simulated design in the evaluation phase.
Finally it is necessary to have an investigation of at least one beam-column joint that is not confined. By means of partial chipping of the concrete cover and with the help of non-destructive instruments, it should be possible to identify the details of the anchorage of the reinforcement of the converging elements, the possible presence of stirrups in the joint, as well as the details of the continuation of vertical reinforcement in the upper floor.

4.1.3.2 Mechanical properties of concrete and of steel

Modelling by means of random variables of the compressive strength of concrete and of the yield strength of steel can be done, as shown in §2.3.2.1, by assuming a of lognormal probability distribution and estimating the two parameters: mean and standard deviation of the logarithm.
With regard to the mean, this can be estimated:

- Starting from the design specifications or from test records, with subsequent updates using the Bayes technique, if this information is available.
- On the basis of investigations carried out at the time of the assessment.

The number of tests that are to be performed must be related to the volume of the building.
In the second case above the number of tests is in general larger than in the first case, and must be adjusted to obtain a stable estimate of the parameter. This number can be reached by means of non-destructive tests only if these have been properly calibrated by using a minimum number of destructive tests.
As regards the standard deviation, this should reflect the actual variability of the mechanical properties within the structure in question and cannot therefore be estimated on the basis of literature data that refer to a sample of a population of contemporary structures. In the absence of more accurate determinations, or as an *a priori* value to

[15] Relatively recent instruments make it possible to reproduce the layout of the reinforcement without having to remove the concrete cover.

be updated by means of the Bayes technique, use can be made of the values given in Table 4.1.

Table 4.1 Recommended values for the standard deviation of the logarithm of the mechanical properties

Properties	Symbol	σ_{ln}
Cylindrical compressive strength of concrete	f_c	0.15
Yield strength of steel	f_y	0.10

As a marginal comment on the above considerations it is appropriate to add that, for the usual values of the average compressive strength of reinforced concrete in the range of 20 to 30 MPa, the results of the assessment is weakly influenced by the particular value used, and that the contribution of the uncertainty on the strength of the concrete on the probability of collapse is in the majority of cases negligible compared to that regarding the uncertainty on the construction details. The comment above has value as long as the quality of the mix is maintained above the lower threshold indicated. In case that lower experimental values are detected, an accurate assessment of the resistance of the concrete is required.
With regard to the steel, albeit within narrower limits, the considerations made concerning the influence of the resistance of the concrete on the outcome of the tests are still valid. Variations of the order of 10÷15% have an influence that is completely marginal. Besides, to reduce the standard error in the estimate of the mean resistance of steel below these values would require a number of tests that would be completely unrealistic, given the double consideration that resistance is a function of the diameter of the bar and that the characteristic strength associated to the various classes is a guaranteed minimum, with variations over the minimum among different batches that are of the same order as mentioned above.

4.2 Response in two and in three dimensions

The models presented below (§4.3.1, §4.3.2 and §4.4) refer, with the sole exception of the beam-columns elements where the sectional behaviour is described by means of a fiber discretization, at a behaviour in a single bending plane. While this does not represent a limitation in the case of beams, or of joints (the external ones since the internal ones are always confined), with the exception of the corner ones, the columns are always subject to a system of biaxial bending.
In the absence of models with a biaxial response capacity, as in the case of *degrading* models currently available (§4.3.1.4), the only option is to adopt in approximation the same model in the two orthogonal bending planes, ignoring the interaction.
In the case of models *without degradation* where the check of the displacement with respect to the deformation thresholds corresponding to limit states is made a posteriori, it is possible to take account of the interaction in an approximate manner through the "elliptical" rule:

$$y = \sqrt{\left(\frac{\theta_2}{\theta_{2,SL}}\right)^2 + \left(\frac{\theta_3}{\theta_{3,SL}}\right)^2} \tag{4.1}$$

where θ_2 and θ_3 are the angular distortions in the planes of bending identified by the local axis 1 (lengthwise of the element) and, respectively, by the local axis 2 and 3, while $\theta_{2,SL}$ and $\theta_{3,SL}$ are the corresponding thresholds (uniaxial) at their limit state (SL). The limit state is reached in the element when $y = 1$.

This rule is proposed in (Biskinis and Fardis, 2010a,b) on the basis of limited experimental evidence from biaxial tests.

4.3 Modelling criteria

4.3.1 Modelling of beams and columns

4.3.1.1 Modes of failure of reinforced concrete beams and columns

Beams and columns are subject to concomitant bending stresses (M), shear (V) and normal stress (N). The interaction between these stresses is one of the most important phenomena in the inelastic response near the collapse of structures in reinforced concrete that are not designed in accordance with criteria of capacity design. Shear related aspects represent in most cases the determining cause of the collapse, whether they precede the damage due to a flexural mechanism or whether they arise due to a reduction of shear resistance caused by cyclic deformation in bending.

The reduction of shear resistance due to the inelastic bending response and the concurrent demand for ductility is a common element in several of the models of shear resistance available in technical literature, usually in the form of a linear reduction factor $k(\mu)$ function of (maximum) ductility μ, as shown in §4.4.6.

The interaction between bending and shear in the determination of the tupe of failure of an element is illustrated in a schematic manner in Fig. 4-1 where for the sake of simplicity reference is made to a monotonic response. There are three instances.

When the initial shear resistance $V_{R,0}$ (i.e., not yet reduced as a result of the flexural response) is less than the shear demand in equilibrium with the bending strength (commonly called "plastic shear" and determined as $V_y = M_y/L_V$) the shear failure occurs in a fragile manner before the bending yield strength, for the value $V_{R,0}$ for an angular deformation, drift or rotation with respect to the chord, θ_V (see §4.4.4.2). The subsequent behaviour is degrading until the formation of a full passing crack and sliding along it, a state where the shear force is reduced to negligible values and the element almost completely loses its bearing capacity, at an angular deformation θ_a (see §4.4.4.3).

When the initial shear strength $V_{R,0}$ is greater than the plastic shear, the element yields in bending. If the value of the residual shear resistance $k(\mu)V_{R,0}$ is smaller than the maximum shear V_{max} (greater than the plastic shear due to hardening), the shear failure occurs after the yield in bending for an intermediate shear value between the initial resistance $V_{R,0}$ and the residual one, at an angular deformation θ_V. The subsequent behaviour is again degrading until the formation of a through crack and of failure with an angular deformation θ_a.

If even the residual value of the shear strength $k(\mu)V_{R,0}$ is greater than the maximum shear, the element continues to deform by bending in the inelastic field until the failure of the compressed part of the section with the buckling of the bars and/or the attainment of the ultimate deformation capacity of the conrete and its expulsion. To these phenomena corresponds a degradation of the bending resistance with an angular deformation θ_f (see §4.4.4.1). The slope of the post-peak branch is associated with the ultimate deformation where the shear force goes to zero, and depends on the process of degradation of the concrete (post-peak slope of the σ-ε law) and on the level of the axial stress to which the element is subjected in relation to the loss of stiffness due to large deformations. The degradation occurs in a sharp manner and the bars are subject to buckling.

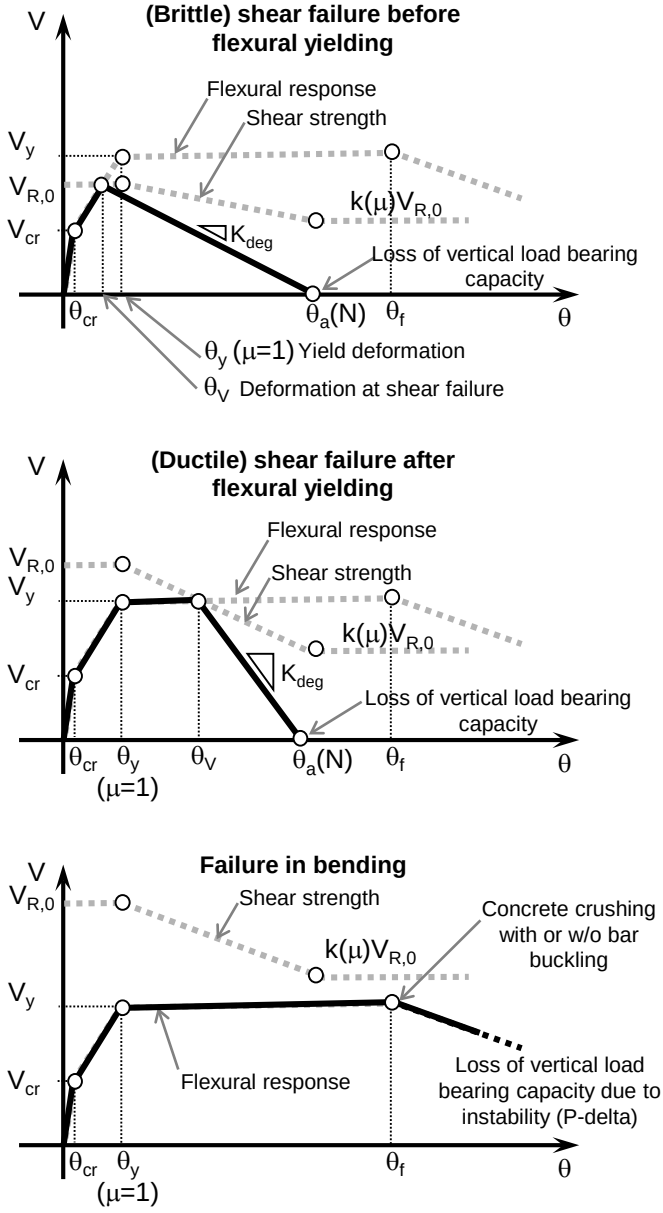

Fig. 4-1 Failure modes of a reinforced concrete element subjected to bending, shear and normal stress

In general, in the case of existing buildings the most frequent failure modes, especially insofar as columns are concerned, are those arising from shear, either in the elastic range (mode 1, in Fig. 4-1) or in the palstic range (mode 2). In the next section models are presented in order to decribe the non-linear pure bending behaviour of the beam-columns elements. These models constitute the basis for more advanced models that describe the bending and shear behaviour, shown in section §4.3.1.4.

4.3.1.2 Models of beam-columns with prevailing flexural behaviour

Available models for the determination of the non-linear response of elements of beam-columns in the most widely udes computer codes belong to the following categories:

- Models with diffused inelasticity:
  - "stiffness" formulation: models where the displacement field is interpolated along the length of the element
  - "flexibility" formulation: models where the force field is interpolated along the length of the element
  - "mixed" formulations: models where multiple fields are interpolated along the length of the element
- Models with concentrated inelasticity, also referred to as "plastic hinges".

Models with diffused inelasticity formulations in flexibility and mixed can be used in all cases. Models with diffused inelasticity with a formulation in stiffness can be used in all the cases but generally require a finer discretization of the structural elements in order to be able to adequately descibe the variation of the deformations along the axis of the elements, or alternatively the use of higher order interpolation functions of displacements.
Models of concentrated inelasticity can be used when the possibility of formation of plasticized zones internal to the element can be ruled out. However, in these elements it is neceessary to estimate the stiffness of the internal 'elastic' zone taking into account of the expected average cracking.
All the listed models make use of sectional response models that provide the link between the section stress resultants and the corrresponding generalized deformations.

4.3.1.3 Section models

Available models for the determination of the response of the section of an element of a beam-column belong to the following categories:

- Fiber models (Fig. 4-2): in these models the section is discretized into component (fiber) portions which are assigned the stress-strain relationship, generally uni-axial, of the corresponding material. The relationship between stress resultants and generalized deformations is obtained starting from the behaviour of the fibers, in the generally adopted assumption of conservation of the plane section.
- Direct models (Fig. 4-3): where the relationship between the stress resultant and generalized deformations is specified in a direct manner.

Fiber models allow the correct description of the interaction between normal force and the two components of the bending moment in the cyclic range. In the version currently in use that is available in the most popular codes these models are not, however, adequate to capture the phenomena of degradation associated with high levels of deformation, such as buckling and slip of the bars, and expulsion of the concrete core in the absence of proper confinement.
In fact, therefore, the fiber section models must be considered as models *without degradation* for the purpose of §2.4 and §2.5.3.

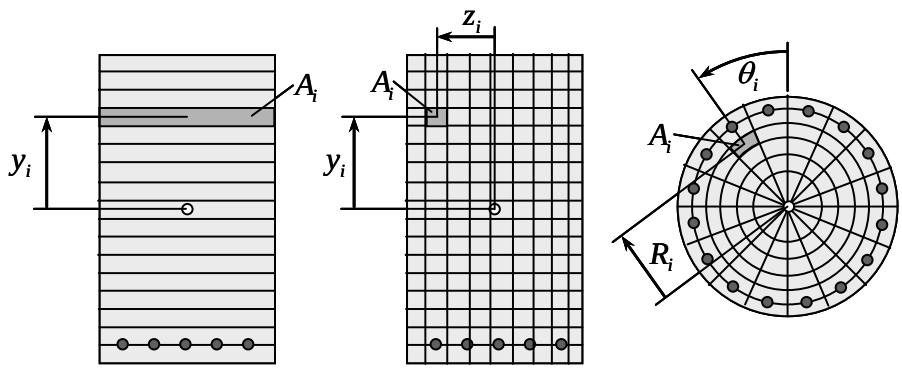

Fig. 4-2 Fiber section models: for plane analyses (left), for spatial analyses (centre and right).

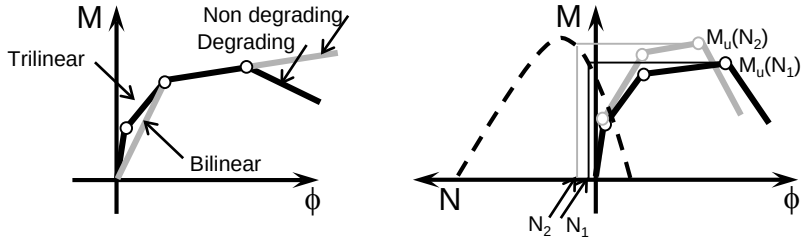

Fig. 4-3 Direct section models: alternatives for the monotonic curve (left), effect of the interaction between the normal force and bending moment (right).

Direct models can describe the phenomena of degradation mentioned above, but are limited in dealing with the interaction between the components of the stress resultants (normal force with bending - Fig. 4-3, right - in particular the latter is biaxial). This limitation is more relevant if the expected level of variation of the axial force in the elements is important. If a check is also carried out for the damage limit state it is preferable to adopt a multi-linear link that distinguishes between the uncracked elastic branches and the cracked elastic (Fig. 4-3, left). In case the link is of the bilinear type (without degradation) or trilinear (with degradation) for the slope of the first branch an intermediate value must be chosen between the initial stiffness and the secant one at yield (for example, secant at 40% of the threshold of yield).
In conclusion, the direct models can be considered as models *with* or *without degradation* for the purpose of §2.4 and §2.5.3, in function of the law adopted (Fig. 4-3, left).

4.3.1.4 Beam-column models with shear or bending-shear failure

Rigorous and robust models of this phenomenon that possess the necessary general features are still the subject of theoretical and experimental research. The available alternatives for a practical application are three:

- Modelling simplified at sectional level where the moment-curvature law is modified by the introduction of a degradation caused by the shear failure, reducing the value of the moment to satisfy the equilibrium with the value of the shear in the post-peak branch (Fig. 4-4, left, corrisponding to the shear failure in the plastic range, mode 2, in Fig. 4-1).
- Modelling of the interaction at the level of the element, adopting a beam formulation that considers shear deformation and a corresponding sectional model that includes the shear and the associated generalized deformation (for example, as shown in Fig. 4-4, right).

- Modelling consisting of an element that describes the bending with interaction NM (normally an element with distributed inelasticity with fiber section) and of one or two elements of zero length at the ends that describe the shear behaviour, the axial failure and eventually the effect of the sliding of the bars (Fig. 4-5, where there is only one element and describes contributions of shear and axial deformations).

Fig. 4-4 (right) illustrates the simplified implementation of the second approach, where the overall response of the section (NMV) is obtained by the assemblage of a coupled NM behaviour with a uni-axial shear hysteretic law of a phenomenological type, independent from M and N. This approach may be considered an acceptable compromise for modelling in the dynamic field *with degradation* when the axial stress N is slightly variable. There are, moreover, other models that, while ignoring the bending stress-shear interaction, include a hysteretic law V-γ as a function of the normal stress.
(Fig. 4-5) illustrates the third option. The column consists of the assembly of an element of a beam-column in bending and normal force and of an element of zero length having shear and axial laws with their corresponding degrees of freedom. The beam element describes the axial flexibility and the bending flexibility of the column. Therefore the shear and axial laws in the element of zero length must have a stiffness that is respectively equal to $K_V = GA_V/L$ (average elastic shear stiffness on the element, with A_V as the shear area) and K_A»EA/L. The total vertical deformation is given by the beam element whereas the horizontal/transversal deformation is given by the sum of $\Delta = \Delta_f+\Delta_V$ of the beam element and the of the shear element. The element with zero length must be able to monitor the total displacement Δ and therefore the corresponding angular distortion $\theta = \Delta/L$. When one of the limits θ_V, θ_f is reached (see Fig. 4-1) the element updates the response curve and imposes a degradation of the force V and/or N also in the beam element. The slope of the degradation branch (negative stiffness) is determined on the basis of the difference between the values of θ_a and θ_V.
As regards the cyclic response, the monotonic shear and axial stress laws must be completed by laws of hysteresis suitably calibrated to reproduce experimental data.

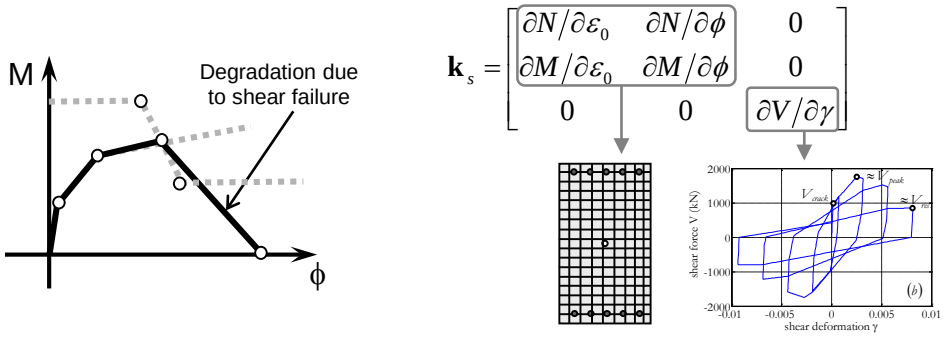

Fig. 4-4 Direct sectional models: alternatives for the monotonic curve (left), effect of the interaction between the stresses (right).

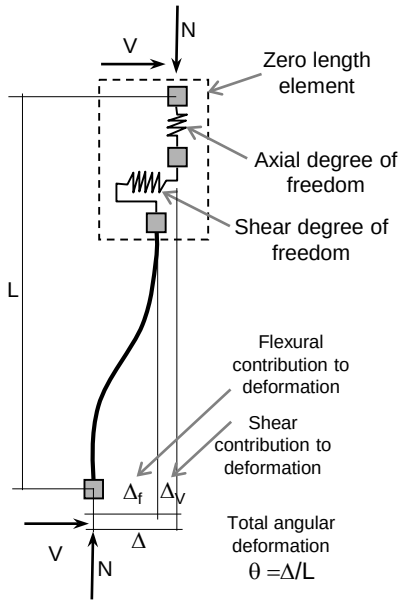

Fig. 4-5 Model consisting of a bending element and of elements at zero length for the shear, the axial failure and the sliding of the bars.

4.3.1.5 Models for cyclic degradation

The phenomenon of degradation is very relevant for elements in reinforced concrete that are not designed in accordance with modern criteria for seismic protection. As shown in §2.4 the degradation concerns both the stiffness as well as the resistance, and it is present both in conditions of increasing monotonic displacement, leading to a negative slope of the monotonic curve, as well as in conditions of cyclic displacement. This type of behaviour is desribed in Fig. 4-6, that shows the monotonic curve of the analytical model together with the cyclic experimental response and with the corresponding simulated response. It can be observed that the state of zero shear is reached in cyclic conditions for lower values of deformation compared to those which correspond to the monotonic condition. The simulation of such a behaviour requires models that allow the description of several cyclic degradation mechanisms:

- Degradation of the strength
- Degradation of the unloading stiffness
- Degradation of the reloading stiffness

In general the parameters of these models vary as function of the ductility and/or the energy dissipated through hysteresis in the cyclic deformation.

By way of example, in the reasonable assumption that every element has a "maximum capacity of energy dissipation by hysteresis" E_t, the yield strength at the inversion after the branch i, $V_{y,i}$, can be made to depend on the dissipated energy E_i and on the strength on the branch $V_{y,i-1}$ (calculated at the inversion point after the branch i-1) in the form (Rahnama and Krawinkler, 1993)(Ibarra et al 2005):

$$V_{y,i} = V_{y,i-1}\left(1-\beta_i\right) \tag{4.2}$$

where:

$$\beta_i = \left(\frac{E_i}{E_t - \sum_{j \le i} E_j} \right)^c \tag{4.3}$$

The use of a model of this type requires the availability of predictive equations for parameters such as, for example, exponent c or the total dissipation energy capacity E_t (the latter is provided as an example in a normalized form by equations such as 4.19).

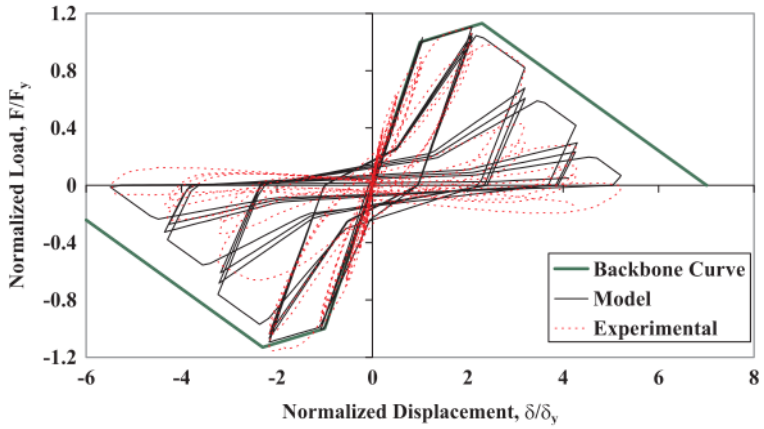

Fig. 4-6 Experimental cyclic response of a reinforced concrete column built according to old concepts and numerical simulation (adapted by Ibarra et al 2005).

4.3.2 Models for beam-column joints

Generally internal joints, confined by beams or by floors on all the four vertical faces, do not represent critical elements. The external joints instead, and in particular those that were built before the introduction of modern seismic codes, constitute critical elements for the response of the building.

Modelling of these elements has not reached a level of development that is comparable to that of the beam-column elements, and the solutions that are adopted in practice consist of rotational springs connected to rigid links to describe the shear deformation of the node (Fig 4-7 , left-centre). The constitutive law is characterized by a weak resistance and by a rapid cyclic degradation (Fig 4-7 , right). In the case of corner nodes usually independent springs are adopted on the two orthogonal planes.

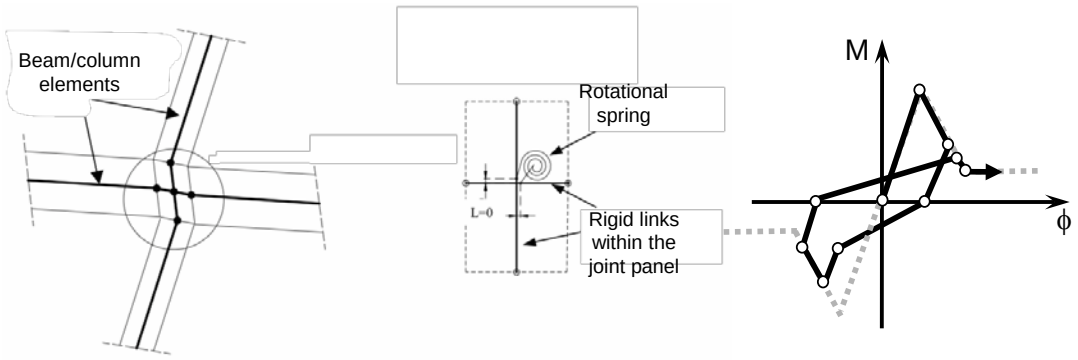

Fig 4-7 Response model for internal nodes: geometry (left), constitutive law (right)

4.3.3 Models for infill walls

External infill walls can have a significant role, positive or negative, in conditioning the response of a framed structure in reinforced concrete. The role is generally positive if the distribution of panels is such as to stiffen and strengthen the structure in a uniform manner, negative in the case of an irregular distribution. Such an irregular distribution can also occur during the response itself, if the damages due to the seis-

mic action are such as to eliminate, for example, a whole level of cladding, leading to a weak floor.
Available models for practical use all refer to an idealization with equivalent struts, arranged cross-wise to form a brace. Expressions are available to determine stiffness, strength and ultimate deformability of the struts for panels without and with openings. Fig. 4-7 shows in a qualitative manner the arrangement of one of the rods and a typical constitutive uniaxial force-deformation law.

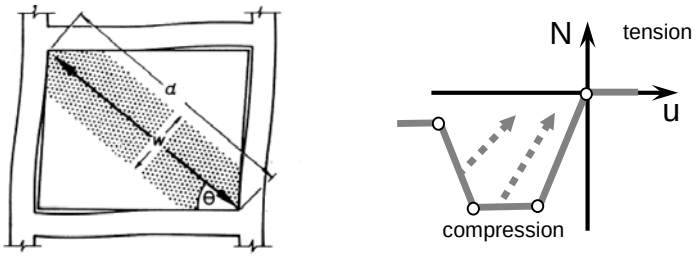

Fig. 4-7 Equivalent strut for a panel (left), and typical cyclic law (left).

4.3.4 Damping for dynamic analyses

The dissipation of energy in a building in reinforced concrete is attributable to the following mechanisms:

1. Dissipation in the structural elements (dependent on the level of displacement and to a limited extent on the frequency)
2. Dissipation in the non-structural elements (dependent on the level of displacement and to a limited extent on the frequency)
3. Dissipation in the portion of soil in direct contact with the foundations that is subject to larger deformations (dependent on the level of displacement and to a limited extent on the frequency)
4. Loss of energy by radiation into the ground (dependent on the frequency)

A correct evaluation of displacements and deformations of the structure requires that the sources of dissipation that are not directly included in the model be explicitly considered. This is usually done with the introduction of an equivalent viscous damping. The level of damping that is to be used must therefore be dependent on the modelling adopted.

4.4 Capacity of structural elements

4.4.1 Introduction

As shown in Fig. 4-1 an element in reinforced concrete can have three types of behaviour. For each type of behaviour characteristic points can be identified corresponding to force-deformation couples. Fig. 4-1, for simplicity, refers to conditions of monotonic deformation, and therefore the thresholds of deformation indicated in them are those that determine the so-called *backbone* curve.
In the following probabilistic models for these thresholds of deformation are presented, indicating which models allow a difference to be made between the value of thresholds for cyclic deformations and those for monotonic deformations (Fig. 4-a). This distinction is in fact important in relation to the type of modelling adopted and hence of the type of control of the limit states. Whereas as the threshold corresponding to the end of the elastic range (SL-DL, §4.4.2) is concerned the distinction be-

tween monotonic or cyclic behaviour is irrelevant, with regard to advanced limit states it is necessary to adopt the correct values of the thresholds depending on whether the model is without or with degradation.
For models with degradation it is necessary to define separately the monotonic curve (using monotonic thresholds) and the rules of cyclic degradation (see §4.3.1.5), obtaining as a result of the analysis a potential failure at a lower threshold of deformation, as a result of the degradation itself.
For models without degradation, and for all those modes of collapse that are not directly modelled, it is necessary to adopt thresholds that take into account cyclic degradation for the control *a posteriori*[16].
It can be observed that in literature the identification of the point where the stiffness becomes negative is not uniform. There are two alternatives: some models adopt the point in correspondence with the peak of the resistance V_{max}, while others adopt a point corresponding to the peak decreased by 20% ($0.8V_{max}$). This difference must be taken into account in the determination of the constitutive law of the elements (calculating, for example, the peak deformation as a funtion of that at $0.8V_{max}$ and of the slope of the branch with negative rigidity, as shown in Fig. 4-b).
Finally, although the structure of this Guide is based on the characterization of the capacity in deformation terms, in §4.4.5.3 models of shear strength V_{max} are introduced, that are necessary for instance to discriminate between elements that are prone to shear failure (fragile or ductile) or to flexural failure (§**C.8.2**).

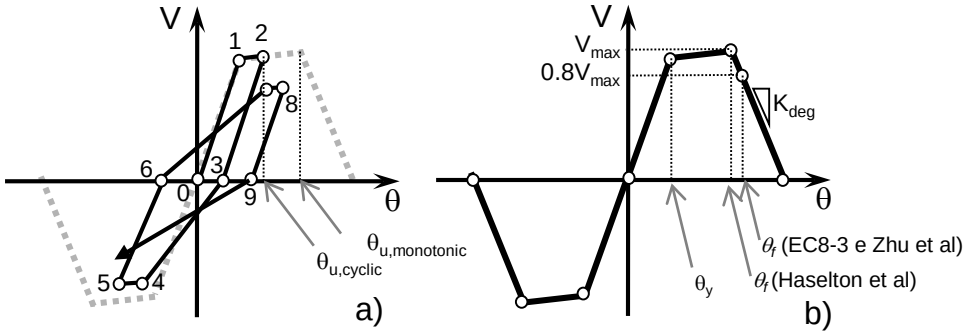

Fig. 4-9 (a) Monotonic threshold (model with degradation) and cyclic threshold (model without degradation) (b) definistion of different thresholds for the start of the negative stiffness.

4.4.2 Capacity for damage limit state (SLD)

The formulation of this limit state indicates negligible damage to structural elements. This condition translates itself into the condition of non exceeding yielding of the reinforcement, both longitudinal and transverse.
The deformation capacity, expressed in terms of rotation with respect to the chord, is therefore equivalent to:

$$\theta_{SLD} = \min\left(\theta_y, \theta_V\right) \tag{4.4}$$

[16] It can be observed that the adoption of this verification system of a limit state involves an inevitable approximation, in that imposed deformation cycles that are prescribed by the different test protocols are definitely different from those that occur during the seismic motion that is under consideration.

If the behaviour of the element is of the type 2 or 3 in Fig. 4-1, yield of the longitudinal reinforcement precedes that of the transverse one and $\theta_{SLD} = \theta_y$, otherwise $\theta_{SLD} = \theta_V$, whose definition is given in § 4.4.4.2.

The angular yield deformation θ_y can be modelled as a variable with a lognormal distribution. For the *mean* of the capacity use can be made of the expressions:

$$\theta_y = \phi_y \frac{L_V}{3} + 0.0013\left(1 + 1.5\frac{h}{L_V}\right) + 0.13\phi_y \frac{d_b f_y}{\sqrt{f_c}} \quad \text{beams and columns} \quad (4.5)$$

$$\theta_y = \phi_y \frac{L_V}{3} + 0.0020\left(1 + 0125\frac{h}{L_V}\right) + 0.13\phi_y \frac{d_b f_y}{\sqrt{f_c}} \quad \text{walls} \quad (4.6)$$

where the three terms represent respectively the contribution of the bending deformation, of the shear deformation and of the sliding of the bars. In particular, ϕ_y is the yield curvature, $L_V = M/V$ is the shear length, i.e. the distance from the end of the element to the section of zero shear, h is the net height of the section and d_b the diameter of the longitudinal bars.

The yield curvature can be obtained from a moment-curvature analysis of the section for the median values of the material properties (§4.1.3.2), or, if the knowledge achieved is not sufficient for a detailed evaluation, by means of the following expression:

$$\phi_y = \alpha \frac{\varepsilon_y}{d} \quad (4.7)$$

where ε_y is the yield strain of the steel, d is the effective height of the section and the factor α depends on the type of the element (for example, 2.1 for beams and colums).

The shear length can be reasonably assumed as constant and equivalent to half of the length of the element.

The standard deviation of the logarithm of θ_y can be assumed equivalent to 0.32 (Biskinis and Fardis, 2010b).

4.4.3 Capacity for SLV

The formulation of this limit state indicates a structure that is characterized by a *diffused* state of damage that renders repair works *uneconomic*. The expression of the limit state variable (2.7) reflects this formulation being expressed in terms of the sum of the conventional costs corresponding to the damage. The capacities to be used in the local relationships *D/C* are those that are relative to the limit state for the prevention of collapse (SLC).

4.4.4 Capacity of the limit state of the prevention of collapse (SLC)

4.4.4.1 Deformation capacity: flexural failure

The deformation capacity θ_f for the mode of failure 3 (Fig. 4-1), expressed in terms of rotation with respect to the chord, is modelled as a variable with a lognormal distibution.

Technical literature provides alternative models for θ_f. The following sections provide three of them. The first model is one of the two provided by the European norm [17] and in the form that is shown, it refers to elements with construction details that are seismically adequate. In the case of existing buildings with elements that lack these details, the European norm indicates reductions to the value of θ_f. The second and third models that are shown, whose experimental bases are less wide but more homogeneous than those in the Eurocode, have the advantage of referring directly to elements that lack proper seismic details (Zhu et al, 2007) or of spanning the behaviour of both "new" as well as "old" members (Haselton et al, 2007).

Model "Eurocode 8 Part 3"

For the *median* use can be made of the formula:

$$\theta_f = 0.016\left(0.3^{\nu}\right)\left[\frac{\max(0.01;\omega')}{\max(0.01;\omega)}\, f_c\right]^{0.225}\left(\frac{L_V}{h}\right)^{0.35} 25^{\alpha\rho_{sx}\frac{f_{yw}}{f_c}}\left(1.25^{100\rho_d}\right) \tag{4.8}$$

where ν is the dimensionless normal force, ω and ω' are the mechanical percentages of the reinforcement in the tension and compression zone, α the confinement factor, ρ_{sx} and ρ_d the precentages of the transverse and diagonal reinforcement (in the coupling beams between the walls).

The standard deviation of the logarithm of θ_f can be assumed equal to 0.40.

The definition adopted for the threshold is that of a decrease of 20% with respect to the maximum shear. Even if the statistical basis is not uniform[18], the model allows for a distinction between a threshold for monotonic deformation (the equation given) and a "cyclic" threshold. Consequently this model is in principle suitable both for use in the case of models with degradation as well as for models without degradation. However, there does not exist a predictive equation obtained on the same experimental basis for the other parameters necessary to establish a full constitutive law such as the negative post-peak stiffness and the parameters of cyclic degradation. In practice, therefore, use of the expression is limited to models without degradation.

Model "Zhu et al 2007"

For the *median*, use can be made of the expression:

$$\theta_f = 0.049 + 0.716\rho + 0.120\frac{\rho_{sx} f_{yw}}{f_c} - 0.042\frac{s}{h} - 0.070\nu \tag{4.9}$$

where *s* is the spacing of the stirrups.

The standard deviation of the logarithm of θ_f can be assumed equal to 0.35.

[17] Eurocode 8 Part 3 provides a "mechanical" and a "statistical" model for the ultimate rotation with respect to the chord. The "mechanical" model has limited usefulness in the case of existing buildings in that no indications are given with regard to the reduction of the capacity as a result of non-seismic details.

[18] The database of the tests assembled by the authors of the model (Fardis and Biskinis, 2010) contains mainly tests where the collapse is reached as a result of bending stresses (mode 3 in Fig. 4-1, 894 tests out of 1195, without taking into account those in which the collapse was not reached), and among these the larger share (778) are cyclical tests on "conforming" elements, in other words with modern seismic details. It is therefore necessary to be aware that factors that take into account the monotonic deformation or the absence of seismic details are based on a much smaller number of tests (respectively 76 and 40). For the sake of completeness of information the number of tests with mode of collapse 1 is 81, while those with mode of collapse 2 is 220.

For this model the definition adopted for the threshold is that of a decrease of 20% of the maximum shear and the experimental basis is constituted by cyclical tests (85 out of 125 tests, all on "non-conforming" elements, as already indicated in §4.4.4), limiting it use to cases of models without degradation.

Model "Haselton et al 2007"
For the *median*, use can be made of the expression:

$$\theta_f = 0.14(1+0.4a_{sl})(0.19)^{\nu}(0.02+40\rho_{sh})^{0.54}(0.62)^{0.01 f_c} \qquad (4.10)$$

where f_c is in MPa.
The standard deviation of the logarithm of θ_f can be assumed equal to 0.46.
For this model the definition adopted for the threshold is that which corresponds to the maximum shear V_{max}.
The experimental basis of this model is constituted by cyclical tests (255 tests, all on "non-conforming" elements). Furthermore, the model, by construction, provides the "monotonic" deformation threshold and can therefore be used only to establish the curve of monotonic load in the case of models with degradation.
Haselton et al also provide a model only for the plastic part deformation at peak, that may be used together with formula (4.4-5) of θ_y:

$$\Delta\theta_f = 0.13(1+0.55a_{sl})(0.13)^{\nu}(0.02+40\rho_{sh})^{0.65}(0.57)^{0.01 f_c} \qquad (4.11)$$

The standard deviation of the logarithm of θ_f can be assumed equal to 0.61.

4.4.4.2 Deformation capacity: shear failure (brittle and ductile)

The deformation capacity θ_V for modes of failure 1 and 2 (Fig. 4-1), expressed in terms of rotation with respect to the chord, is modelled as a variable with a lognormal distribution.
Also in this case the literature provides several alternative models. Only that of Zhu et al (2007) is given here, compatible with those of θ_f and θ_a and usable in the case of models without degradation as indicated in paragraph 4.4.5.2.

Model "Zhu et al 2007"
For the *median*, use can be made of the expression:

$$\theta_V = 2.02\rho_{sx} - 0.025\frac{s}{h} + 0.013\frac{L_V}{h} - 0.031\nu \qquad (4.12)$$

The standard deviation of the logarithm of θ_V can be assumed equival to 0.27. For this model the definition adopted for the threshold is that of a decrease of 20% compared to the maximum shear and the experimental basis is constituted by cyclical tests (40 out of 125 tests, all on "non-conforming" elements, as already indicated in §4.4.4), limiting their use to cases of models without degradation.

4.4.4.3 Deformation capacity: loss of axial bearing capacity

The deformation capacity θ_a for modes of failure 1 and 2 (Fig. 4-1), expressed in terms of rotation with respect to the chord, is modelled as a variable with lognormal distribution.

Also in this case the literature provides several alternative models. Two are reported here: that of Zhu et al (2007), that refers to the loss of bearing capacity after the shear failure (brittle or ductile) and is compatible with those of θ_f and θ_V and usable in the case of models without degradation as indicated in paragraph 4.4.5.2, and that of Haselton et al (2007), that refers to the case of loss of bearing capacity for bending failure, and is usable in the case of models with degradation.

Model "Zhu et al 2007"
For the *median*, use can be made of the expression:

$$\theta_a = 0.184 \exp(-1.45\mu) \tag{4.13}$$

where the effective friction coefficient μ on the crack of shear failure is given by the formula:

$$\mu = \frac{\dfrac{N}{A_{sw} f_{yw} d_c / s} - 1}{\dfrac{N}{A_{sw} f_{yw} d_c / s} \cot\alpha + \tan\alpha} \tag{4.14}$$

where $\alpha = 65°$ and $d_c = h\text{-}c$ is the dimension of the confined core parallel to the direction of the shear.
The standard deviation of the logarithm of θ_a can be assumed equival to 0.35. For this model the experimental base is quite small (28 tests, all on "non-conforming" elements, as already indicated in §4.4.4) and constituted by tests of cyclic type, thus limiting it use to cases of models without degradation.

Model "Haselton et al 2007"
For the *median*, use can be made of the expression:

$$\Delta\theta_a = \theta_a - \theta_f = 0.76(0.031)^{\nu}(0.02 + 40\rho_{sh})^{1.02} \le 0.10 \tag{4.15}$$

The standard deviation of the logarithm can be assumed equival to 0.72.
The experimental basis of this model is constituted by tests of a cyclic nature (255 tetsts, all on "non-conforming" elements). Furthermore, the model, by construction, provides the threshold for "monotonic" deformation and is therefore usable only to establish the curve for a monotonic load in the case of models with degradation.

4.4.5 Operational guidance for modelling

The definition of a constitutive law of the elements must be based on a set of predictive models (for deformation thresholds, for levels of stiffness, for degradation parameters) that are consistent with each other (in other words, obtained at the same time on the same experimental basis). The next two paragraphs contain indications that are relevant as function of the type of modelling.

4.4.5.1 Model with degradation

At present the only set of coherent usable models to establish the constitutive cyclic law of beam-columm elements in reinforced concrete is constituted by the equations of Haselton et al (2007). These equations have been obtained by means of regression on 255 cyclic tests using as a base model of the response that of Ibarra, Medina and Krawinkler (2005). The model requires seven parameters, five of which are necessary

to establish the monotonic curve and two for degradation. Of these last two, one is identically equivalent to 1.0. In addition to the equations for θ_f and $\Delta\theta_a$ already provided, the following equations are necessary.

Secant stiffness at 40% of the yield moment
To be used as an intermediate value between the initial one and that at the yield (the model of Ibarra does not differentiate between stiffness at stage I and II), median value:

$$k_{0.4My} = \frac{EI_{0.4M_y}}{EI_0} = 0.17 + 1.61\nu \begin{cases} \geq 0.35 \\ \leq 0.80 \end{cases} \tag{4.16}$$

with standard deviation of the logarithm equival to 0.38.

Secant stiffness at yield
Necessary to identify the yield point together with the corresponding moment, median value:

$$k_y = \frac{EI_y}{EI_0} = 0.065 + 1.05\nu \begin{cases} \geq 0.2 \\ \leq 0.6 \end{cases} \tag{4.17}$$

with standard deviation of the logarithm equival to 0.36.

Ratio between the ultimate and yield moment
Median:

$$\frac{M_u}{M_y} = 1.25(0.89)^{\nu}(0.91)^{0.01 f_c} \cong 1.13 \tag{4.18}$$

with standard deviation of the logarithm equival to 0.10 (f_c in *MPa*).

Degradation parameter γ
Median:

$$\gamma = \frac{E_t}{M_y \theta_y} = 170.7(0.27)^{\nu}(0.10)^{s/d} \tag{4.19}$$

with standard deviation of the logarithm equivalt to 0.50. The equation provides in a normalized form the the total energy dissipation for hysteresis used in models such as the one in Eq.(4.3)

4.4.5.2 Model without degradation

In the case of models without degradation it is possible to use both mechanical formulations (fiber section models) as well as phenomenological (multi-linear models of the moment-rotation law).
In both cases the *a posteriori* check of the limit states must be carried out by means of the Eurocode model for θ_y (SLD) and of the models of Zhu for θ_f e θ_V (SLS and SLC).

4.4.5.3 Statistical dependence

The parameters of the constitutive law of an element are linked among themselves by physical constraints, a fact that introduces a statistical dependence among the random variables describing them. Strictly speaking, therefore, rather than a group of predictive marginal models such as those indicated in the previous two paragraphs, it would be necessary to make use of a joint probabilistic model of the parameters vector. Under the current state of the art a model of this type is not available.
Besides the internal statistical dependence on an element just indicated, there is also statistical dependence between the parameters of different elements. This dependence arises from two causes. The first one concerns the median of the models, where common variables often enter such as, for example, the strength of materials, that in turn present a statistical dependence. The second concerns the error terms (epsilon) that measure the variability around the medians. These latter can be considered as the sum of two terms that are linked to factors that are not included in the median, the first that does not vary from one element to another and that consequently introduces dependence (quality of execution, curing conditions of the concrete, etc), and the second that varies from one element to another thus reducing the dependence. In literature models of this type are not available.
Appendix C (§C.6.2) gives an example of how the problem can be faced in practice, with reference to structures in reinforced concrete.

4.4.6 Shear strength

Technical literature provides alternative models for shear strength V_{max}. Common characteristics for all models are: a) the presence of three additive contributions, due to the axial force *N*, the concrete and the steel; b) the presence of a term that reduces the resistance in function of the maximum ductility reached.
In the following two among the three currently more widely used are presented. The first is that provided in the European norm (CEN, 2005) with reference to elements with construction details that are inadequate from the seismic point of view (existing buildings). The second model is that of Sezen and Mohele (2004) and is reported because it is used to discriminate between shear (brittle or ductile) and flexural failure associated with the models for deformation capacity of (Zhu et al, 2007). In both cases the *shear strength* under cyclic action is modelled as a variable with lognormal distribution and the expressions are given may be used to determine the median.

Model "Eurocode 8 Part 3"
This model envisages two distinct equations for columns and beams and for squat walls. For beams and columns, the *median* is provided by the following expression (units MN and m):

$$V_R = \frac{h-x}{2L_V}\min\left(N;0.55A_c f_c\right) + \left(1-0.05\min\left(5;\mu_{\Delta,pl}\right)\right)\times \\ \times\left[0.16\max\left(0.5;100\rho_{tot}\right)\left(1-0.16\min\left(5;\frac{L_V}{h}\right)\right)\sqrt{f_c}A_c\right] + V_w \tag{4.20}$$

where:
h total height of the section
d effective height of the section
x depth of the neutral axis

N normal force, positive if in compression, zero if in tension
A_c area of the section bd for rectangular section, $\pi D_c^2 / 4$ for circular section
D_c confined core diameter
p_{tot} total geometric percentage of the longitudinal reinforcement
V_w contribution by the reinforcement equal to $p_w b z f_y$, for rectangular sections, and to $e\frac{\pi}{2}\frac{A_{sw}}{s} f_y (D-2c)$, for circular sections
A_{sw} area of circular stirrups
s spacing of stirrups
D diameter of the section
c concrete cover

The term $\mu_{\Delta,pl} = \mu_\Delta - 1 \cong \theta / \theta_y - 1$ represents the plastic part of the ductility experienced by the element.
For squat walls the median of the *shear strength* under cyclic action must not exceed the limit corresponding to the crushing of diagonal struts given by the following expression (units MN and m):

$$V_{R,\max} = 0.85\left(1 - 0.06\min\left(5;\mu_{\Delta,pl}\right)\right)\left(1 + 1.8\min\left(0.15;\frac{N}{A_c f_c}\right)\right)\times \\ \times\left(1 + 0.25\max\left(1.75;100\rho_{tot}\right)\right)\left(1 - 0.2\min\left(2;\frac{L_V}{h}\right)\right)\sqrt{f_c} b_w z \tag{4.21}$$

The standard deviation of the logarithn may be assumed in both cases eqival to 0.25.

Model "Sezen e Mohele 2002"
The model refers only to columns and the *median* is given by the following expression (units MN and m):

$$V_R = k\left(\mu_\Delta\right)\cdot\left(\frac{0.5\sqrt{f_c}}{L_V / h}\sqrt{1 + \frac{N}{A_g 0.5\sqrt{f_c}}}0.8A_g + V_w\right) \tag{4.22}$$

where $A_g = bh$ is the whole area of the section, and the term of the reduction due to the (total) displacement ductility equals $k\left(\mu_\Delta\right)$ equals 1.0 for $\mu_\Delta \le 2$ and 0.7 for $\mu_\Delta \ge 2$, with a linear variation in the middle. In this model the influence of the normal force does not translate itself into a separate contribution to the resistance but into a change of the term giving the contribution of concrete. Further the reductive factor $k\left(\mu_\Delta\right)$ is applied to the total contribution by concrete and steel, instead of only to the first term.
The standard deviation of the logarithm may be assumed to be equival to 0.15.

4.5 Capacity of the non-structural elements

Non-structural elements can be divided in three general categories:

1. Architectural elements: for example, external infill walls and partitions, doors, ceilings, etc.
2. Installations: for example, water services, electricity, gas, lifts and elevators, air conditioning, etc.
3. Contents: for example, furniture, equipment, any other object that contributes towards an economic assessment of the damage.

From the point of view of the capacity to withstand seismic action, non-structural elements are divided into:

1. Elements that are mainly sensitive to inter-storey movement
2. Elements that are mainly sensitive to the acceleration of the storey

The capacity of non-structural elements is expressed by means of a distribution, assumed to be lognormal and referred to as the "fragility curve" of the element, for each limit state (generally two, damage limit state (SLD) and limit state for the prevention of collapse (SLC)) characterized by two parameters:

- the median of the capacity (in terms of drift or of acceleration at the storey, depending on the type of the element)
- standard deviation of the logarithm

The values that are to be used depend on the type of element under consideration and must be established on the basis of literature data or on the basis of specific tests.

When the infill walls are included in the modelling through equivalent struts, their state of the damage can be recovered directly from the analysis. The constitutive law of the equivalent struts must obviously be consistent with the fragility curves of the infill walls being taken into account.

4.6 Quantification of the limit state for the prevention of collapse

4.6.1 Modelling with degrading elements

The quantification of reaching or exceeding the limit state is obtained in global terms. The methods are different according to the method of analysis that is used.

In cases where the analysis of the response is made through non-linear static analysis (methods B and C, §2.6.3-2.6.4), the global threshold of displacement corresponding to the limit state of collapse δ_{SLC} is identified in the capacity curve and corresponds to the end of the segment with a negative post-peak stiffness. The limit state variable is therefore determined by the expression (2.11).

In cases where the analysis of the response is done through non-linear dynamic analysis (method A, §2.6.2), the curves IDA are drawn in the plane θ_{max}-S and for every time history of acceleration the value of the intensity leading to the limit state for the prevention of collapse is that which corresponds to the first attainment of a tangent to the curve equival to the 10% of the initial one.

4.6.2 Modelling with non degrading elements

The quantification of reaching or exceeding the limit state is carried out in global terms through the local aggregated relationships *D/C* by means of the formulation (2.8) of the variable limit state Y_{SLC}. This formulation requires the preliminary identification of all the cut sets, an operation that is not trivial in dynamic cases, since the critical cut sets depend on the dynamic response and can therefore change from one time-history to the other.

In general, in the evaluation of Y_{SLC} there must be included at least the following sets:

- Single columns and squat walls:
  - collapse due to bending: relationship θ/θ_u with capacity given for example by the equation (4.10)
  - shear collapse; relationship V/V_u with capacity given for example by the equations (4.20) and (4.21)
- Storeys:
  - exceedance of the yield drift threshold by all the columns (a condition corresponding to an important decrease of the stiffness of the floor and to a localization of the displacement demand). For each column the relationship θ/θ_y is obtained, for example, using equation (4.5). For each storey, the storey drift is assumed as the minimum among the story columns.

5 Bibliographical references

5.1 Monographs and articles

Anthoine, A., Magonette, G., Magenes, G. 1995. Shear-compression testing and analysis of brick masonry walls, Proc. 10th European Conference on Earthquake Engineering, Wien, Austria, Duma editor, Balkema: Rotterdam, The Netherland.

Asteris, P.G., Antoniou, S.T., Sophianopoulos, D.S. & Chrysostomou, C.Z. 2011. Mathematical Macromodeling of Infilled Frames: State of the Art. *ASCE Journal of Structural Engineering*. 137(12), 1508-1517.

Baggio, C., Trovalusci, P. 1998. Limit analysis for no-tension and frictional three-dimensional discrete systems. *Mech Struct Mach*, 26(3), 287–304

Baker, J.W. 2014. Efficient analytical fragility function fitting using dynamic structural analysis. *Earthquake Spectra*

Belmouden, Y. & Lestuzzi, P. 2009. An equivalent frame model for seismic analysis of masonry and reinforced concrete buildings. *Construction and Building Materials*, 23, 40-53.

Bertoldi, S., Decanini, L.D. & Gavarini, G.C. 1993. Telai tamponati soggetti ad azioni sismiche. Un modello semplificato. Confronto sperimentale e numerico. ANIDIS VI, Perugia, Italia

Beyer, K. 2012. Peak and residual strengths of brick masonry spandrels. *Engineering Structures*. 41, 533-547.

Beyer, K., Dazio, A. 2012. Quasi-static monotonic and cyclic tests on composite spandrels. *Earthquake Spectra*, 28(3), 885-906.

Beyer, K., Dazio, A. 2012. Quasi-static cyclic tests on masonry spandrels. *Earthquake Spectra*, 28(3), 907-929.

Biskinis, D. & Fardis, M.N. 2010. Flexure-controlled ultimate deformations of members with continuous or lap-spliced bars. *Structural Concrete*, 11(2), 93-108.

Biskinis, D. & Fardis, M.N. 2010. Deformations at flexural yielding of members with continuous or lap-spliced bars. *Structural Concrete*, 11(3), 127-138.

Bradley, B., 2013, Ground motion selection for seismic risk analysis of civil infrastructure, Handbook of seismic risk analysis and management of civil infrastructure systems (Tesfamariam and Goda eds), Woodhead Publ. Ltd, UK, ISBN 978-0-85709-268-7

Calderini, C. & Lagomarsino, S. 2008. A continuum model for in-plane anisotropic inelastic behaviour of masonry. *ASCE Journal of Structural Engineering*, 134(2), 209-220.

Calderini, C., Cattari, S. & Lagomarsino, S. 2009. In-plane seismic response of unreinforced masonry walls: comparison between detailed and equivalent frame models, in Proc. of ECCOMAS Thematic Conference on Computational Methods in Structural Dynamics and Earthquake Engineering (COMPDYN 2009), Rhodes, Greece, 22-24 June 2009.

Caliò, I., Marletta, M. & Pantò, B. 2012. A new discrete element model for the evaluation of the seismic behaviour of unreinforced masonry buildings, *Engineering Structures*, 40, 327-338.

Casapulla, C., Maione, A. 2011. Out-of-plane local mechanisms in masonry buildings. The role of the orientation of horizontal floor diaphragms. *Proc. of 9th Australasian masonry conference*, Queenstown, New Zealand, pp 225–235

Cattari, S., Lagomarsino, S., 2008. A strength criterion for the flexural behaviour of spandrels in un-reinforced masonry walls. *Proc. of 14th WCEE*, Beijing, China, 2008.

Cattari, S. & Lagomarsino, S. 2013. Seismic assessment of mixed masonry-reinforced concrete buildings by non-linear static analyses. *Earthquakes and Structures*, 4(3), 241-264.

Chen, S.Y., Moon, F.L. & Yi, T. 2008. A macroelement for the nonlinear analysis of in-plane unreinforced masonry piers. *Engineering Structures*, 30, 2242-2252.

Chopra, A.K. & Goel, R.K. 2002. A modal pushover analysis procedure for estimating seismic demands for buildings. *Earthquake Engineering & Structural Dynamics*, 31(3), pp.561–582.

Clemente, P. 1998. Introduction to dynamics of stone arches. *Earthq Eng Struct Dynam*, 27(5), 513–522

Cornell, C. et al., 2002. Probabilistic basis for 2000 SAC Federal Emergency Management Agency Steel Moment Frame Guidelines. *Journal of Structural Engineering*, 128(4), pp.526–533.

D'Ayala, D., Speranza, E. 2003. Definition of Collapse Mechanisms and Seismic Vulnerability of Historic Masonry Buildings. *Earthq Spectra*, 19(3), 479–509

Decanini, L.D., Gavarini, G.C., Bertoldi, S. & Mollaioli, F. 1994. Modelo simplificado de paneles da mamposteria con aberturas incluidos en marquos de concreto renforzado y metalicos. Comparacion y calibracion con resultados experimentales y numericos. 9th Intnl Seminar on Earthq. Prognostics, San Josè, Costa Rica.

De Canio, G., Clemente, P., Mongelli, M., Roselli, I., Rinaldis, D., Saitta, F., Lagomarsino, S., Rossi, M. 2012. Performance based assessment of the obelisco lateranense in Rome, *Proc. of 8th International Conference on Structural Analysis of Historical Constructions (SAHC)*, October 15-17 2012, Wroclaw, Poland.

de Felice, G., Giannini, R. 2001. Out-of-plane seismic resistance of masonry walls. *J Earthq Eng*, 5(2), 253–271

Deliverable D26. 2012. Modelling strategies for seismic global response of building and local mechanisms. PERPETUATE (EC-FP7 Project), www.perpetuate.eu.

Doherty, K., Griffith, M.C., Lam, N.T.K. & Wilson, J.L. 2002. Displacement-based analysis for out-of-plane bending of seismically loaded unreinforced masonry walls. *Earthq Eng Struct Dynam*, 31(4), 833–850

Dolsek, M., Fajfar, P. 2005. Simplified non-linear seismic analysis of infilled concrete frames. *Earthquake Engineering and Structural Dynamics*, 34(1):49–66.

Elwood, K. 2004. Modelling failures in existing reinforced concrete columns. *Canadian Journal of Civil Engineering*, 31, pp.846–859.

Fragiadakis, M. & Vamvatsikos, D. 2010. Fast performance uncertainty estimation via pushover and approximate IDA. *Earthquake Engineering & Structural Dynamics*, 39, pp.683–703.

Gattesco, N., Clemente, I., Macorini, L., Noè, S. 2008. Experimental investigation on the behaviour of spandrels in ancient masonry buildings. *Proc. of 14th WCEE*, Beijing, China, 2008.

Grande, E., Imbimbo, M. & Sacco, E. 2011. A beam finite element for nonlinear analysis of masonry elements with or without fiber-reinforced plastic (FRP) reinforcements. *Int. J. Architectural Heritage*, 5, 693-716.

Graziotti, F., Magenes, G., Penna, A. 2012. Experimental cyclic behaviour of stone masonry spandrels. *Proc. of 15th WCEE*, Lisbon, Portugal.

Grunthal, G. 1998. European Macroseismic Scale. Centre Européen de Géodynamique et de Séismologie. Luxembourg. Vol. 15.

Han, S. & Chopra, A. 2006. Approximate incremental dynamic analysis using the modal pushover analysis procedure. *Earthquake Engineering & Structural Dynamics*, 35, pp.1853–1873.

Haselton, C.B., Liel, A.B., Taylor Lange, S. & Deierlein, G.G. 2008 Beam-Column Element Model Calibrated for Predicting Flexural Response Leading to Global Collapse of RC Frame Buildings, PEER report 2007/03.

Haselton, C.B. & Deierlein, G.G. 2007 Assessing Seismic Collapse Safety of Modern Reinforced Concrete Moment Frame Buildings, Blume center Technical report 156.

Housner, G.W. 1963. The behavior of inverted pendulum structures during earthquakes. *Bull Seismol Soc Am*, 53, 403–417

Ibarra, L.F., Medina, R.A. & Krawinkler, H. 2005. Hysteretic models that incorporate strength and stiffness deterioration. *Earthquake Engineering & Structural Dynamics*, 34(12), pp.1489–1511.

Jalayer, F., Franchin, P. & Pinto, P.E. 2007. A scalar damage measure for seismic reliability analysis of RC frames. *Earthquake Engineering & Structural Dynamics*, 36, pp.2059–2079.

Jalayer, F. & Cornell, C.A. 2009. Alternative non-linear demand estimation methods for probability-based seismic assessments. *Earthquake Engineering & Structural Dynamics*, 38, pp.951–972.

Kappos A.J., Penelis G.G. & Drakopoulos, C.G. 2002. Evaluation of Simplified models for lateral load analysis of unreinforced masonry buildings. *ASCE J. of Structural Engineering*, 128(7), 890-897.

Lagomarsino, S. 2014. Seismic assessment of rocking masonry structures, *Bulletin of Earthquake Engineering*, DOI:10.1007/s10518-014-9609-x.

Lagomarsino, S., Penna, A., Galasco, A. & Cattari, S. 2013. TREMURI Program: an equivalent frame model for the nonlinear seismic analysis of masonry buildings. *Engineering Structures*, 56, 1787-1799.

Lignos, D. & Krawinkler, H. 2012. Sidesway Collapse Of Deteriorating Structural Systems Under Seismic Excitations. Blume center Technical report 177.

Lin, T., Haselton, C. B., & Baker, J. W. (2013). Conditional spectrum-based ground motion selection. Part I: Hazard consistency for risk-based assessments. *Earthquake Engineering & Structural Dynamics*.

Lourenço, P.B., Rots, J.G. & Blaauwendraad, J. 1995. Two approaches for the analysis of masonry structures: micro and macro-modeling, *Heron*, 40(4), ISSN 0046-7316.

Lourenço, P.B., Milani, G., Tralli, A. & Zucchini, A. 2007. Analysis of masonry structures: review of and recent trends in homogenization techniques. *Canadian J. Civil Engineering*, 34, 1443-1457

Lowes, L.N., Mitra, N. & Altoontash, A. 2004. A Beam-Column Joint Model for Simulating the Earthquake Response of Reinforced Concrete Frames, PEER report 2003/10.

Magenes, G. & Della Fontana, A. 1998. Simplified non-linear seismic analysis of masonry buildings. *Proc. of the British Masonry Society*, 8, 190-195.

Makris, N., Konstantinidis, D. 2003. The rocking spectrum and the limitations of practical design methodologies. *Earthq Eng Struct Dyn*, 32(2), 265–289

Mann, W., Müller, H. 1980. Failure of shear-stressed masonry – An enlarged theory, tests and application to shear-walls. *Proc. Int. Symposium on Load-bearing Brickwork,* London, UK, 1-13.

Marques, L. & Lourenço, P.B. 2011. Possibilities and comparison of structural component models for the seismic assessment of modern unreinforced masonry buildings, *Computers and Structures*, 89, 2079-2091.

McKenna, F., Scott, M.H. & Fenves, G.L. 2010. Nonlinear Finite-Element Analysis Software Architecture Using Object Composition. *ASCE Journal Of Computing In Civil Engineering*24(1), pp.95-107.

Milani, G., Pizzolato, M. & Tralli, A. 2013. Simple numerical model with second order effect for the out-of-plane loaded masonry walls. *Eng Struct*, 48, 98–120

Orduña, A. & Lourenço P.B. 2005. Three-dimensional limit analysis of rigid blocks assemblages. Part II: load-path following solution procedure and validation. *Int J Solids Struct*, 42, 5161–5180

Pasticier, L., Amadio, C. & Fragiacomo, M. 2008. Non-linear seismic analysis and vulnerability evaluation of a masonry building by means of the SAP2000 V.10 code. *Earthquake Engineering & Structural Dynamics*, 37(3), 467-485.

Portioli, F., Casapulla, C., Cascini, L., D'Aniello, M. & Landolfo, R. 2013. Limit analysis by linear programming of 3D masonry structures with associative friction laws and torsion interaction effects. *Arch Appl Mech*, 83(10), 1415–1438

Rahnama, M. & Krawinkler, H. 1993. Effects Of Soft Soil And Hysteresis Model On Seismic Demands. Blume center Technical report 108.

Reyes, J. & Chopra, A. 2011. Three dimensional modal pushover analysis of buildings subjected to two components of ground motion, including its evaluation for tall buildings. *Earthquake Engineering & Structural Dynamics*, 40, pp.789–806.

Rots, J.G. 1991. Numerical simulation of cracking in structural masonry, *Heron* 36(2), 49-63.

Salonikos, T., Karakostas, C., Lekidis, V. & Anthoine, A. 2003. Comparative inelastic pushover analysis of masonry frames. *Engineering Structures*, 25, 1515-1523.

Scott, M.H. & Fenves, G.L. 2006. Plastic hinge integration methods for force-based beam–column elements. *ASCE Journal of Structural Engineering*. 132, 244-252.

Sezen, H. & Mohele, J.P. 2004. Shear Strength Model for Lightly Reinforced Concrete Columns. *ASCE Journal of Structural Engineering*. 130(11), 1692-1703.

Turnšek, V., Čačovič, F. 1970. Some experimental results on the strength of brick masonry walls. *Proc. of the 2nd International Brick Masonry Conference,* Stoke-on-Trent, 1149-156.

Turnšek, V., Sheppard, P. 1980. The shear and flexural resistance of masonry walls. *Proc. Int. Research Conference on Earthquake Engineering*, Skopje, Japan, 517-573.

Vaculik, J., Griffith, M.C. & Magenes, G. 2012. Dry stone masonry walls in bending - part II: analysis. *Int J Archit Herit*. doi:10.1080/15583058.2012.663060

Vamvatsikos, D. & Cornell, C.A. 2002. Incremental dynamic analysis. *Earthquake Engineering & Structural Dynamics*, 31(3), pp.491–514.

Vamvatsikos, D. & Cornell, C. 2005. Direct Estimation of Seismic Demand and Capacity of Multidegree-of-Freedom Systems through Incremental Dynamic Analysis of Single Degree of Freedom. *Journal of Structural Engineering*, 131(4), pp.589–599.

Zhu, L., Elwood, K. & Haukaas, T. 2007. Classification and seismic safety evaluation of existing reinforced concrete columns. *Journal of Structural Engineering*, (September), pp.1316–1330.

5.2 Norms and technical guidelines

(ASCE/SEI 41/06) American Society of Civil Engineers, Reston –VA, 2007. “Seismic Rehabilitation of Existing Buildings”

(NTC2008) Ministero Infrastrutture, 2008. D.M.14/1/2008 “Norme Tecniche per le Costruzioni” (Testo integrato con la Circolare n°617/C.S.LL.PP. del 2/2/2009)

(EC8-3) Comité Européen de Normalisation, 2005. “Eurocode 8: Design of structures for earthquake resistance - Part 3: Assessment and retrofitting of buildings”

(NZSEE 2006) New Zealand Society for Earthquake Engineering 2006. “Assessment and Improvement of the structural performance of buildings in earthquake, Recommendation of a NZSEE study group, Wellington, New Zealand.

A Comments to the text of the Guide

A.1 Reliability basis of evaluation methods (Comment on §2)

From the formal perspective of structural reliability theory, the problem of evaluating the average annual frequency of exceedance of a limit state λ_{SL} can be posed in the following terms.
All sources of uncertainty which appear in the problem (geometry and activity of seismogenic sources, mechanical characteristics of the wave propagation path, including the upper soil layers at the site, and of the structure, epistemic uncertainty in all models) are described by means of random variables grouped in a vector **x**. This vector is characterised probabilistically by its probability distribution, expressed for example by means of a joint density function $f(\mathbf{x})$.
To check for violation of the limit state, one may use a function of **x**, formulated so that its value is one when the limit state is violated and zero in other cases, called the limit state "indicator" function $I_{SL}(\mathbf{x})$.
Simulation is the most robust method for determining the frequency λ_{SL}: it is based simply on a large number of experiments and observation of the results, followed by their statistical analysis.
The methods considered in this Guide belong to a specific subset of simulation methods, the effectiveness of which is based on the use of a hazard curve $\lambda_S(s)$, i.e. the marginal distribution of a seismic action intensity parameter S, and of a set of motion time histories to describe the variability of the seismic action, given the same value of S.
This section outlines the general Monte Carlo simulation approach and its specialised application to the problem under consideration, framing the methods proposed in this Guide within a broader theoretical context.

The probability of an event E, defined as the union of mutually exclusive elementary events e_i, is equal, according to the axioms of probability, to the sum of the probabilities of the elementary events: $p_E = \sum p_{ei}$.
If the event in question is the violation of the limit state, and the generic elementary violation event e_i corresponds to the occurrence of the value **x** of the random variables, and hence $p_{ei} = f(\mathbf{x})d\mathbf{x}$, the probability of the compound event can be written in integral form as:

$$p_{SL} = \int_{\mathbf{x}\in SL} f(\mathbf{x})d\mathbf{x} \tag{A.1}$$

where SL indicates the portion of the space of the random variables where the limit state is violated.
The preceding integral equation can be rewritten introducing the function $I_{SL}(\mathbf{x})$:

$$p_{SL} = \int_{\mathbf{x}\in SL} f(\mathbf{x})d\mathbf{x} = \int I_{SL}(\mathbf{x}) f(\mathbf{x})d\mathbf{x} = \mathrm{E}\left[I_{SL}(\mathbf{x})\right] \tag{A.2}$$

in which the integration is extended to the entire space of the random variables. It can be observed that the probability of exceedance of the limit state coincides in the preceding equation with the expected value of the function $I_{SL}(\mathbf{x})$.
The Monte Carlo simulation amount to the estimation of the previous expected value by means of the arithmetic mean across a sufficiently high number of samples of **x**:

$$p_{SL} = \mathrm{E}\left[I_{SL}(\mathbf{x})\right] \cong \frac{1}{N}\sum_{i=1}^{N} I_{SL}(\mathbf{x}_i) = \frac{N_{SL}}{N} = \hat{p}_{SL} \qquad \text{(A.3)}$$

It can be shown that the estimator $\hat{p}_{SL}$ converges to p_{SL}, and that the variance around its mean p_{SL} decreases with N and is proportional to p_{SL} itself:

$$\mathrm{Var}\left[\hat{p}_{SL}\right] = \frac{p_{SL}(1-p_{SL})}{N} \qquad \text{(A.4)}$$

An important result that can be derived is the rule which provides the minimum number N of simulations required to obtain a given confidence in the estimate[19]:

$$N \geq 10\frac{1-p_{SL}}{p_{SL}} \cong \frac{10}{p_{SL}} \qquad \text{(A.5)}$$

Such a result is immediately justified in qualitative terms too, since being $\hat{p}_{SL} = N_{SL}/N$, if p_{SL} and therefore $\hat{p}_{SL}$ are very small, violation of the limit state is clearly a very rare event and an extremely high number of simulations (N) is required to obtain a number (N_{SL}) of results that are favourable to the event itself.

The average annual frequency of exceedance of the structural limit state λ_{SL} is determined as follows. The probabilistic model (joint distribution) $f(\mathbf{x})$ contains a portion relating to seismogenic sources from which events can be sampled in terms of location, magnitude and other parameters such as the faulting mechanism, etc. The model normally includes several sources, which are indexed by i. If λ_i is the mean annual rate of events[20] generated in the i^{th} source, we may write:

$$\lambda_{SL} = \sum_{i=1}^{N} \lambda_i p_{SL|i} = \lambda_0 \sum_{i=1}^{N} (\lambda_i/\lambda_0) p_{SL|i} = \lambda_0 \sum_{i=1}^{N} p_{SL|i} \cdot p_i = \lambda_0 p_{SL} \qquad \text{(A.6)}$$

where $\lambda_0 = \sum_{i=1}^{N} \lambda_i$ is the overall event generation rate in the area that has an effect on the site of interest, $p_i = \lambda_i/\lambda_0$ is the probability that the event is generated by the i^{th} source, and p_{SL} is the probability that the limit state is violated, conditioned on the occurrence of an event in any one of the sources. The Monte Carlo simulation is used to determine p_{SL}. To this end the probabilistic model $f(\mathbf{x})$ also contains the portions relating to the determination of the seismic motion at the site, given the event, and to the response and capacity of the structure. Fig. A-1 illustrates the simulation process with reference to the generic event i. The simulation begins with the sampling of the active seismogenic zone Z (the first random variable in the vector $\mathbf{x}$), followed by sampling of the magnitude of the event M and the epicentre E. From the positions of epicentre and site, the distance R is calculated. The values of M and R constitute the minimum information needed to implement a stochastic motion model, which is used to produce artificial time histories of seismic motion at the site (such models often filter and modulate a random stationary acceleration time history with uniform frequency content, termed "white noise" and denoted as $\mathbf{x}_5$ in the figure, in order to match target

[19] In particular, equation A.5 ensures a probability of 30% of the estimate $\hat{p}_{SL}$ falling within the interval $(1 \pm 0.33)\, p_{SL}$

[20] The average annual rate of events is the (only) parameter of the Poisson distribution implicitly assumed in the whole document as a model for describing the temporal frequency of events. This assumption is at the basis of the most up-to-date seismic hazard analysis on a national scale.

frequency content and duration compatible with M and R). The subsequent phases involve the determination of the motion at the surface and of the corresponding structural response, by means of the relevant models. The uncertainty on the mechanical characteristics of the site and of the structure, as well as that on all models parameters, are included in the vector **x** through the sub-vectors $\mathbf{x}_4$, $\mathbf{x}_6$ and $\mathbf{x}_7$.

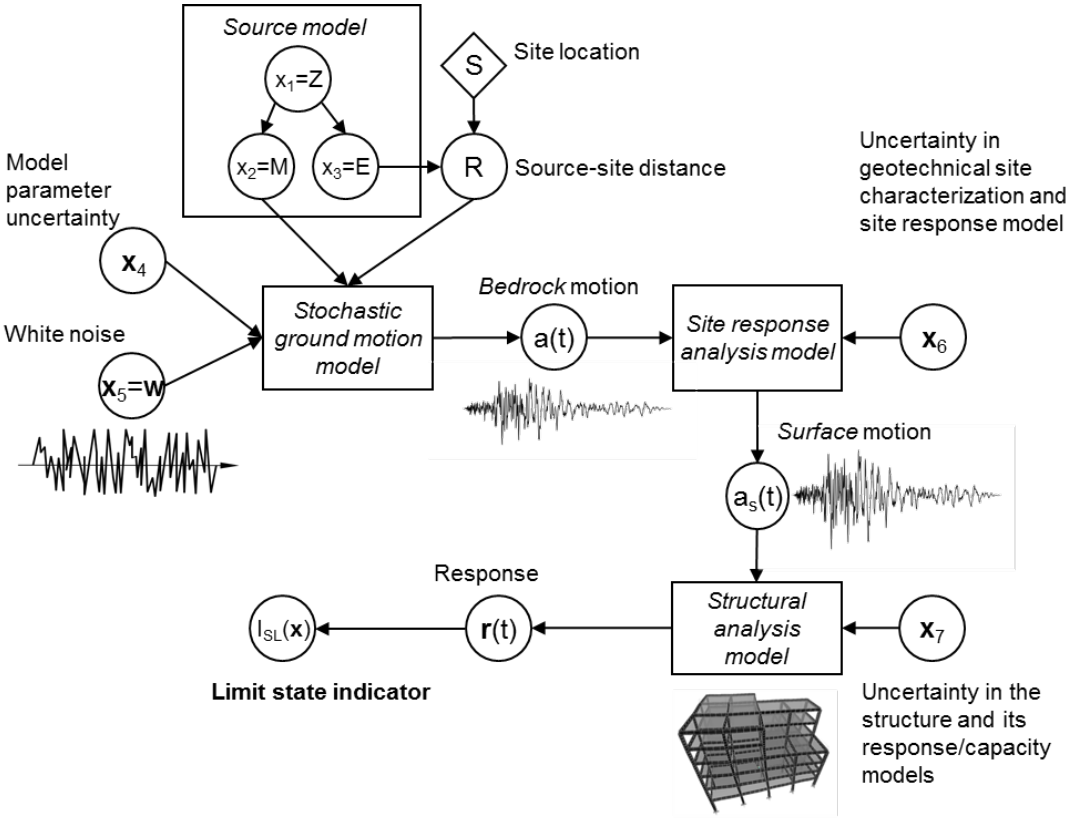

Fig. A-1 Diagram of simulation procedure with reference to generic event.

Calculation of the mean annual frequency in accordance with the procedure just described generally requires – as mentioned above – a very high number of simulations. For example, for a value of $\lambda_{SL} = 10^{-3}$, which corresponds to a mean return period for violation of the limit state equal to $T_{R,SL} = 1000$ years, the number of simulations in accordance with Eq. (A.5) in the order of 10000 (λ_{SL} and p_{SL} are numerically coincident for values of $\lambda_{SL} < 0.1$).

To reduce the number of simulations, it is necessary to act on the variance of the estimator $\hat{p}_{SL}$. Various techniques, termed *variance reduction techniques*, exist for this purpose. Some of these techniques consist in setting the value – which is then varied parametrically – of a number of the variables (conditioning), thus performing a series of lower-order simulations before removing the conditioning by weighting the results obtained with the probability of occurrence of the values of the variables for which conditioning was applied (total probability theorem).

The methods considered in this Guide belong to this category, and are based on the following rewriting of Eq. (A.6):

$$\lambda_{SL} = \sum_{i=1}^{N} \lambda_i p_{SL|i} = \sum_{i=1}^{N} \lambda_i \int_0^{\infty} p_{SL|S}(s) f_{S|i}(s) ds = \int_0^{\infty} \underbrace{p_{SL|S}(s)}_{fragility} \underbrace{\sum_{i=1}^{N} \lambda_i f_{S|i}(s)}_{hazard} ds \quad \text{(A.7)}$$

the last member of which coincides with Eq. (2.12) provided in §2.6.1. The main advantage of this formulation is that it separates the contributions of the seismicity of the site in question at the frequency λ_{SL} and the fragility of the structure. As the predominance of the former contribution over the latter is well known and verified, this separation introduces the possibility of making an approximate – and thus "economical", in computational terms – estimation of the fragility curve $p_{SL}(s)$. Different approaches to estimating the parameters of the fragility curve exist. The main alternatives available given the current state of the art are described in the next section.

A.1.1 Alternative approaches to determining the fragility curve (Comment on §2.6)

The average annual frequency of exceedance of the limit state is calculated by means of the integral of the total probability (2.12), which requires the fragility curve of the structure $p_{SL}(s)$ to be known.
In the literature, an alternative approach to the one represented by Eq. (2.14) for calculating $p_{SL}(s)$ can also be found. This approach uses a direct definition of the fragility curve:

$$p_{SL}(s) = p\left(Y_{SL} \geq 1 \middle| S = s\right) = 1 - \Phi\left(\frac{\ln 1 - \mu_{\ln Y|S=s}}{\sigma_{\ln Y|S=s}}\right) = \Phi\left(\frac{\mu_{\ln Y|S=s}}{\sigma_{\ln Y|S=s}}\right) \qquad \text{(A.8)}$$

where, by making the usual assumption of lognormal distribution for the limit-state variable, the parameters to be determined are the mean $\mu_{\ln Y|S=s}$ and the standard deviation $\sigma_{\ln Y|S=s}$ of the logarithm of the limit-state variable Y_{SL} conditioned on the intensity level $S = s$.
Figure A-2 illustrates how the fragility curve is determined starting from the IDA curves, using either Eq. (2.14) or Eq. (A.8). The first case (vertical section in the response-intensity plane) uses the distribution of the seismic intensity values S which lead to the limit state (Y_{SL}=1), while the second (horizontal sections in the response-intensity plane) is based on the distribution of the values of Y_{SL} associated with a fixed seismic intensity ($S = s$) (Vamvatsikos & Cornell, 2002).
The parameters $\mu_{\ln Y|S=s}$ and $\sigma_{\ln Y|S=s}$ of the distributions conditioned on $S = s$ can be obtained both from horizontal segments of the IDA curves and from the result of analyses conducted by scaling the selected records to increasing $S = s$ levels. In the literature, this procedure is called MSA (Multiple Stripe Analysis) and is described, for example, in (Jalayer & Cornell, 2009). A conceptual advantage of MSA over IDA is that use can be made of a different selection of seismic motions for each stripe, which more accurately reflects the characteristics of the events that primarily determine the hazard at the intensity level considered. However, this approach requires specialist skills and tools for selecting the motions, which make it less attractive in practical terms (Bradley, 2013) (Lin et al, 2013).
The fragility curves provided by the two methods are nevertheless very similar to each other, as shown for instance in (Jalayer et al, 2007). The important difference regards the computational efficiency of the alternative approaches. A recent discussion of the advantages and disadvantages of the two techniques can be found in (Baker, 2014).

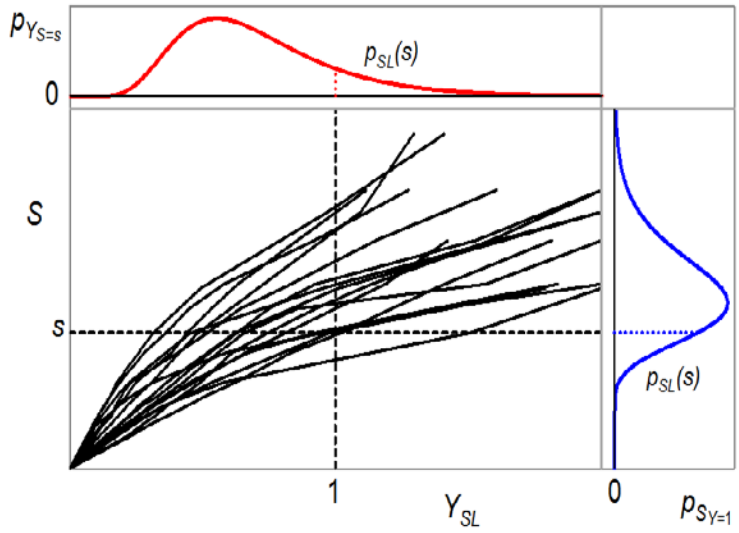

Fig. A-2 Evaluation of fragility starting from the IDA curves using Eqs. (2.14) and (A.8).

A.1.1.1.1 Example with reference to Method C

This section provides an example of the horizontal-section approach by specialising it to the case of Method C. In this case, the method required *n* distinct probability distributions of the variable Y_{SL} to be known for the *n* values of seismic intensity considered, i.e. the estimation of the parameters $\mu_{\ln Y|S=s}$ and $\sigma_{\ln Y|S=s}$. This variant is therefore more laborious in terms of processing the data, although it is easy to automate. However, it does not increase the computational burden as the pushover analyses that need to be performed are the same. The total probability integral, in this case, must necessarily be calculated in numerical form.

Calculation of the median of Y conditioned on S

For each value of seismic intensity $S=s_i$ (i=1,…,n), the median of Y_{SL} is obtained by considering the seismic action and the capacity curve used in §2.6.4.2.
The mean value $\mu_{\ln Y|S=s}$ of the logarithm of Y_{SL} is determined by calculating the displacement *demand* with the median spectrum (50% fractile) of the motions selected in accordance with §2.2.2, scaled to intensity $S = s_i$, and relating it to the displacement *capacity* corresponding to the limit state under consideration (§3.4 o §4.4) on the median capacity curve.

Calculation of uncertainty in seismic demand β_S

For each value of seismic intensity $S=s_i$ (i=1,…,n), the term β_S is calculated – assuming lognormal distribution of Y conditioned on S, as a function of the values $Y_{SL,16}$ and $Y_{SL,84}$ of Y_{SL} calculated, on the median capacity curve, using the 16th and 84th fractile response spectra of the time histories selected in accordance with §2.2.2, scaled to the intensity $S = s_i$:

$$\beta_S = \frac{\ln Y_{SL,84} - \ln Y_{SL,16}}{2} \tag{A.9}$$

Figure A-3 shows the values to be used to calculate β_S by means of Eq. (A.9), compared with those used to calculate dispersion in the case of the method described in §2.6.4.2.

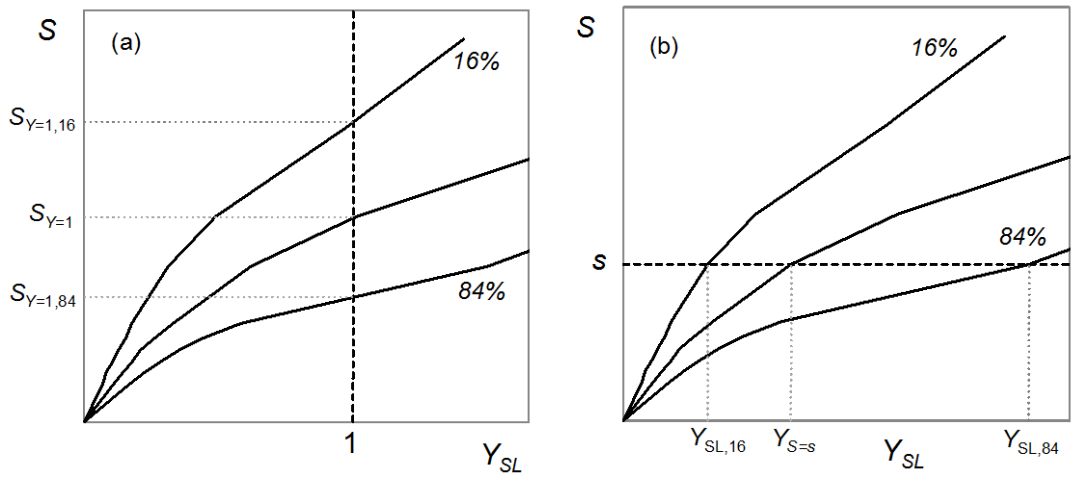

Fig. A-3 Calculation of β_S in the two methods by means of the formulas illustrated in: a) Eq. (2.17); b) Eq. (A.9).

Calculation of uncertainty in capacity β_C

For each value of seismic intensity $S=s_i$ (i=1,…,n), the influence on the variable Y_{SL} of the continuous random variables (§2.3.2.1) relating to the mechanical and geometric properties of the structure is estimated by means of a linear response surface:

$$\ln Y_{SL} = \alpha_0 + \sum_{k=1}^{N} \alpha_k x_k + \varepsilon \tag{A.10}$$

which expresses the logarithm $ln(Y_{SL})$ in the space of the normalised random variables x_k, defined in §2.6.4.3 by Eq. (2.18). Calculation of β_C then proceeds in the same way as for the case of vertical sections.

A.2 The need to verify the limit state for the prevention of collapse (Comment on §2.1)

The design of new buildings entails compliance with a series of requirements which ensure a high degree of overall ductility. Therefore, a positive outcome of the severe damage limit state (SLS) verification implies also an adequate margin of protection with respect to the limit state for the prevention of collapse (SLC).[21] This is usually not the case for existing structures, which not infrequently exhibit a behaviour such as that shown in Fig. A-4, where safety for the SLS does not imply satisfaction of the SLC verification, which then needs to be checked explicitly.

[21] This is also why many technical standards refer to the severe damage limit state as the life safety limit state, since it is used as a proxy for the collapse one.

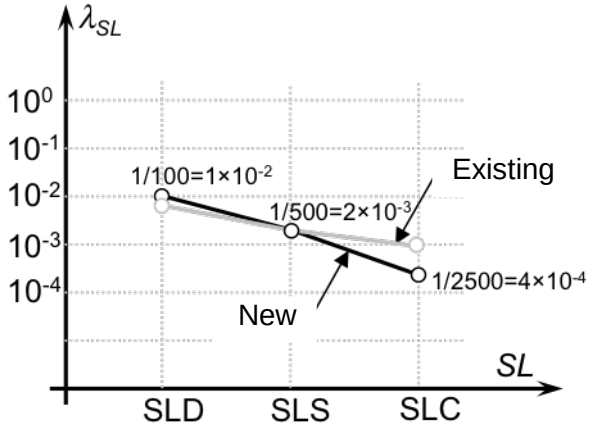

Fig. A-4 Variation in average annual frequency of exceedance of limit states for new and existing buildings.

A.3 Remarks on epistemic uncertainty in the seismic hazard curve (Comment on §2.2)

The seismic hazard curve for the site $\lambda_S(s)$ which appears in the integral (2.12) of the risk is itself characterised by epistemic uncertainty. The sources of this uncertainty include, for example, the definition of the boundaries of seismogenic zones, of the lower and upper limit values for magnitude in each zone and the different available attenuation laws. The treatment of such uncertainties by means of a logic tree is an integral part of the probabilistic analysis of seismic hazard. The results are usually reported in terms of a median curve $\lambda_{S,50\%}(s)$ and fractile curves, for example $\lambda_{S,16\%}(s)$ e $\lambda_{S,84\%}(s)$. Fig. A-5 shows, for illustrative purposes, the logic tree used to determine the seismic hazard in Italy in the study conducted for the purpose of drawing up a seismic hazard map according to the Prime Ministerial Order 3274/2003 (OPCM), in which the parameters considered are:

1. ranges of completeness of the earthquake catalogue
2. ranges of the maximum magnitude for each source
3. use of different attenuation relationships.
4. use of different definitions of magnitude

The weight of each branch (each branch leads to a hazard map for the whole country) appears in the right-hand column. The results have been presented in the form of median and fractile maps of peak ground acceleration.

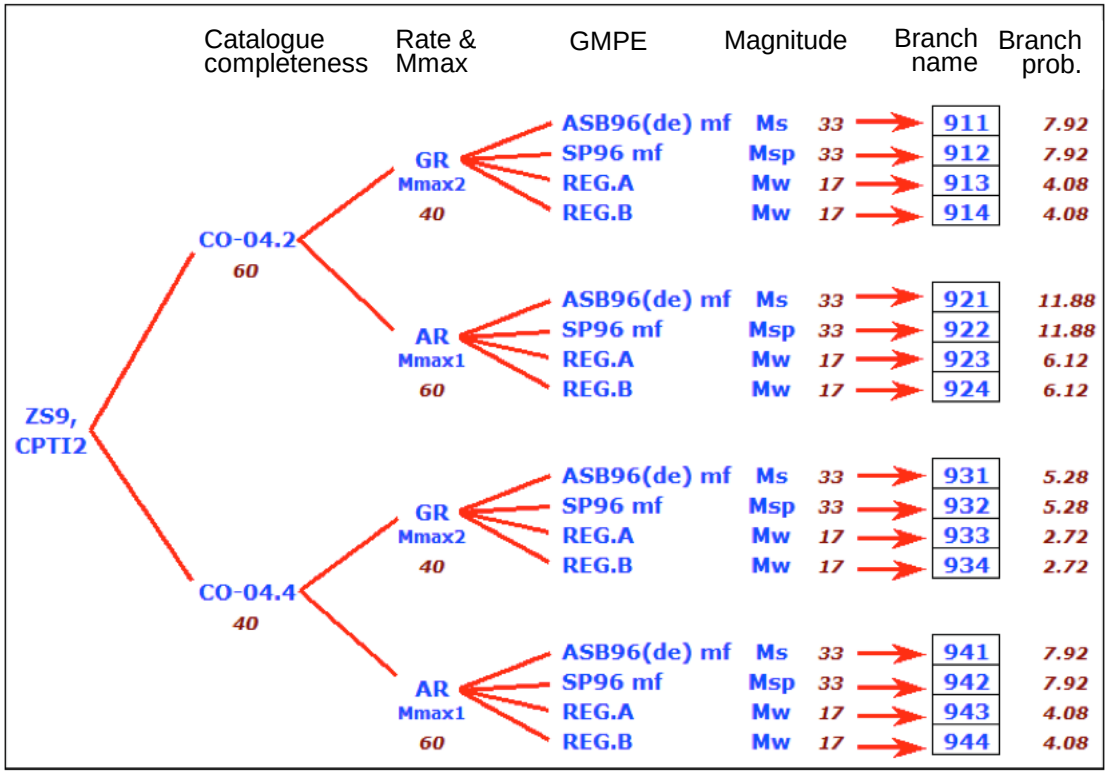

Fig. A-5 Logic tree used in (INGV, 2004) to determine distribution of peak ground acceleration.

If in the integral (2.12) we introduce the epistemic uncertainty associated with determination of the seismic hazard curve, represented by means of a random variable ε_H, the expected value of the risk with respect to the epistemic uncertainty on the hazard takes the following form:

$$\lambda_{SL} = \int_0^\infty \left[\int_0^\infty p_{SL}(s) \left| \frac{d\lambda_S(s,\varepsilon_H)}{ds} \right| ds \right] f(\varepsilon_H)\, d\varepsilon_H \qquad \text{(A.11)}$$

As the fragility curve $P_{SL}(s)$ is not dependent on the variable ε_H, it is possible to change the order of integration and, under suitable conditions of regularity, the order of integration with respect to ε_H with the order of derivation in respect of s, obtaining:

$$\lambda_{SL} = \int_0^\infty p_{SL}(s) \left[\int_0^\infty \left| \frac{d\lambda_S(s,\varepsilon_H)}{ds} \right| f(\varepsilon_H)\, d\varepsilon_H \right] ds =$$

$$= \int_0^\infty p_{SL}(s) \left| \frac{d\left[\int_0^\infty \lambda_S(s,\varepsilon_H)\, f(\varepsilon_H)\, d\varepsilon_H \right]}{ds} \right| ds = \int_0^\infty p_{SL}(s) \left| \frac{d\overline{\lambda}_S(s)}{ds} \right| ds \qquad \text{(A.12)}$$

in which the internal integral represents the expected value with respect to the distribution of ε_H of the derivative of the hazard curve, assumed equal to the derivative of the mean (i.e., unconditioned with respect to ε_H) hazard curve.
Assuming for the variable ε_H a lognormal distribution (Cornell *et al*, 2002) it is possible to obtain the mean hazard curve $\overline{\lambda}_S(s)$ starting from the median hazard curve $\lambda_{S,50\%}(s)$ by means of the following equation:

$$\overline{\lambda}_S(s) = \lambda_{S,50\%}(s)\exp\left(\frac{1}{2}\beta_H^2\right) \qquad \text{(A.13)}$$

which corresponds to Eq. (2.2) in §2.2.

The standard deviation of the logarithm of ε_H, $\beta_H = \sigma_{\ln \varepsilon_H}$ is actually not constant with variation in intensity *S*. It can then be estimated in approximation starting from the median and from a fractile value of λ_S around the intensity $S = s_{\lambda_{SL}}$ which corresponds on the median hazard curve to the risk value λ_{LS} calculated with Eq. (2.12).

A.4 Criteria for choosing seismic motion time histories (Comment on §2.2.2)

In current professional practice, the most advanced procedure used to select seismic signals for the purpose of non-linear dynamic analysis of structures consists of four stages (represented graphically in Fig. A-6). They involve:

1. obtaining – starting from a probabilistic analysis of the seismic hazard of the site under examination – the design elastic spectrum for the limit state considered: for example the uniform hazard spectrum[22] (UHS);
2. obtaining, from the *disaggregation of seismic hazard*, the magnitude-distance pairs (also called *design earthquakes*) which contribute most to the mean frequency of exceedance of a chosen threshold of the spectrum ordinate associated with the fundamental period of the structure;[23]
3. accessing a database of accelerograms to identify groups of records with similar characteristics (magnitude and distance) to those derived from the disaggregation. This ensures that, as an initial approximation, the accelerograms selected are consistent with the source and propagation characteristics that are most *important* for the seismic activity of the site in question;
4. Finally, selecting from among them the accelerograms which not only come from events that are similar to design earthquakes but also have a spectral shape that is similar to that of the reference elastic spectrum, for example by imposing on the mean spectrum of the records, including those that are *scaled*[24] in amplitude, an assigned degree of spectral compatibility in a range of periods.

[22] The UHS is the spectrum whose ordinates all have the same probability of being exceeded during the time interval concerned (e.g. fifty years). These spectra are often assumed by codes as elastic design spectra. However an UHS does not represent the spectrum of any specific earthquake, as it accounts for all of the possible earthquakes (for example in terms of magnitude and distance) involved in the hazard analysis for the site in question. Alternatives which enable this limitation to be overcome do, however, exist.

[23] Disaggregation often leads to at least one design earthquake being identified for each of the sources involved in the hazard analysis for the site in question. Strictly speaking, for each design earthquake identified, it is necessary to use an independent sample of accelerograms as, despite the fact that they contribute to the exceedance of the same spectrum ordinate, they represent earthquakes which differ in terms of other characteristics (e.g. significant duration). Furthermore, design earthquakes change according to the spectrum ordinate and the return period considered. Finally, it should be noted that in addition to magnitude and distance from source, often disaggregation is expressed in terms of *epsilon* (ε). This parameter measures the degree to which the spectrum for the reference earthquake deviates from the one predicted *on average* for the design earthquake in question.

[24] Scaling linearly in amplitude means simply multiplying the accelerograms by the ratio between the value of the design spectrum that it is desired to achieve and the value of the accelerogram before it is scaled.

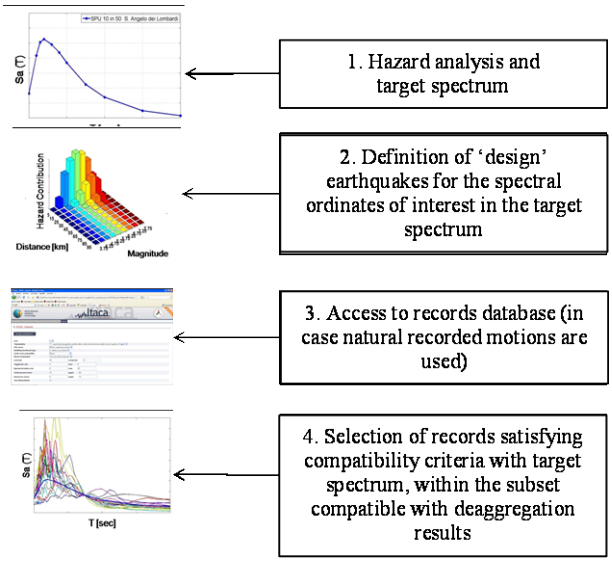

Fig. A-6 Fundamental steps in the process of selection of seismic motion time histories.

The procedure described above requires that the selection process be based on design earthquakes and the spectral shape. Magnitude and distance influence the spectral shape, and the latter (in particular around the fundamental period) contains a large quantity of information regarding the evaluation of the seismic response of multi-degree-of-freedom non-linear structures, especially in terms of deformation parameters. It might therefore seem superfluous to seek accelerograms with magnitude and distance obtained from disaggregation, as opposed to selecting them in order to have a spectral shape similar to the reference shape. On the other hand, it should be observed that considering also earthquake accelerograms obtained from disaggregation helps to ensure that, in selecting time histories, account is also implicitly taken of certain intensity measures of the shaking which are not represented in the elastic spectrum (e.g. significant duration and/or potential for inducing cyclic damage), which depend more directly on the characteristics of the source and propagation of the seismic waves.[25]
The importance of the spectral shape in the selection also explains why it is appropriate to make the spectra of the individual accelerograms as similar as possible to the reference spectrum, at least around the fundamental oscillation period of the structure. This in fact helps to reduce variability in the seismic response of the structure *from accelerogram to accelogram*, which means being able to evaluate the behaviour of the structure conditioned on the scenario, with less uncertainty (or, equivalently, with greater confidence), for the same number of analyses.

The procedure discussed, despite representing the best current practice for defining shaking time histories, does not take into account of the so-called *near-field* phenomena, although these are significant for seismic design. Indeed, when a seismic event occurs, the zones near the source may be influenced by the effects of the *directionality of the source*. Such effects are connected to the prevailing directions of propagation of the fracture and the slip of the fault. Because of these, ground motion at a site that is in certain specific geometric conditions in proximity to the source, and particularly the time history of velocity in an orthogonal direction to the fault, during the initial

[25] Representing the cyclic damage potential of an earthquake is important especially for structures characterised by degrading constitutive laws, as is often the case with existing structures. Nevertheless, it has been shown that only structures with strongly degrading characteristics are actually sensitive to parameters connected with the duration of the shaking.

phases of the signal may exhibit a low-frequency cycle (*impulse*) in which is contained most of the energy that the entire signal carries with it.
What actually happens is schematically represented in Fig. A-7a, for the sake of simplicity with regard to a hypothetical strike-slip fault. It can be stated, roughly but effectively, that discretising the fracture into point-localised sources of mechanical waves, the initial zone of the fracture is the first to radiate towards the site while the subsequent parts radiate afterwards but have less distance to cover, this may cause *constructive interference* of the seismic waves and therefore the formation of a low-frequency, high-energy impulse (Site 2). Far from the source or for sites which the fracture moves away from, this effect is lost and the energy carried by the signal is distributed more uniformly (Site 1).
In cases where it occurs, the impulse brings about the amplification only at the frequencies of the signal that approximate the impulse period (defined as Tp), as schematically represented in Fig. A-7b. It will be noted that directionality implies a systematic variation in the spectral shape compared with earthquakes which do not exhibit these characteristics (so-called *ordinary* earthquakes), and therefore how it can be significant for the selection of time histories based on the spectral shape. Generally, in fact, the impulse period Tp falls within the range of periods of structural relevance (0.0 s ÷ 3.0 s) and even the structures that have a fundamental period equal to a certain fraction of the impulse period (e.g. 0.4 ÷ 0.5) may be subjected to an anomalous elastic as well as inelastic demand, where the anomaly is intended in relation with the demand from ordinary earthquakes.
The current state of the art in research provides models which make it possible to modify (at least theoretically) standard seismic hazard analysis to account for any directional phenomena, and thus readapt the selection procedure described above to take the phenomenon into account.[26] However, near-field hazard analyses require highly detailed yet often unavailable information about individual faults. Explicit modelling of directional effects would therefore seem only feasible for critical infrastructures, where a more detailed knowledge of the seismogenic characteristics of the region is necessary to guarantee a very high level of safety.

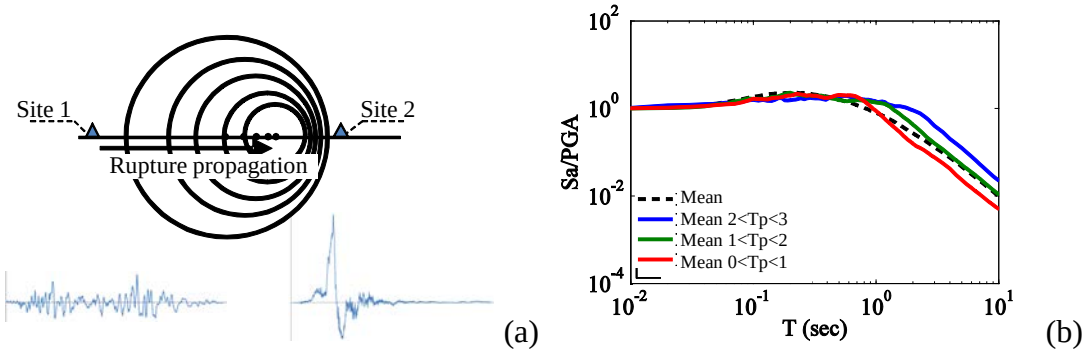

Fig. A-7 (a) Simplified illustration of the impulsive effects of directionality and example relating to the Landers earthquake, California (1992). (b) Mean elastic acceleration spectra in the case of impulsive and ordinary signals; all of the spectra are normalized to the same PGA values. Note the systematic difference around the pulse period.

[26] This requires the probability, based on site-source geometry. of observing impulsive signals, to be evaluated. It also needs empirical relationships between event magnitude and impulse period. Apart from these modifications, *near-field hazard* analysis proceeds in the same way as standard analysis. Its disaggregation, in fact, enables Tp to be added to the parameters which identify design earthquakes. Thus the procedure schematically illustrated in Fig. A-6, at least in principle, may be adapted to take impulsive signals into account.

A.5 Determination of the overall state of a structure from the state of its component parts (Comment on §2.5.3 and §4.6.2)

As observed in the Introduction (§1), the step from the qualitative description of the various limit states to an explicit definition of them with reference to the state of all of their structural components often leaves room for margins of subjective interpretation which may significantly affect the outcome of the evaluation. Moreover, the situation varies according to the limit state in question (§2.5). With regard to the collapse limit state, as already stated in §2.5.3, two formulations are possible. The second, which is adopted in the case of modelling with non-degrading constitutive laws, is based on an expression which aggregates the local D/C ratios of the structural elements (Jalayer et al. 2007):

$$Y_{SLC} = \max_{i=1,N_S} \min_{j \in I_i} \frac{D_j}{C_{j,SLC}} \tag{2.8}$$

where N_s is the number of sub-systems and I_i is the set of components in the i^{th} sub-system. The formulation of Y shown is based on the breakdown of the structure into a *series* of sub-systems made up of components arranged in *parallel*. Failure in a parallel sub-system occurs when *all* of its components exceed the corresponding capacity and, given the connection in series of the sub-systems, failure of *a single one* of them is sufficient to bring about the failure of the whole system.
The definition can be justified by observing that choosing the minimum *D/C* ratio in a given sub-system implies that the remaining components are in "worse" conditions; if in any case this minimum is still less than one, the sub-system does not fail. The system, in contrast, fails when the maximum of the minima reaches the value of one.
Fig. A-8 illustrates how the value of Y is calculated with reference to a simple two-storey, two-bay frame. In the example, for illustrative purposes, structural collapse may occur through a ductile mechanism of generalised loss of stiffness on one storey (the "weak storey": in the example two mechanisms of this type are possible), corresponding to generally high, uncontrollable maximum and residual deformations, or as a result of fragile shear failure of members. Ultimately there are eight mechanisms in series: the soft storey at the first level, soft storey at the second level, and six shear failure mechanisms. The soft storeys in turn constitute sub-systems in parallel which require the plastic deformation of all of the members of the storey. The figure illustrates the *D/C* values for each elementary component and the corresponding aggregation into Eq. (2.8).

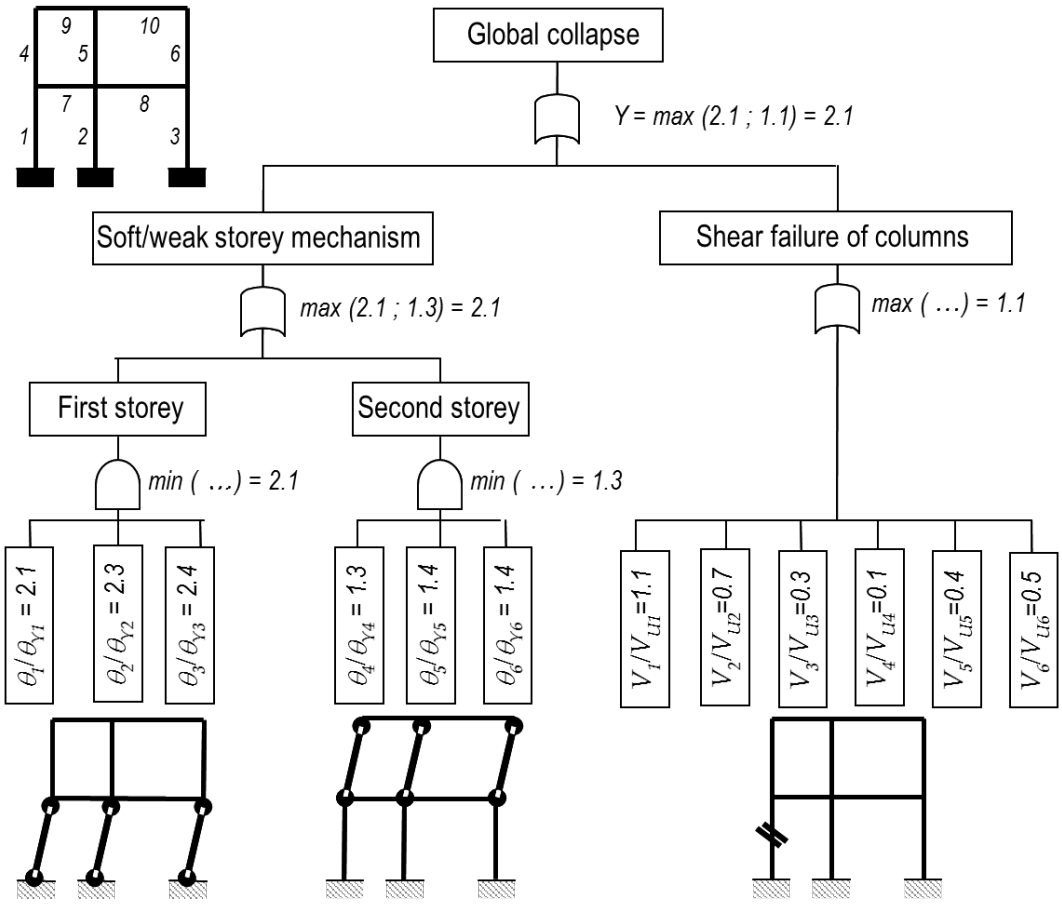

Fig. A-8 Representation of structural failure as a combination of alternative sub-systems (mechanisms).

It should also be noted that the above mentioned formulation for structures of realistic dimensions becomes particularly laborious as, strictly speaking, it requires all possible failure mechanisms to be considered (sub-systems in parallel). Finally, it should also be added that that the previous considerations refer to problems that are static in nature. Under highly non-linear behaviour the critical mechanisms cannot be determined *a priori*, as they depend of the response of the structure, which is in turn strongly influenced by the frequency characteristics of each individual motion.
In practice, in the case of the collapse limit state it is frequently assumed for the sake of simplification that the critical mechanism consists in the collapse of the weakest element, i.e.:

$$Y_{SLC} = \max \frac{D_j}{C_{j,SLC}} \tag{A.14}$$

which means having the collapse coinciding with the beginning as opposed to the end of the downward-sloping section of the curve (c) in Fig. 2-5. The degree of approximation associated with this choice is variable and highly dependent on the importance of the critical element to the global equilibrium.

A.6 Quantification of limit states in irregular masonry buildings for methods B and C (Comment on §3.2.1.5 and §3.3.1)

Simulation of the seismic behaviour of irregular buildings using methods B and C requires the definition of several equivalent non-linear oscillators and the correct combination of their responses.
In cases where for a given mode significant torsional effects are present (i.e. the ratio between the minimum and maximum participation factors is greater than 10%), it is necessary to combine the effects produced by the two components of the seismic motion.
In addition, when the pushover analysis is conducted with a distribution of forces derived from a deformation associated with a participating mass less than 75% of the total mass, it is necessary to consider the contribution of the higher modes, after having performed a multi-mode non-linear static analysis.

A.6.1 Quantification of limit states considering the two excitation components

In the case of irregular-in-plan buildings, the modal forms exhibit a coupling of displacements in the two directions as a result of the torsional effects.
Supposing, by way of example, that the i^{th} mode is considered and for this mode the main direction (i.e. the one with the greatest participating mass) is X, the curve obtained from non-linear static analysis refers to the base shear V_X according to this direction. The seismic response must however consider the contribution of the two excitation components.
A measure of the importance of these effects is provided by the participation factors Γ_{iX} and Γ_{iY} of the i^{th} mode for to the two directions:

$$\Gamma_{iX} = \frac{\varphi_i^T \mathbf{M}\, \mathbf{t}_X}{M_i} \quad \Gamma_{iY} = \frac{\varphi_i^T \mathbf{M}\, \mathbf{t}_Y}{M_i} \qquad \left(M_i = \varphi_i^T \mathbf{M}\, \varphi_i\right) \tag{A.15}$$

where φ_i is the modal form (the superscript T denotes the vector transposition operation), $\mathbf{M}$ is the mass matrix, M_i is the modal mass of mode i, $\mathbf{t}_X$ and $\mathbf{t}_Y$ are the drag vectors in the X and Y directions (the components of which are equal to 1 if the degree of freedom is a translation in the X or Y direction, and zero in other cases).
The procedure described below must be applied when $\Gamma_{iY} / \Gamma_{iX} > 0.1$.
The capacity curve which enables the contribution of seismic motion to the displacement demand at the base directed in the X direction is obtained by converting the curve obtained from pushover analysis:

$$a_X = \frac{V_X}{\Gamma_{iX} M_i} \quad \delta_X = \frac{d_X}{\Gamma_{iX}} \tag{A.16}$$

where d_X is the single-degree-of-freedom control displacement in the X direction.
The capacity curve which enables the contribution of seismic motion to the displacement demand at the base directed in the Y direction is obtained by converting the same curve, but by means of the corresponding participation factor Γ_{iY}:

$$a_Y = \frac{V_X}{\Gamma_{iY} M_i} \qquad \delta_Y = \frac{d_X}{\Gamma_{iY}} \tag{A.17}$$

As $\Gamma_{iY} < \Gamma_{iX}$, the curve representing the response to actions in the Y direction has larger acceleration capacities and therefore the corresponding contribution to the overall response is smaller than the contribution due to the excitation in X direction.
The definition of the limit state variables requires the evaluation of the same response parameters used in §3.3.1, §3.3.2 and §3.3.3, which are all a function of the displacement δ_X that is: $\Sigma_{SLD,F}$, $\Sigma_{SLD,M}$, $\Sigma_{SLC,M}$, $\square_G$, $\delta_{SLD,G}$, $\delta_{SLC,G}$, $\theta_{p,l}$, ($p = 1,\ldots,N_p$ – number of piers; $l = 1,\ldots,N_l$ – number of levels).
By using the relevant, appropriately reduced (overdamped or anelastic) response spectrum for the two directions, it is possible to express the functional relationships between the seismic intensity and the displacement demands due to the two excitation components:

$$\delta_X = f_X\left(S_a(T_1)\right) \quad \delta_Y = f_Y\left(S_a(T_1)\right) \tag{A.18}$$

where $S_a(T_1)$, which is the measure of the intensity of the event consisting of the simultaneous application of the two components of ground motion, is defined as the geometric mean of spectral accelerations at T_1 in the two directions, X and Y:

$$S_a(T_1) = \sqrt{S_{aX}(T_1) S_{aY}(T_1)} \tag{A.19}$$

and the relationships between $S_a(T_1)$ and the intensities in the two directions $S_{a,X}(T_1)$ and $S_{a,Y}(T_1)$ are implicit in the definition of the functions f_X and f_Y.
The partial limit state variables must be defined, for each intensity value, by combining the effects produced by the two components of motion.
Check at local scale is performed by combining the cumulative damage indicators, using the SRSS rule. To do so, a single cumulative function is defined as a function of the displacement on the capacity curve corresponding to the response due to the X component, while taking into account the fact that the displacement demand due to the Y component corresponds to a point $\delta_{X|Y}$ on this capacity curve which precedes δ_X, which is the displacement demand only due to the X component. $\delta_{X|Y}$ is computed as follows:

$$\delta_{X|Y} = \frac{\Gamma_{iY}}{\Gamma_{iX}} f_Y\left(f_X^{-1}(\delta_X)\right) \tag{A.20}$$

It is thus possible to define, for example, for the SLS in the spandrels, the cumulative function which takes account of the complete seismic excitation response, starting from the response derived only for the X direction:

$$\Sigma_{SLD,F}^{XY}(\delta_X) = \sqrt{\Sigma_{SLD,F}^2(\delta_X) + \Sigma_{SLD,F}^2\left[\frac{\Gamma_{iY}}{\Gamma_{iX}} f_Y\left(f_X^{-1}(\delta_X)\right)\right]} \tag{A.21}$$

With analogous expressions the cumulative damage functions for piers at the SLS and SLC are obtained, from which the limit state variables at the structural element level are given as:

$$Y_{SLD}^{XY} = \frac{1}{\tau_{SLD}} \max\left(\Sigma_{SLD,F}^{XY}; \Sigma_{SLD,M}^{XY}\right) \tag{A.22}$$

$$Y_{SLC}^{XY} = \frac{1}{\tau_{SLC}} \Sigma_{SLC,M}^{XY} \tag{A.23}$$

It is therefore possible to define $\delta_{SLD,S}$ and $\delta_{SLC,S}$, on the capacity curve resulting in the X direction, as the points at which $Y_{SLD,S}^{XY}$ and $Y_{SLC,S}^{XY}$ reach the value equal to 1.
Check at the macro-element (wall) scale is performed by defining the variable:

$$\theta_P(\delta_X) = \max\left|\theta_{p,l}(\delta_X)\right| \quad \left(p = 1,..N_p \; ; \; l = 1,..N_l\right) \tag{A.24}$$

If the effects are combined using the SRSS rule, the following is obtained:

$$\theta_P^{XY}(\delta_X) = \sqrt{\theta_P^2(\delta_X) + \theta_P^2\left[\frac{\Gamma_{iY}}{\Gamma_{iX}} f_Y\left(f_X^{-1}(\delta_X)\right)\right]} \tag{A.25}$$

The displacement $\delta_{SLD,M}$ on the capacity curve resulting in the X direction corresponds to the condition $\theta_P^{XY} = \theta_{SLD,M}$; similarly, the displacement $\delta_{SLC,M}$ is defined.
For check at the global scale, for each intensity value the relationship between the displacement demand and the corresponding limit value is evaluated. The values for the two directions are combined using the the SRSS rule, thus obtaining:

$$Y_{SLD,G}^{XY}(\delta_X) = \frac{1}{\delta_{SLD,G}^X} \sqrt{\delta_X^2 + \left[\frac{\Gamma_{iY}}{\Gamma_{iX}} f_Y\left(f_X^{-1}(\delta_X)\right)\right]^2} \tag{A.26}$$

where $\delta_{SLD,G}^X$ is the displacement on the capacity curve associated to excitation in the X direction defined by means of check on the SDL at the global scale; it will be observed that the second addend under the square root increases the limit state variable as a result of the concomitant excitation in the Y direction.
The displacement $\delta_{SLD,G}$ is the value of the capacity curve in the X direction for which $Y_{SLD,G}^{XY}$ reaches the value equal to 1.
The values of δ_{SLD} and δ_{SLC} are obtained from Eqs. (3.31) and (3.37), as the minimum among the values defined above deriving from the checks performed at the various scales of the multi-criteria approach; these are always lower than or equal to those obtained by neglecting the contribution of the seismic excitation in an orthogonal direction with respect to the direction of verification.
Finally, for the SLS, the overall repair cost variable is obtained starting from the function $C_G(\delta_X)$ determined from the response in the direction of verification:

$$C_G^{XY}(\delta_X) = \sqrt{C_G^2(\delta_X) + C_G^2\left[\frac{\Gamma_{iY}}{\Gamma_{iX}} f_Y\left(f_X^{-1}(\delta_X)\right)\right]} \tag{A.27}$$

The displacement δ_{SLS} on the capacity curve for the response in X direction is the one corresponding to the condition $C_G^{XY} = C_{SLS}$, under the further condition that $\delta_{SLS} \leq \delta_{SLC}$.
After establishing in a suitable position the points on the capacity curve corresponding to the points at which the three limit states are reached, the verification is conducted considering the displacement demand due exclusively to the seismic input component in the direction of verification.

A.6.2 Quantification of limit-states in the case of multi-modal analysis

It is necessary to consider the contribution of higher modes when a percentage of 75% of the total mass is not reached, either by the first mode (in case of sufficiently stiff diaphragms) or by a SRSS combination of the modes for which displacement in the direction of verification do not change sign along the height (such as the case of highly flexible diaphragms, a case in which each mode corresponds to one or more walls).
In these cases, in addition to the principal mode, identified by the index *1* and defined as above, for performing a multi-modal analysis it is necessary to consider a number N_{mm}-1 of higher modes, until over 75% of participating mass is reached.
In the discussion that follows, for the sake of simplicity, the index denoting the direction of verification is omitted, as the combination takes into consideration modes which act in the same direction.
Having performed the pushover analysis for the generic mode *i* and once calculated the capacity curve, it is possible to evaluate the response parameters for the i^{th} mode, required for the application of the multi-scale criterion, as a function of δ_I that is: the cumulative damage in piers and spandrels ($\Sigma^i_{SLD,F}$, $\Sigma^i_{SLD,M}$, $\Sigma^i_{SLC,M}$); the overall repair cost function (C^i_G); the interstorey drift in the various walls and at the different levels ($\theta^i_{p,l}$ - p = 1,...,N_p; l = 1,...,N_l). In addition, displacements for which SLS and SLC conditions at the global scale occur ($\delta^i_{SLD,G}$, $\delta^i_{SLC,G}$) are evaluated.
Having established the appropriately reduced (overdamped or anelastic) response spectrum, the function expressing the displacement demand of the i^{th} equivalent oscillator is derived for each mode as a function of the seismic intensity:

$$\delta_i = f_i\left(S_a(T_1)\right) \quad \left(i = 1,..N_{mm}\right) \tag{A.28}$$

The displacement demand for higher modes can be expressed as a function of the demand on the principal mode:

$$\delta_i(\delta_1) = f_i\left(f_1^{-1}(\delta_1)\right) \quad \left(i = 2,..N_{mm}\right) \tag{A.29}$$

The partial limit state variables must be defined, for each intensity value, by combining the effects produced by the various modes.
Check at the local scale is performed by combining the various cumulative damage functions, all expressed as a function of δ_1, using the SUM rule, as it may be conservatively assumed that the first elements to be damaged on each mode are different. We may thus define, for example for the SLS in the spandrels, the cumulative function which takes account of the multi-modal response:

$$\Sigma^{mm}_{SLD,F}\left(\delta_1\right) = \Sigma^1_{SLD,F}\left(\delta_1\right) + \sum_{i=2}^{N_{mm}} \Sigma^i_{SLD,F}\left[f_i\left(f_1^{-1}(\delta_1)\right)\right] \tag{A.30}$$

With similar expressions the cumulative functions for the masonry piers at the SLS and SLC are derived, and from these the limit state variables at the structural element scale are obtained:

$$Y^{mm}_{SLD} = \frac{1}{\tau_{SLD}} \max\left(\Sigma^{mm}_{SLD,F}; \Sigma^{mm}_{SLD,M}\right) \tag{A.31}$$

$$Y_{SLC}^{mm} = \frac{1}{\tau_{SLC}} \Sigma_{SLC,M}^{mm} \tag{A.32}$$

$\delta_{SLD,S}$ and $\delta_{SLC,S}$ can then be defined, on the capacity curve in the X direction, as the points at which $Y_{SLD,S}^{mm}$ and $Y_{SLC,S}^{mm}$ reach the value equal to 1.

Check at macroelement scale (wall) is performed by combining the effects for each wall and storey of the building using the SRSS rule:

$$\theta_{p,l}^{mm}(\delta_1) = \sqrt{\left[\theta_{p,l}^{1}(\delta_1)\right]^2 + \sum_{i=2}^{N_{mm}}\left[\theta_{p,l}^{i}\left(f_i\left(f_1^{-1}(\delta_1)\right)\right)\right]^2} \tag{A.33}$$

and defining the variable:

$$\theta_P^{mm}(\delta_1) = \max\left(\theta_{p,l}^{mm}(\delta_1)\right) \quad \left(p = 1,..N_p \; ; \; l = 1,..N_l\right) \tag{A.34}$$

The displacement $\delta_{SLD,M}$ on the capacity curve for the principal mode corresponds to the condition $\theta_P^{mm} = \theta_{SLD,M}$; similarly the displacement $\delta_{SLC,M}$ is defined.

For check at global scale, for each intensity value the relationships between the displacement demand and the limit value on each mode $\delta_{SLD,G}^{i}$ are evaluated; these are combined using the SRSS rule, thus obtaining:

$$Y_{SLD,G}^{mm}(\delta_1) = \sqrt{\left[\frac{\delta_1}{\delta_{SLD,G}^{1}}\right]^2 + \sum_{i=2}^{N_{mm}}\left[\frac{f_i\left(f_1^{-1}(\delta_1)\right)}{\delta_{SLD,G}^{i}}\right]^2} \tag{A.35}$$

The displacement $\delta_{SLD,G}$ is the value on the capacity curve of the principal mode for which $Y_{SLD,G}^{mm}$ reaches the value equal to 1.

A similar formula is adopted to determine the function $Y_{SLC,G}^{mm}(\delta_1)$ and the displacement $\delta_{SLC,G}$.

The values of δ_{SLD} and δ_{SLC} are obtained from Eqs. (3.31) and (3.37), as the minimum among the values defined above derived from checks carried out at the various scales of the multi-scale approach; these are always lower than or equal to those obtained when only the principal mode is considered.

Finally, for the SLS the overall repair cost variable is obtained starting from the functions $C_G^i(\delta_i)$ evaluated on the modes considered in the multi-mode analysis:

$$C_G^{mm}(\delta_1) = \sqrt{\left[C_G^1(\delta_1)\right]^2 + \sum_{i=2}^{N_{mm}}\left[C_G^i\left(f_i\left(f_1^{-1}(\delta_1)\right)\right)\right]^2} \tag{A.36}$$

The displacement δ_{SLS} on the capacity curve representative of the response of the principal mode is the one corresponding to the condition $C_G^{mm} = \tau_{SLS}$, under the further condition that $\delta_{SLS} \leq \delta_{SLC}$.

After having established on the capacity curve, in a suitably forward position, the points of the principal mode corresponding to the points at which the three limit states are reached, the verification is conducted considering the displacement demand δ_1 calculated on this capacity curve.

A.7 Viscous damping models for non-linear dynamic analyses (Comment on §4.3.4)

In linear and non-linear dynamic analyses, the most widespread practice is to use a constant level of viscous damping – in addition to the hysteretic damping modelled in accordance with the cyclic constitutive laws of structural elements – e.g. of 5% for reinforced concrete structures. For multi-degrees-of-freedom structures the most commonly used damping model is Rayleigh's model, which provides a damping matrix proportional to those of mass and (initial) stiffness: $\mathbf{C} = \alpha\mathbf{M}+\beta\mathbf{K}_i$. In this model the viscous damping ratio is not constant, but is frequency dependent. The proportionality coefficients are calculated in such a way as to obtain a critical damping ratio of approximately 5% within a given range of frequencies connected with the vibration modes of the structure.

Theoretical considerations and the limited experimental data available suggest that such a practice may, at high levels of ductility, lead to an overestimation of viscous forces, and therefore an underestimation of the response of the structure.

An alternative proposal is to utilise a viscous damping matrix which is proportional exclusively to the tangent stiffness matrix: $\mathbf{C} = \beta\mathbf{K}_t$ i.e. the istantaneous value of the stiffness matrix at each steps of the response analysis. The issue is still debated, and pending a widely agreed solution, the use of critical damping ratios lower than 5% to model the energy dissipation at low amplitude vibration may be justified.

B Example of application to a masonry building

B.1 Premise

The procedure for the evaluation of seismic safety on masonry buildings of Chapters 2 and 3 has been applied to an existing residential building, damaged during the earthquake of May 29, 2012 in Emilia. The availability of the damage survey has allowed us to validate the equivalent frame model used in the evaluation.
Despite this, for the aims of the exemplification of the procedure, the assessment has been carried out by considering the same seismic hazard adopted for the application on the reinforced concrete structure (Appendix C, §C.4) and therefore not consistent with that of the Emilia region.
A sensitivity analysis was performed in order to plan the investigations of structural details and material properties and to limit the number of uncertain variables to be taken into account in the risk analysis.
The risk analysis referred to two of the three methods proposed in this document. Method A (non-linear dynamic analysis on the MDOF model of the building) is considered as the best estimate. The method C is what is proposed for a more frequent and engineering practice oriented use, since it is based on the use only of non-linear static analyses, and so does not require that the model is able to describe the cyclic behavior of the elements and presents a significantly reduced computational effort.
Given the characteristics of the building, which has good wall-to-wall connections and rigid diaphragms, the local mechanisms were not taken into account; the damage survey after the earthquake that hit the building confirmed the reliability of this hypothesis.

B.2 Description of the building

The building is a three-storey residential unreinforced masonry structure made of solid bricks and lime mortar (Figure B-1) and built in the first half of the last century. The diaphragms are composed of steel beams and hollow clay tiles (with concrete screed), while the timber roof of pitched trusses and struts. The thickness of the load-bearing walls, including the perimeter ones, is only 24 cm, as is typical in those areas of the Emilia region; in the perimeter walls, the lintels of openings, supporting spandrel elements, are made through a brick masonry flat arch. No chains or reinforced concrete curbs have been detected. The building is isolated and the planimetric configuration is fairly simple and regular; indeed, in the main façade presents a modest recess and some openings are not vertically aligned. The state of maintenance is quite poor.
As already mentioned, on the occasion of the Emilia earthquake of 29 May 2012 the building substantially showed a global seismic response, with a severe in-plane damage of walls but without the activation of local mechanisms. The global failure mode mainly activated is that associated to a spread damage on spandrels at various levels

higher than that of piers (of both internal and external walls), which present cracks mainly on the ground floor. The damage level occurred on spandrels (Figure B-2) was very severe (in some cases corresponding to the incipient collapse of the flat arch), with the activation of both the flexural mechanism (with cracks concentrated in the end sections) and the shear mechanism (with a stair-stepped path, that is with cracks through the mortar joints). The activation of the shear mode, although in the absence of tensile-resistant elements coupled to the spandrel, is made possible by the horizontal tensile strength of masonry, guaranteed by the interlocking and friction on the horizontal mortar joints. In the piers of internal walls a diagonal shear cracking mainly occurred (Figure B-3a), while the response of piers of external walls was dominated by flexural cracks (Figure B-3b) or a mixed failure mode.

(a) (b)

Fig. B-1 View of South and West façades (a) and the East façade (b).

Fig. B -2 Damage in spandrels, with activation of both flexural and shear damage modes.

(a) (b)

Fig. B -3 Cracks in piers: (a) shear failure in an inner wall; (b) flexural failure in a pier, located at the second floor of a perimeter wall, characterized by a low axial load.

B.3 Assessment procedure

The example of application is done with reference to the assessment methods A and C described in paragraph 2.6.2 and 2.6.4, respectively.

B.4 Seismic action

As indicated in §2.2.1, the seismic action is defined by a hazard curve and a set of records of natural motions (or artificial time histories) compatible with the local characteristics and the mechanisms generating the dominant events of the site.
Table C-1 shows the values of the three parameters (a_g, F_0 and T_C*) which define the code spectral shape adapted to the iso-likely spectra at 16%, 50% and 84%, for the nine return periods considered by the INGV Hazard map.
The seismic intensity measure is the spectral acceleration at the fundamental period of the structure (S_a (T_1)). This period is assumed to be equal to the value provided by the simplified formula proposed in NTC2008 (T_1=0.05 $H^{3/4}$=0.26 s) which, as will be seen below, is very close to the values obtained from the modal analysis with the mean values of the parameters (§B5.3). As regards the site effects, similarly to the application on the reinforced concrete building discussed in Appendix C (§C.8.1), they were considered in a simplified manner through a deterministic factor, equal to 1.25, independent of the period of vibration and the intensity.
Table B-1 shows the parameters of the hazard curve (Figure B-4), as a function of S_a (T_1) (16%, 50% and 84% percentile and the mean value) and the parameter β_H related to the epistemic uncertainty on the hazard.

Table B-1 Parameters that describe the hazard curve and the relative uncertainty.

T_r	λ	$S_a(T_1)_{16\%}$	$S_a(T_1)_{50\%}$	$S_a(T_1)_{84\%}$	β_H	$S_a(T_1)_m$
30	3.33E-02	0.102	0.131	0.150	0.192	0.133
50	2.00E-02	0.144	0.173	0.199	0.160	0.175
72	1.39E-02	0.174	0.205	0.251	0.185	0.208
101	9.90E-03	0.211	0.245	0.303	0.183	0.249
140	7.14E-03	0.249	0.286	0.358	0.181	0.291
201	4.98E-03	0.291	0.337	0.424	0.188	0.343
475	2.11E-03	0.431	0.528	0.660	0.214	0.540
975	1.03e-03	0.562	0.713	0.891	0.231	0.732
2475	4.04E-04	0.780	1.063	1.371	0.282	1.106

The mean curve, defined in nine points, is then fitted by a quadratic function in the logarithmic space which is given by the expression (2.13). The parameters that minimize the error are in this case the following:

$$k_0 = 5.14 \times 10^{-4} \quad k_1 = 2.257 \quad k_2 = 0.0946 \qquad \text{(B.1)}$$

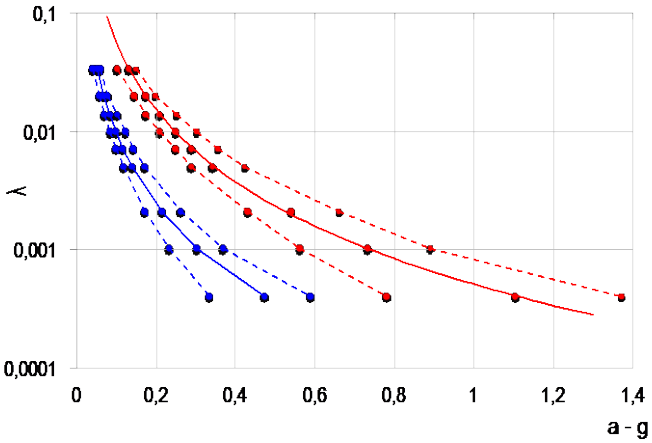

Fig. B-2 Mean hazard curve (continuous line) and fractiles 84% and 16% (dotted line), in terms of peak ground acceleration (blue) and spectral ordinate $S_a(T_1 = 0.26$ s) (red) for the site under examination.

Records of seismic motion used in the analysis were selected from disaggregated data (relative to the mean hazard curve in terms of peak ground acceleration), listed in §C.4.2 . Table B-2 provides details of the 30 selected events, each consisting of the two components NS and EW; compared to Table C-4, there are herein provided the values of the spectral acceleration of the two components corresponding to the period used as a representative of that fundamental of the masonry building examined (T_1=0.26 s). Figures C-7, C-8 and C-9 show some time histories and the corresponding acceleration response spectra.

For the purposes of verification, as intensity measure of the event, which consists in the simultaneous application of the two components of the ground motion, the geometric mean of the spectral accelerations in both directions NS and EW ($S_{a,NS}(T_1)$ and $S_{a,EW}(T_1)$) is assumed as reference computed as:

$$S_a(T_1) = \sqrt{S_{a,NS}(T_1) \cdot S_{a,EW}(T_1)} \qquad \text{(B.2)}$$

Table B-2. Features of the selected motions (R in km, peak ground accelerations in m / s ^{2}) and value of the intensity measure S_a (T_1) to be used for scaling.

#	DB	event	M	station	R	a_{gX}	$S_{aX}(T_1)$	a_{gY}	$S_{aY}(T_1)$	$S_a(T_1)$
1	AND	Friuli (as)	6.0	ST28	14.0	1.386	3.443	2.322	5.059	4.174
2	AND	Montenegro (as)	6.2	ST75	17.0	1.731	3.510	2.721	3.126	3.312
3	AND	Preveza	5.4	ST123	28.0	1.404	5.704	1.330	3.430	4.423
4	AND	Umbria Marche (as)	5.6	ST86	20.0	0.963	1.972	1.316	2.155	2.061
5	AND	Umbria Marche (as)	5.6	ST265	21.0	1.073	2.105	0.802	1.913	2.007
6	AND	Izmit (as)	5.8	ST575	15.0	0.716	2.110	3.118	10.115	4.620
7	AND	Ano Liosia	6.0	ST1100	16.0	2.611	3.935	3.018	8.598	5.817
8	AND	Ano Liosia	6.0	ST1101	17.0	1.173	3.043	1.070	2.689	2.861
9	AND	Ano Liosia	6.0	ST1257	18.0	1.091	3.051	0.843	2.478	2.750
10	AND	Ano Liosia	6.0	ST1258	14.0	2.392	8.042	2.164	4.862	6.253
11	AND	South Iceland (as)	6.4	ST2482	21.0	1.088	3.683	1622	4.285	3.973
12	AND	South Iceland (as)	6.4	ST2557	15.0	1.251	3.305	1.140	2.541	2.898
13	AND	South Iceland (as)	6.4	ST2497	20.0	0.505	1.208	1.033	1.995	1.552
14	AND	South Iceland (as)	6.4	ST2556	20.0	1.047	1.791	0849	1.899	1.844
15	S	Near Miyakejima Island	6.4	TKY011	21.0	1.276	3.320	1.972	3.891	3.594
16	S	NW Kagoshima Pref.	6.1	KGS002	12.0	5.431	4.337	7.999	3.726	4.020
17	S	NW Kagoshima Prefecture	6.0	KGS002	16.0	4.529	2.714	7.818	4.993	3.681
18	S	South Iceland	6.4	102	24.0	1.275	1.325	0618	1.592	1.452
19	S	South Iceland	6.4	105	21.0	1.108	3.720	1.662	4.323	4.010
20	S	South Iceland	6.4	305	20.0	0.539	1.200	1.057	1.994	1.547
21	S	South Iceland	6.4	306	20.0	1.067	1.821	0892	1.924	1.872
22	S	Umbria-Marche (3rd shock)	5.6	NRC	20.0	1.314	2.149	0939	1.954	2.049
23	S	L'Aquila (as)	5.6	GSA	16.8	2.811	6.558	2.485	3.491	4.785
24	S	Parkfield	6.0	36177	19.4	3.430	9.661	2.248	5.183	7.076
25	S	Parkfield	6.0	36445	15.2	1.437	3.499	2.225	4.679	4.046
26	S	East Fukushima Pref	5.9	FKS011	24.0	1.798	2.212	1.564	2.569	2.384
27	S	Mid Niigata Pref	6.2	NIG021	21.0	2.499	4.876	2.799	8.427	6.410
28	S	Mt Fuji Region	5.9	SZO009	22.0	1.442	2.544	1.225	2.563	2.553
29	S	Mt Fuji Region	5.9	YMN006	20.0	2.373	3.337	1.629	2.771	3.041
30	The	Friuli (4th Shock)	5.9	SRC0	16.4	1.288	3.148	2.444	5.488	4.156

Figure B-5a shows the response spectra of the 30 NS components, applied in this case in the X direction of verification (Figure B-7), normalized to the unit value of the in-

tensity measure $S_{a,NS}(T_1)$. Figure B-5b shows the response spectra of the 30 EW components, applied in the Y direction, normalized to the value $S_{a,NS}(T_1)$=1 (that is, maintaining its original ratio between the intensities of the two orthogonal components of each motion) .

Figure B-6 shows the response spectra at fractiles 16%, 50% and 84%, of the individual records listed in Table C-4, necessary for the application of the method C (§2.6.4).

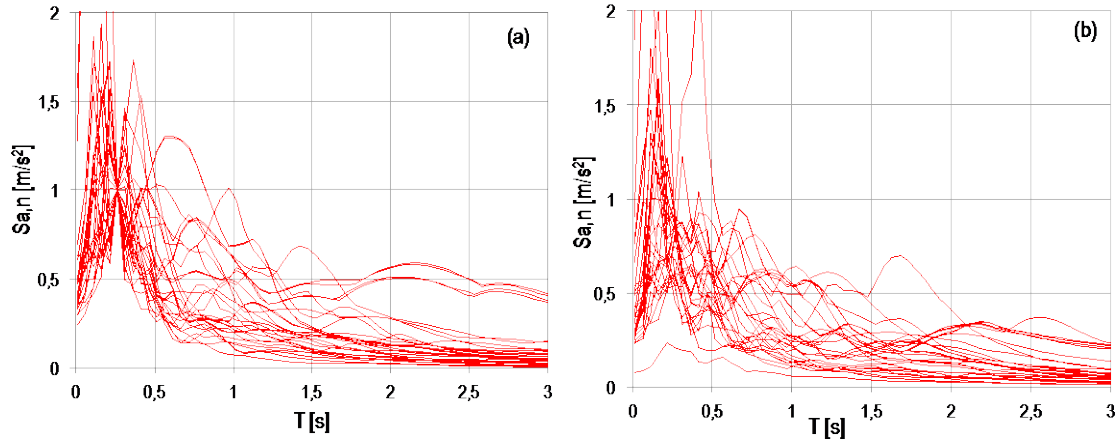

Fig. B -5 Response spectra normalized to the value $_iS_a(T_1)$=1: a) in the X direction; b) in the Y direction.

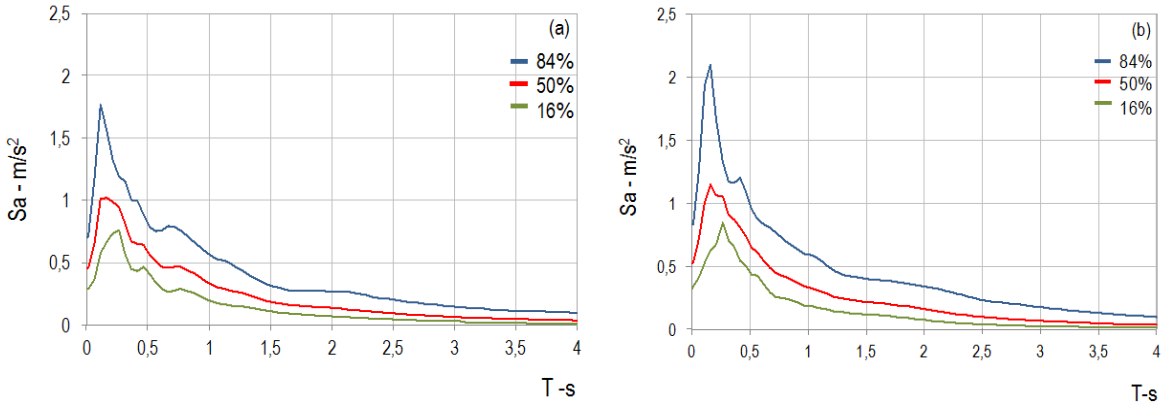

Fig. B -6 Median spectrum and those corresponding to the fractiles 16% and 84%: a) in the X direction; b) in the Y direction

B.5 Knowledge of the structure

B.5.1 Modeling of the building and analysis criteria

The building was modeled according to the equivalent frame approach. The structure is identified by the walls (elements bearing the vertical and horizontal actions) and the diaphragms (elements able to redistribute the horizontal seismic actions among the walls). Each wall is idealized according to a frame in which the non-linearity is concentrated in the structural elements (piers and spandrels) connected through rigid portions (nodes). The diaphragms are modeled as elastic orthotropic membrane finite (plane stress) elements. The flexural behavior of the latter ones, in respect to the vertical loads, and the out-of-plane response of the walls are not considered in this model and should be evaluated by appropriate local verifications.
The choice of such an approach seems particularly appropriate for the case under examination, characterized by a rather regular distribution of the openings, which limits the arbitrariness of the idealization of the walls into the equivalent frame; moreover, since the building is characterized by a masonry made of solid bricks and lime mortar, the reliability of the constitutive law adopted for piers and spandrels is supported by the evidences of many cyclic tests carried out in laboratory and available in literature.
Figure B-7 shows the plan layout of the building at the ground floor, where you can identify the load-bearing walls (in total number of 5 and 6 in the X and Y directions, respectively).

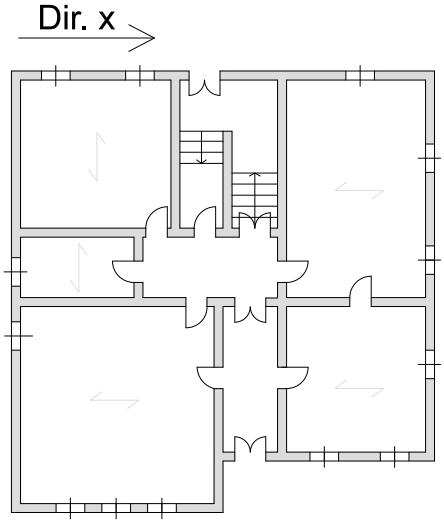

Fig. B-7 Ground floor plan

Figure B-8 shows the three-dimensional structural model and a possible equivalent frame mesh of the external façades: the piers, spandrels and rigid nodes are marked respectively in red, green and cyan. In particular, one observes in the wall 1 (east façade) the offset of the openings in the central part (in correspondence to the stairwell of the structure) compared to the adjacent ones: the identification of the spandrels portions, misaligned with respect to the adjacent rows, reflects the evidence of damage shown in Fig. B-1b. Additional considerations about other possible alternatives mesh for the equivalent frame are discussed at §B.5.2.

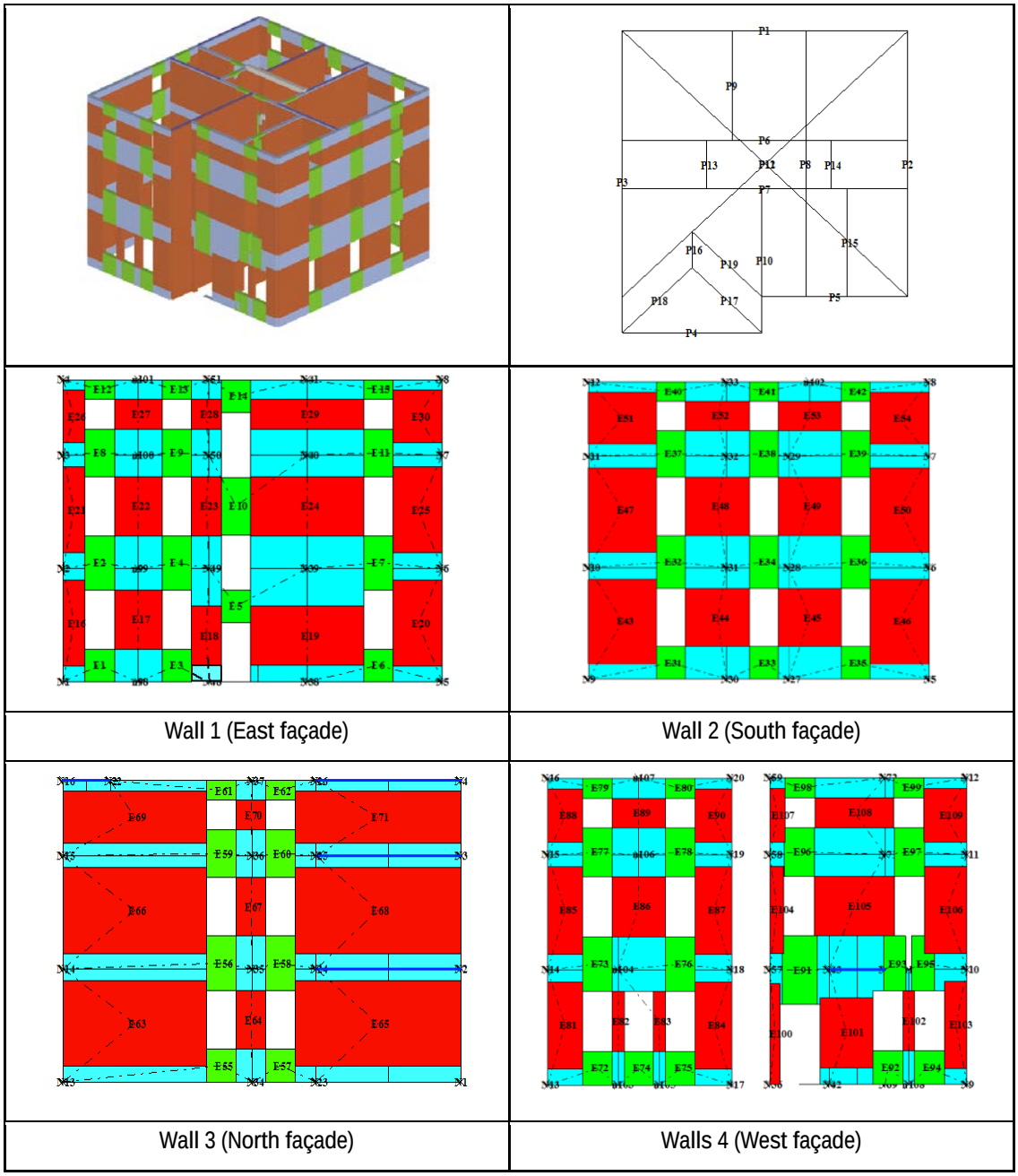

Fig. B -8 Three-dimensional structural model, numbering plan of the walls and a possible equivalent frame idealization of the main façades (the dotted lines graphically identify the position of the center of gravity of the structural element with respect to the end nodes which it is attached to)

The nonlinear static analysis is performed by adopting two load patterns: one proportional to the first modal shape in the two directions X and Y; one proportional to the masses. The latter is thought to be the most consistent with the actual response, in particular close to the attainment of the SLC, as resulting from the simulations performed for validating the model (§B7.1). For the computation of the displacement demand through the nonlinear static analysis there is used the method of the overdamped spectra, which has the advantage of not requiring the transformation of the capacity curve into an equivalent bilinear system and which is more reliable also for elevated ductility demand.

B.5.2 Aleatory and epistemic uncertainties

A preliminary model has been defined starting from the data available even in the absence of specific diagnostic investigations (geometry, construction details and materials).
For the floors an estimate of the permanent and accidental load leads to assume a value between 2.0 and 3.0 kN/m^2. For the timber roof there was assumed a value of the permanent load between 1.2 and 1.8 kN/m^2.
Table B-3 shows the ranges of the values assumed for the stiffness parameters of diaphragms which have been calibrated by assuming: an effective connection of the diaphragms to the perimeter walls and, in the case of the roof, a good connection of the timber elements with the top of the masonry walls. In particular, the Young moduli, $E_{1,eq}$ and $E_{2,eq}$, represent the normal stiffness of the membrane in the direction of the main warping of the diaphragms and in the orthogonal direction, respectively; in particular, they affect the in-plane coupling among piers, hence influencing the axial force computed in the spandrels. The shear modulus G_{eq} instead influences the redistribution of the seismic actions among the walls, both in the elastic and non-linear phases. The assumed variability of the moduli that define the diaphragms stiffness is very large because these parameters would represent in equivalent manner a set of constructive, geometric and materials aspects.

Table B-3 Stiffness parameters assumed for orthotropic membrane elements that simulate the diaphragms

Type	t [cm]	$E_{1,eq}$ [MPa]	$E_{2,eq}$ [MPa]	G_{eq} [MPa]
Plan	4	5000-50000	5000-50000	1250-12500
Coverage	4	2000-20000	1000-10000	100-1000

For masonry panels there was assumed a non-linear beam model described by a piecewise-linear behaviour and based on a phenomenological approach (Deliverable D26 2012). It allows one to describe: i) the non-linear monotonic response of the panel associated with increasing levels of damage (denoted by i ranging from 1 to 5, up to collapse), assigning progressive residual strength (β_{Ei}) in correspondence with predetermined limit thresholds (θ_{Ei}) of the drift θ (computed by the expression 3.11 or 3.12); ii) the hysteretic cyclic response. On the basis of an appropriate assignment of parameters (both in a monotonic and cyclic context), such model is able to describe the distinctive features of the various failure modes (rocking and crushing, shear and mixed as well), which characterize the two different structural elements (piers and spandrels). The shear strength of the panel (V_u) is then calculated as the minimum value among those associated with the different failure modes, as a function of the normal stress acting in the element; mixed failure modes are activated at assigned intervals of normal stress.

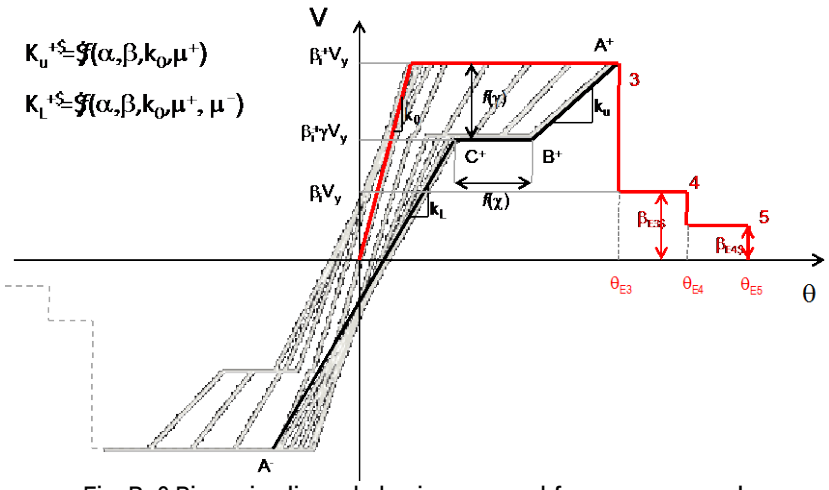

Fig. B -9 Piecewise-linear behavior assumed for masonry panels

With reference to the criteria stated in §3.2.1, to interpret the diagonal shear cracking, there has been adopted the criterion proposed by Mann and Müller (3.6), while in the case of spandrels there was used the expression (3.11).

As regards the stiffness and strength mechanical parameters, preliminary analyses were performed by adopting the ranges proposed for the *masonry of solid bricks and mortar of lime* in Table C8A.2.1 of the Commentary to NTC 2008 (Circular No 617, 2 February 2009), shifted slightly to the low values to account for the poor state of maintenance and quality of the walls that was not particularly good in the Emilian area. Table B-4 shows the intervals assumed.

Table B-4. Mechanical parameters adopted for the masonry (M = piers; F = spandrels)

		Mechanical parameters				
		E [MPa]	G [MPa]	f_m [MPa]	$\bar{f}_{vm0}$ [MPa]	$\hat{\mu}$
M/F		542-808	181-269	2.1-3.5	0.08-0.12	0.30-0.40
		Drift limit and residual strength				
		θ_{E3}	θ_{E4}	θ_{E5}	β_{E3}	β_{E4}
M	flex	0.0046-0.0074	0.0078-0.0122	0.012-0.018	-	0.80-0.90
	shear	0.0023-0.0037	0.0039-0.0061	0.0056-0.0084	0.60-0.80	0.25-0.55
F	flex shear	0.0015-0.0025	0.0045-0.0075	0.015-0.025	0.30-0.70	0.30-0.70

As regards the limit values of drift and the residual strength, as well as the parameters describing the cyclic response, there were assumed the intervals proposed in Tables 3.2 and 3.3. Figure B-10 shows the simulation of experimental tests available: on two masonry piers characterized by a prevailing flexural (combined axial force and bending) and diagonal cracking shear response, respectively; and on a spandrel with a lintel of the same type as those of the building under examination.

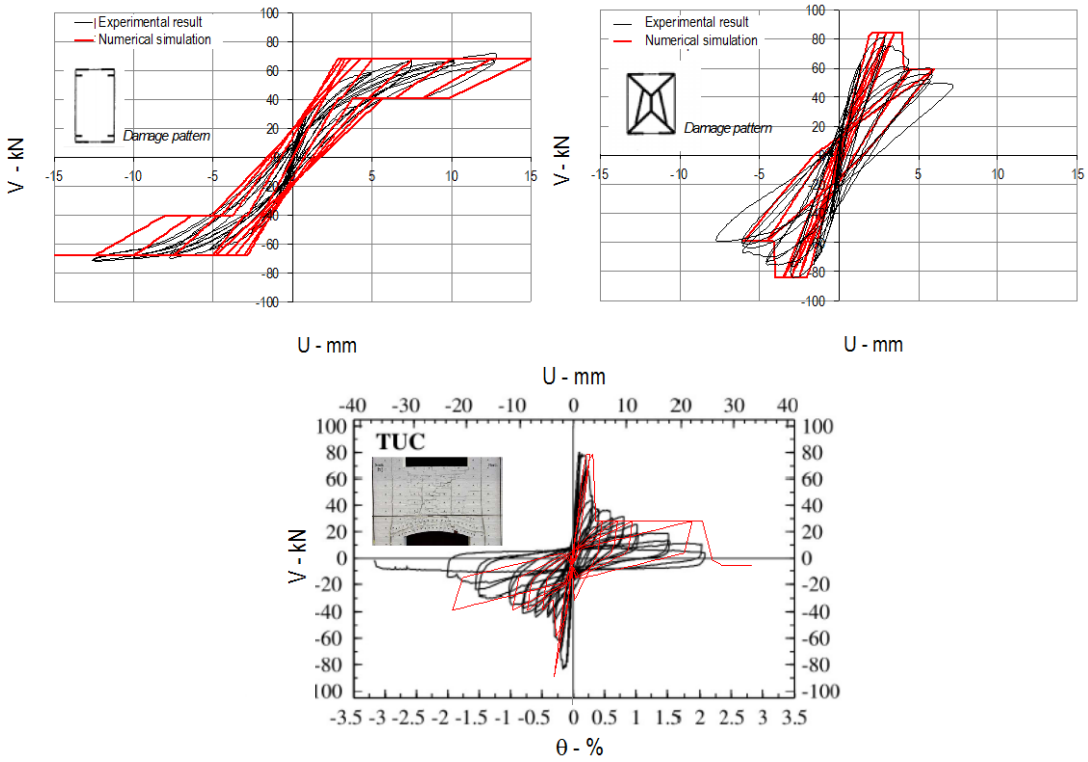

Fig. B -10 Numerical simulation of some panels tested in laboratory, aimed at calibrating the hysteretic parameters of the piecewise-linear model adopted (in the case of piers reference was made to the experimental results of Anthoine et al. 1995, in the case of spandrels to those of Beyer and Dazio, 2012)

As regards the model uncertainties two aspects have been considered: a) the definition of the geometry of the equivalent frame; b) the flange effect in correspondence of the wall-to-wall connection. In particular, this latter effect can be simulated by linking the piers belonging to two walls to the same node (for simulating the case of full connection) or maintaining distinct nodes in the two walls, then connected by a fictitious beam of a stiffness equivalent to that offered by the interlocking.

Both aspects lead to a different equivalent frame mesh, for which these uncertainties cannot be described by a random variable but must be treated through the logical tree approach.

Regarding the assumptions adopted to define the geometry of the piers, two possible alternatives mesh were considered: Mesh-1) in which the height of the external piers has been taken as the average of that of the adjacent opening and the height of the incident nodes; Mesh-2) in which the height of the external piers is equal to that of the adjacent openings.

In the case of flange effect, the conditions of perfect coupling (Amm-1) and that representative of an intermediate condition (Amm-2) were considered; further consideration on this aspect are described in §B.5.3.

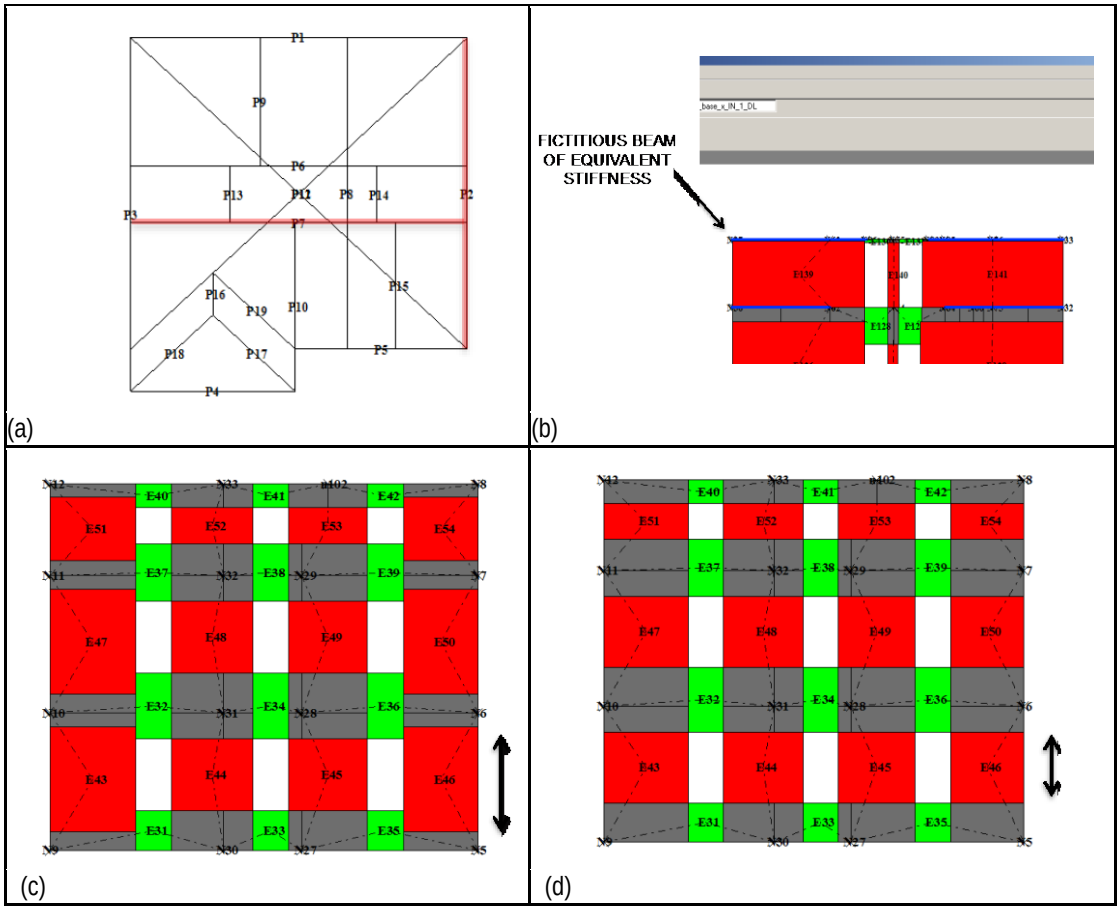

Fig. B -11. Equivalent frame model (piers in red, spandrels in green, rigid nodes in grey): (a) plan view of masonry walls; (b) internal wall 7 in which the fictitious beams adopted for simulating the flange effect are indicated; (c/d) exemplification of the two assumptions adopted for the geometry of piers, by way of example in the case of wall 2: (c) Mesh-1 and (d) Mesh-2.

B.5.3 Sensitivity analysis

The sensitivity of the response to several uncertain parameters was investigated through a series of non-linear static analyses performed by adopting for all parameters the central value of the range except one, to which was attributed either the maximum or minimum value of the set interval, respectively.

Altogether the following parameters or groups of parameters are considered:

1. Material: this is a group comprising the elastic modulus E, the shear modulus G, the shear strength of the masonry $\bar{f}_{vm0}$, the equivalent friction coefficient $\bar{\mu}$, the compressive strength f_m.
2. Floor diaphragm stiffness: a group comprising the equivalent shear modulus G_{floor}, the elastic modulus in the main warping direction E_{1floor} and the elastic modulus in the direction perpendicular to warping E_{2floor} (all for a slab of conventional thickness t = 4 cm).
3. Roof diaphragm stiffness: a group comprising the equivalent shear modulus $G_{roof,}$, the elastic modulus in the main direction of warping E_{1roof} and the elastic modulus in the direction perpendicular to warping E_{2roof} (all for a slab of conventional thickness t = 4 cm).
4. Floor masses: permanent and accidental load (factored) $p_{floor.}$

5. Roof masses: accidental and permanent load (factored) $p_{roof.}$
6. Constitutive law of piers : this is a group comprising the drift thresholds corresponding to the attainment of progressing levels of damage (θ_{M3}, θ_{M4}, θ_{M5}) and the corresponding percentages of residual strength ($\beta_{M3,}$ β_{M4}). Such values are also differentiated for the two main failure modes considered, that is crushing and diagonal shear cracking.
7. Constitutive law of spandrels: this is a group comprising the drift thresholds corresponding to the attainment of progressing levelsof damage (θ_{F3}, θ_{F4}, θ_{F5}) and the corresponding percentage of residual strength (β_{F3}, β_{F4}).
8. Energy dissipation (method A) / damping (method C): in the case of method A, the dissipation of energy derives directly from the cyclic hysteretic behavior of piers and spandrels (in addition to the viscous component), hence from the set of parameters that regulate it; if one uses instead the method C, based on the use of non-linear static analysis, the energy dissipation affects the computation of the displacement demand trhough the use of overdamped spectra, which are based on the concept of equivalent damping. In particular, in the case of method C, in the sensitivity analysis there was used a correlation law between damping and ductility (3.15), assuming as uncertain the parameter ζ, that is the asymptotic value of the hysteretic damping.

Each group of parameters is considered as a single random variable; in the sensitivity analysis the parameters within the same group have been alternatively changed or placed all at the extreme upper or lower end of the range assigned.

The acceleration that leads to the attainment of the limit states SLD and SLC has been assumed as response parameter to assess the sensitivity and it has been conventionally evaluated considering the median spectral shape shown in Fig. B-6 .The sensitivity to the parameters has been calculated as explained in §3.1.2, by adopting the expression (3.1) in the case of those of random nature and the expression (3.4) in the case of epistemic uncertainties leading to alternative models. Being j = 2 and m = 2 (see §3.1.2) the number of uncertain epistemic factors and the corresponding modeling options, the expressions to compute the sensitivity parameters assume the following form:

$$\Delta_1^{'} = 2\frac{\max\left(\frac{a_{11}+a_{12}}{2},\frac{a_{21}+a_{22}}{2}\right)-\min\left(\frac{a_{11}+a_{12}}{2},\frac{a_{21}+a_{22}}{2}\right)}{\max\left(\frac{a_{11}+a_{12}}{2},\frac{a_{21}+a_{22}}{2}\right)+\min\left(\frac{a_{11}+a_{12}}{2},\frac{a_{21}+a_{22}}{2}\right)}$$

$$\Delta_2^{'} = 2\frac{\max\left(\frac{a_{11}+a_{21}}{2},\frac{a_{12}+a_{22}}{2}\right)-\min\left(\frac{a_{11}+a_{21}}{2},\frac{a_{12}+a_{22}}{2}\right)}{\max\left(\frac{a_{11}+a_{21}}{2},\frac{a_{12}+a_{22}}{2}\right)+\min\left(\frac{a_{11}+a_{21}}{2},\frac{a_{12}+a_{22}}{2}\right)} \quad \text{(B.3)}$$

where the acceleration *a* is relative to the limit state of interest and, in the subscript, the first index refers to the option taken for the uncertainty on the mesh (j = 1), that is the height of the piers, and the second refers to the option taken on the flange effect (j = 2); this subscript uniquely identifies the acceleration associated with each branch of the logic tree.

The following are the results for the analyses performed in directions X and Y (see also Fig.B-7) with load pattern proportional to the masses.

Tables B-5 and B-6 show the results of the sensitivity analysis for the random variables, respectively in directions X and Y and in the positive direction; by way of ex-

ample, result refer to the choice of the first option for both the epistemic uncertainties (Mesh-1, Amm-1).
Tables B-7 and B-8 instead show the results consequent to the epistemic uncertainties; the value of $\Delta_j^{'}$ resulting from each of epistemic uncertainty is associated with the more punitive (i.e. associated with the highest value) direction, whether positive or negative.

Table B-5. Results of sensitivity analysis in the X direction (random variables).

Parameter	VAR.	VALUE	SLD	SLC	SLD	SLC
			a [m/s^2]	a [m/s^2]	$\Delta_k^{'}$	$\Delta_k^{'}$
		Mean	2.53	3.29	-	-
Masonry material	1	Maximum	2.76	3.80	0.2231	0.2714
		Minimum	2.20	2.90		
Floor diaphragms stiffness	2	Maximum	2.41	3.31	0.0070	0.0217
		Minimum	2.39	3.24		
Roof stiffness	3	Maximum	2.47	3.29	0.0467	0.0096
		Minimum	2.35	3.26		
Floor mass	4	Maximum	2.43	3.25	0.0036	0.0313
		Minimum	2.44	3.35		
Roof mass	5	Maximum	2.36	3.24	0.0976	0.0269
		Minimum	2.61	3.33		
Constitutive law of piers	6	Maximum	2.53	3.49	0.0004	0.1368
		Minimum	2.53	3.03		
Constitutive law of spandrels	7	Maximum	2.41	3.40	0.2057	0.0732
		Minimum	1.89	3.16		
Damping	8	Maximum	2.67	3.52	0.1194	0.1418
		Minimum	2.37	3.05		

Table B-6. Results of sensitivity analysis in the Y direction (continuous random variables).

Parameter	VAR.	VALUE	SLD	SLC	SLD	SLC
			a [m/s^2]	a [m/s^2]	$\Delta_k^{'}$	$\Delta_k^{'}$
		Mean	2.50	3.78	-	-
Masonry material	1	Maximum	2.68	4.59	0.0855	0.3007
		Minimum	2.46	3.46		
Floor diaphragms stiffness	2	Maximum	2.68	3.76	0.0115	0.0680
		Minimum	2.71	4.02		
Roof stiffness	3	Maximum	2.53	3.80	0.0159	0.0002
		Minimum	2.49	3.80		
Floor mass	4	Maximum	2.82	3.91	0.1106	0.0549
		Minimum	2.54	4.11		
Roof mass	5	Maximum	2.65	3.78	0.0406	0.0060
		Minimum	2.55	3.81		
Constitutive law of piers	6	Maximum	2.49	4.38	0.0036	0.1912
		Minimum	2.50	3.65		
Constitutive law of spandrels	7	Maximum	2.66	3.84	0.0888	0.0885
		Minimum	2.44	4.17		
Damping	8	Maximum	2.56	4.07	0.0807	0.1386
		Minimum	2.36	3.55		

Table B-7. Results of sensitivity analysis in the X direction (epistemic uncertainties).

MODEL AND WAY OF ANALYSIS			BRANCH	SLD a [m/s^2]	SLC a [m/s^2]	VAR.	SLD Δ'_j	SLC Δ'_j
Amm-1 (j=2, p=1)	Mesh-1 (j=1, p=1)	+	11	2.53	3.29	Mesh (j=1)	0.0772	0.0127
		-		1.77	3.01			
	Mesh-2 (j=1, p=2)	+	21	2.48	3.35			
		-		1.87	3.06			
Amm-2 (j=2, p=2)	Mesh-1 (j=1, p=1)	+	12	1.96	2.85	Amm (j=2)	0.5005	0.5087
		-		1.84	3.24			
	Mesh-2 (j=1, p=2)	+	22	1.94	2.76			
		-		2.03	3.27			

Table B-8. Results of sensitivity analysis in the Y direction (epistemic uncertainties).

MODEL AND WAY OF ANALYSIS			BRANCH	SLD a [m/s^2]	SLC a [m/s^2]	VAR.	SLD Δ'_j	SLC Δ'_j
Amm-1 (j=2, p=1)	Mesh-1 (j=1, p=1)	+	11	2.50	3.78	Mesh (j=1)	0.0928	0.0350
		-		2.46	3.82			
	Mesh-2 (j=1, p=2)	+	21	2.87	4.05			
		-		2.42	3.90			
Amm-2 (j=2, p=2)	Mesh-1 (j=1, p=1)	+	12	2.75	4.65	Amm (j=2)	0.4508	0.4947
		-		2.84	4.35			
	Mesh-2 (j=1, p=2)	+	22	2.88	4.68			
		-		2.41	4.08			

The analysis of the results shows that, among the random variables, the groups 1 (masonry material), 6 (constitutive law of piers), 7 (constitutive law of spandrels) and parameter 8 (damping) involve a significant sensitivity of the response. In the case of the epistemic uncertainties, the height of piers does not have a great influence with respect to other parameters, while the flange effect is very significant.

In the case examined, the sensitivity to the wall-to-wall connection quality is highly variable in relation to the direction of verification (X or Y) and the way of application of load pattern (positive or negative). This result is due to the architectural and planimetric configuration of the structure, which for example, in the X direction, has on one side two inner walls coupled with continuity at all levels while, on the other side, only one. Figure B-12 shows a plan view of the intersections between inner and outer walls that affect the sensitivity of the response to the wall-to-wall connection.

In order to better clarify this aspect, Figure B-13 illustrates the capacity curves in X and Y directions, considering the load pattern applied to both positive and negative direction. In addition to the two conditions on wall-to-wall connection already introduced (Amm-1 and Amm-2), by way of example, there has been considered a further condition representative of the complete absence of coupling. The curves show that in the latter case the global response significantly changes (in this case one would also need to consider the activation of local mechanisms). In general it is evident that, for the examined case, the analyses in X and Y directions with positive sense are the ones most sensitive to this factor. The condition associated to the total absence of coupling is not realistic for the present case, considering the real seismic response exhibited by the building during the event of 2012 and the masonry type (since in general with brickwork it is constructively possible to achieve good conditions of coupling).

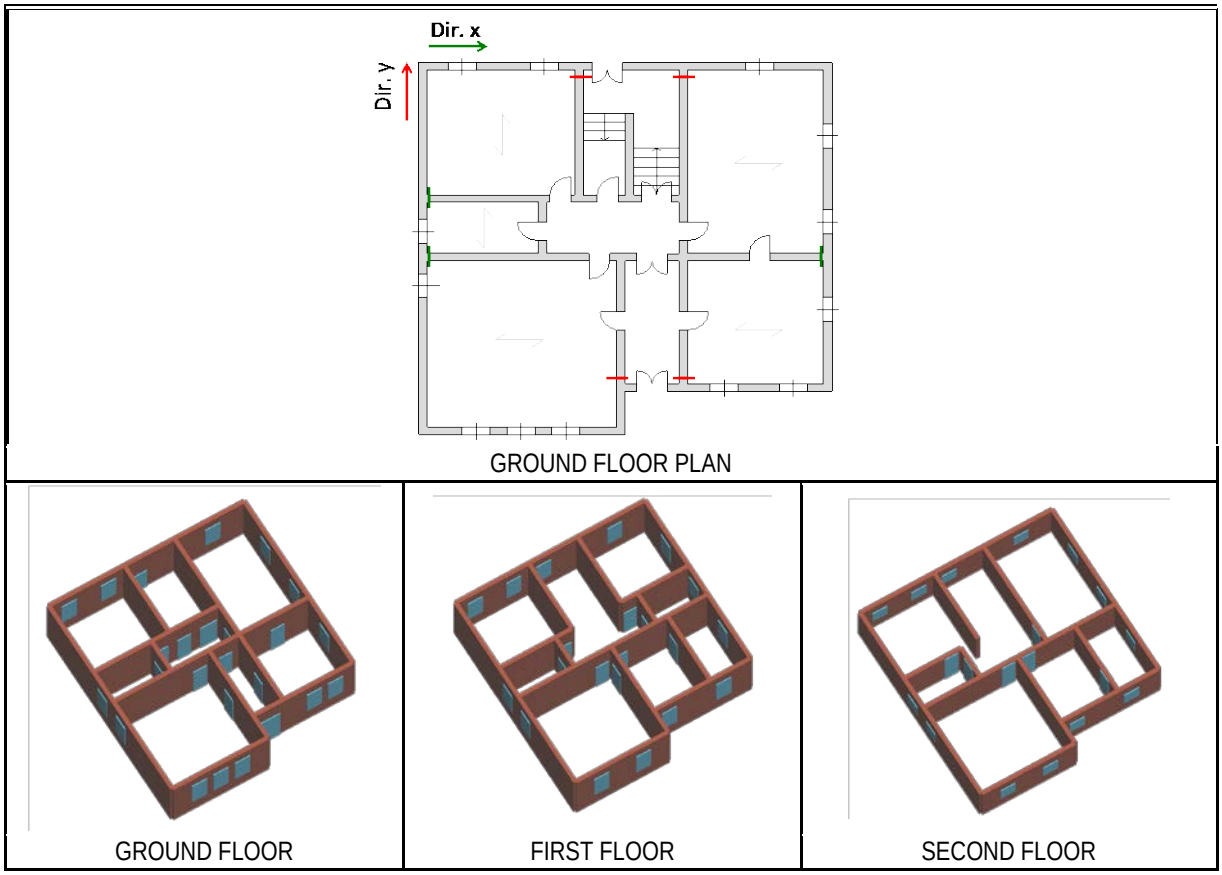

Fig. B-12 Localization on the plan view of the points where the conditions on the wall-to-wall connection were changed and planimetric configuration at the three floors which highlights how some internal walls are not continuous at all levels in X direction (reducing the sensitivity to this factor in particular in the negative sense)

Based on the results discussed above, in the risk analysis illustrated in the following paragraphs the effect of following parameters has been assessed:1, 6, 7 and 8, for the random variables; the wall-to-wall connection (conditions Amm-1 and Amm-2) for the epistemic factors.

B.5.4 Diagnostic surveys and investigations

The sensitivity analysis made it possible to highlight what are the parameters that most influence the seismic response of the building under consideration. This enables to plan the campaign of diagnostic investigations in order to minimize the residual uncertainties, compatibly with the available resources and the need to limit the invasiveness of slightly destructive investigations, being the latter an important aspect especially in the presence of heritage buildings. These investigations appear therefore justified only when supported by a real need of deepening.
In this case, among the uncertain parameters that have emerged as significant, the only ones on which it would be possible to learn more are those on the mechanical properties of the masonry. In this example we consider, for simplicity, that it was possible to perform a limited number of tests, sufficient to confirm the range of values initially adopted for the sensitivity analysis. As for the epistemic uncertainties of the model, the investigations on the structural details highlighted a good quality of the interlocking between perimeter and internal walls, but this does not allow us to state that two

piers belonging to two orthogonal walls behave as a single, rigidly connected element (under the hypothesis of plane section). Thus, both models (Amm-1 and Amm-2) will be then brought forward in the analysis.

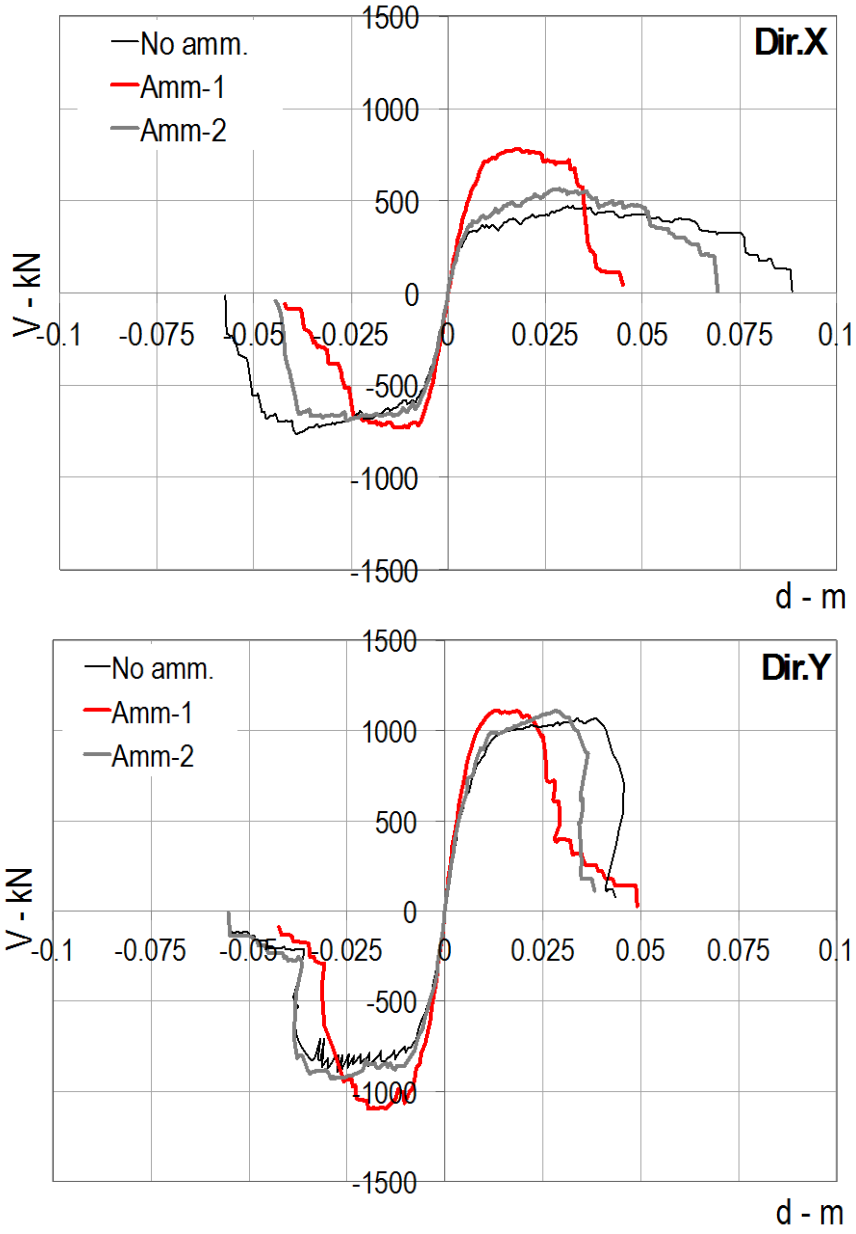

Fig. B-13 The resulting pushover curves in X and Y direction (positive and negative) as a function of the three hypotheses assessed for the wall-to-wall connection (Amm-1, Amm-2 and absence of connection)

B.6 Modeling and limit states

B.6.1 Modeling of the site response

As indicated in § 2.2.2, the change in the characteristics of the motion associated with the seismic response of the site under examination requires a detailed analysis of the local seismic response, which takes into account the uncertainty in the mechanical parameters of the soil. In this application, assuming that the building is on a type C soil,

it has been decided (§C.8.1) not to address in detail the issue and to take into account for the amplification in an approximate manner by a deterministic factor equal to 1.25 that amplifies the intensity measure on rigid soil.

B.6.2 Modeling of the uncertainties

B.6.2.1 Logic tree

Downstream of the results of the sensitivity analysis it was decided to perform risk analysis with two distinct models: the first of which considers a perfect coupling between orthogonal masonry panels while the second in which there is an elastic connection aimed to simulated an intermediate interlocking. Based on observation of the structural details it was decided to give more weight to the first hypothesis (p_1= 0.6); consequently for the second hypothesis $p_2 = 1-p_1 = 0.4$. This choice is also supported, in this specific case, from the observation of seismic damage, which does not show any cracking in correspondence of the wall-to-wall connection.
The size of the piers in the equivalent frame *mesh* (with respect to which the response was almost insensitive) was taken intermediate between the two hypotheses considered in the sensitivity analysis. Figure B-14 illustrates the mesh adopted for the five perimeter walls (as numbered in Figure B-8). In most cases there has been adopted a mesh consistent with the criterion "Mesh-2" described in §B.5.2 (also supported by the position of some cracks that occurred as a result of the seismic response to the event of May 2012), only in case of wall 3 instead was adopted the criterion"Mesh-1" (in order to avoid of defining unrealistically squat piers).

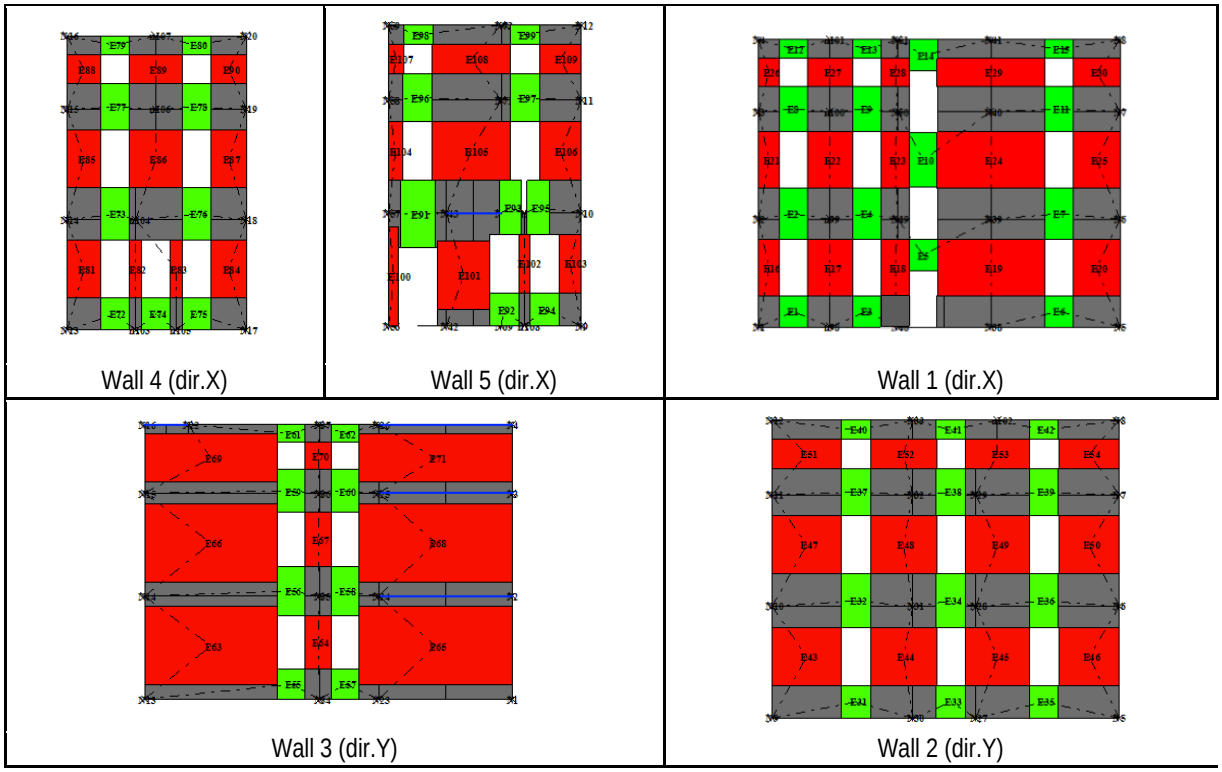

Fig. B-14 Final mesh adopted in the risk analysis

B.6.2.2 Continuous random variables

Diagnostic investigations have confirmed that the mechanical properties of the masonry of solid bricks and lime mortar are similar to those in the Table C8A.2.1 of Appendix C8A present in the Commentary to NTC 2008 (Circular No 617, 2 February 2009), and are among the lowest values of the range. Since it was not possible, due to the limited number of tests performed and their poor reliability, to probabilistically characterize these parameters, there was assumed for all of them a lognormal distribution, with mean values centered in the range used for the sensitivity analysis and dispersion β obtained considering the extremes of that range as corresponding to percentiles at 16% and 84%.

Table B-10. Probabilistic characterization of the random variables: the mean μ and the standard deviation β of the logarithm for lognormal variables; and shape parameters p and q for Beta variables.

Set	Parameter	Variable	Distribution	μ / p	β / q	Expected value
1	Masonry	E	Lognormal	6.49	0.2	675
		G		5.40	0.2	225
		$\hat{\mu}$		-1.06	0.15	0.35
		$\bar{f}_{vm0}$		-2.32	0.2	0.1
		f_m		1.00	0.25	2.8
6	Constitutive law of piers	δ_{T3}	Lognormal	-5.84	0.24	0.003
		δ_{T4}		-5.32	0.22	0.005
		δ_{T5}		-4.98	0.2	0.007
		δP_{F3}		-5.14	0.24	0.006
		δP_{F4}		-4.63	0.22	0.01
		δP_{F5}		-4.22	0.2	0.015
		β_{T3}	Beta	0.77	0.33	0.7
		β_{T4}		0.24	0.36	0.4
		β_{PF}		1.317	0.233	0.85
7	Constitutive law of spandrels	$\delta_{T3} = \delta_{PF3}$	Lognormal	-6.24	0.24	0.002
		$\delta_{T4}=\delta_{PF4}$		-5.15	0.25	0.006
		$\delta_{T5} = \delta_{PF5}$		-3.94	0.25	0.02
		$\beta_{T3} = \beta_{T4} = \beta_{PF}$	Beta	0.125	0.125	0.5
8	Energy dissipation of piers*	α_{mT}	Beta	0.120	0.08	0.6
		β_{mT}		Deterministic assumption		0.8
		γ_{mT}		-0.010	-0.09	0.1
		δ_{mT}		Deterministic assumption		0
		α_{mPF}		0.480	0.12	0.8
		β_{mPF}		Deterministic assumption		0.8
		γ_{mPF}		0.840	0.56	0.6
		δ_{mPF}		0.750	0.75	0.5
8	Energy dissipation of spandrels*	$\alpha_{mT=}\alpha_{mPF}$	Beta	-0.023	-0.1275	0.15
		$\gamma_{mT}=\gamma_{mPF}$		0.330	0.77	0.30

* The values of the quantities governing the hysteretic cyclic behavior of piers and spandrels (in addition to a viscous component) are used in the case of method A, while in the case of the method C, there was used a damping law, by assuming a range of variation of the parameter ζ (the asymptotic value of the hysteretic damping) between 0.25 and 0.4. Such values are assumed to correspond to the fractiles16% and 84%.

The parameters defining the constitutive laws of piers and spandrels and the related levels of damage have been gathered from laboratory tests and cannot be verified on situ. The stochastic characterization is performed, similarly to the case of the elastic properties and strength of masonry, assuming the interval used in the sensitivity analysis as corresponding to the above percentiles. For the values of drift corresponding to the different levels of damage a lognormal distribution is assumed, while for the residual strength (which varies between 0 and 1) a Beta distribution is assumed.
Table B-10 shows the stochastic characterization of uncertain parameters.
Figure B-15 illustrates, by way of example in the case of piers, the effects of the variation of the parameters α_m, γ_m and δ_m on the hysteretic response; in particular, the figure illustrates the maximum variation in the case where the parameters are set respectively to the values at the 16% and 84% fractiles, with which the minimum or maximum dissipation is obtained respectively.
The sampling of the 30 arrays of values of the random variables needed for the application of method A was performed as follows. For each group there was sampled a standard normal variable u . The value of each variable X_i of the group was then obtained by the transformation:

$$x_i = F_i^{-1}\left[\Phi(u)\right] \qquad \text{(B.2)}$$

in which F_i and Φ are respectively the cumulative distribution of Xi and the normal standard distribution. The sampling was carried out independently for each of the groups of random variables.

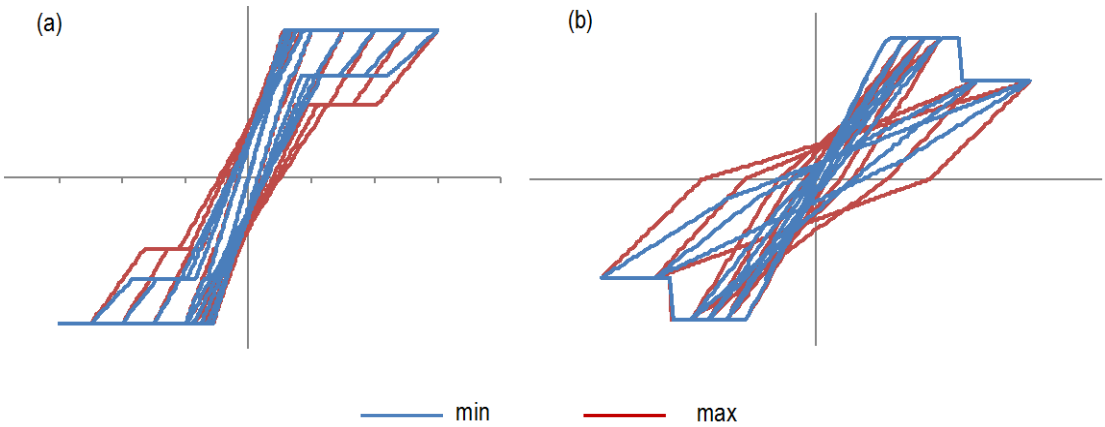

Fig. B-15 Effect of the parameters α_m, γ_m and δ_m on the hysteretic response at scale of the single masonry panel: a pier with a prevailing flexural (a) or shear (b) response

Figure B-16 shows the distributions obtained for four uncertain parameters, each one belonging to a different group of random variables (Table B-10).

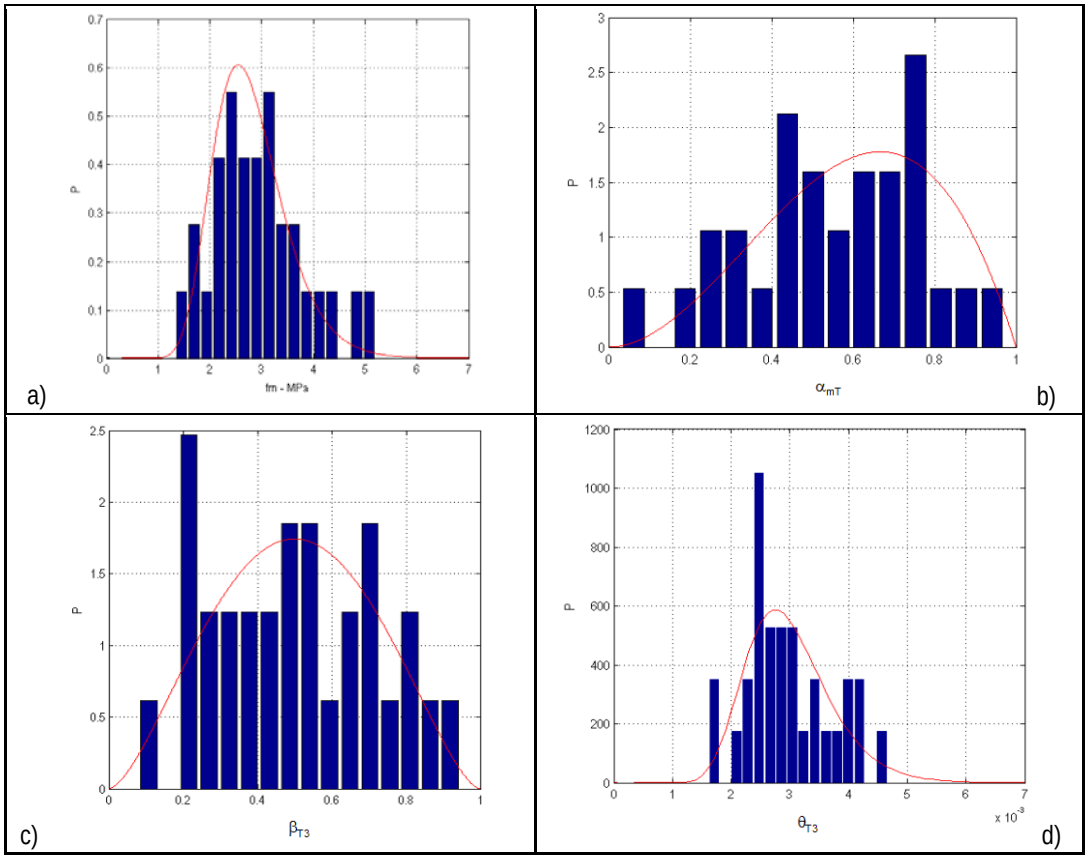

Fig. B-16 Histograms relating to the distribution of the stochastic sampling obtained for some of the variables belonging to four of the sets of random variables considered: a) the compressive strength of the masonry f_m (from set 1 - Masonry); b) α_{mT} (from set 8 - Energy dissipation of piers); c) β_{T3} (from set 7 – constitutive law of spandrels); θ_{T3} (from set 6 - constitutive law of piers).

B.6.3 Limit state variables

For the three limit states considered proper variables were used as defined in §2.5, with specific indications for the global response of masonry buildings as clarified in §3.3.1. Limit states SLD and SLC are based on a multi-scale approach, which considers the damage and the seismic response at different scales: that of piers and spandrels, through checks on the cumulative damage indicators; the masonry walls, through the interstorey drift (in this case checks on angular strain of diaphragms were not considered as they are almost rigid); the global response, described by the capacity curve.

The limit state SLS is instead defined by an integral measure of the cost of repair of all the elements (piers and spandrels), evaluated according to the level of local damage through a proper cost function.

Regarding the application of the multi-scale approach to non-linear dynamic analysis with method A, the indications of §3.3.1 have been used. In particular the (3.25) has been used for the SLD, while the (3.34) for the SLC. In the case of the SLS we have assumed a conventional cost $\tau_{SLS} = 0.6$. For the calculation of the cost function of global repair C_G (3.32), the reference thresholds assumed correspond to a damage level slightly preceding the severe level ($C_j = 0.5\theta_3$), in the case of piers, and to the severe level ($C_j = \theta_3$), in the case of spandrels; the latter assumption is consistent

with the lintel type that characterizes the building, that is a flat brick arch without tie-rods .
In the case of the non-linear static analysis (method C), the points corresponding to the attainment of each limit state are identified on the capacity curve; then, for SLC and SLD, the limit state variable Y is defined by the ratio between demand and capacity in terms of displacement of the equivalent non-linear single degree of freedom. In the case of SLS, the limit state variable is instead calculated through (3.33), taking as a conventional global cost value $\tau_{SLS} = 0.3$, half of that adopted in method A. This choice is motivated by the fact that with the method A the two components of seismic motion are applied simultaneously (so the damage is spread in all the walls) while with the nonlinear static analysis only one direction is mainly activated. Moreover with the dynamic analysis the damage spreads further along the height, due to the contribution of the higher modes.

B.7 Analysis and Verification

B.7.1 Validation of the model

The reliability of the modeling approach adopted was evaluated by simulating the seismic response of the structure after the event of May 29, 2012 (M_L = 5.8, depth 9.6 km with its epicenter near Mirandola). For the numerical simulation the recording of the station SAN0 located in San Felice sul Panaro (less than 500 meters away from the building under examination) were adopted, being installed after the previous event of 20 May 2012 in addition to those of the Rete Accelerometrica Nazionale (RAN)[27] already present in the area. Figure B-17 illustrates the recordings in terms of acceleration and the relative response spectra; the NS component is mainly acting in the X direction, while the EO in the Y direction.

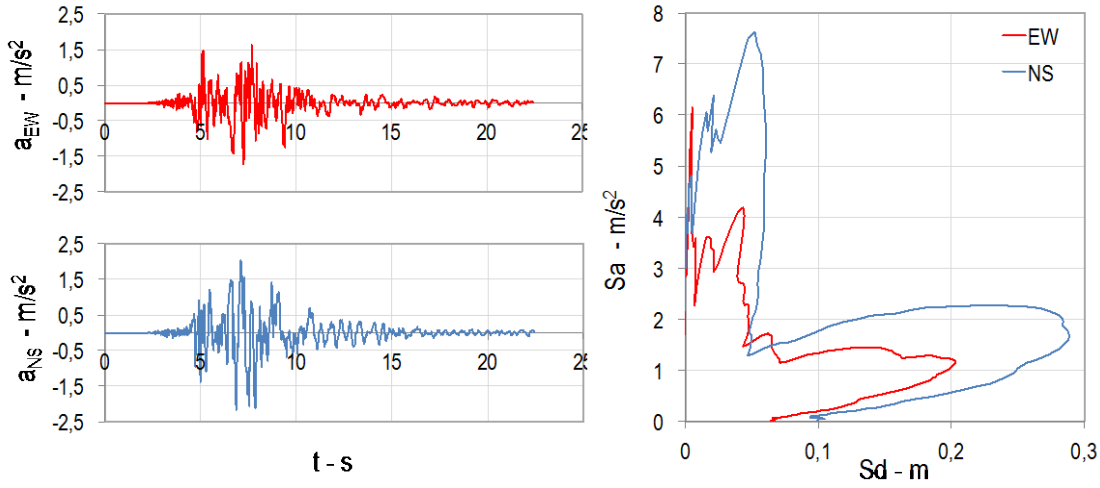

Fig. B-17) a) Accelograms from SAN0 registration of 29 May 2012; b) response spectra in ADRS format.

[27] http://www.protezionecivile.gov.it/jcms/it/ran.wp

The numerical simulation was carried out by performing nonlinear static and dynamic analyses, taking as reference the mean values of the mechanical parameters as introduced in B6.2.2.
Figure B-18 illustrates the results of non-linear static analysis (by way of example with a positive direction) performed in the X and Y directions as a function of various load patterns adopted, respectively, proportional to: 1) masses; 2) the product in each node of the mass and the corresponding height; 3) the first modal shape.

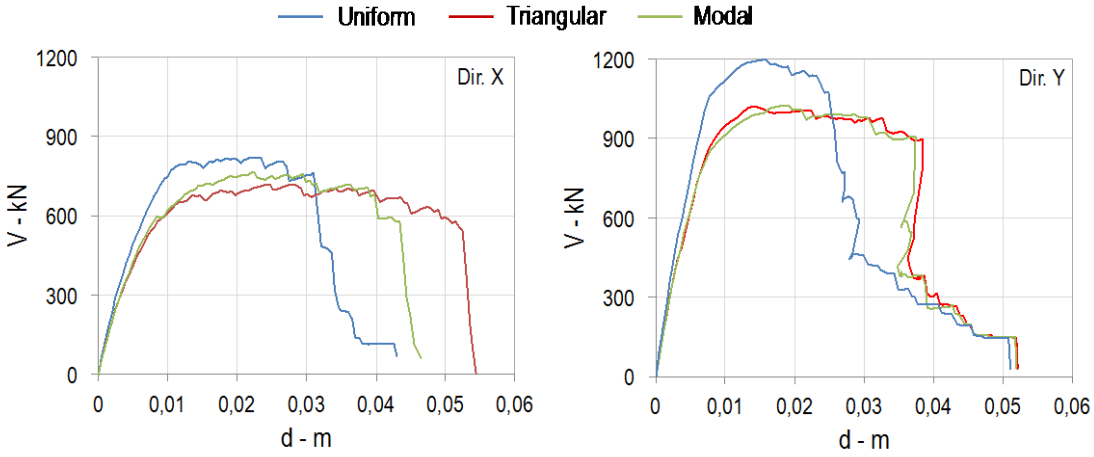

Fig. B-18 Results of the non-linear static analyses in X and Y directions as a function of the various load patterns adopted

In Figure B-19 (for the X direction) and B-20 (for the Y direction) the comparison, in terms of V-d curves, between the results of nonlinear dynamic and static analyses is shown. Dynamic analyses were performed by applying in addition to the NS and EW components also the vertical component (the results of the application of records with positive and negative ways are marked in grey and black, respectively). In the case of the non-linear static analysis, among the different load patterns adopted, the one proportional to the masses in general provides results more consistent with those obtained by the dynamic analysis. In the case of such distribution, in Figures B-19 and B-20 the displacement thresholds corresponding to the attainment of limit states SLD, SLS and SLC, as defined according to the criteria previously introduced (§B6.3), are also represented. The maximum displacement obtained from the dynamic analysis lies between the thresholds of limit states SLD and SLS defined from the static analysis, in the X direction, and slightly before the SLD, in the direction Y. This result is in agreement with the global damage level observed on the structure. These curves clearly show that in the X direction the structure has reached a higher level of non-linearity of the response than Y direction; this is also consistent with the observed damage, which is more severe in the walls oriented along NS (X, Figure B-1). Moreover, the damage simulated by the nonlinear dynamic analyses matches well with that observed in terms of extent, severity and prevailing failure modes on panels (Figure B-21).
Finally, the maximum acceleration compatible with the SLC, evaluated in the X direction with the non-linear static procedure based on the use of overdamped spectra (obtained starting from those of Figure B-17b) is comprised between 1.64 and 8.2 m/s^2 (as a function of the load pattern adopted): a value that is compatible with the peak acceleration at the ground of the real seismic event, equal to 2.16 m/s^2.

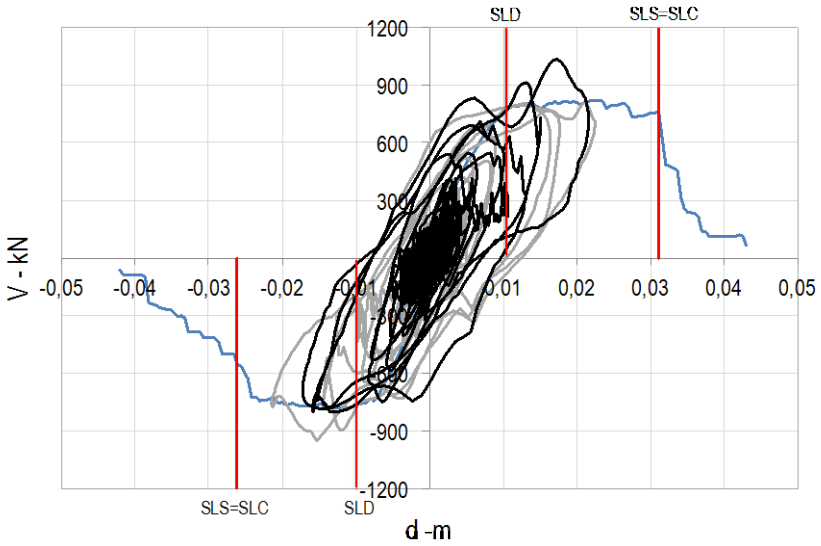

Fig. B-19 Direction X: comparison of the results of non-linear static and dynamic analysis

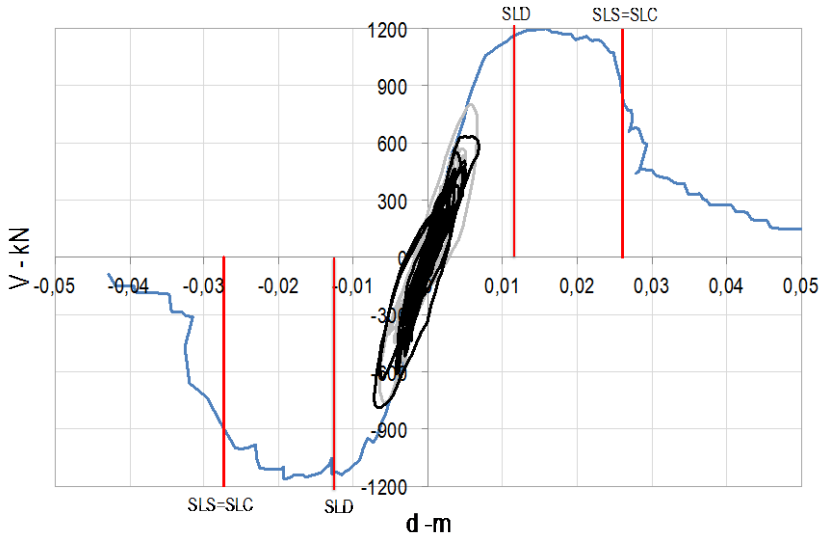

Fig. B-20 Direction Y: comparison between the results of non-linear static and dynamic analyses

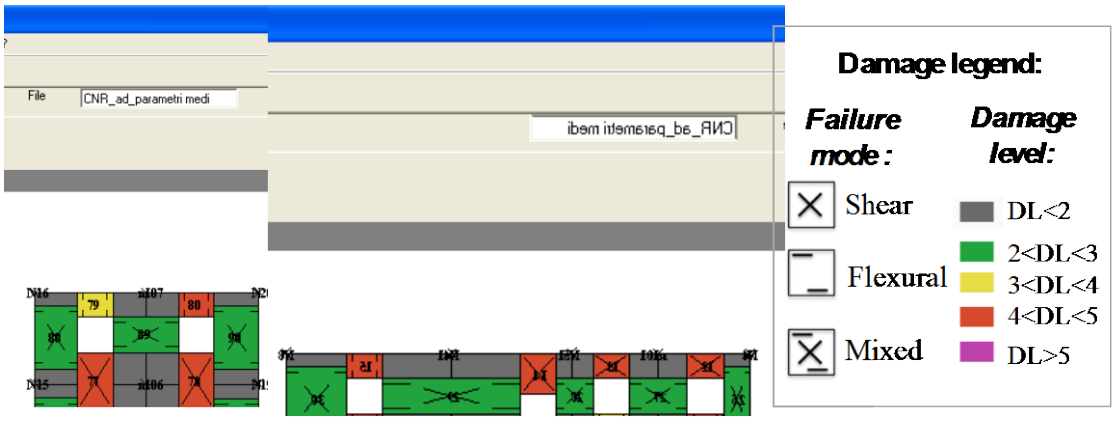

Fig. B-21 Damage simulated for the walls 4 and 1 oriented in the X direction

B.7.2 Modal analysis and methods of non-linear analysis

Before the application of the methods addressed to the risk analysis, a modal analysis has been performed on the two models of the logic tree, by referring to the mean values of the random variables (Table B-10). The fundamental period of vibration varies between 0.26 s and 0.27 s respectively for the case of the model Amm-1 (perfect coupling) and Amm-2 (intermediate wall-to wall connection simulated by an elastic connection); it activates a participating mass in the X direction of 86%. The first significant mode in the Y direction corresponds to a period equal to 0.23 s for both models, with a participating mass comprised between 82% and 86% in the two cases. Figure B-22 illustrates the plan deformed shapes associated with the fundamental modes in X and Y directions, for the model Amm-1 (first branch of the logic tree). Figure B-23 shows the two modal shapes in height, in terms of average floor displacement components; one observes how such deformed trends are well approximated by a triangular shape. The fundamental period well agrees with that obtained by the formula suggested by the NTC 2008 (§B4), which was used to compute the seismic intensity measure $S_a(T_1)$.

The ratio between the participation factors of first modes is equal to: $\Gamma_{1Y} / \Gamma_{1X} = -0.033$, in the direction X; and $\Gamma_{3X} / \Gamma_{3Y} = 0.055$, in the Y direction.

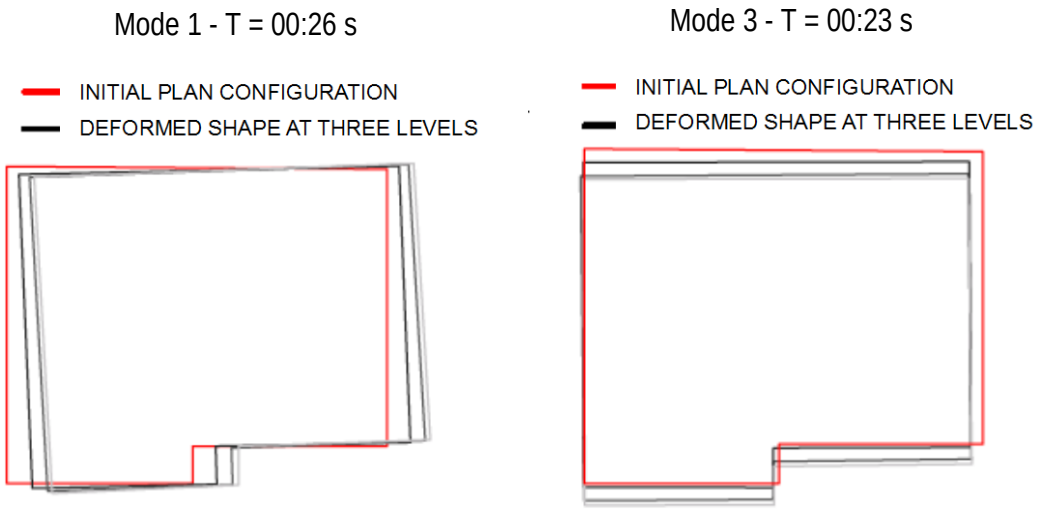

Fig. B-22 Plan deformed shape related to the modes 1 and 3 for model Amm-1 (first branch of the logic tree); the different colors are associated with the different levels of the building.

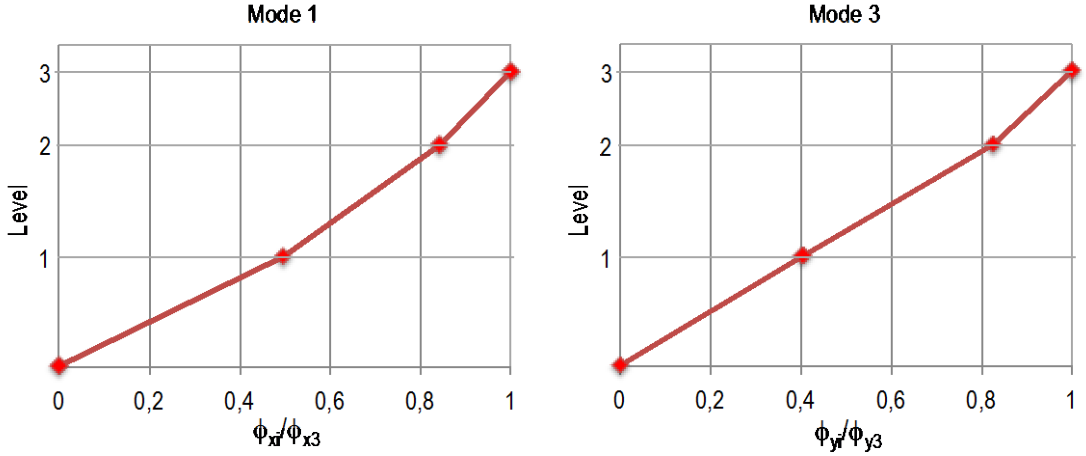

Fig. B-23 Deformed shape in height of the modes 1 and 3 for model Amm-1 (first branch of the logic tree).

In applying the method C, in line with what is indicated in §3.2.1.5, the regularity of the dynamic response of the building allows, for both directions of verification, the use of non-linear static analysis considering only the first mode; moreover, it is not necessary to consider, for each direction of verification, the contribution due to excitation in the orthogonal direction (bidirectional effect).

B.7.3 Verification with Method A

For simplicity and economy in the description of the case study, the method A is applied only to the first branch of the logic tree (Amm-1).
For the non-linear dynamic analysis, 30 different models were used characterized by parameters generated in accordance with the probability distributions assumed; then, each of them is associated with one of the 30 selected records, applying the NS

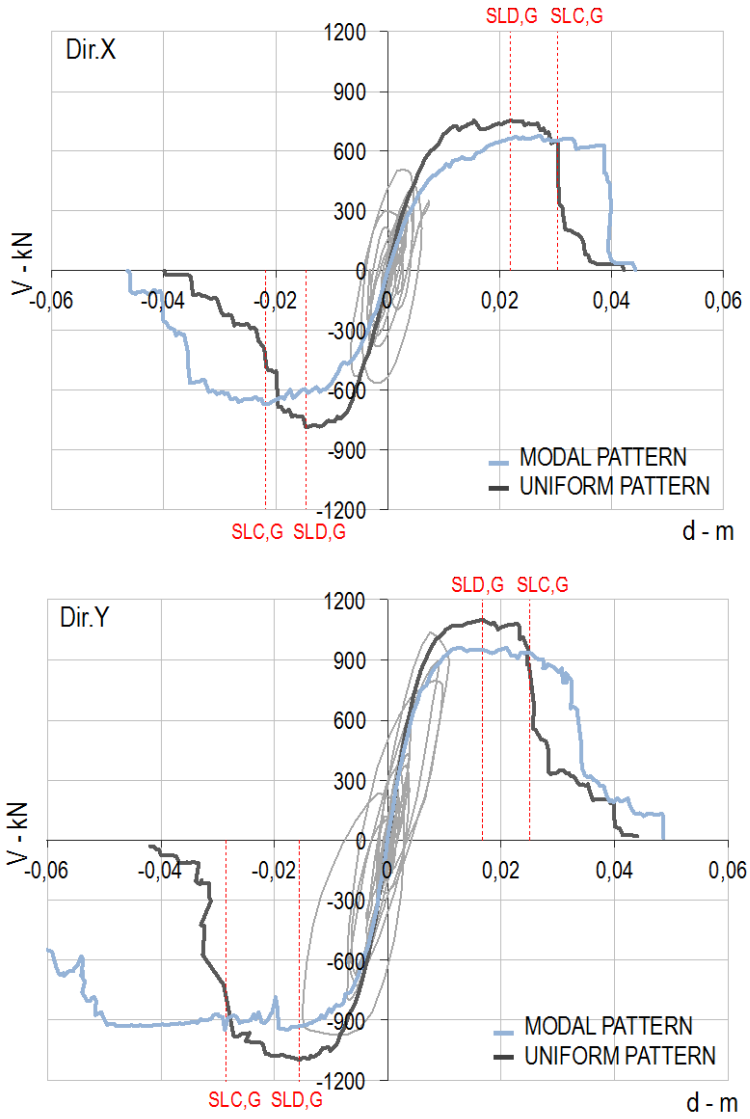

Fig. B-24 Cyclic response in X and Ydirections following the application of the event 1, scaled to the value $S_a(T_1)$=6.25 m/s² and comparison with the pushover curves obtained from non-linear static analysis.

component according to the direction X. The incremental dynamic analysis is performed by scaling the records so that the intensity measure takes on increasing values until, for each seismic event, the three limit states are achieved.

The definition of limit state variable used for the application of the multi-scale approach in the case of the dynamic non-linear analyses has been discussed at §B.6.3.
In order to exemplify the procedure, the results corresponding to the event 1 of Table B-2 (Friuli - M = 6.0 - station ST28), are illustrated in the following, being the components of the event shown in Figure C-7.
The Figures B-24 and B-25 illustrate the cyclic response (base shear / average top displacement of the structure), for the two main directions of the building, for the seismic event 1 scaled to two different levels of intensity $S_a(T_1)$: 6.25 and 10.84 m/s ^{2}. The cyclic response is compared with the pushover curves obtained by nonlinear static analysis, performed in both directions and with two load patterns: a) proportional to the first modal shape; b) proportional to the masses. On these curves the points at which the three SLs are achieved in the case of the load pattern proportional to the masses and by considering only the checks at the global scale, are also indicated.

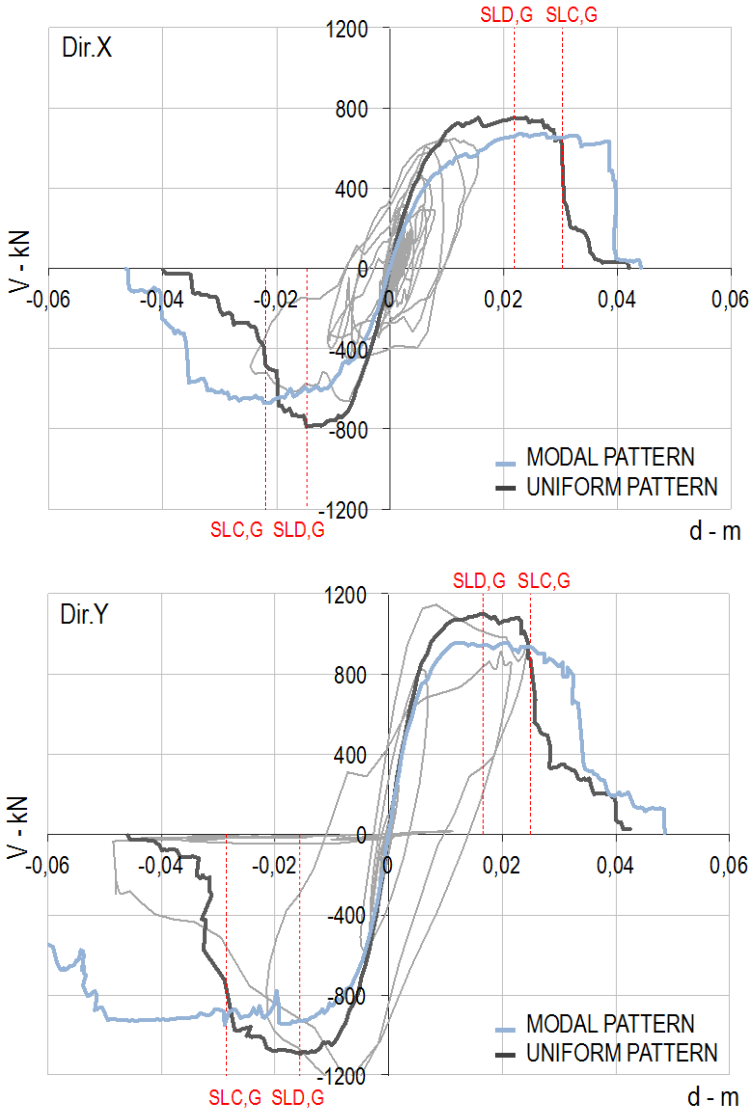

Fig. B-25 Cyclic response in X and Y directions following the application of event 1, scaled to value $S_a(T_1)$=10.84 m/s^2, and comparison with pushover curves obtained from the non-linear static analysis.

One can observe how the dynamic response is consistent with that resulting from the non-linear static analysis; in particular, for relatively low values of the seismic intensity (Fig. B-24), those that lead to the SLD, both the two load patterns are in agreement with the result of non-linear dynamic analysis, while for increasing values of the seismic intensity (Fig. B-25), the dynamic response is more consistent with the prediction of the SLC obtained from the load pattern proportional to the masses.
As regards the checks at the scale of structural elements introduced by multi-scale approach, Fig. B-26 shows the variation with time of the entities necessary for computing the limit state variables$Y_{SLD,S}$ and $Y_{SLS,S}$; results refer to the dynamic response already illustrated in Fig. B-24. The SLD has already been attained since the accumulated damage in spandrels, for the damage level 3, has exceeded the threshold of 3% (while only two piers have reached the damage level 2). For the SLS the cost variable C_G reaches at the end the value 0.3, which is lower than the limit threshold assumed (C_{SLS} = 0.6). No figure is shown relative to the SLC because no pier has yet reached the damage level 5.

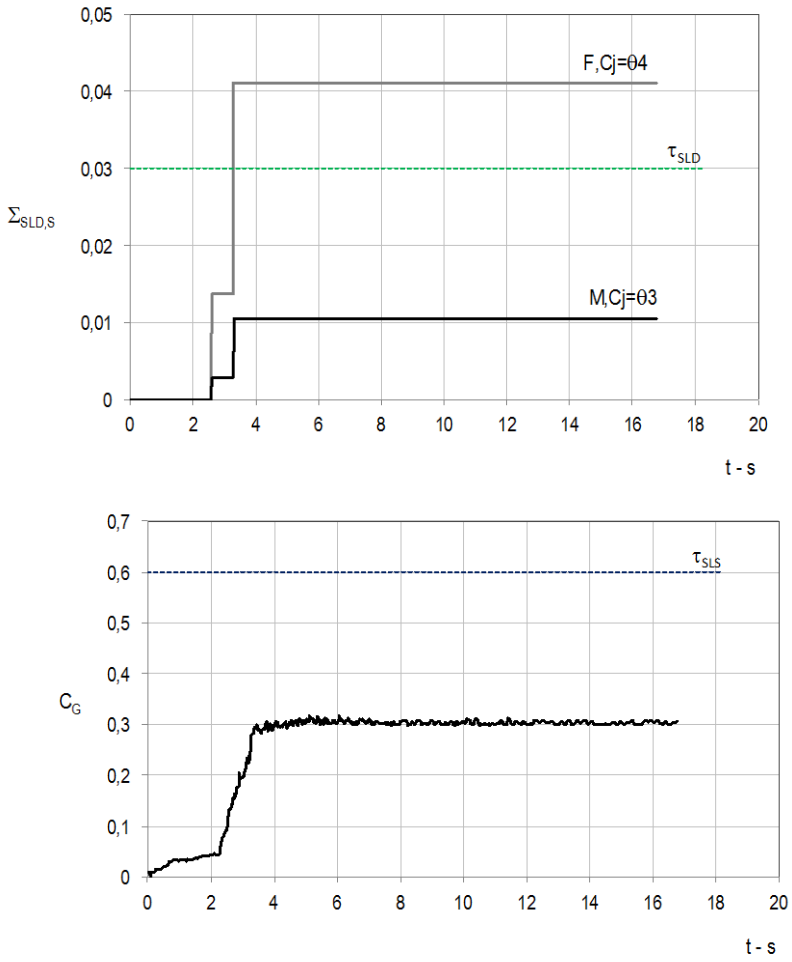

Fig. B-26 Variation with time of the entities necessary for the calculation of the limit state variables at the scale of the element (the cumulative damage indicator Σ_{SLD}) and the cost function (C_G), resulting from the application of the event 1 scaled to the value $S_a(T_1)$ =6.25 m/s^2.

Figure B-27 shows the variation with time of the entities necessary for computing the limit state variable $Y_{SL,S}$ for the three limit states, in the case of the dynamic response of Fig. B-25. The damage accumulated in piers, with reference to the damage level 2, and that in spandrels, with reference to the damage level 3, which are necessary for

the check on the attainment of SLD, are further increased with respect the level of seismic intensity already shown. The cost variable C_G has exceeded the limit assumed for the attainment of SLS (τ_{SLS} = 0.6). Finally, for the SLC, the damage accumulated in piers with reference to the damage level 5 has exceeded the threshold of 3%.

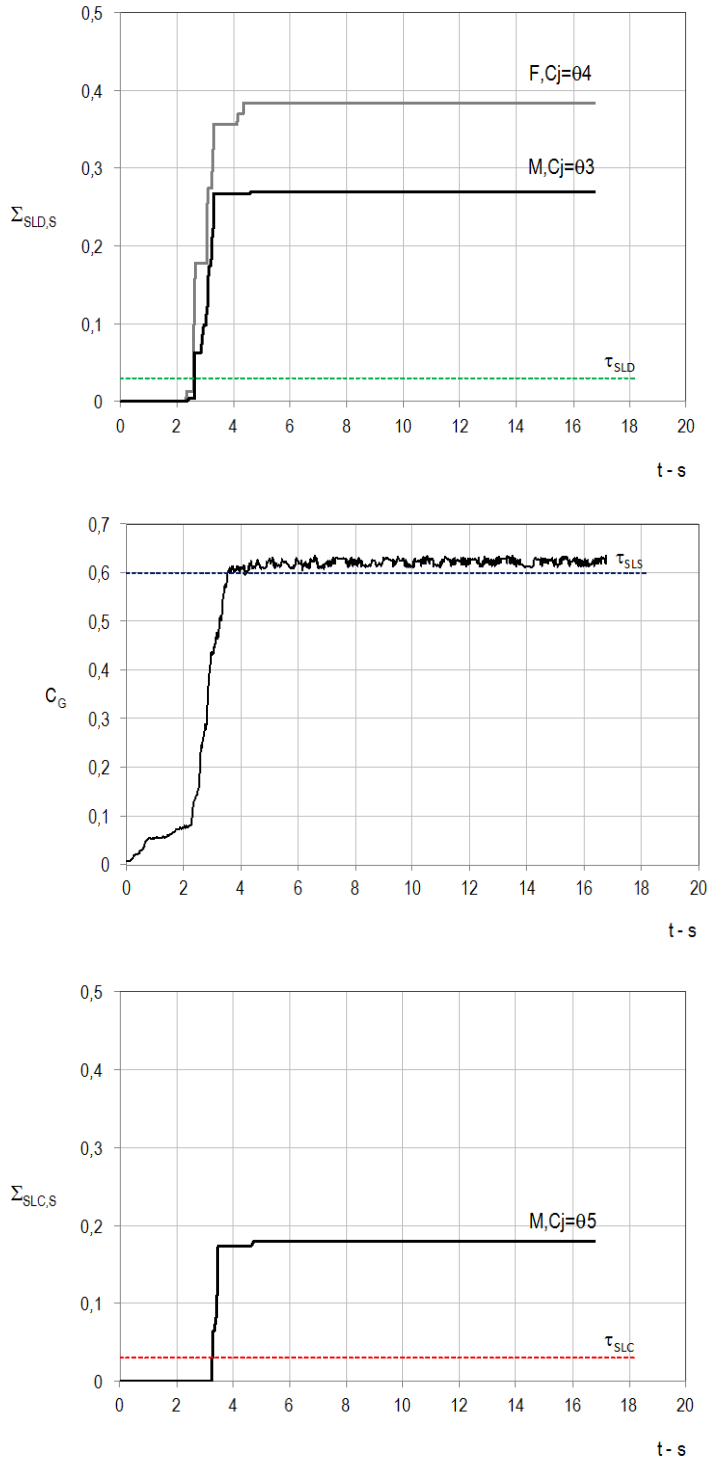

Fig. B-27 Variation with time of the entities necessary for the calculation of the limit state variables at the scale of the element (the cumulative damage indicators Σ_{SLD} , Σ_{SLC}) and cost function (C_G), resulting from the application of the event 1 scaled to the value $S_a(T_1)$ =10.84 m/s^2.

As regards the checks of the multi-scale approach at the scale of macroelements, Figure B-28 shows the variation with time of the maximum interstorey drift (which herein occurs in the wall 13 on the 3rd floor), obtained for the two levels of the seismic intensity already considered in the previous figures. It can be observed that in the first case the threshold of 0.2%, assumed as reference for the evaluation of the limit state $Y_{SLD,M}$, is exceeded, while, in the second case, even the threshold of 0.6%, adopted for the limit state variable $Y_{SLC,M}$, is exceeded.
Table B-11 shows the values of the three limit state variables for the two levels of intensity considered, obtained from (3.25) and (3.34) as the highest among the partial limit state variables, considered by the multi-scale approach.

Table B-11. Limit state variables obtained from the multi-scale approach, from the response of the building shown in Figures B-25/26/27/28/29.

$S_a(T_1)$ [m/s^2]	*SLD*				*SLS*	*SLC*			
	$Y_{SLD,S}$	$Y_{SLD,M}$	$Y_{SLD,G}$	Y_{SLD}	Y_{SLS}	$Y_{SLC,S}$	$Y_{SLC,M}$	$Y_{SLC,G}$	Y_{SLC}
6.25	1:37	2.72	0.96	2.72	0.77	12:00	0.91	0.60	0.91
10.84	12.79	6.93	3.12	12.79	1.19	5.98	2.31	1.95	5.98

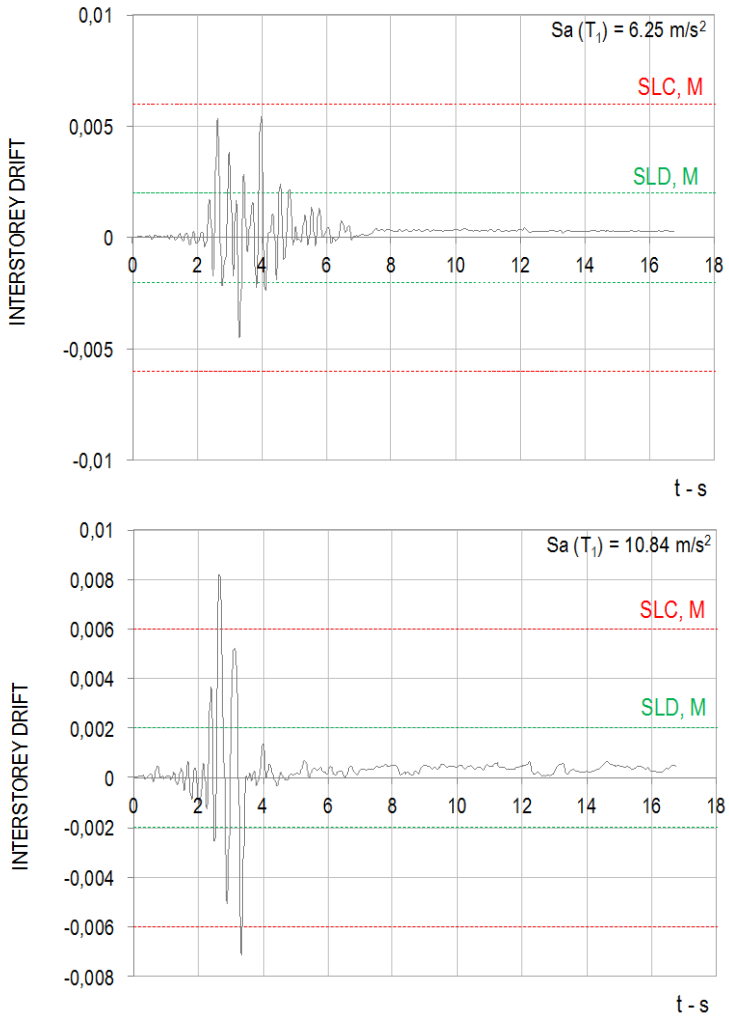

Fig. B-28 Variation with time of the interstorey drift, relatively to the wall and diaphragm that present the maximum values, for the two levels of the intensity measure shown in the previous Figures.

The result processing described above has been performed for all 30 models, obtaining the variation of all the parameters of response and of the limit state variables as a function of the seismic intensity.
Figure B-29 shows the maximum displacement of the top of the building as a function of the seismic intensity, for the 30 models considered (and the relative recordings); on each curve the reaching of the limit states is indicated with a different colored dot. One observes, in particular for limit states SLS and SLC, how they are achieved by values very scattered both in intensity and displacement. Furthermore, in some cases, according with the analytical definition proposed for the SLS, these two SLs coincide; this happens when the condition of SLC occurs before the damage has spread significantly, that is when the condition $C_G < C_{SLS}$ occurs on the cost function . This result is consistent with the behavior that often occurs in masonry buildings, with limited ductility and a rather brittle response, resulting in the activation of a failure mechanism that may involve a limited number of structural elements.
Figure B-30 shows the curves resulting from the incremental dynamic analysis (IDA curves) in terms of the limit state variables Y_{SLD} , Y_{SLS} and Y_{SLC} , plotted against the seismic intensity measure $S_a(T_1)$. The values of the seismic intensity measure for which each curve reaches the value 1 are analyzed statistically, assuming that they are distributed as a lognormal; the corresponding parameters are shown in the top of each of three graphs illustrated in Figure B-30.

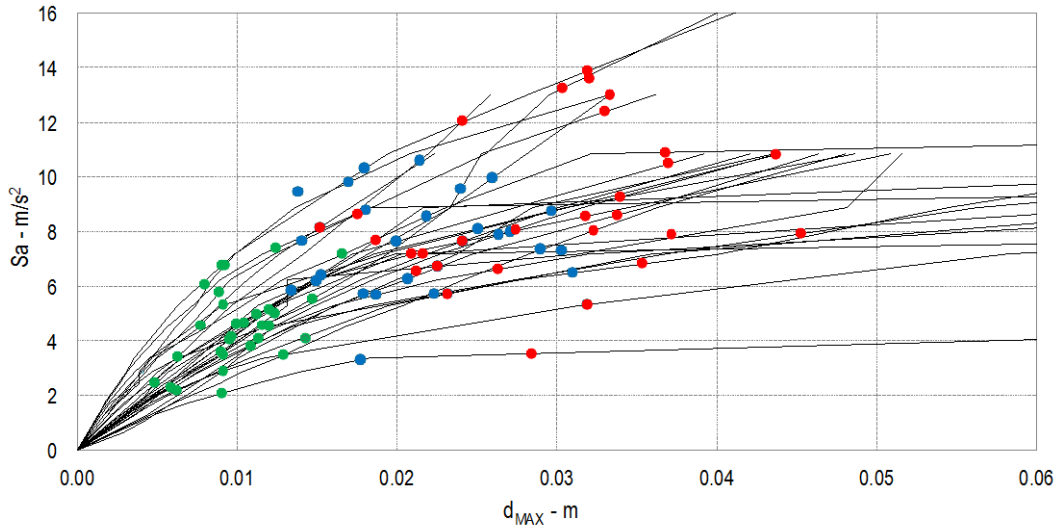

Fig. B-29 Incremental Dynamic Analysis (IDA) curves in terms of maximum displacement at the top of the building versus the seismic intensity measure, for the 30 models considered; the green , blue and red dots correspond to the achievement of the SLD, SLS and SLC, respectively.

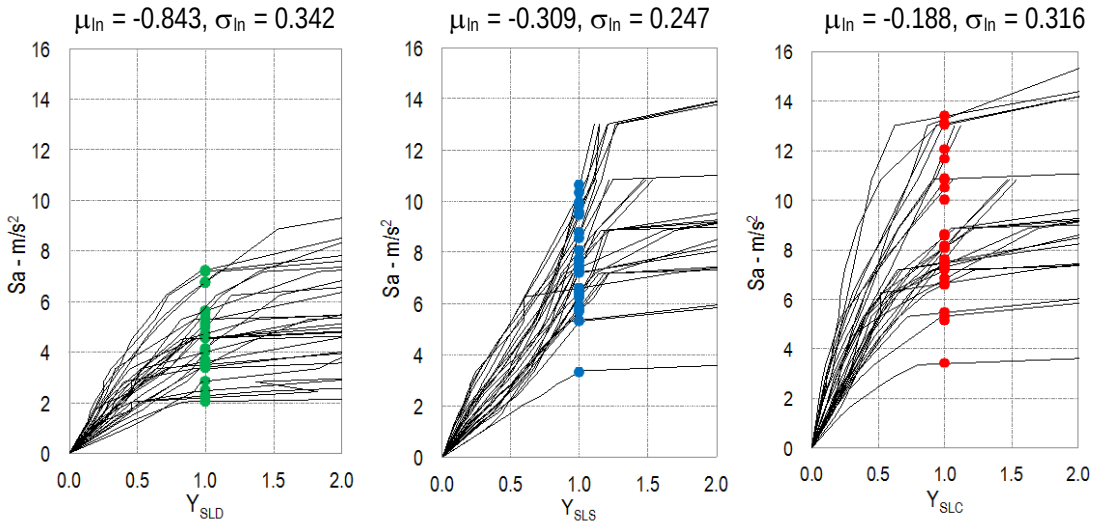

Fig. B-30 Incremental Dynamic Analysis (IDA) curves in terms of limit state variable Y_{SL} (up above, the parameters that define the lognormal distribution adopted for statistically processing the intensity measures that lead to SLD, SLS and SLC).

The mean annual frequency of exceedance of each LS is obtained from (2.12) discretizing the curve of hazard evaluated in §B4. The resulting values are listed in Table B-11, where they are compared with the reference limit thresholds presented inTable 2-1, having assumed a class of use II, since the building is private and for residential use. The building complies the safety requirements for the SLD and SLS, while is vulnerable towards the SLC.

Figure B-31 shows the fragility curves for the three limit states, defined by (2.13). It is worth noting how the curves associated to the SLS and SLC are very close, which means that this building, if it does not collapse, is repairable. It appears useful to recall that the introduction of the cost function aims to quantitatively define the limit condition of reparability associated with a concept of economic convenience; instead, the criteria at the base of the SLC are able to highlight conditions of fragility of the construction, which can lead to the collapse even in the presence of a not very widespread damage.

Finally, Figure B-32 shows the contribution of the different levels of seismic intensity to the total probability. The median value of the distribution of the seismic intensity measure which leads to the corresponding SL is indicated as well.

Table B-11. Mean annual frequency of exceedance of the limit states SLD, SLS, SLC and their corresponding return periods; comparison with the maximum tolerated threshold values.

	λ_{SLD}	λ_{SLS}	λ_{SLC}
Method A	0.0082	0.0023	0.0020
Maximum tolerated thresholds	0.045	0.0047	0.0023
	$T_{r,SLD}$	$T_{r,SLS}$	$T_{r,SLC}$
Method A	122	426	508

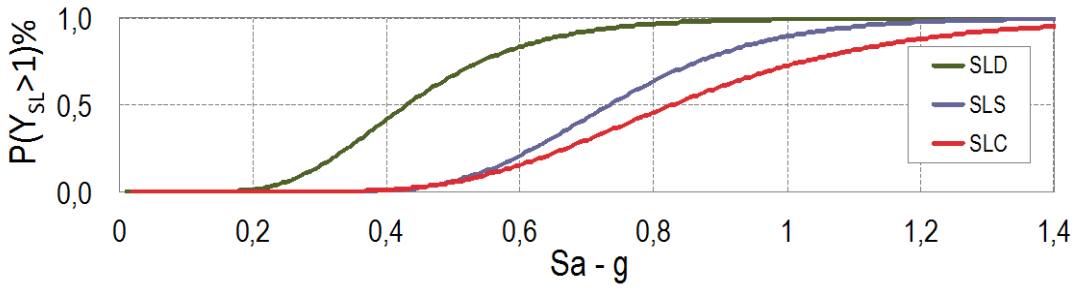

Fig. B-31 Fragility curves of the three limit states.

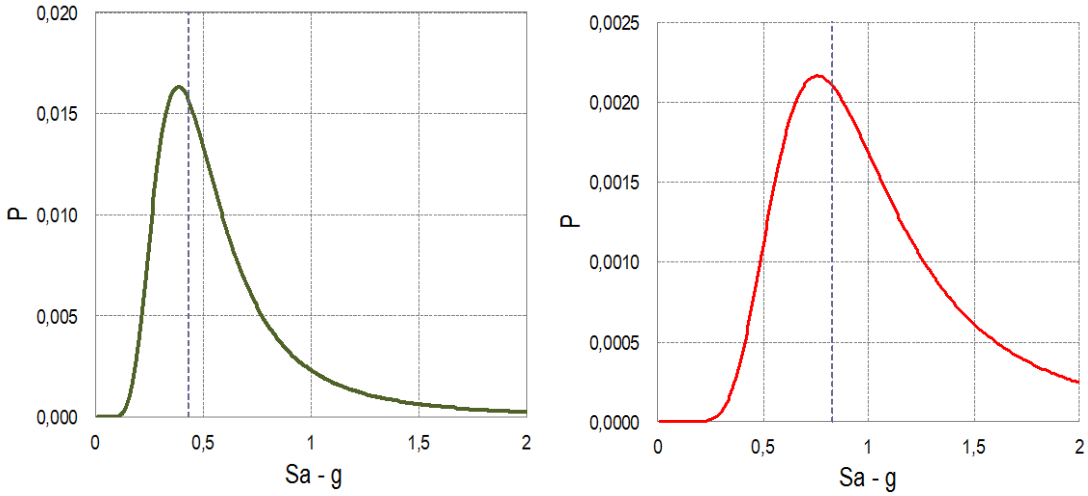

Fig. B-32 Distribution of the conditional probability for the computation of the limit states SLD and SLC (the vertical dotted line indicates the median value of the seismic intensity measure which leads to the attainment of SL).

B.7.4 Verification with Method C

The following shows the risk analysis according to the method C.
In particular, the non-linear static analyses have been performed by adopting exclusively the load pattern proportional to the masses, being this choice motivated by the comparison between the dynamic and static analyses described in §B7.3 that showed in this case a greater agreement in particular at the SLC. This load pattern is associated with a much more brittle behavior of the response, as shown in Figure B-18, because of the activation of a soft story mechanism at the ground floor.
In more general terms, it would be necessary to consider other load patterns, then taking as final value of the risk analysis that obtained by a combination of the results through the logic tree technique. Conversely, in the absence of comparison of data with non-linear dynamic analyses or other evidence on the structural behavior, when it is therefore not possible to attribute a degree of reliability to each of the load patterns considered, the final value of the risk analysis can be adopted, on the safe side, as the greater of those obtained by all the load patterns considered.
Figures B-33 and B-34 show the results of non-linear static analyses in X and Y directions (positive and negative directions) for the two branches considered of the logic tree (Amm-1 and Amm-2); the analyses refer to the adoption of the mean values for all the random variables.

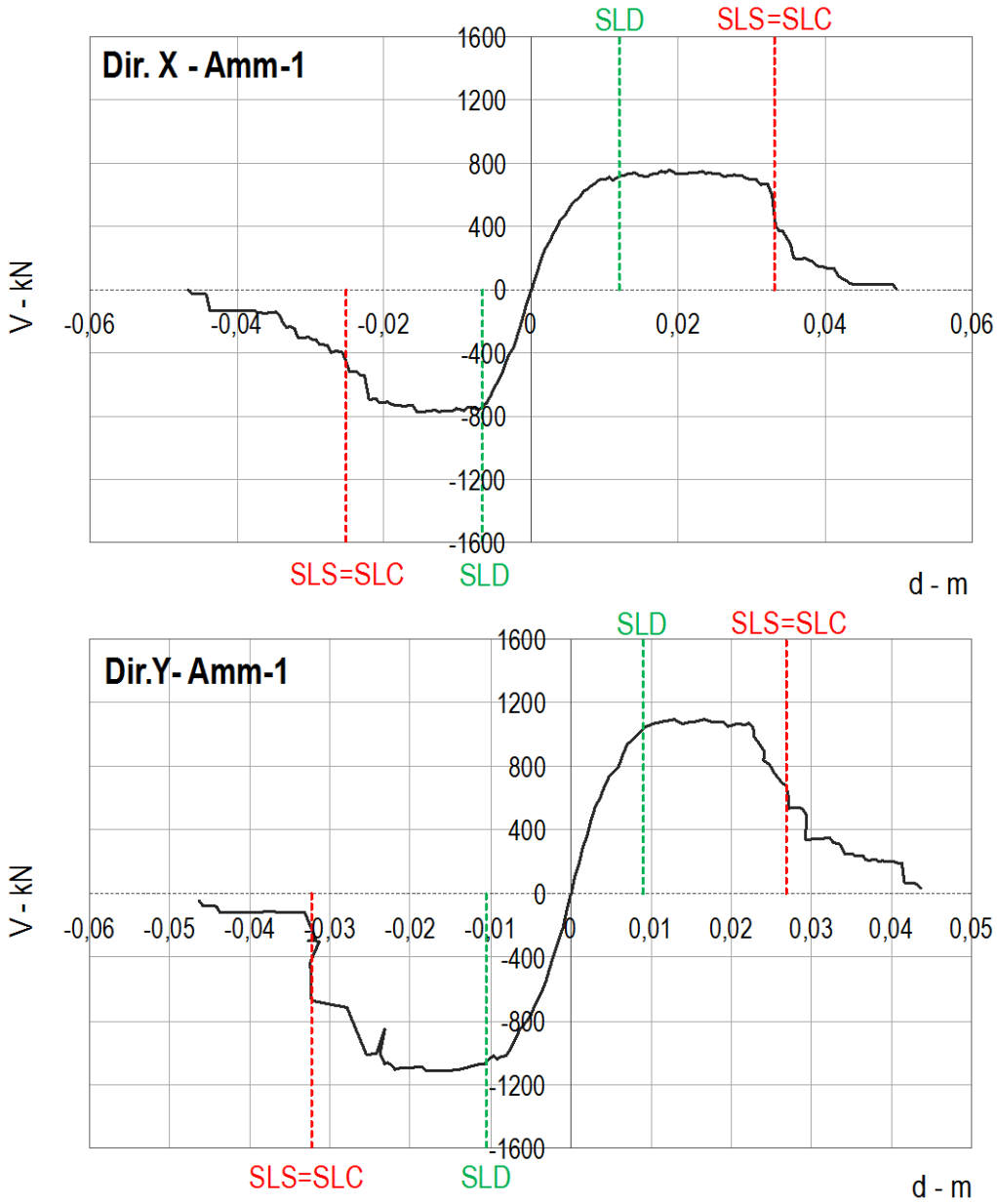

Fig. B-33 Results of the non-linear static analyses for the first branch of the logic tree (Amm-1) in the direction X and Y, with positive and negative direction (mean values for all the random variables)

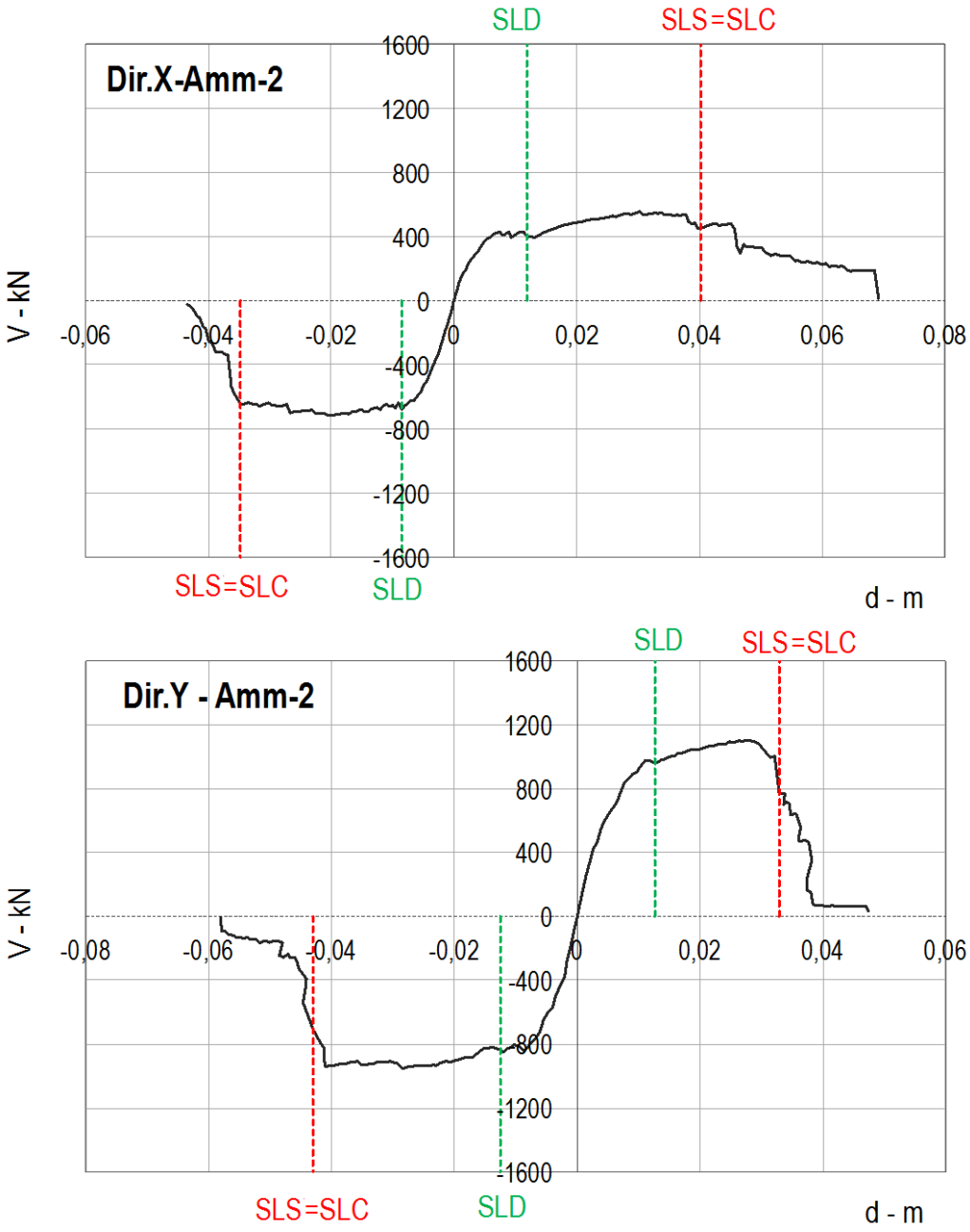

Fig. B-34 Results of the non-linear static analyses for the second branch of the logic tree (Amm-2) in the directions X and Y, with positive and negative direction (mean values for all the random variables)

In Figure B-35 the pushover curves are converted into the corresponding capacity curves representing the equivalent single degree of freedom (by the factors Γ and m*). These capacity curves are assumed as the median value of the response of the building.

In Figures B-33, B-34 and B-35 the positions of the limit states (SLD, SLS and SLC) are shown as resulting from the checks at different scales (structural element, wall and global) illustrated at §B6.3. In this case the limit states SLS and SLC coincide. For the definition of the SLS (via the (3.33)) the threshold $\tau_{SLS} = 0.3$ was assumed, that is equal to half of that conventionally adopted in method A, where the cost function is calculated by non-linear dynamic analyses. This choice is motivated by the fact that the pushover analysis is performed by applying the load pattern only in one and single (if positive or negative) direction. In this regard, Figure B-37 illustrates the compari-

son between the damage pattern of the walls 1 and 2 (as identified in plan in Fig B-36a), obtained at the end of the dynamic analysis (for the recording 1 scaled to the value of $S_a(T_1)$ equal to 6.25 m/s^2), and that resulting from the non-linear static analysis performed in the X-positive direction and Y-negative direction (with load pattern proportional to the masses); the latter has been taken in correspondence of the step of the analysis on which a displacement equal to the maximum obtained from the dynamic analysis is attained. In general one observes how in the case of the dynamic analysis the damage is more widespread (consequence of the activation also of the higher modes): for example, in the case of wall 1, one notes how the damage in the case of the non-linear static analysis in the Y direction is concentrated exclusively in piers of the ground floor, while in the case of the dynamic analysis it extends even to some piers of the upper levels. Moreover, in the case of the static analysis, it is confirmed how the damage in the walls directed orthogonally to the direction of the analysis is much less widespread and with a severity level lower than that obtained by the dynamic analysis. Finally, Figure B-36b, by way of example for the static analysis in the X direction, illustrates the evolution of the cost function that, in correspondence of the maximum displacement, results equal to 0.185, thus significantly lower than the value of 0.6 obtained by the dynamic analysis.

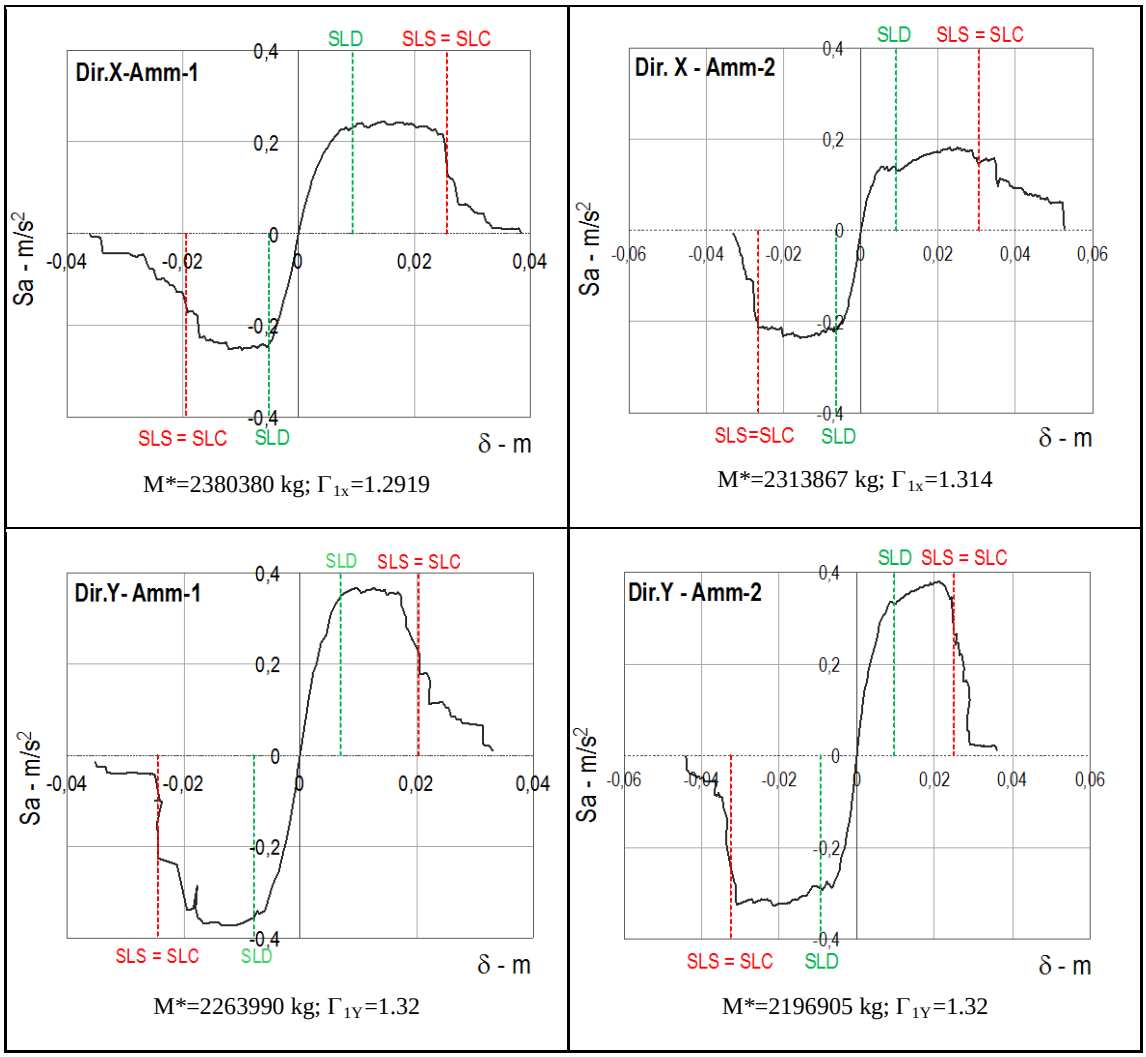

Fig. B-35 Results of non-linear static analyses in terms of capacity curve (conversion of pushover curves into the equivalent single degree of freedom): X direction - positive and negative directions for the two branches of the logic tree (mean values for all the random variables)

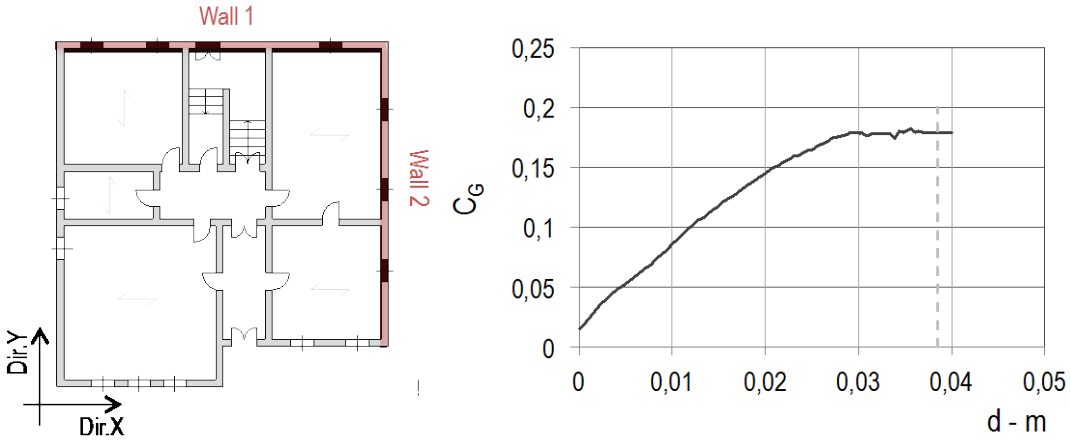

Fig. B-36 a) Identification in plan of the walls 1 and 2; b) cost function resulting from the non-linear analysis in X- positive direction.

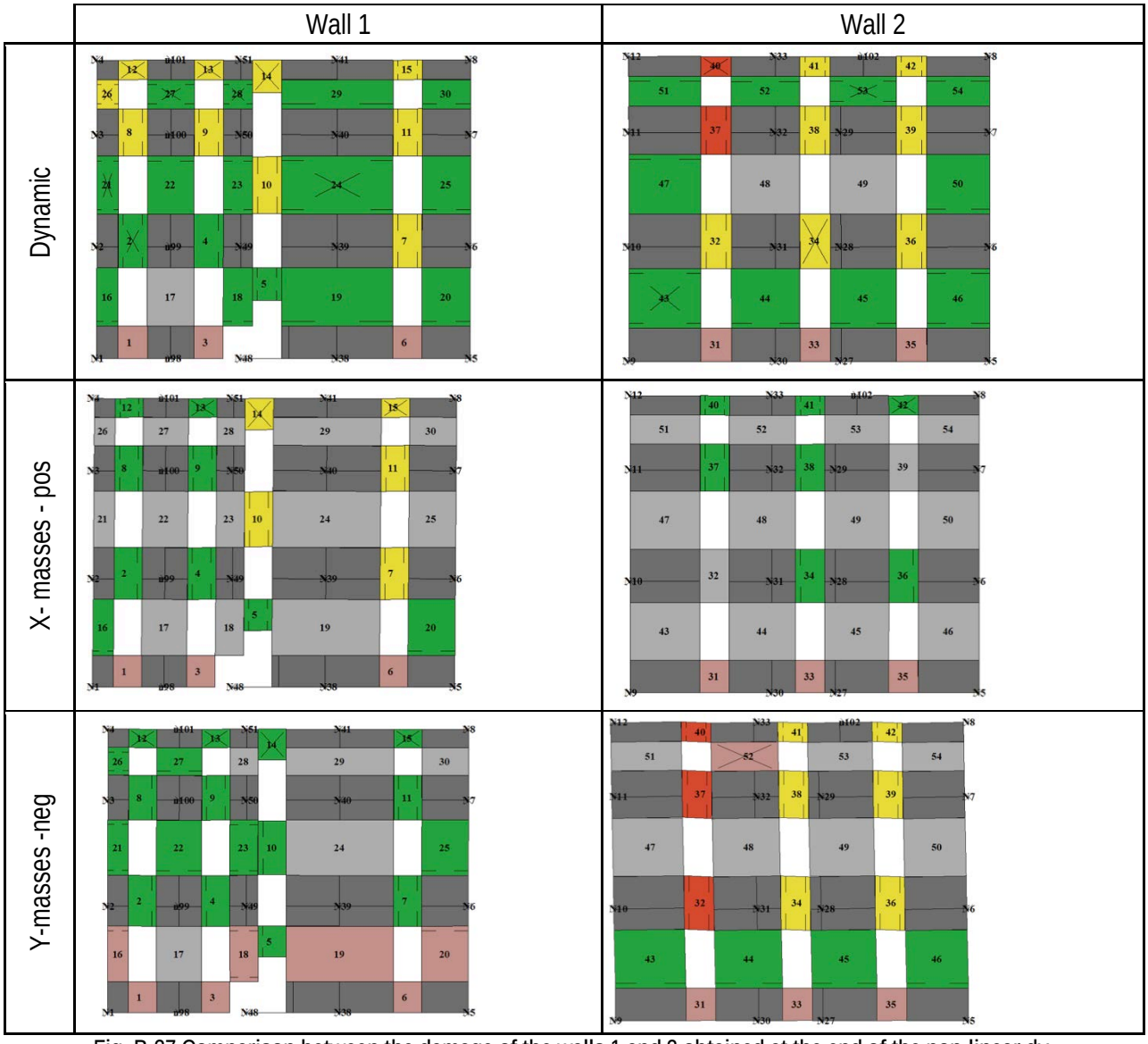

Fig. B-37 Comparison between the damage of the walls 1 and 2 obtained at the end of the non-linear dynamic analysis (event 1 scaled to the value S_a (T_1) = 6.25 m / s²) and that resulting from the non-linear static analysis (X- positive direction and Y- negative direction) in correspondence of the step in which the maximum displacement obtained from the dynamic analysis is attained

Tables B-12 (for the first branch of the logic tree - Amm-1) and B-13 (for the second branch - Amm-2) summarize the displacement capacity associated with the different limit states resulting from the checks at different scales and the final value associated with the more demanding condition.

Table B-12. Displacement capacities for the different limit states, resulting from the checks at the scale of the structural elements (S), walls (M) and global (G): first branch of the logic tree (Amm-1) - median values of the capacity

Dir. X (Amm-1) – Median capacities						
		$\delta_{SL,S}$ [m]		$\delta_{SL,M}$ [m]	$\delta_{SL,G}$ [m]	δ_{SL} [m]
SLD	+	0.0262	0.0141	0.0497	0.0120	0.0120
	-	0.0191	0.0171	0.0466	0.0066	0.0066
SLS	+	0.0497				0.0331
	-	0.0287				0.0251
SLC	+	0.0332	0.0497	0.0332	0.0331	0.0331
	-	0.0252	0.0466	0.0282	0.0251	0.0251
Dir. Y (Amm-1) – Median capacities						
		$\delta_{SL,S}$ [m]		$\delta_{SL,M}$ [m]	$\delta_{SL,G}$ [m]	δ_{SL} [m]
SLD	+	0.0221	0.0121	0.0437	0.0091	0.0091
	-	0.0049	0.0049	0.0069	0.0032	0.0032
SLS	+	0.0437				0.0269
	-	0.0324				0.0323
SLC	+	0.0269	0.0437	0.0271	0.0270	0.0269
	-	0.0323	0.0463	0.0323	0.0323	0.0323

Table B-13. Displacement capacities atthe different limit states, resulting from the checks at the scale of the structural elements (S), walls (M) and global (G): second branch of the logic tree (Amm-2) – median values of the capacity

Dir. X (Amm-2) – Median capacities						
		$\delta_{SL,S}$ [m]		$\delta_{SL,M}$ [m]	$\delta_{SL,G}$ [m]	δ_{SL} [m]
SLD	+	0.0318	.0120	0.0174	0.0258	0.0120
	-	0.0272	.0151	0.0434	0.0085	0.0085
SLS	+	0.0692				0.0402
	-	0.0347				0.0347
SLC	+	0.0452	0.0692	0.0402	0.0463	0.0402
	-	0.0363	0.0434	0.0368	0.0366	0.0363
Dir. Y (Amm-2) – Median capacities						
		$\delta_{SL,S}$ [m]		$\delta_{SL,M}$ [m]	$\delta_{SL,G}$ [m]	δ_{SL} [m]
SLD	+	0.0289	0.0127	0.0127	0.0201	0.0127
	-	0.0005	0.0034	0.0068	0.0032	0.0005
SLS	+	0.0475				0.0330
	-	0.0447				0.0430
SLC	+	0.0357	0.0475	0.0330	0.0347	0.0330
	-	0.0447	0.0581	0.0430	0.0444	0.0430

Figures B-38 and B-39 illustrate, by way of example for the analyses in the X-negative direction and Y-positive direction of the first branch of the logic tree (Amm-1), the evolution of: the cumulative damage indicators; the variable representative of the global repair cost; and the inter-story drift of walls. On the abscissa the displace-

ment of the equivalent non-linear single degree of freedom is represented. The vertical dashed lines indicate the displacements at which the limit states SLD and SLC were attained. One observes that the cumulative damage indicator in piers, associated to the damage level 3, reaches the threshold of 3% for a displacement greater than that which leads to the SLD: in this case the check at the global scale proves to be a decisive factor, as evident from the Table B-12; the same happens in spandrels, where the damage level 4 is the reference one to be checked. The cost function, in the case of the analysis in X direction, reaches the reference value C_{SLS} = 0.3 for a displacement slightly higher than that which leads to the SLC, for which, consistently with (3.33), the SLS is achieved simultaneously with the SLC; in the Y direction the cost function remains below 0.3.

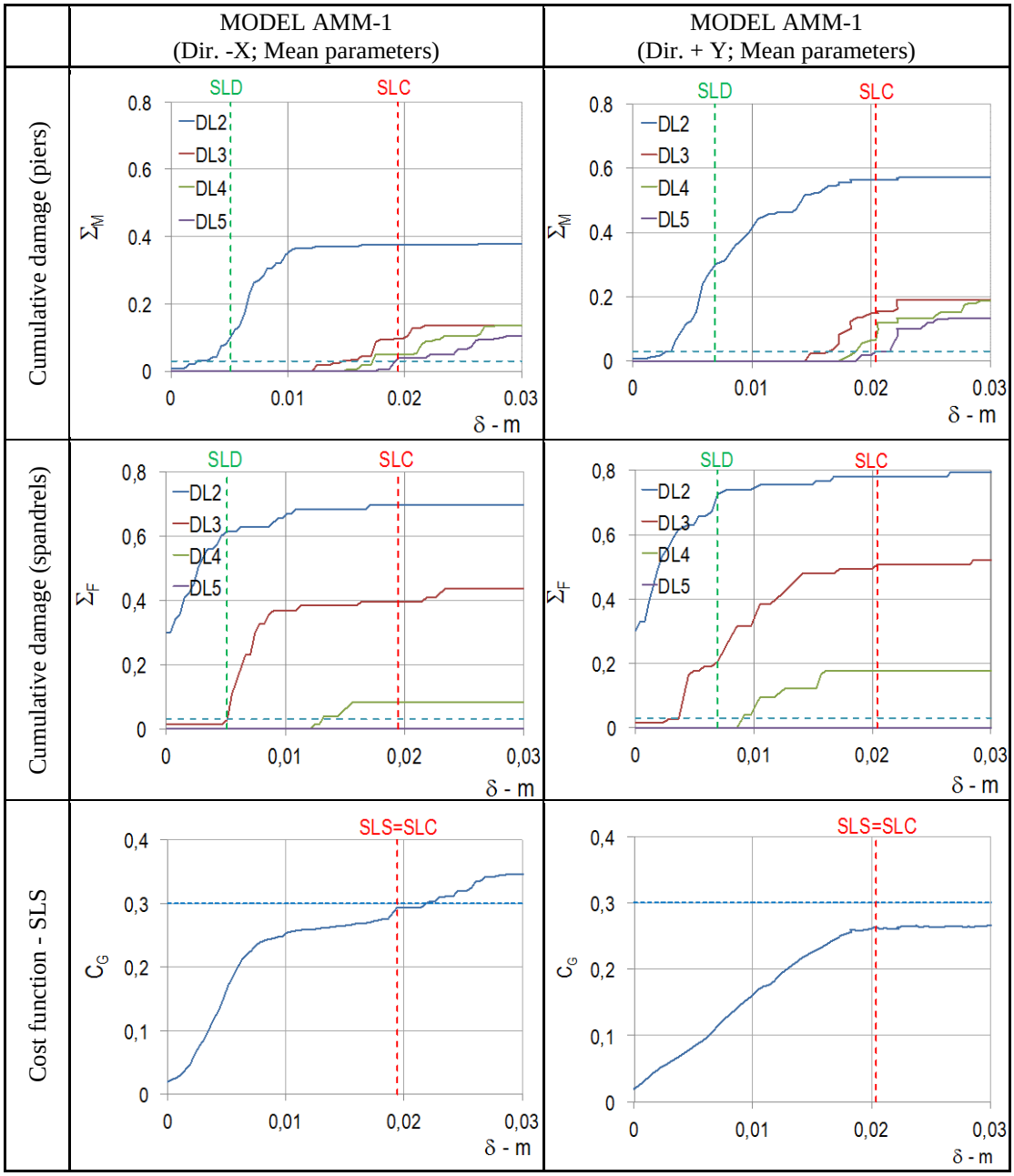

Fig. B-38 Evolution of the cumulative damage indicators of piers and spandrels and the global repair cost variable

Figure B-39 shows the evolution of the interstory drift at different levels for each wall of the building; the presence of rather rigid diaphragms produces quite uniform values among different walls. One observes that the interstorey drift is concentrated on the ground floor but still reaches the limit threshold always after the SL has been reached on the basis of one of the other two checks (structural element and global scales).

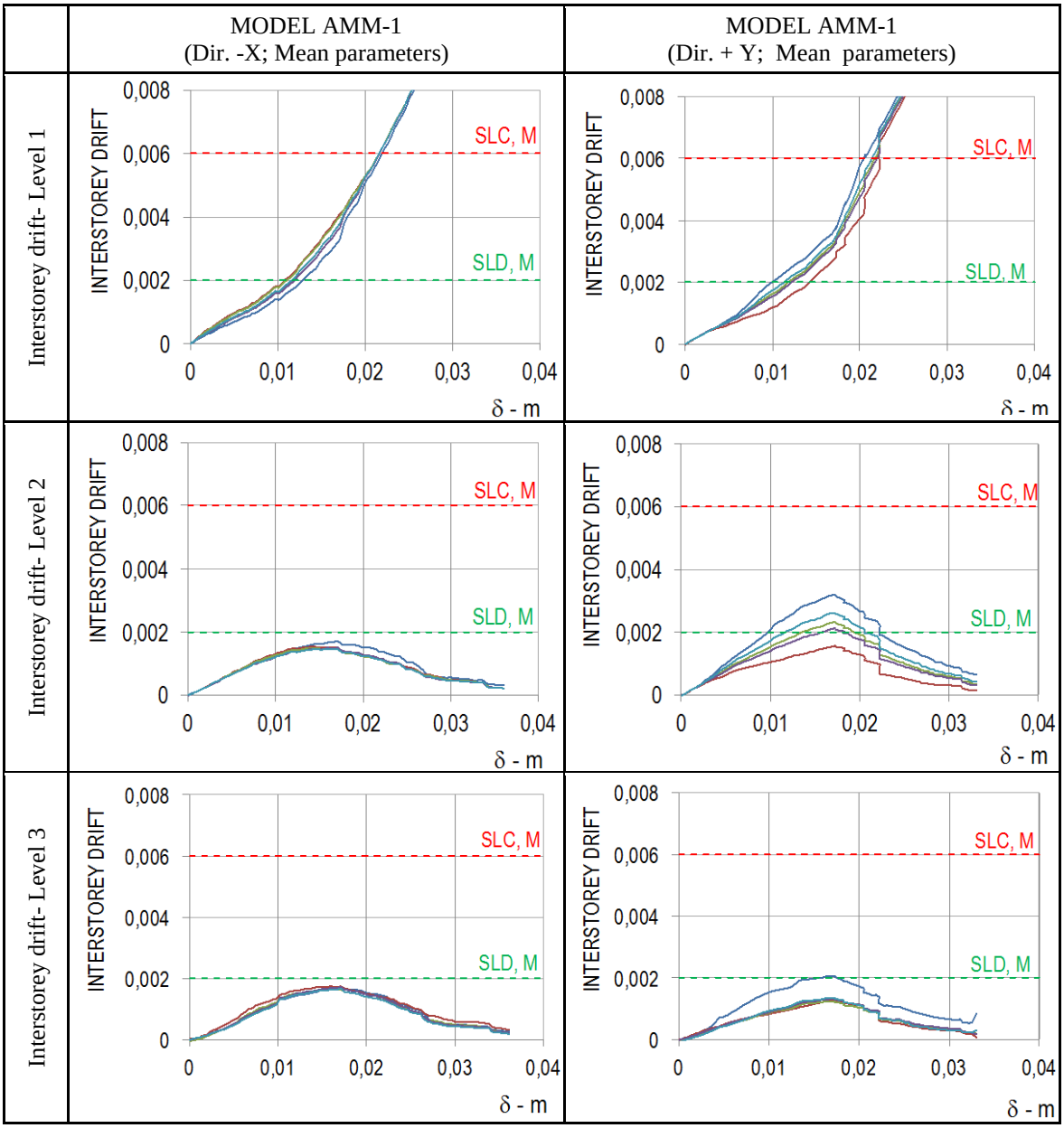

Fig. B-39 Evolution of the interstorey drift, at different levels of the building.

Now we proceed to calculate the mean annual frequency of exceedance of the three limit states according to what is described in §2.4.6; in particular it is computed through (2.12), which requires the assessment of the fragility through (2.14) by the evaluation of the parameters of the distribution of $S_{Y=1}$, that is, the intensity S that leads to the attainment of a given limit state LS (Y = 1).

In the following, the procedure is described and exemplified in detail in the case of Amm-1 and for the X direction.

Figures B-40 and B-41 illustrate the ISA (Incremental Static Analysis) curves that correspond to fractiles 16%, 50% and 84% obtained from the non-linear static analy-

sis and the use of a procedure based on the overdamped response spectra (§2.4 .6.2). They were plotted with reference to the limit states SLD (Figure B-40) and SLC (Figure B-41), which in this case coincides with the SLS, consistent with what previously discussed on the definition of SLs for the structure under examination (which it is characterized by a rather brittle behavior).
Based on these ISA curves it is possible to calculate the entities required for the calculation of the contribution β_S relative to the impact on $S_{Y=1}$ of the uncertainty of the seismic demand as shown in §2.4.6.3, and graphically, in Figure A-8.

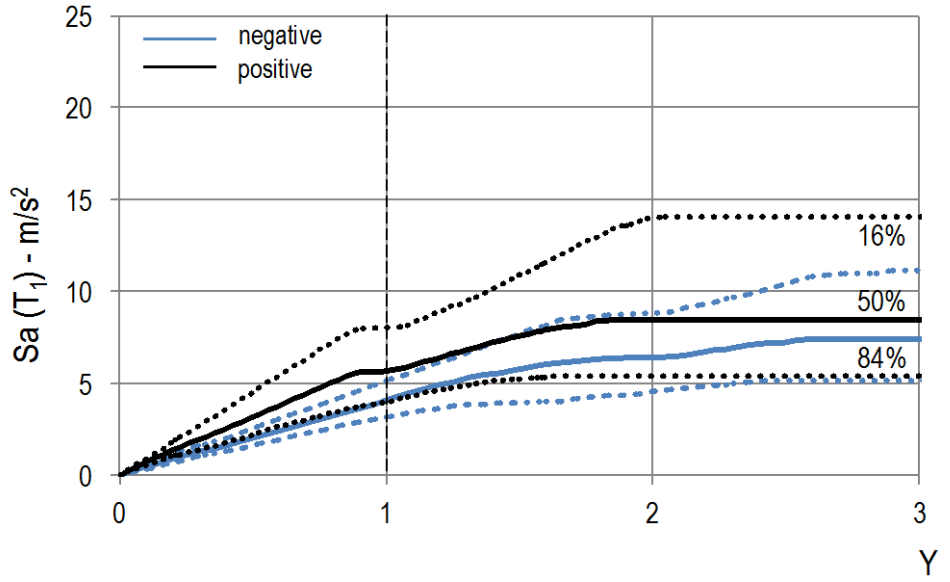

Fig. B-40 ISA curves obtained by comparing the median capacity curve and the median response spectrum (at the 16% and 84% percentiles): Amm-1, X-direction (positive and negative direction) and SLD.

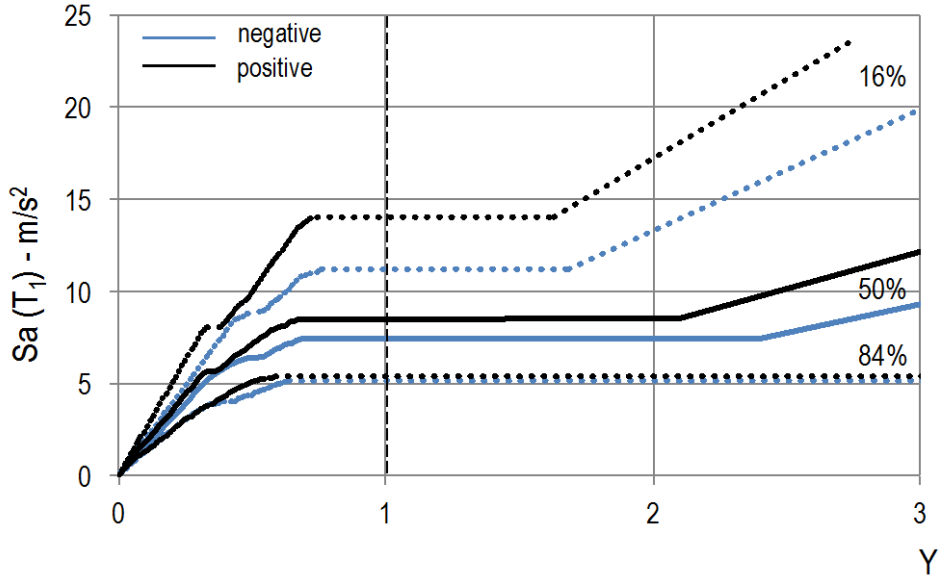

Fig. B-41 ISA curves obtained by comparing the median capacity curve and the median response spectrum (at the 16% and 84% percentiles): Amm-1, X-direction (positive and negative direction) and SLC (which in this case also coincides with SLS).

Table B-14 shows the resulting values of $S_{Y=1}$ (necessary for the calculation of the fragility through (2.14)) and $S_{Y=1,16\%}$ and $S_{Y=1,84\%}$ (used for the calculation of β_S through (2.16)). In particular, for the first branch of the logic tree (Amm-1), there are

shown the values for both directions examined (X and Y) with reference to the direction of load pattern application (if positive or negative) that proved most demanding (i.e., associated with the lower value of $S_{Y=1}$).

Table B-14. Values of $S_{Y=1}$ obtained by comparing the capacity curve associated with the mean values of the random variables (median capacity curve) and the median response spectrum, at the 16% and 84% fractiles for the limit states SLD, SLS and SLC (first branch of the logic tree Amm-1)

		SLD	SLS = SLC
Amm.1 - X (-)	$S_{Y=1}$ (m/s^2)	3,495	8,486
	$S_{Y=1,16\%}$ (m/s^2)	5,126	11,152
	$S_{Y=1,84\%}$ (m/s^2)	3,192	5,128
Amm.1 - Y (+)	$S_{Y=1}$ (m/s^2)	5,780	7,317
	$S_{Y=1,16\%}$ (m/s^2)	7,347	10,816
	$S_{Y=1,84\%}$ (m/s^2)	4,484	4,949

The dispersion β_C, associated to the effect on $S_{Y=1}$ of the uncertainty in the capacity curve, is calculated by applying the response surface technique, as illustrated in §2.6.4.4. Table B-15 summarizes the 16 cases ($M = 2^N$) obtained from the complete factorial combination at two levels of $N = 4$ random variables ; in the matrix of the **Z** experiments the values -1 and +1 refer to the use of the fractiles of the random variables respectively at 16% and 84%. Table B-15 shows the minimum values of $S_{Y=1}$, for the three limit states considered, obtained from the comparison between the median spectrum and the capacity curves obtained in the two directions (positive and negative) from each of M combinations. Thus it is possible to calculate the coefficients α and β_C using equations (2.19) and (2.20).

Table B-15 Experiment matrix of the M possible combinations of the N random variables and resulting values of $S_{Y=1}$ (as a function of the three limit states considered) corresponding to the analyses performed in the X direction to the first branch of the logic tree (Amm- 1)

Matrix experiments Z				$S_{Y=1}$ (m / s^2)		
Masonry material	Constitutive law of piers	Constitutive law of spandrels	Damping	SLD	SLS	SLC
-1	-1	-1	-1	4.469	5.003	5.003
-1	-1	-1	+1	4.976	5.802	5.802
-1	-1	+1	-1	4.471	4.904	4.904
-1	-1	+1	+1	4.504	5.640	5.640
-1	+1	-1	-1	4.343	6.676	6.676
-1	+1	-1	+1	4.923	7.777	7.777
-1	+1	+1	-1	4.675	6.263	6.263
-1	+1	+1	+1	4.675	7.292	7.292
+1	+1	+1	-1	4.947	8.077	8.077
+1	+1	+1	+1	5.268	9.442	9.442
+1	+1	-1	-1	5.091	8.356	8.356
+1	+1	-1	+1	5.690	9.792	9.792
+1	-1	+1	-1	4.949	6.502	6.502
+1	-1	+1	+1	5.268	7.563	7.563
+1	-1	-1	-1	5.127	7.916	7.916
+1	-1	-1	+1	5.225	7.313	7.313

In Table B-16 the values of the contributions β_C and β_S are summarized, as well as the total β values, obtained for the two directions X and Y, in the case of the first branch of the logic tree (Amm.1) as a function of the three limit states considered. On the basis of these values and those of $S_{Y=1}$ (already introduced in Table B-14), the fragility curves can then be plotted as illustrated in Figure B-42. As already noted, the SLS is always achieved at the same time of the SLC (the curves in fact coincide). This result is due to the quite pronounced brittle behavior of this masonry building, meaning that the building reaches the collapse with a not too widespread damage. Moreover, one notes that this building is, in respect of SLD, more vulnerable in the X direction, while at the SLC it is more vulnerable in the Y direction (although for this limit state the response in the two directions is more similar).

Table B-16 Contributions to the calculation of β: first branch of the logic tree (Amm-1) for the analyses performed in the X and Y directions

		SLD	SLS = SLC
Amm.1 - X	β_S	0.237	0.388
	β_C	0.067	0.194
	β	0.246	0.434
Amm.1 - Y	β_S	0.247	0.391
	β_C	0.094	0.188
	β	0.264	0.434

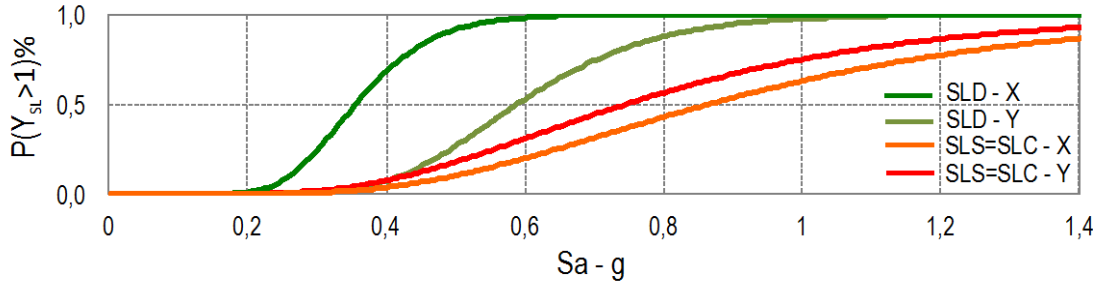

Fig. B-42 Fragility curves for the three limit states, obtained for the first branch of the logic tree, considering the response in the two X and Y directions.

The fragility of the building is obtained by assuming, for each level of the seismic intensity, the greater of those obtained in the two directions X and Y. Figure B-43 shows the final fragility curves for the first branch of the logic tree (Amm-1).

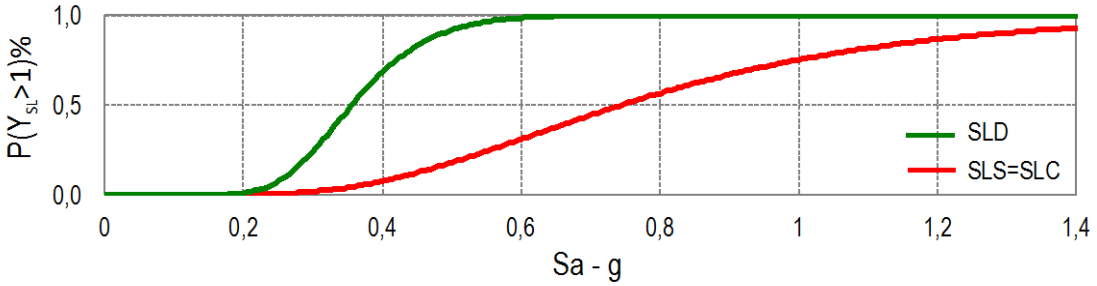

Fig. B-43 Fragility curves for the three limit states, obtained for the first branch of the logic tree (Amm-1).

Repeating the same procedures for the second branch of the logic tree (Amm-2), some analogous fragility curves are obtained as shown in Figure B-44, in which they are al-

so compared with those of Figure B-43. It is worth noting that, despite the capacity curves obtained for the two models are rather different, in terms of seismic safety the results are very similar, at least with regard to the SLC.

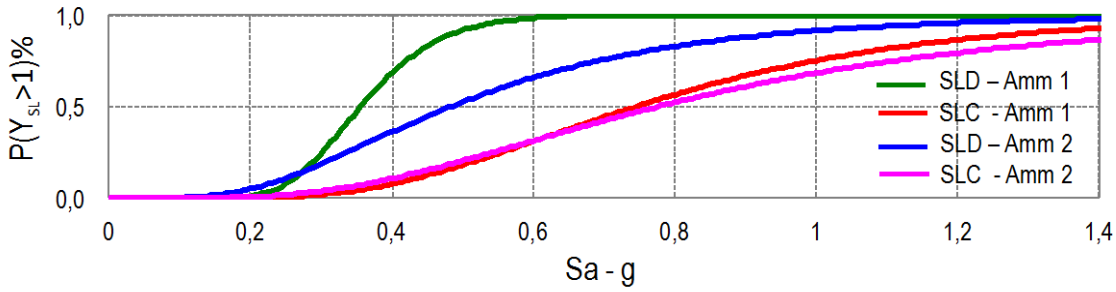

Fig. B-44 Fragility curves for the three limit states, obtained by the two branches of the logic tree.

On the basis of the different weight assumed for the two branches of the logic tree, the final fragility curves can be easily obtained as illustrated in Figure B-45; in particular, it is useful to recall that a different subjective probability has been attributed to the two branches of the logic tree, equal to 0.6 for the hypothesis of perfect wall-to-wall connection (Amm-1) and 0.4 for the second branch (Amm-2).

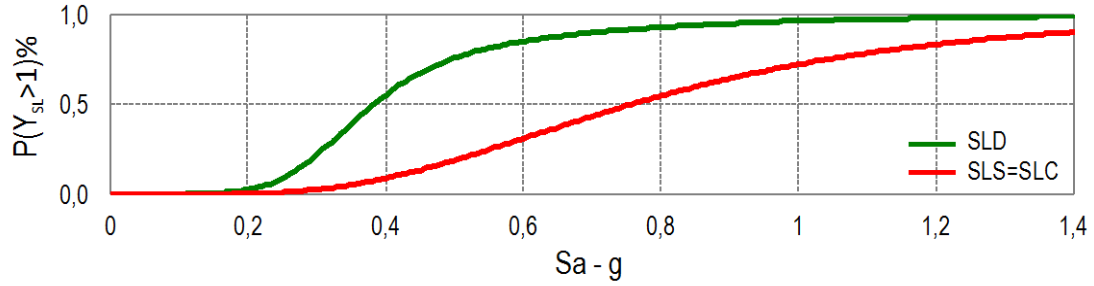

Fig. B-45 Final fragility curves for the three limit states, resulting from the combination of the results obtained in the two branches of the logic tree (Amm-1 and Amm-2).

Finally, we proceed to calculate the mean annual frequency of exceedance of the limit state (λ_{SL}) applying the theorem of total probabilities, i.e. through the use of (2.12). The calculation of the integral requires to extend the summation to a number of points such as to make stable the estimate of λ_{SL}; in particular, to this end, we recall how the mean hazard curve has been approximated by a quadratic function in the logarithmic space whose parameters are defined in (B.1).
Table B-17 shows the values of the mean annual frequency of exceedance of the limit

Table B-17 Calculation of the mean annual frequency of exceedance of the limit state, obtained by combining the results of the two branches of the logic tree

	λ_{SL} (Amm-1)	λ_{SL} (Amm-2)	λ_{SL}	Target (Class II)	Outcome of the verification	$T_{r,SL}$
SLD	0.01080	0.00891	0.00997	0.045	YES	100
SLS	0.00301	0.00336	0.00315	0.0047	YES	318
SLC	0.00301	0.00336	0.00315	0.0023	NO	318

states for the two branches of the logic tree. The estimate of λ_{SL} is obtained by weighing the values obtained from the two branches through their subjective probabilities

(Amm-1, probability 0.6 and Amm-2, probability 0.4). The verification is then performed by comparing these values with the corresponding maximum admissible thresholds (Table 2.1); in this case, being a residential building, the thresholds proposed for class of use II have been assumed.
In the specific case the building would not be verified in respect of SLC

B.7.4.1 Assessment by the method described in §A.1.1.1

In the following the application of the alternative method for the evaluation of the fragility illustrated in Appendix A.1.1.1 and based on the use of non-linear static analysis is exemplified.
In this case, the parameters that define the fragility (preliminary step necessary for the calculation of the mean annual frequency of exceedance of the limit states) are calculated with respect to the limit state variable Y_{SL} computed as a function of the level of intensity S = s, rather than with respect to the variable $S_{Y=1}$ as described in B.7.4.
The procedure requires that, for each intensity value, the fragility is evaluated for both directions and then the highest value is chosen. Similarly to what carried out in the case of method C, in the following the procedure is described and exemplified only in the case of Amm-1 and for the X direction.
Figure B-46 illustrates the ISA curves obtained by applying a nonlinear static procedure based on the use of overdamped spectra; the curves refer to the comparison between the median capacities curves (obtained from the analysis with the positive and

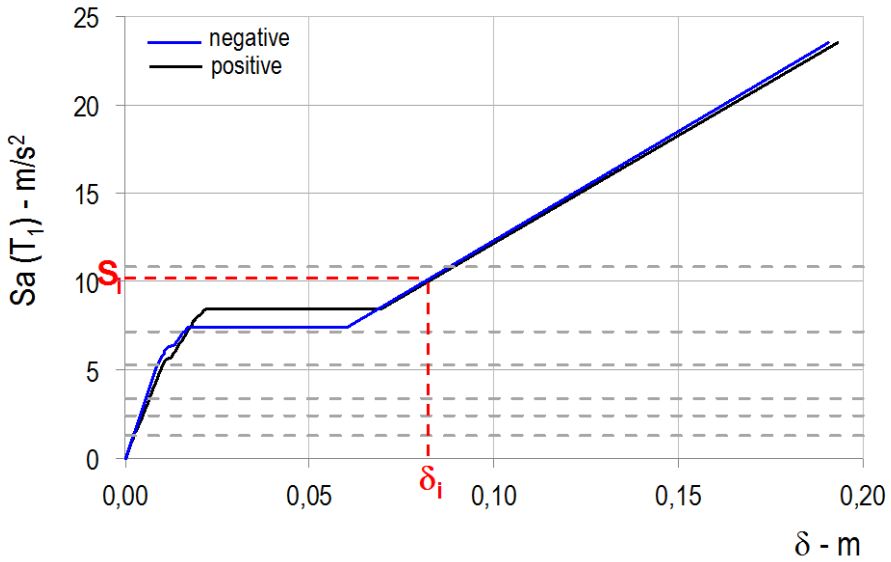

Fig. B-46 ISA curves obtained from the comparison between the median capacity curve and the median response spectrum as a function of the positive and negative directions (X direction -Amm.1): the horizontal dotted lines exemplify the potential use of such curves for 6 different values of the seismic intensity as shown in Table B-18.

Table B-18. Values of Y_{SL} obtained by comparing the median spectrum and the capacity curve associated with the mean values of the random variables (first branch of the logic tree Amm-1)

T_R	30	101	201	475	975	2475
$S_a(T_1)$	0131	0245	0337	0528	0713	1,063
$+\delta$ [□]	0.00223	0.00452	0.00623	0.00977	0.01614	0.08553
$\delta -$ [□]	0.00194	0.00387	0.00533	0.00838	0.01533	0.08442
Y_{SLD}	0.38	0.76	1.04	1.64	3.00	16.55
Y_{SLS}	0.10	0.20	0.27	0.43	0.79	4.34
Y_{SLC}	0.10	0.20	0.27	0.43	0.79	4.34

negative directions) and the median response spectrum; in the abscissa the value of the displacement demand δ is illustrated . Entering in this curve with a generic value of the intensity, the displacement demand may be obtained and, from this, one calculates the limit state variable Y_{SL}, that is then used to calculate the fragility.

By way of example, Table B-18 shows the resulting values of δ^+ (positive direction) and δ (negative direction) that, when related to the displacements corresponding to the attainment of different SLs (Table B-12), allow to evaluate the values of Y_{SL} (e.g. for values of intensity corresponding to some of the return periods considered by the INGV hazard).

We proceed now to the calculation of the different contributions of β (total standard deviation of the logarithm of the variable Y_{SL}) according to the procedure outlined in Appendix A.6.

The contribution β_S due to the uncertainty on the shape of the response spectrum is evaluated from the median capacity and the displacement demand produced by the response spectra at 16% and 84% fractiles. Figure B-47 shows the resulting ISA curves for two directions (positive and negative) of load pattern in the X direction; the horizontal dotted lines correspond to the intensity values listed in Table B-18. The calculation of β_S is carried through the (A.13) and the result is shown in Table B-19.

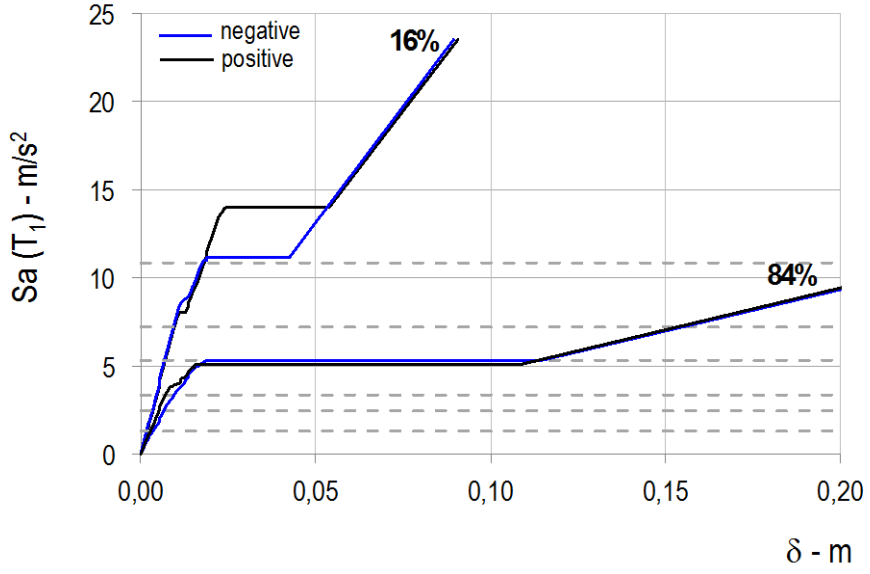

Fig. B-47 ISA Curves calculated by comparing the median capacity curve with the response spectra at 16% and 84% percentiles

Table B-19. Values of β_S calculated according to the approach set out in Appendix A.1.1.1- first branch of the logic tree (Amm-1)

	T_R	30	101	201	475	975	2475
β_S	SLD	0.278	0.225	0.240	1.399	1.399	1.295
	SLS	0.278	0.232	0.250	1.399	1.399	1.295
	SLC	0.278	0.232	0.250	1.399	1.399	1.295

It is worth noting how, according to such approach, a different value of the dispersion β_S is obtained for each level of intensity, and not a single value as in the case of the application of method C described in §2.6.4 and exemplified in §B.7.4. It is observed that the dispersion β_S is very limited for the low return periods, when the response is almost linear and the spectral acceleration at the period T_1 provides a good measure of the seismic intensity, while with the increase of T_R , when the structure progresses into the non-linear range, the variability of the shape of the response spectrum significantly affects and increases the value of β_S. It is also noted that, for given values of the return period, the value of β_S is almost always independent of the SL; this is because the way of application of the load pattern for which the building results more vulnerable is almost always the same.
The dispersion β_C due to the randomness on the capacity curve is obtained with the response surface technique.

Table B-20 Experiment matrix of M possible combinations of N random variables and values of Y_{SL} corresponding to T_R = 201 years - first branch of the logic tree (Amm-1)

Matrix of Z experiments				T_R = 201 years		
Masonry material	Constitutive law of piers	Constitutive law of spandrels	Damping	Y_{SLD}	Y_{SLS}	Y_{SLC}
-1	-1	-1	-1	0.830	0.218	0.218
-1	-1	-1	+1	0.830	0.218	0.218
-1	-1	+1	-1	0.830	0.218	0.218
-1	-1	+1	+1	0.830	0.218	0.218
-1	+1	-1	-1	0.831	0.218	0.218
-1	+1	-1	+1	0.830	0.218	0.218
-1	+1	+1	-1	0.830	0.218	0.218
-1	+1	+1	+1	0.830	0.218	0.218
+1	+1	+1	-1	0.742	0.195	0.195
+1	+1	+1	+1	0.701	0.184	0.184
+1	+1	-1	-1	0.763	0.200	0.200
+1	+1	-1	+1	0.663	0.174	0.174
+1	-1	+1	-1	0.742	0.195	0.195
+1	-1	+1	+1	0.701	0.184	0.184
+1	-1	-1	-1	0.752	0.197	0.197
+1	-1	-1	+1	0.660	0.173	0.173

In Table B-20 are summarized the 16 cases (M=2^N) obtained by the complete factorial combination at two levels of N = 4 random variables and the matrix of experiments Z. Table B-20 shows the maximum values of Y_{SL} obtained from the comparison between the median spectrum and the capacity curves obtained for the two directions of load pattern and for each of M combinations: by way of example the values corre-

sponding to the seismic intensity with a return period equal to T_R=201 years are shown.
Thus it is possible to calculate the coefficients α and β_C using equations (2.19) and (2.20).

Once computed the values of β_S and β_C for the three limit states and the intensity levels considered, it is possible to combine them through (2.15) in order to define the value of the total dispersion β. Table B-21 summarizes the partial and total values of the dispersion. It is possible to observe how with the increase of the level of seismic intensity s, in particular from T_R = 475 years, the contribution of β_S becomes preponderant in relation to that associated to the capacity.
Having repeated the analysis for the Y direction, it is possible to obtain, for different levels of seismic intensity, the values of Y_{SLD} , Y_{SLS} and Y_{SLC} , and the corresponding dispersions β_{SLD} , β_{SLS} and β_{SLC} . By (2.14) one can then calculate the fragility.
Figure B-48 shows the fragility curves obtained, for the first branch of the logic tree (Amm-1), considering the response in the two directions X and Y.

Table B-21 Contributions to the calculation of β: first branch of the logic tree (Amm-1) - direction X.

	T_R	30	101	201	475	975	2475
β_S	SLD	0.278	0.225	0.240	1.399	1.399	1.295
	SLS	0.278	0.232	0.250	1.399	1.399	1.295
	SLC	0.278	0.232	0.250	1.399	1.399	1.295
β_C	SLD	0.106	0.087	0.083	0.405	0.606	0.167
	SLS	0.327	0.318	0.314	0.641	0.835	0.322
	SLC	0.327	0.318	0.315	0.642	0.836	0.323
β	SLD	0.297	0.241	0.254	1.457	1.525	1.305
	SLS	0.429	0.393	0.401	1.539	1.629	1.334
	SLC	0.429	0.394	0.402	1.539	1.630	1.334

It is possible to observe how the trend of the fragility curves is not that of a lognormal distribution, and is quite irregular since the value of the dispersion estimated with the proposed procedure is not constant. In this specific case, the dispersion increases with increasing intensity, as both the dispersion of the spectral shape and the variability of the capacity curve increase.

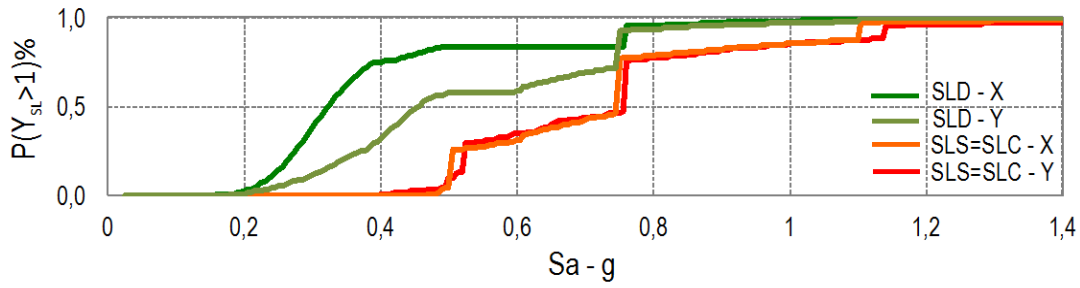

Fig. B-48 Fragility curves for the three limit states, obtained for the first branch of the logic tree, considering the response in the two directions X and Y according to the approach proposed in Appendix A.1.1.1..

The fragility of the building is obtained by taking, for each level of intensity, the greater of those obtained in the two directions X and Y. Figure B-49 shows the final fragility curves for the first branch of the logic tree (Amm-1).
Repeating the same procedure for the second branch of the logic tree (Amm-2) the fragility curves shown in Figure B-50 are obtained and thus compared with those of

Figure B-49. It is noted that, despite the capacity curves obtained for the two models are rather different, in terms of seismic safety the results are more similar.
Finally the results are combined using the technique of the logic tree, analogously to what illustrated in §B.7.4 and assuming the subjective probability equal to 0.6 for the first branch (Amm.1); the resulting fragility curves are shown in Figure B-51.

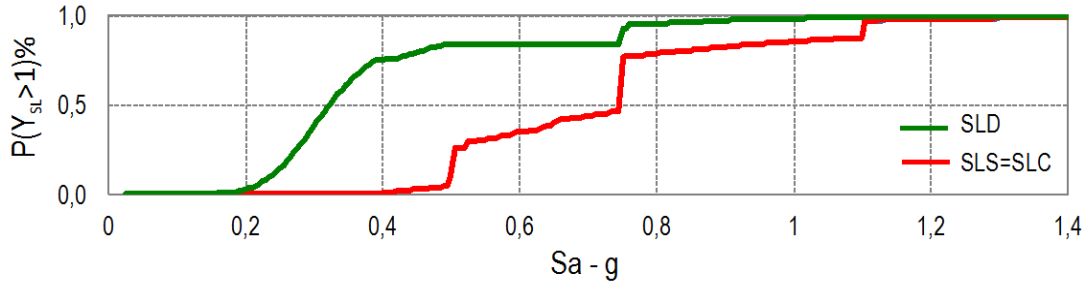

Fig. B-49 Fragility curves for the three limit states, obtained for the first branch of the logic tree (Amm-1).

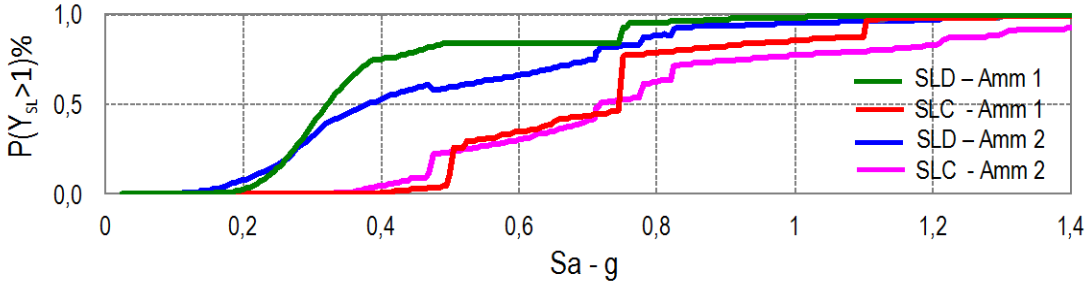

Fig. B-50 Fragility curves for the three limit states, obtained by the two branches of the logic tree.

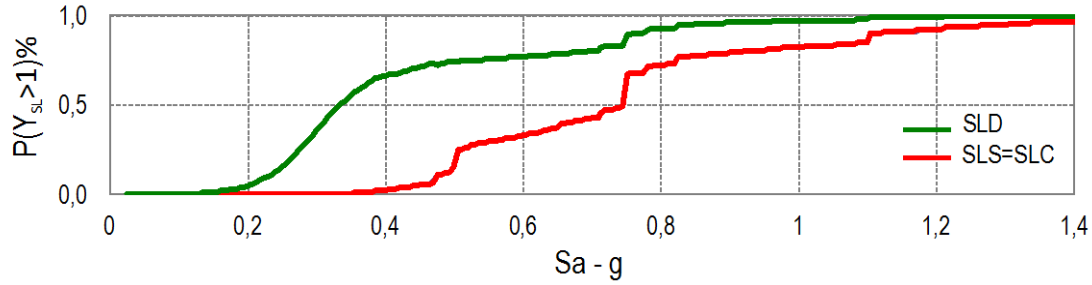

Fig. B-51 Final fragility curves for the three limit states, obtained by combining the results obtained for the two branches of the logic tree (Amm-1 andAmm -2).

One can then proceed to the calculation of the mean annual frequency of exceedance of the limit state by applying the theorem of total probability, as explained in §B.7.4.1. It is useful to highlight how, in this case, the computation of the integral must be carried out necessarily in numerical form, since the values of the parameters defining the fragility (μ,β) vary depending on the intensity level S = s. Table B-22 shows the values obtained.

Table B-22 Computation of the mean annual frequency of exceedance of the limit state according to the approach proposed in Appendix A.1.1.1., combining the results of the two branches of the logic tree

	$\lambda_{□□}$ (Amm-1)	$\lambda_{□□}$ (Amm-2)	$\lambda_{□□}$	Target (Class II)	Outcome of verification	$T_{r,SL}$
SLD	0.0125	0.0120	0.0123	0.045	YES	81
SLS	0.00260	0.00262	0.00261	0.0047	YES	383
SLC	0.00260	0.00262	0.00261	0.0023	NO	383

In the following a comparison of results obtained by applying the method C illustrated in §B.7.4.1 and the alternative procedure proposed in Appendix A.1.1.1 is illustrated. Figure B-52 shows the comparison in terms of fragility curves for the three limit states considered, while Table B-23 in terms of the values of the mean annual frequencyof exceedance of the limit state (and their return periods).

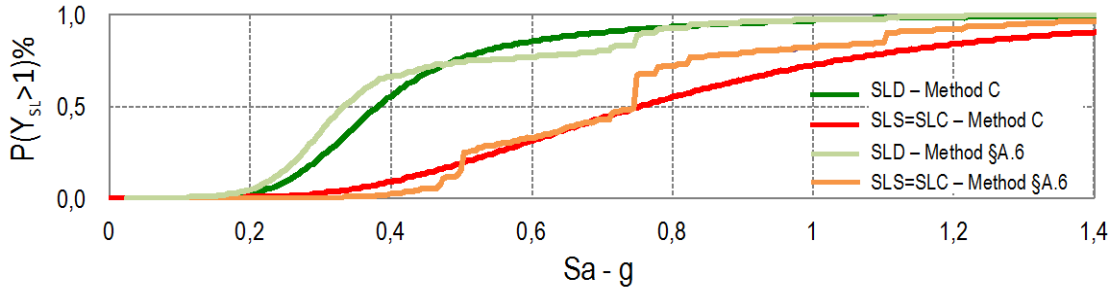

Fig. B-52 Final fragility curves for the three limit states compared as obtained by the method C and method illustrated in §A.1.1.1. (as resulting from the combination of two branches of the logic tree)

It is noted that the results are in good agreement and provide substantially similar results in terms of verification.

Table B-23 Comparison of mean annual frequency of exceedance of the limit state as obtained from the application of the method C and from that proposed in Appendix A.1.1.1.

	Method C		Method Appendix A.1.1.1.	
	λ_{SL}	$T_{r,SL}$	λ_{SL}	$T_{r,SL}$
SLD	0.00997	100	0.0123	81
SLS	0.00315	318	0.00261	383
SLC	0.00315	318	0.00261	383

B.7.5 Comparison of the two methods

The comparison between the results obtained for the masonry building under examination by using the methods A and C confirms their reliability in the evaluation of the seismic safety through the adoption of non-linear analysis methods. The two methods are entirely similar from the point of view of the calculation of the fragility, computed with respect to the seismic intensity S that leads to a given limit state LS (Y=1).
In Figure B-53 the fragility curves obtained for the three limit states are compared; Table B-24 summarizes the values of the parameters that describe the fragility ($S_{Y=1}$ and β) in the two cases.
It is observed how the method C is always a little more on the safe side than the method A, as one might hope, since it is based on a more approximate method of analysis (i.e. static rather than dynamic), although non-linear. Method A also allows one to distinguish a minimum difference between limit states SLS and SLC, which instead coincide in the case of method C, given the rather brittle nature of the response of the building examined as discussed in §B.7.4.
The median value of the seismic intensity $S_{Y=1}$ is in a good agreement in the two cases; in general, the value obtained by method C is more on the safe side, apart the case of the SLS that this method cannot distinguish from the SLC; in this case, the value

obtained is still slightly higher. The values of β were higher in the case of method C for SLS and SLC, while there is a lower dispersion in the case of the first limit state.

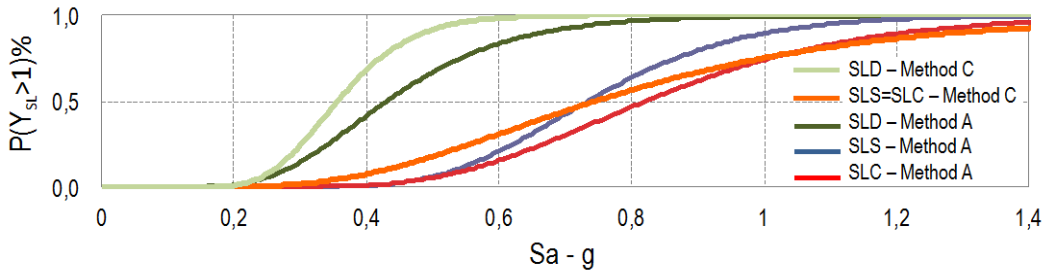

Fig. B-53 Final fragility curves for the three limit states, obtained by combining the results of the two branches of the logic tree (Amm-1 and Amm-2).

Table B-24. Comparison of the results provided by the Methods A and C: median value of the intensity that leads to the attainment of three limit states examined and corresponding values of β

		SLD	SLS	SLC
Method A	$S_{Y=1}$	4.224	7.201	8.126
	β	0.342	0.247	0.315
Method C	$S_{Y=1}$	3.495	7.317	7.317
	β	0.246	0.434	0.434

Table B-25 finally compares the values of the mean annual frequency of exceedance of the limit states SLD, SLS, SLC and the corresponding return periods of occurrence. As one would expect, already from the comparison of fragility curves, the values provided by the two methods are similar and more on the safe side in the case of method C.

Table B-18. Comparison of the results provided by the Methods A and C: mean annual frequency of exceedance of the limit states SLD, SLS, SLC and corresponding return periods (compared with the maximum tolerated thresholds).

	λ_{SLD}	λ_{SLS}	λ_{SLC}
Method A	0.0082	0.0023	0.0020
Method C	0.0108	0.0030	0.0030
Maximum tolerated thresholds	0.045	0.0047	0.0023
	$T_{r,SLD}$	$T_{r,SLS}$	$T_{r,SLC}$
Method A	122	426	508
Method C	100	318	318
Maximum tolerated thresholds	22	213	435

C Application example of a reinforced concrete building

C.1 Premise

The procedure for the evaluation of seismic safety of concrete structures described in chapters 2 and 4 was applied to a school building actually existing, of which, however, were varied both the position, and hence the hazard at the site, and the properties of the materials.
The risk analysis was repeated adopting both a modelling *without degradation and with degradation* (§2.4). The first one corresponds to the current state of the art of non-linear analysis of reinforced concrete structures, and rests on foundations to be considered as well established both from a procedural viewpoint and that of the models available.
However, it was decided to introduce also the second, while recognizing that it is the subject of ongoing research, the knowledge of which is not yet widespread in the technical-scientific community. There are lacking, for example, proposals for the interaction between the stress resultants and in particular for the biaxial behaviour. The experimental results supporting the modelling of extreme behaviour such as the collapse of the columns for loss of vertical bearing are still of an inadequate number. Furthermore it should be noted that these models exhibit a lower level of computational robustness than the consolidated models mentioned above.
Therefore, the value of this second approach is to provide a frame of reference pending further developments in research and at the same time an order of magnitude of the differences that can be expected from the application of the two approaches.

C.2 Description of the building

The school complex consists of three separate buildings. The application refers to the main body, of which there are shown two facades in Fig. C-1 and C-2. The spatial geometry of the frame and a layout are shown, respectively in Fig. C-10 and C-11.
The structure was probably built in the early 60s. It consists of a reinforced concrete frame with emerging beams present in both directions and is on three levels (basement, ground floor and first floor); the average height of the floors above ground is ~ 3.8m, of the basement ~ 4.4m.
The layout of the building (~ 530 m^2) is very irregular with a large (in percentage) offsets on all fronts. The basement does not occupy all the footprint but two distinct portions: one part to the southwest directly accessible from the outside (~ 150 m^2), and a smaller portion (~ 90 m^2) at the north-west stairwell. The foundations are of the direct type and placed on different levels.The walls against the soil of the underground rooms are built in reinforced concrete.
The floor diaphragms are of brick and cement with an estimated thickness of 20+5cm. The bays of the floor diaphragms alternate rather irregular spans: from a minimum of 3m to a maximum of 9m (ground floor atrium cover).

Upon a visual examination, the state of conservation of the structure looks rather good.

Fig. C -1 Photo NE view.

Fig. C -2 Photo NW view.

C.3 Assessment procedure

The application example is carried out with reference to the assessment method B described in section 2.6.3 . The corresponding procedure for assessing the degree of protection with respect to the three limit states SLD, SLS and SLC for the building in

question consists of the following steps (in brackets there is indicated the section in which each step is described in detail for the case):

1. Determination of seismicity of the site in question (§C.4)
    a. Data acquisition of the hazard at the site (§ (§C.4.1) in terms of spectral ordinates in acceleration (fractiles 16%, 50% and 84%, for the nine average return periods from NTC2008) and possibly the values of M and R from the disaggregation procedure.
    b. Selection of a set of N recordings of motion (§C.4.2 , three orthogonal components) compatible with the hazard mentioned in point 1.a, using the criteria described in §2.2.2 and §A.4.
2. Acquisition of data related to the soil, building materials, geometry, renforcement and construction details (§ (§C.5)
3. Assessment of available data and modelling of the uncertainties through a logic tree and random variables (§ (§C.6)
    a. Choice of the uncertainties to be modeled by a logic tree, the corresponding levels (branches) and weights (§ C.6.1)
    b. Determination of the probability distribution of the other random variables
4. Choice of the method of analysis (in this case the method B, § C.7)
5. Establishment of a structural model (§C.8) appropriate for the method of analysis and for the chosen mode of quantification of the limit states (model with degradation or without degradation, in this example both options are presented)
    a. Modeling of the site for the local seismic response (§ C.8.1)
    b. Modelling of the structure (§C.8.2)
6. For each branch of the logic tree:
    a. Sampling of N realizations of the set of random variables. Each implementation is associated with one of the N recordings of point 1.b and determines a distinct realization of the site-structure model.
    b. Execution of modal analysis of each structural model. Selection of significant modes. Determination of the *average* fundamental period T_1
    c. Determination from the data referred to in 1.a of the *average* hazard curve (§2.2.1) on rock for the spectral ordinate at the fundamental period $S_a(T_1)$
    d. For each model:
        i. In accordance with the evaluation method B, and with the chosen variant of static nonlinear analysis (*pushover* modal method, § §C.7.1), two pushover analyses are carried out (positive and negative signs of the pushing) with distribution of modal forces for each significant mode (point 6.b)
        ii. Determination of the characteristics of the equivalent oscillator (not symmetrical) for each significant mode (§C.7.1.1)
        iii. Determination of the incremental dynamic analysis curve by combining at each step the responses of the equivalent oscillators to the current seismic motion (at least two horizontal components, § §C.7.1.2)
    e. Determination of the fragility curves for the three SLs
    f. Determination of the average annual frequency of exceeding the three SLs, λ_{SLD}, λ_{SLs} and $\lambda_{SLC.}$

The step 6.d is the only specific element of the evaluation method B, all others are common to all methods.

C.4 Seismic action

As indicated in § §2.2.1 , the seismic action is defined by a hazard curve and a set of recordings of natural motions (or artificial time histories) compatible with the dominant mechanisms that generate events at the site on rock/rigid soil. The next two sections present the derivation of the average hazard curve for the site from the data provided in NTC2008, and the selection of natural records in a number equal to the minimum of twenty, as indicated in §2.2.2 .

C.4.1 Hazard curve

The starting data for the determination of the average hazard curve are the fractiles at 16%, 50% and 84% of the spectral ordinates in acceleration provided for nine average return periods in NTC2008. Fig. C.3 shows the nine *median* response spectra.

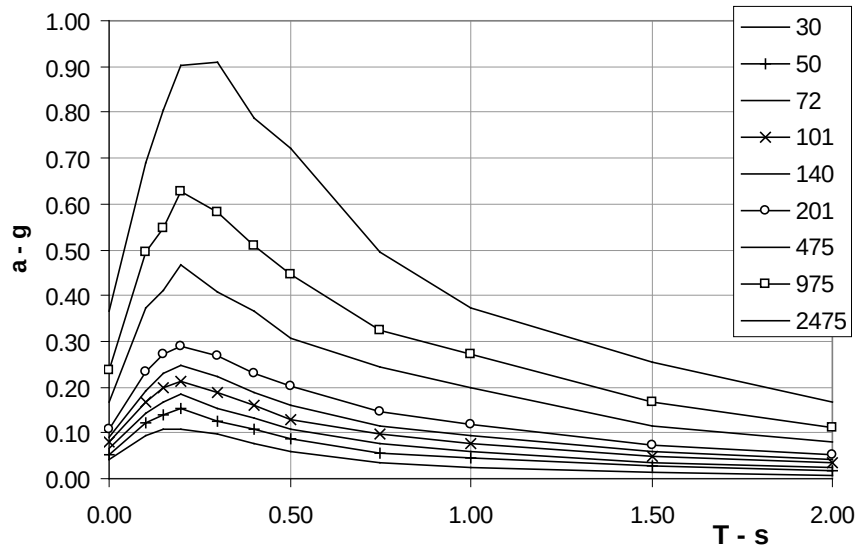

Fig. C.3 Median isoprobable spectra on rock for the site in question.

Table C-1 shows the values of the three parameters a_g, F_0 and T_C^* of the normative spectral shapes approximating to the iso-probable spectra at 16%, 50% and 84%. The table also shows the corresponding frequency $\lambda_S=1/T_r$. Fig. C.4 shows the fractile hazard curves in terms of peak ground acceleration (black) and of spectral acceleration for the average period of the models (see § C.8.2) corresponding to the first branch of the logic tree (§C.6.1) .
The difference between the fractiles allows one to obtain the value of the term of epistemic uncertainty β_H on the hazard according to equation (2.3), calculated as below, with reference to the first branch of the logic tree:

$$\beta_H = \frac{\ln S_{84\%} - \ln S_{16\%}}{2} \qquad \text{(C.1)}$$

This value allows to amplify the median curve to obtain the mean curve, according to Equation (2.2). The calculated values for the nine return periods are shown in Table C-2.

Table C-1 parameters of the normative spectral form approximating to the isoprobabile response spectrum and dominant event for varying average frequencies of exceedance at the site in question.

T_r	λ	a_g	F_o	T_C^*	$a_{g16\%}$	$a_{g84\%}$
30	3.33E-02	0.041	2.549	0.278	0.032	0.047
50	2.00E-02	0.054	2.565	0.295	0.045	0.062
72	1.39E-02	0.066	2.480	0.329	0.056	0.081
101	9.90E-03	0.079	2.477	0.340	0.068	0.098
140	7.14E-03	0.092	2.487	0.350	0.080	0.115
201	4.98E-03	0.109	2.474	0.386	0.094	0.137
475	2.11E-03	0.168	2.515	0.388	0.137	0.210
975	1.03E-03	0.236	2.417	0.414	0.186	0.295
2475	4.04E-04	0.365	2.329	0.430	0.268	0.471

Table C-2 First branch of the logic tree: calculation of the uncertainty on the hazard curve and transition to the mean curve.

T_r	λ	$S_a(T_1)_{16\%}$	$S_a(T_1)_{50\%}$	$S_a(T_1)_{84\%}$	β_h	λ_m
30	3.33E-02	0.008	0.013	0.020	0.43	3.66E-02
50	2.00E-02	0.019	0.026	0.037	0.34	2.12E-02
72	1.39E-02	0.026	0.035	0.052	0.34	1.47E-02
101	9.90E-03	0.034	0.046	0.065	0.32	1.04E-02
140	7.14E-03	0.044	0.059	0.080	0.30	7.48E-03
201	4.98E-03	0.054	0.073	0.098	0.30	5.20E-03
475	2.11E-03	0.086	0.113	0.151	0.28	2.19E-03
975	1.03E-03	0.122	0.163	0.224	0.31	1.07E-03
2475	4.04E-04	0.188	0.250	0.371	0.34	4.28E-04

To the mean curve, defined in nine points, is then adapted a quadratic function in logarithmic space given by the expression (2.13). The parameters that minimize the deviation are in this case:

$$k_0 = 8.134 \times 10^{-5} \quad k_1 = 3.254 \quad k_2 = 0.303 \qquad \text{(C.2)}$$

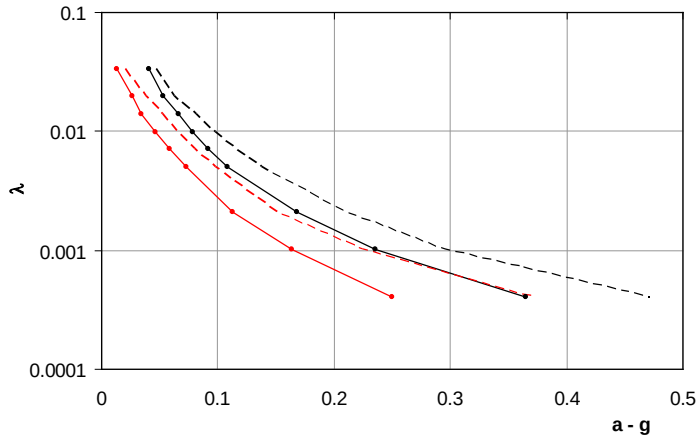

Fig. C-4 Median curve hazard (solid line) and 84% fractile (hatched), in terms of peak ground acceleration (black) and of spectral ordinate Sa ($T_1 \cong 1.52$ s) (red) for the site under consideration.

C.4.2 Choice of records of seismic motion

Table C-3 shows the data of disaggregation (relative to the median hazard curve in terms of peak ground acceleration) for the site in question. The table provides the values of magnitude and distance for the average periods of exceedance from 30 to 2,475 years. The values for all the corresponding frequencies are presented graphically in Fig. C-5.

Table C-3 Disaggregation of the median value of the average frequency of exceeding of the peak ground acceleration for the site in question.

Tr	λ	M	R_{epi}	ε
30	3.33E-02	5.644	51.221	0.233
50	2.00E-02	5.703	43.917	0.280
72	1.39E-02	5.728	38.624	0.317
101	9.90E-03	5.742	34.767	0.348
140	7.14E-03	5.755	31.585	0.381
201	4.98E-03	5.765	28.666	0.422
475	2.11E-03	5.810	23.058	0.566
975	1.03E-03	5.877	20.526	0.718
2475	4.04E-04	6.025	18.779	0.958

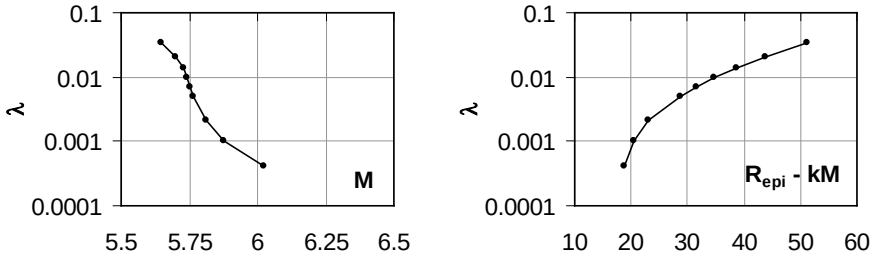

Fig. C-5 Magnitude and distance from the dominant event provided by the disaggregation as function of the average frequency of exceedance.

The recordings have been selected in a range of magnitude between the values 5.6 and 6.5, and of distance between 10km and 30km. These intervals, indicated in §2.2.2 as a choice generally appropriate in the absence of specific data from disaggregation, are in this case roughly centered around the values of disaggregation. The Fig. C-6 shows the indicated range and the recordings selected, within the database used (aggregation of European ESD databases, and Italian databases SIMBAD and ITHACA).

Table C-4 provides details of the selected recordings. In particular, it provides the values of the peak ground acceleration and spectral acceleration at the average fundamental period of the models in the first branch of the logic tree (§C.6.1). Three sample motions, which consists of two orthogonal components of horizontal acceleration, are shown in the following figures, together with the corresponding response spectra. The figures report in the caption also the name of the files containing the time series, according to the name of the database used.

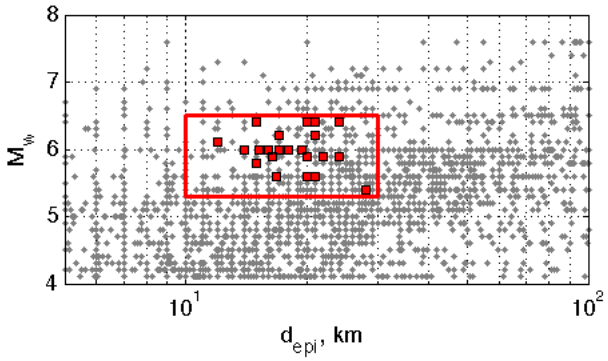

Fig. C-6 Magnitude-distance couplings of the recordings of the database (5 km <R_{epi} <100 km). There are highlighted the points relative to the selected recordings and the bounds of the target ranges.

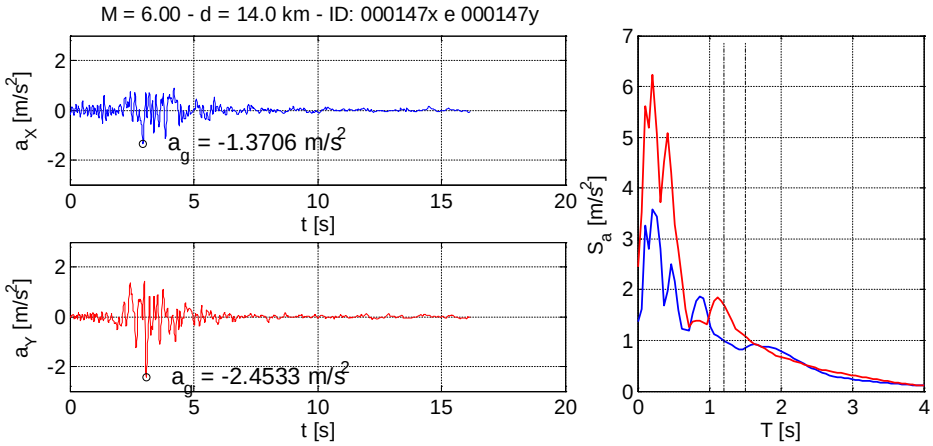

Fig. C-7 Record No. 1: time histories of the orthogonal components of horizontal acceleration, and respective response spectra (the two vertical lines indicate the range of variation of the fundamental periods of the 30 realizations of the models A or B).

Table C-4. Characteristics of selected motions (R_{epi} in km, peak ground and spectral acceleration in m/s^2, "as" indicates an aftershock).

#	DB	Event	M	station	R_{epi}	a_{gX}	$S_{aX}(T_1)$	a_{gY}	$S_{aY}(T_1)$
1	E	Friuli (as)	6.0	ST28	14.0	1.386	1.029	2.322	1.734
2	E	Montenegro (as)	6.2	ST75	17.0	1.731	0.750	2.721	0.840
3	E	Preveza	5.4	ST123	28.0	1.404	0.522	1.330	0.537
4	E	Umbria Marche (as)	5.6	ST86	20.0	0.963	0.629	1.316	1.353
5	E	Umbria Marche (as)	5.6	ST265	21.0	1.073	1.201	0.802	1.077
6	E	Izmit (as)	5.8	ST575	15.0	0.716	0.522	3.118	0.524
7	E	Ano Liosia	6.0	ST1100	16.0	2.611	0.924	3.018	1.054
8	E	Ano Liosia	6.0	ST1101	17.0	1.173	0.571	1.070	0.805
9	E	Ano Liosia	6.0	ST1257	18.0	1.091	0.835	0.843	0.544
10	E	Ano Liosia	6.0	ST1258	14.0	2.392	1.039	2.164	0.763
11	E	South Iceland (as)	6.4	ST2482	21.0	1.088	0.579	1.622	0.921
12	E	South Iceland (as)	6.4	ST2557	15.0	1.251	1.135	1.140	0.559
13	E	South Iceland (as)	6.4	ST2497	20.0	0.505	0.736	1.033	0.758
14	E	South Iceland (as)	6.4	ST2556	20.0	1.047	0.946	0.849	0.875
15	S	Near Miyakejima Island	6.4	TKY011	21.0	1.276	1.070	1.972	1.006
16	S	NW Kagoshima Pref.	6.1	KGS002	12.0	5.431	0.711	7.999	0.552
17	S	NW Kagoshima Prefecture	6.0	KGS002	16.0	4.529	1.517	7.818	0.952
18	S	South Iceland	6.4	102	24.0	1.275	0.842	0.618	0.562
19	S	South Iceland	6.4	105	21.0	1.108	0.580	1.662	0.920
20	S	South Iceland	6.4	305	20.0	0.539	0.760	1.057	0.732
21	S	South Iceland	6.4	306	20.0	1.067	0.927	0.892	0.839
22	S	Umbria-Marche (3rd shock)	5.6	NRC	20.0	1.314	1.355	0.939	0.615
23	S	L'Aquila (as)	5.6	GSA	16.8	2.811	0.582	2.485	0.668
24	S	Parkfield	6.0	36177	19.4	3.430	1.487	2.248	0.921
25	S	Parkfield	6.0	36445	15.2	1.437	2.332	2.225	2.784
26	S	East Fukushima Pref	5.9	FKS011	24.0	1.798	1.583	1.564	1.363
27	S	Mid Niigata Pref	6.2	NIG021	21.0	2.499	0.764	2.799	0.873
28	S	Mt Fuji Region	5.9	SZO009	22.0	1.442	0.660	1.225	0.581
29	S	Mt Fuji Region	5.9	YMN006	20.0	2.373	0.797	1.629	0.552
30	I	Friuli (4th Shock)	5.9	SRC0	16.4	1.288	0.937	2.444	1.933

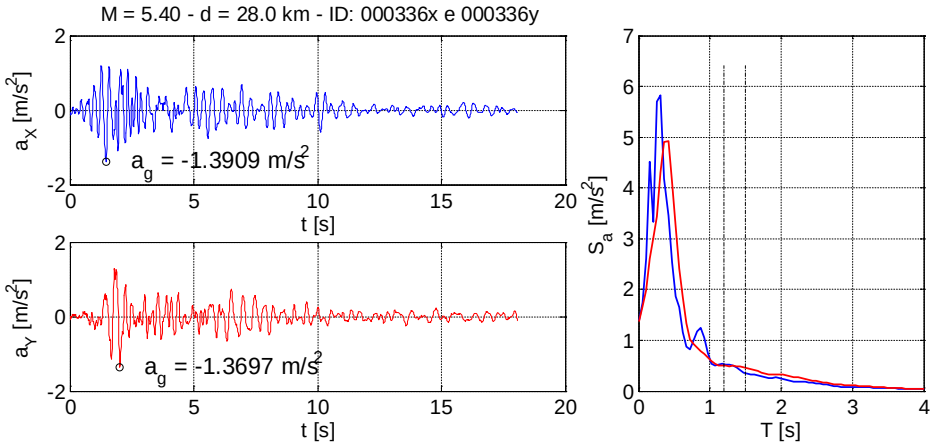

Fig. C -8 Record No. 3: time histories of the orthogonal components of horizontal acceleration, and respective response spectra.

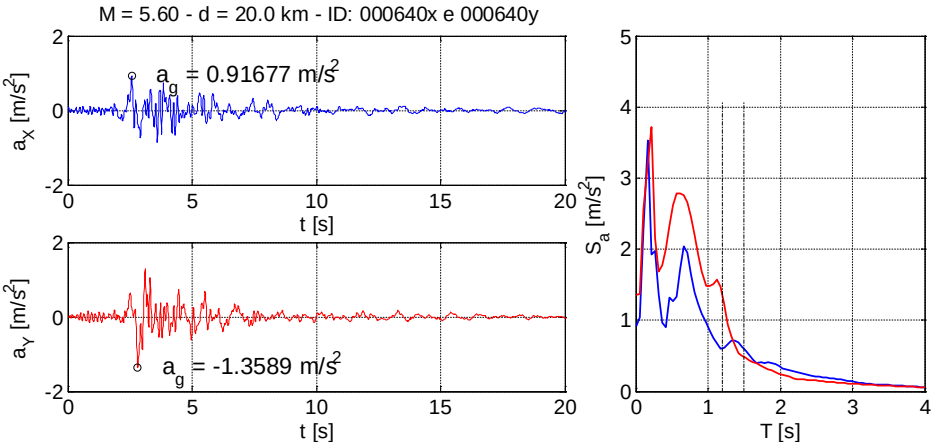

Fig. C -9 Record No. 4: time histories of the orthogonal components of horizontal acceleration, and respective response spectra.

C.5 Knowledge of the structure

For the structure in question the documents of the original structural design are not available. Based on a pre-existing architectural survey a structural survey was then carried out from scratch, which made it possible to reconstruct the structural system. Based on the reconstructed structural geometry and estimated values of the loads, and with assumptions made for the materials and amounts of reinforcement (geometric percentages in the columns according to the regulations in force at the time of construction and reinforcement in the beams from a simulated design), a preliminary linear model was set up that allowed an approximate evaluation of the different importance of the elements, and was then used to direct the subsequent tests campaign. The Fig. C-10 shows the model (the floors, modeled with equivalent rods as required by the code OpenSees used for subsequent nonlinear analysis, are not shown). The figure also shows in red the arrangement and the relative intensity of the loads on the beams.

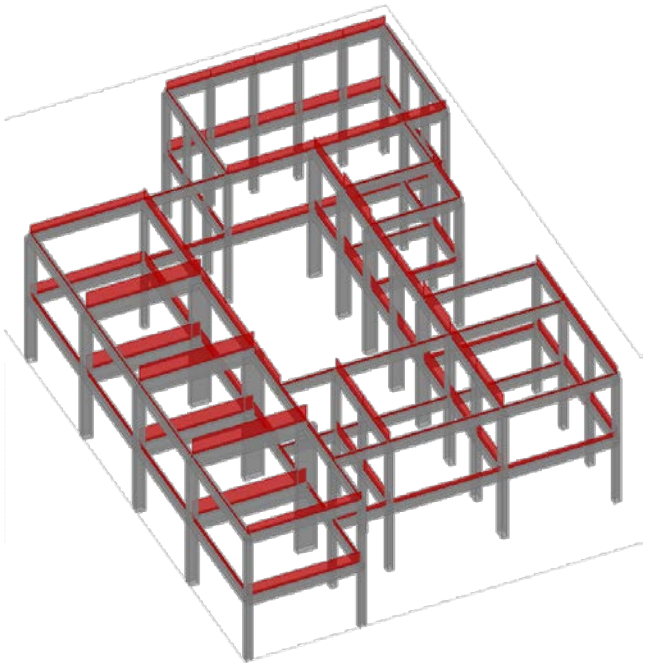

Fig. C-10 Preliminary model and load distribution from the floors on the beams.

The premilinary model constitutes the first step of the final model described in §C.8.2 , in which the geometry (nodes, elements, masses) is the final one, while for the elements a linear behaviour with cracked stiffness was adopted. The analysis performed is of a modal type with a response spectrum and the state of stress of the elements (calculated with reference only to the columns) is measured by the expression:

$$y = \sqrt{\left(\frac{M_2}{M_{y2}}\right)^2 + \left(\frac{M_3}{M_{y3}}\right)^2} \qquad \text{(C.3)}$$

where the moments acting on the two planes of bending are those obtained by the modal combination.

The Fig. C-11 shows the plan of the ground floor of the building with indication of the most stressed columns and of those chosen for carrying out the tests on the steel bars and the extraction of material for strength tests. The columns were chosen in general among those most stressed and adopting the criterion of repetitiveness. The reinforcement samples have been extracted from the columns of a larger cross section among those chosen, through not at the underground floor (not modeled). The results of the tests are shown in Table C-5 .

As for the strength of concrete, the average value of the tests is 14.7 MPa, with a standard deviation of 2.82 MPa. It has been finally chosen to adopt an average of 14 MPa with a 20% coefficient of variation. As regards the yield strength of the steel it was decided to adopt the mean value of 355 MPa, with a dispersion from literature equal to 10%.

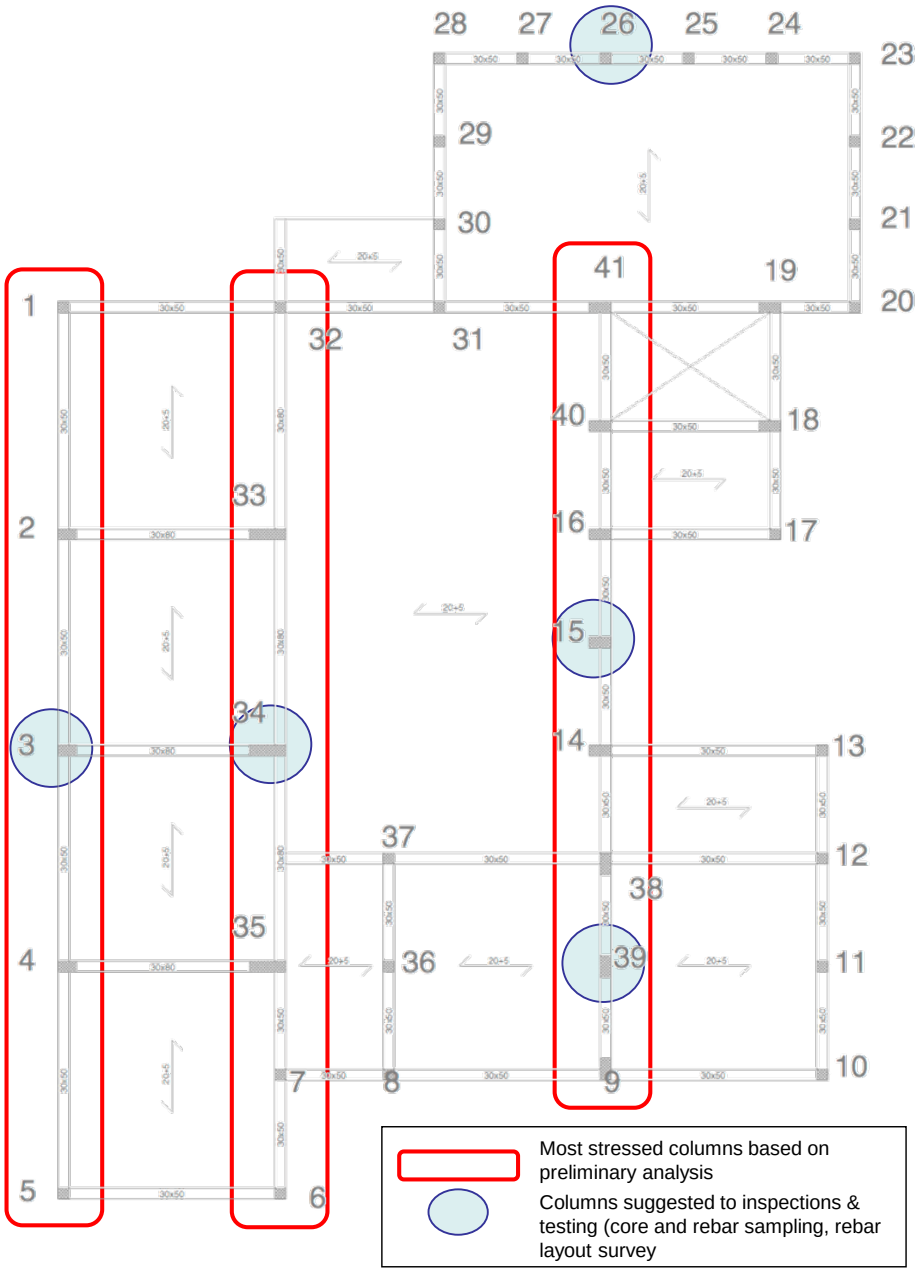

Fig. C-11 Position of the elements subject to testing.

Table C-5. Results of tests on the columns

Element	**B (mm)**	**H (mm)**	**Rebar long.**	**Rebar trasv.**	f_c **(MPa)**	f_y **(MPa)**
P3	300	500	6 ϕ 20	2 ϕ 6/200	16.7	-
P15	300	600	6 ϕ 20	2 ϕ 6/200	15.4	-
P26	300	300	4 2 ϕ1	2 ϕ 6/200	17.8	-
P34	300	1000	8 20 ϕ	2 ϕ 6/200	11. 9	337
P39	300	500	6 2 ϕ1	2 ϕ 6/200	11. 6	370

C.6 Modelling of the uncertainties

C.6.1 Logic tree

For the purpose of this application it has been modelled by a logic tree only the epistemic uncertainty on the effect of the infills on the response of the structure. As is known, the infills can have a positive or negative effect, depending on their distribution in plan and in elevation, and on the ratios of stiffness and strength with respect to those of the structural members. The two choices are given equal weights. The Fig. C-12 shows the in-plan distribution of the main infills to which a structural function can be attributed. The modeling with equivalent rods is described in § §C.8.2 .

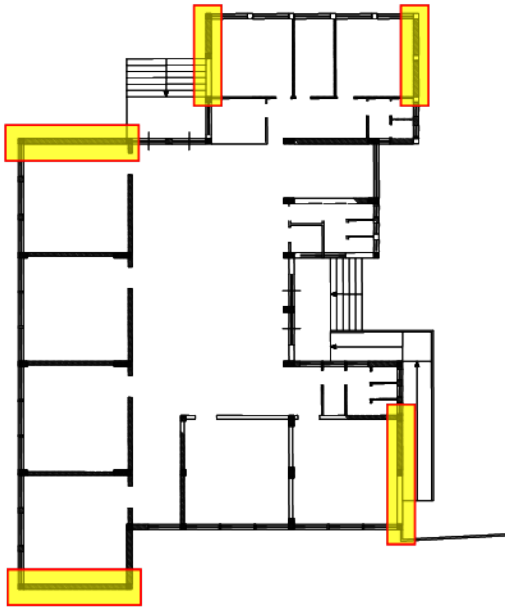

Fig. C-12 Distribution of the infills in plan.

C.6.2 Continuous random variables

In this application continuous random variables are used to describe the following uncertainties:

- Uncertainty in the strength of materials f_c and $f_{y,}$ and in the ultimate deformability of the concrete ε_{cu};
- Model uncertainty relative to the thresholds of *monotonic* deformation, $\theta_{y,}$ $\Delta\theta_f$ and $\Delta\theta_{a,}$ in the sectional phenomenological laws for the degrading beam-column elements (see §C.8.2);
- Model uncertainty relative to the thresholds of *cyclic* deformation, θ_V, θ_f and $\theta_{a,}$ for the a posteriori verification of the beam-column elements without degradation (see § §C.8.2);
- Uncertainty about the parameter of cyclic degradation of the elements γ;

- Uncertainty related to the resistance and deformability of the infills N_{tu} and $u_{tu,}$ for the branch of the logic tree in which they are included.

For all the mentioned variables it was adopted a marginal distribution of the lognormal type, defined by two parameters: the median and standard deviation of the logarithm β.

As regards the statistical dependence among the variables, in general different types of variables were considered as independent from each other (eg: $fc \perp f_y$), with the exceptions consisting of:

- variables K_{40} and $K_{y,}$ representing the error in stiffness at 40% of the yield strength and at the yield strength, that are considered perfectly correlated to ensure the condition $K_{40} > K_{y.}$ In practice, then, it is sampled a single standard normal variable $\varepsilon \sim$ N(0,1), which is amplified by the specific dispersion of each variable obtaining the factors $\exp(\varepsilon\sigma_{\ln K_{40}})$ and $\exp(\varepsilon\sigma_{\ln K_y})$ which multiply the corresponding medians.
- variables $\Delta\theta_f$ (Haselton *et al 2007)* and $\Delta\theta$a (Zhu *et al* 2007) which represent the threshold of monotonic deformation at the peak strength of the constitutive law of the element and the cyclic threshold for collapse due to loss of vertical bearing, to be used in the a posteriori verification, are considered perfectly correlated to avoid unrealistic situations in which a very ductile element ($\Delta\theta_f >> 1$) finds itself losing vertical bearing prematurely ($\Delta\theta_a << 1$). As in the previous case one proceeds by sampling a single standard normal variable and amplifying it with the appropriate dispersion.

As for the statistical dependence for variables of the same type between one element and another (spatial distribution of mechanical properties of materials, or correlation between the error terms of deformation models), it was adopted in a simplified manner a model of equicorrelation, with the values shown together with the parameters of the marginal distribution in Table C-6 .

As regards the variables that describe the properties of materials, the constant correlation adopted is a simplification that ignores the dependence on the distance between the elements (an alternative model could have adopted a trend with a decay of the correlation coefficient with increasing distance, slower for elements of the same floor and faster from one floor to another, to reflect the construction sequence).

As for the model errors, the indicated correlation values are assigned on the basis of the judgment of the authors, as the adopted model (the set of deformation thresholds of Haselton *et al 2007)* does not provide the correlation between the errors[28].

[28] It is necessary in any case to impose a correlation between such terms since the sampling of independent variables would inevitably lead to a high number of unrealistic combinations, for which, among other things, the structural analysis would not achieve convergence.

Table C-6. Continuous random variables: median, dispersion and correlation

Variable	Median	Dispersion	Correlation
f_c (MPa)	14.0	0.2	0.7
ε_{cu}	0.006	0.2	0.7
f_y (MPa)	338.0	0.1	0.8
K_{40}	Eq.(4.16)	0.38	0.8
K_y	Eq.(4.17)	0.36	0.8
θ_y	Eq.(4.11)	0.33	0.8
$\Delta\theta_f$	Eq.(4.11)	0.61	0.8
$\Delta\theta_\alpha$	Eq.(4.15)	0.72	0.8
θ_f	Eq.(4.9)	0.35	0.8
θ_V	Eq.(4.12)	0.27	0.8
θ_a	Eq.(4.13)	0.35	0.8
γ	Eq.(4.19)	0.5	0.8
N_{tu}	Eq.(C.20)	0.25	0.7
u_{tu}	§C.8.2	0.25	0.7

The simulation of correlated values is implemented by expressing the generic lognormal error ε (which multiplies the corresponding median) as a product of independent lognormal variables[29]:

$$\varepsilon_i = \tilde{\varepsilon}_i \eta \tag{C.4}$$

in which $\tilde{\varepsilon}_i \sim \text{LN}(0,\beta_\varepsilon)$, $\tilde{\varepsilon}_i \perp \tilde{\varepsilon}_j$, and $\eta \sim \text{LN}(0,\beta_\eta)$. The latter variable is sampled only once for the entire vector ε. The dispersions $\beta\varepsilon$ and β_η are obtained as functions of the total dispersion of the model and of the correlation coefficient assigned using the expressions:

$$\beta_\eta = \sqrt{\ln\left(1+\rho\left(e^{\beta^2}-1\right)\right)} \tag{C.5}$$

$$\beta_\varepsilon = \sqrt{\beta^2 - \beta_\eta^2} \tag{C.6}$$

In practice, then, for each random quantity (for example the strength of concrete), if *m* is the number of the structural elements, there are sampled *m* +1 lognormal independent variables (the *m* variables $\tilde{\varepsilon}_i$ and η).

The Fig. C-13 shows the histograms of the relative frequency of the sampled values of variabiles of the strength of the concrete, $f_{c,}$ and of the steel, $f_{y.}$ The figure also shows the lognormal densities from which the values were sampled (whose parameters are those shown in Table C-6).

[29] The two factors in the expression of the error of the model correspond respectively to the component common to all the elements of the same type and to that which varies from one element to the other, even if nominally equal. The term η corresponds, for instance, to those among the potential *hidden variables* not present in the model,which take on equal values for elements of the same type, as well as for the lack of fit, which is characterisitic of the analytical form chosen for the model and not of the element. The second term $\tilde{\varepsilon}_i$ corresponds to the *hidden variables* that take on different values for nominally equal elements.

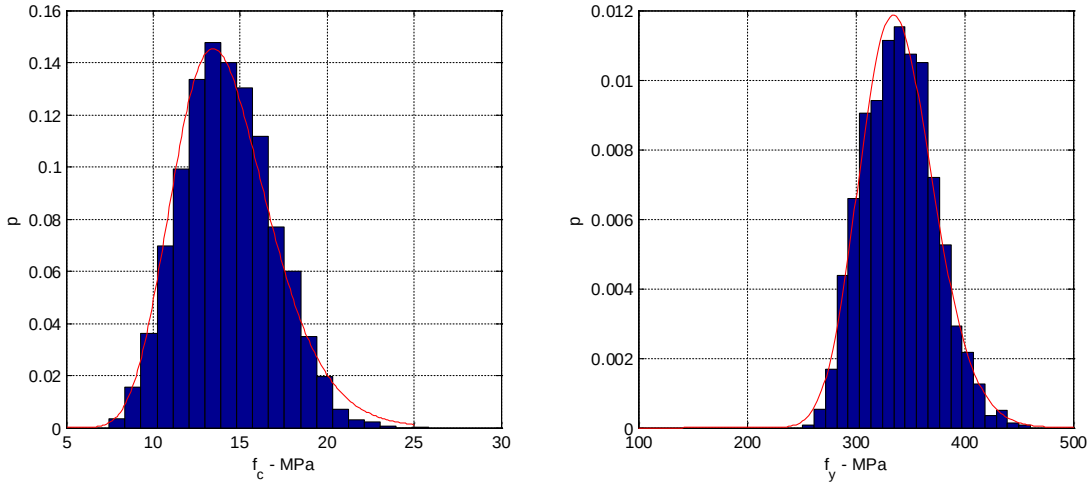

Fig. C -13 Properties of the materials: histograms of the relative frequency of sampled values and corresponding density (histograms are obtained with all the sampled values, i.e. for all elements in all the N simulations).

The Fig. C-14 shows the effect of the randomness of the materials and of the model errors on the constitutive law M- θ of the plastic hinge. The figure shows in blue the laws with degradation (continuous) and without degradation (dotted horizontal line after the peak) obtained with the median values of all random variables. The laws obtained with a single realization of the variables are shown in the red line. The realization of the strength is below the median, while that of the threshold of deformation is above the median. The figure also shows on the horizontal axis the cyclical thresholds corresponding to the start of the degradation and axial collapse (§C.8.3).

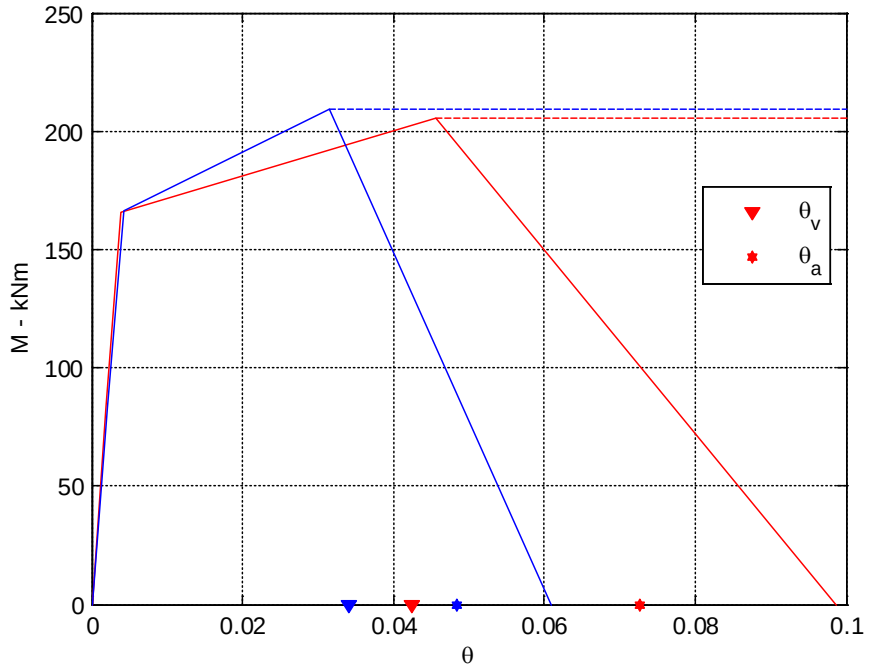

Fig. C -14 Error models: M-θ constitutive relationship relative to a member with median values of the random variables (blue) and for one of the samples (red).

C.7 Analysis

As indicated in §2.6.3 , the assessment method B shares the limitations of the adopted static nonlinear analysis.
In literature there are several proposals for the determination of the curve of incremental dynamic analysis from non-linear static analysis, for example (Vamvatsikos and Cornell, 2005) (Dolsek and Fajfar, 2005) (Han and Chopra, 2006).
Among these variants of the one that is chosen is due to (Han and Chopra, 2006) which is based on the modal non-linear static analyses (Chopra and Goel, 2002). This method is easy to implement in commercial programs, because it uses invariant force distributions, and is directly applicable to the actual buildings with spatial geometry (Reyes and Chopra, 2011).

C.7.1 Static modal analysis method

The modal static nonlinear method of analysis was introduced by Chopra and Goel (2002) with reference to plane frames. The method was then extended to spatial structures having a regular or irregular layout, still subject to one horizontal component of seismic motion, and finally to spatial structures excited by two orthogonal components (Reyes and Chopra, 2011a).
Here below the basic steps of the method with reference to spatial structures are presented. The proposed variant differs from that in (Reyes and Chopra, 2011a) which requires two separate analyses for the two components of motion and the use of a directional combination rule (for example the SRSS).

The equations of motion of a discrete dynamical system with n degrees of freedom subject to two orthogonal components a_X (t) and a_Y (t) of the seismic acceleration are written:

$$\mathbf{M}\ddot{\mathbf{u}} + \mathbf{C}\dot{\mathbf{u}} + \mathbf{F}(\mathbf{u}) = -\mathbf{M}(\mathbf{t}_X a_X + \mathbf{t}_Y a_Y) \qquad \text{(C.7)}$$

in which **M** and **C** are the mass and damping matrices, **F(u)** is the vector of resisting forces, a non-linear function of displacements (depending on the modelling adopted, §C.8.2), $\mathbf{t}_X$ and $\mathbf{t}_Y$ are the drag vectors in direction X and Y (the components of which are equal to 1 if the degree of freedom is a translation in the direction X or Y, and zero otherwise), and for simplicity the time dependence of excitation and the response has been omitted.

The method proposes to adopt in approximation the modal decomposition even in the presence of nonlinear resistant forces. Equation (C.7) then takes the form:

$$M_i\ddot{q}_i + C_i\dot{q}_i + F_i = -(L_{iX}a_X + L_{iY}a_Y) \quad i = 1,\ldots,n \qquad \text{(C.8)}$$

where q_i is the i-th modal coordinate, $M_i = \boldsymbol{\varphi}_i^T\mathbf{M}\boldsymbol{\varphi}_i$ and $C_i = \boldsymbol{\varphi}_i^T\mathbf{C}\boldsymbol{\varphi}_i$ are the corresponding modal mass and damping, $F_i = \boldsymbol{\varphi}_i^T\mathbf{F}(\mathbf{u})$ is the projection of the resisting forces on the i-th mode, and $L_{iX,Y} = \boldsymbol{\varphi}_i^T\mathbf{M}\mathbf{t}_{iX,Y}$. Dividing by the modal mass, one obtains:

$$\ddot{q}_i + 2\xi_i\omega_i\dot{q}_i + \frac{F_i}{M_i} = -\left(\Gamma_{iX}a_X + \Gamma_{iY}a_Y\right) \quad i = 1,\ldots,n \tag{C.9}$$

where ξ_i e ω_i are the damping and the natural frequency of the i-th mode, and Γ_{iX} e Γ_{iY} are the factors of modal participation of the two orthogonal components of excitation. Dividing by the larger participation factor (for example, that in X direction) corresponding to the "prevailing" direction of the mode, one obtains:

$$\ddot{D}_i + 2\xi_i\omega_i\dot{D}_i + \frac{F_i}{L_{iX}} = -\left(a_X + \frac{\Gamma_{iY}}{\Gamma_{iX}}a_Y\right) \quad i = 1,\ldots,n \tag{C.10}$$

The preceding equation is that of a nonlinear oscillator have a resisting force F_i/L_{iX}, subject to excitation $-\left(a_X + a_Y\Gamma_{iY}/\Gamma_{iX}\right)$, in which the component parallel to the secondary direction is weighted by the ratio between the participation factors. The following steps, described in the next paragraph, are those necessary for the determination of the constitutive non-linear law of the modal oscillator from a nonlinear static analysis.

C.7.1.1 Determination of the equivalent oscillator

As already indicated in 6.d.i of the assessment procedure (§C.3), for each significant mode two non-linear static analyses are carried out, corresponding to the two signs of thrust, positive and negative. If the structure is symmetrical with respect to the considered mode, one non-linear static analysis is sufficient.
The result of the nonlinear static analysis consists of a database of local responses of the structure, hereinafter referred to as *db* and containing for example matrices of displacements of the nodes, or forces and deformations in the elements (of a size respectively equal to $n_{steps} \times n_{nodes}$ and $n_{steps} \times n_{elements} \times n_{deformations)}$ and in a curve that expresses the relationship between the shear at the base V_b and the displacement of a chosen control degree of freedom u_c.
The curves relative to the first prevailing modes in the two orthogonal directions will be typically characterized by a first ascending portion, by a peak or plateau and by one section with negative stiffness (whose starting point and slope depend on the type of modelling adopted and will correspond to an anticipated crisis of the structure in the case of a model *with degradation,* where in addition to strength degradation due to the geometric effect there will the addition of that of mechanical nature). The curves relating to higher modes will have in general a trend approximately linear or bilinear without negative stiffness.
For spatial structures the shear at the base is that in the "prevailing" direction of the mode, for which participation factor is greater. For example, if the prevailing direction is the X, the base shear is given by the expression:

$$V_{biX} = \mathbf{t}_X^t\mathbf{F}_i \tag{C.11}$$

Dividing the base shear by the corresponding participation factor one obtains:

$$\frac{V_{biX}}{\Gamma_{iX}} = \frac{\mathbf{t}_X^t \mathbf{F}_i}{\left(\frac{\boldsymbol{\varphi}_i^t \mathbf{M} \mathbf{t}_X}{\boldsymbol{\varphi}_i^t \mathbf{M} \boldsymbol{\varphi}_i}\right)} = \frac{\mathbf{t}_X^t \lambda \mathbf{M} \boldsymbol{\varphi}_i}{\mathbf{t}_X^t \mathbf{M} \boldsymbol{\varphi}_i} \boldsymbol{\varphi}_i^t \mathbf{M} \boldsymbol{\varphi}_i = \lambda M_i \qquad \text{(C.12)}$$

with the substitution $\mathbf{F}_i = \lambda \mathbf{M} \boldsymbol{\varphi}_i$, where λ is the multiplier of loads and $\mathbf{M}\boldsymbol{\varphi}_i$ expresses the modal distribution of the forces of the i-th mode. The last term of the previous expression coincides with the resisting force of the oscillator in the equation (C.4), but for the factor $L_{iX:}$

$$F_i = \boldsymbol{\varphi}_i^t \mathbf{F}_i = \boldsymbol{\varphi}_i^t \lambda \mathbf{M} \boldsymbol{\varphi}_i = \lambda M_i \qquad \text{(C.13)}$$

One thus finds the transformation rule of the results of the static non-linear analysis in the law of the equivalent modal oscillator, for what concerns the resisting forces:

$$\frac{F_i}{L_{iX}} = \frac{1}{L_{iX}} \frac{V_{biX}}{\Gamma_{iX}} = \frac{V_{biX}}{L_{iX}^2} M_i \qquad \text{(C.14)}$$

As for the displacement, assuming that the fact that the displacements caused by a distribution of forces proportional to $\mathbf{M}\boldsymbol{\varphi}_i$ are proportional to $\boldsymbol{\varphi}_i$ (i.e. $u_c = \varphi_{i,c} q_i$) maintains validity in a non-linear context and taking into account that $q_i = \Gamma_{iX} D_{i,}$ one obtains the transformation rule for the displacements:

$$D_i = \frac{u_c}{\Gamma_{iX} \phi_{ic}} \qquad \text{(C.15)}$$

The next step consists in the approximation of the relation F/L-D with an hysteretic analytic law generally of a multi-linear kind. The Fig. C-15 shows, to the left with reference to the model A, the relationship V_b -u_c for the two directions of pushover relative to the distribution of forces of the first, second and third mode, and their relative trilinear approximations. In the figure one observes the general case in which the analysis, though pushed well beyond the peak along the descending portion, does not converge down to the point of zero shear at the base, where instead the trilinear approximating curve arrives. It can then occur the case during the following incremental dynamic analysis where the maximum displacement of the oscillator D_{max} corresponds to a maximum displacement of the control point $u_c(D_{max})$ larger than the maximum $u_{c,end}$ provided in the database *db*.

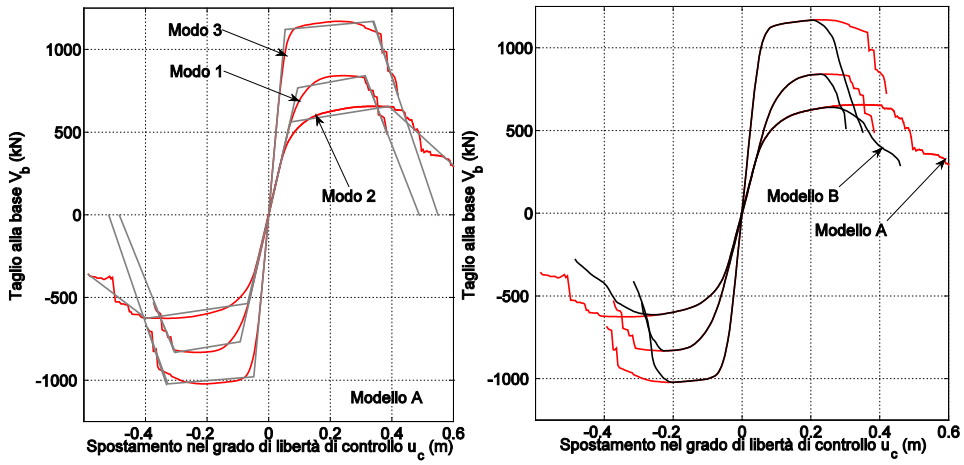

Fig. C -15 Capacity curve: trilinear approximationn for the model A, without degradation, to the left, and comparison between model A and model B with degradation, right. The negative tangent in the model without degradation is due to the geometric contribution to the stiffness.

The figure on the right contains the comparison between model A and model B in terms of curves V_b-u_c for the three previous modal distributions, which shows that the two curves coincide up to the value of the displacement of the control degree of freedom relative to the first local rupture, identified only by the model B during the analysis.

The approximation of the curve F/L-D using a multi-linear relation can be carried out in different ways. With reference to the modes for which the analysis has produced a curve with a plateau and a section with negative stiffness, i.e. a tri-linear law as that for example of Ibarra et al (2005), whose monotonic load curve is defined by the force-displacement couples of three points (yield, peak or capacity, and ultimate), or by transformations thereof, one can proceed as in (Fragiadakis and Vamvatsikos, 2010) by first determining the parameters of the first two segments (linear and hardening), then determining the negative slope of the post-peak branch[30]:

1. One identifies the maximum point on the curve D_{max} - $(F/L)_{max}$
2. One finds the initial k_{el} and post-elastic k_h stiffnesses, for example with the criterion of equal areas (underlaid by the bilinear and by the curve DF/L in the segment between $D = 0$ and $D = D_{max}$)
3. One finds the post-peak stiffness k_c of a linear branch passing through D_{max} - $(F/L)_{max}$, having equation $F/L-(F/L)_{max} = k_c\,(D-D_{max})$, by minimizing the mean square error with respect to the analytical curve in the section $D > D_{max}$.

When the curve produced by the analysis presents different trends, as can happen for load distributions corresponding to higher modes, a linear or bilinear approximation can be adopted.

In the case of models with degradation, the constitutive law includes the appropriate parameter values of cyclic degradation of the equivalent oscillator. In rigour, the determination of the values of these parameters should be performed by subjecting the

[30] In the application, actually, it was used an optimization procedure that simultaneously determines the three points of yield, peak and ultimate, resulting in a slightly lower overall error.

whole structure to imposed cyclic deformations: the corresponding analytical effort would be however not consistent with the approximation of the method B. In approximation one may adopt, for example, as values of the parameters of degradation: a) the average of all the columns of the structure, b) average of the columns of the most stressed storey, if one such appears clearly from the examination of the inelastic deformation, c) the average weighed along the deformed shape, for example at the peak $(F/L)_{max}$. In the application it has been chosen to adopt the average value on the columns.

C.7.1.2 Determination of the IDA curve

For each of the *n* significant modes one proceeds by performing an incremental dynamic analysis of the corresponding asymmetrical equivalent oscillator subjected to a signal $-\left(a_X + a_Y \Gamma_{iY} / \Gamma_{iX}\right)$ or $-\left(a_Y + a_X \Gamma_{iX} / \Gamma_{iY}\right)$, depending on the prevailing direction of the mode under consideration.
The result consists of a set of *n* IDA curves that express the link between the intensity of the earthquake S, on the ordinate, and the displacement of the oscillator D, in the abscissas ("IDA curve").
For each curve, using the equation (C.9), it is possible to derive at each intensity level the corresponding value of the displacement in the control degree of freedom u_{ci} ($S = s$), and with this it is possible to determine, interpolating in the database db_i (see §C.7.1.1), all local responses of interest (in particular, for the application under consideration, the drift θ in the columns[31] and the interstory displacements Δ, as shown in the following in §C.8.3) relative to the *i*-th mode.
In performing the interpolation, in order to obtain modal responses for equal intensities to produce, through an appropriate rule of modal combination (SRRS or CQC), the overall response of the structure, it is necessary to take account of the fact that, in general, the curves will not have the same number of points and that these will not be at the same levels of intensity S. In particular, the curves relative to those equivalent oscillators whose response does not present a section with negative stiffness will not have a plateau corresponding to the dynamic instability (Vamvatsikos and Cornell, 2005) (Han and Chopra, 2006), as shown in Fig. C-16 (left). The deformation contained in the database of the mode whose IDA curve presents a plateau with an intensity lower than s_{min} (the Mode 1 in the Fig. C-16[32]) will have very high value at the approach of this intensity. Therefore, whatever the chosen combination rule, the displacements of the structure will be conditioned by those of that mode and will present significant increases for small variations of the intensity near s_{min}. In the interpola-

[31] The fact that only the columns are considered allows the simplification of avoiding the subtraction of the response due to the gravitational loads from that of each mode, and its summation to the result of the modal combination, as indicated in (Chopra and Goel, 2002)(Han and Chopra, 2006) and (Reyes and Chopra, 2011).
[32] The figure shows two IDA curves characterized by a plateau, those relative to the first and second modes. The figure schematically represents the typical situation of a 3-D building in which there are two “first modes”, one prevailing in the X direction and the other in the Y direction. The difference in maximum intensity reflects a difference in the resistance between the two modes. The third mode represents a higher mode that is included since it has a participation that is still not negligible, though actually modest and such as to leave the structure substantially elastic.

tion[33], it is thus not necessary to consider intensities larger s_{min} since the overall curve has already reached a plateau of dynamic instability. One will choose a number of points adequate to determine the relationship between the limit state indicators (as shown in the following §C.8.3) and the intensity S, equally spaced between the extremes S = 0 and S = s_{min} (for example ten points), as shown in Fig. C-16 (left).

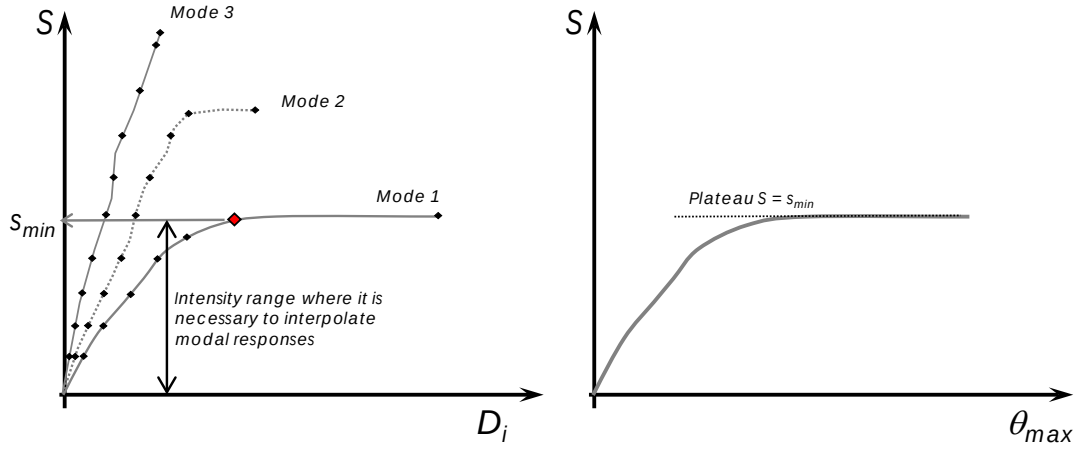

Fig. C -16 The IDA curves of the modes (left) and that of the entire structure (right).

The figure (right) also shows the combined curve corresponding to the IDA for the considered structured-model-record, expressed in terms of seismic intensity S and the parameter commonly used to express the maximum deformation in a building, θ_{max}. The latter is defined in the application as the maximum interstorey displacement with the subtraction of the rotation of the beams. In particular, the formulation adopted in the application is:

$$\theta_{\max} = \max_j \max\left(\theta_{12,j}, \theta_{13,j}\right) \quad j = 1, \ldots, n_{elementi} \tag{C.16}$$

that takes account of the two planes of bending (see §4.2 and §C.8.3).
Having obtained the overall IDA curve S- $\theta_{\max}$, one can determine the intensity corresponding to the attainment of each limit state, s_{SL} interpolating at the unit value of the corresponding variable Y_{SL} = 1. These intensities can be represented as shown in Fig. C-17 , where it is shown in qualitative terms both the case of the model with degradation and the model without degradation.

[33] It may happen that, as indicated in §C.7.1.1, at some intensities near s_{min}, the displacement D_{max} corresponds to a displacement in the control degree of freedom larger than the maximum one $u_{c,end}$ in the database. In these cases, in approximation, one can *extrapolate* the modal deformation to the last point by amplifying it by the factor $u_c(D_{max})/u_{c,end}$.

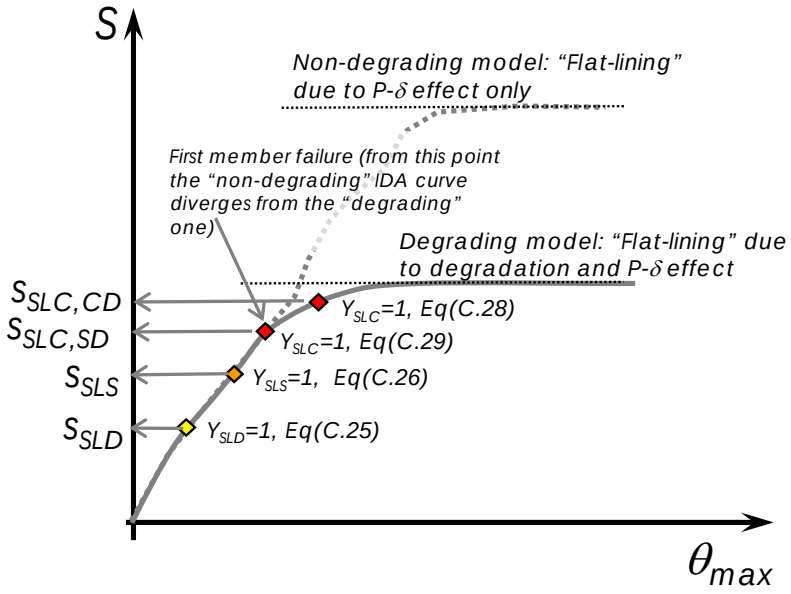

Fig. C -17 The IDA curve of the entire structure and representation of the attainment of the three SLs, for the two types of modelling considered.

C.8 Modelling

C.8.1 Modelling of the site response

As indicated in §2.2.2 , the change in the characteristics of the motion associated with the seismic response of the site under consideration requires in rigour an analysis of the local seismic response, which should take into account the uncertainty in the mechanical parameters of the soil.
In this application, by way of simplification, it has been decided not to address this issue and to take account of the amplification with a deterministic factor independent of the period of vibration and intensity equal to 1.25.

C.8.2 Modelling for the structural analysis

The structural analyses (static nonlinear analyses on the 3D model and incremental nonlinear dynamic anlysis on the equivalent oscillators) have been performed with the code OpenSees (McKenna et al, 2010).
The behavior of the beam-column joints has not been modelled.
The beams and columns have been modeled with an assembly of an elastic element and two *zeroLength* elements at its ends. The two end sections have been assigned independent uniaxial laws for the different degrees of freedom (linear in particular for the torsion). The moment-rotation law adopted is the trilinear one of Ibarra et al (2005) modeled with the link *ModIMKpeakOriented* (Lignos and Krawinkler, 2012), as shown in Fig. C-18a.

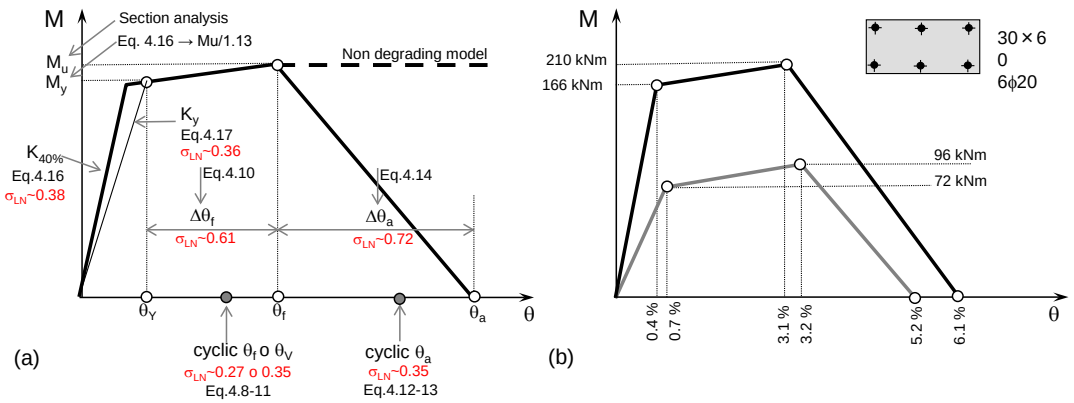

Fig. C -18 Constitutive law of plastic hinge (a) and laws in the two planes of bending for a rectangular column (b).

A conceptually equivalent alternative would be to use the finite element *beamWithHinges* (Fenves and Scott, 2006). The modeling strategy adopted is however more robust from the computational aspect as it always leaves the global algorithm, over which the user has more control, the task of reducing the unbalanced forces during the analysis. The analysis was in fact carried out also with the *BeamWithHinges* element[34], obtaining completely comparable results, but with considerable convergence problems.

For the columns two distinct and independent laws in the two planes of bending have been assigned (Fig.C-18b). The figures also show the corresponding laws *without degradation*. The laws were evaluated for a normal stress constant equal to zero for the beams and equal to that produced by the vertical loads in the seismic combination, obtained by a static analysis on the preliminary model, for the columns.

The equation which gives the ratio M_u / M_y has been used to obtain M_y from M_u , and the dispersion was neglected, which is however very low ($\sigma_{LN} = 0.10$). The figure also shows the thresholds of cyclic deformation, lower than the corresponding monotonic thresholds, used to determine the limit state variables as detailed in §C.8.3. These thresholds are calculated with the model of Zhu *et al* (2007) and in order to discriminate collapse due to ductile shear from that due to flexure a criterion proposed by the authors has been used, which anticipates shear failure (brittle or ductile) if the geometric percentage of shear reinforcement $\rho_{sh} \le 0.002$, or if the element is squat $L_V / h \le 2$, or the ratio between plastic shear $V_p = 2M_u / L$ and shear strength (evaluated according to the model of Sezen and Mohele, Eq.4.21) is $V_p / V_R \ge 1.05$. The indicated equations were used to determine the median of the corresponding quantities, multiplied by the lognormal random variables described in §C.6.2. In the event that according to the above criterion failure is anticipated to occur in flexure (Mode 3), it has been assigned $\theta_a = \theta_f$ (since the model for θ_a expects the preceding failure to be of Mode 1 or 2) .

[34] In assigning the moment-rotation laws to the sections in this case, the deformation thresholds have been divided for the same length of the plastic hinge required as input by the *beamWithHinges* element, for which it has been adopted the expression:

$$l_p = 0.1L_V + 0.17h + 0.24\phi\, f_y / \sqrt{f_c}$$

For each column N values of the total hysteretic normalized energy γ entering the model of cyclical degradation of Ibarra *et al* (2005) were also sampled according to Eq. 4.19.
It should be noted that the parameter of degradation provided by Eq. 4.19 is defined in Haselton et al (2007) according to (Rahnama and Krawinkler, 1993) and (Ibarra et al, 2005) as the ratio of the total hysteretic energy E_t and the product $M_y\theta_y$. The model *ModIMKpeakOriented* used in OpenSees implements the law of Ibarra et al as modified by Lignos and Krawinkler (2012), in which the total hysteretic energy is normalized with respect to the product $M_y\theta_p$, i.e. between the yielding moment and the plastic part of the rotation, the latter resulting in a more stable parameter. Finally, the implementation of *ModIMKpeakOriented* requires as input the value of the so-called cumulative plastic rotation $\Lambda = \lambda\theta_p$(Lignos and Krawinkler, 2012). It is therefore necessary to take into account of this difference, in the allocation of the value of γ, to the constitutive law:

$$\left.\begin{aligned}\gamma &= \frac{E_t}{M_y\theta_y}\\ \lambda &= \frac{E_t}{M_y\theta_p}\\ \Lambda &= \lambda\theta_p\end{aligned}\right\} \rightarrow \Lambda = \gamma\theta_y \qquad \text{(C.17)}$$

As stated above (§C.7.1.1) for the purpose of the incremental dynamic analysis of the equivalent oscillator the average value of γ (actually the value $\overline{\Lambda} = \overline{\gamma}D_y$) has been used. Figure C-19 shows the distribution of γ on the columns of the structure for two of the N simulations.

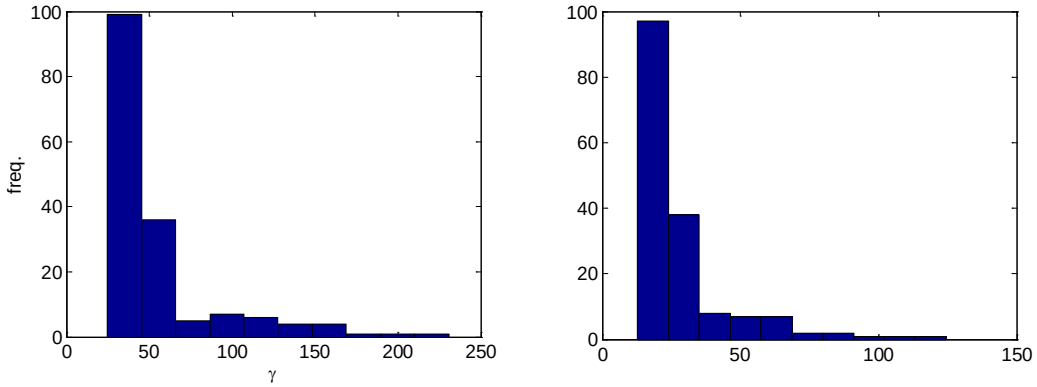

Fig. C -19 Distribution of γ on the columns for two of the N = 30 simulations.

The infills have been modeled, in the branch of the logic tree corresponding to the case of model *with degradation*, by means of equivalent rods. Among the possible modeling alternatives by rods (Asteris *et al* , 2011) it has been chosen the easiest, with only two rods that join the beam-column nodes. This modeling does not allow to capture local effects of increased shear to beams and columns, but allows one to describe the effect on the global response due an irregular distribution of the panels in-plan and elevation.

A rectangular section has been assigned to the equivalent struts, with width equal to the actual thickness t = 0.15m of the masonry and height w determined as a function of the strut length d according to (Bertoldi *et al* , 1993):

$$\frac{w}{d} = \frac{K_1}{\lambda^* H} + K_2 \tag{C.18}$$

in which H is the height of the infilled story and λ^* is a parameter of relative infill-frame stiffness proposed by Stafford-Smith (1962, 1966) given by the expression:

$$\lambda^* = \sqrt[4]{\frac{E_m t \sin 2\theta}{4 E_c I H_m}} \tag{C.19}$$

where E_m = 5 GPa and E_c are respectively the Young modules of concrete and masonry, θ the angle of inclination of the diagonal with respect to the horizontal, I the moment of inertia of the adjacent columns and H_m the free height of the infill. The two parameter K_1 and K_2 are determined in function of the product $\lambda^* H$ (Table C.7).

Table C-7. Parameters K_1 and K_2 of the equivalent rod model.

Coefficient	$\lambda^* H < 3.13$	$3.13 < \lambda^* H < 7.85$	$7.85 < \lambda^* H$
K_1	1.300	0.707	0.470
K_2	-0.178	0.010	0.040

The compressive strength of the equivalent connecting rod can be obtained by the product:

$$N_u = t \cdot w \cdot \min(\sigma_u) \tag{C.20}$$

between the area of the cross section of the rod and the minimum critical stress between those corresponding to the four mechanisms (Bertoldi *et al* , 1993) reported in Table C-8, in which f_m = 1 MPa and τ_m = 0.3 MPa are the resistances to compression and to shear of the masonry, and τ_g = 0.2 MPa is the resistance to sliding in the joints.

Table C-8. Resistance for the four failure mechanisms.

Mechanism	Rupture strength
Diagonal tension	$\sigma_u = (0.6\tau_m + 0.3 f_m) / \left(\frac{K_1}{\lambda^* h} + K_2 \right) = \frac{d}{w}(0.6\tau_m + 0.3 f_m)$
Sliding joints	$\sigma_u = \frac{d}{w}\left[(1.2\sin\theta + 0.45\cos\theta)\tau_g + 0.3 f_m \right]$
Corner crushing	$\sigma_u = \frac{f_m 1.12 \sin\theta\cos\theta}{K_1 (\lambda^* h)^{-0.12} + K_2 (\lambda^* h)^{0.88}}$
Diagonal compression	$\sigma_u = \frac{1.16 f_m \tan\theta}{K_1 + K_2 \lambda^* h}$

Mass, stiffness and resistance of the infills can be reduced by taking into account the actual position and size of the openings present, following the indications in Decanini *et al.*(1994). In the present case, however, the openings have been neglected because of their modest size.
The constitutive link, shown in Fig. C-20 , is completed by the values of the displacements u_d and u_u which mark respectively the end of the "plastic" sections with the beginning of the degradation and the collapse of the panel. These limits were defined, using indications from the literature, as equal to 2 and 4 times the elastic displacement limit $u_y = N_u/k$ (where the stiffness k of the connecting rod is equal to $E_m wt/d$).

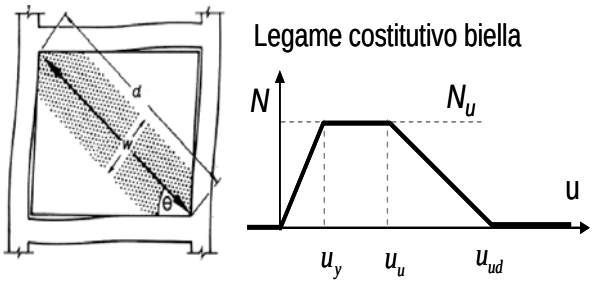

Fig. C -20 Constitutive law of the equivalent rods for infills.

Finally, as regards the uncertainty on the properties of the infills, as indicated in §C.6.2, the mechanical properties of the masonry material have not been modeled as random variables. Two variables have been included, which describe, respectively, the overall effect of the uncertainty on the materials and on the model on the resistance, ε_{Nu}, and on the deformability/ductility, $\varepsilon_{Uu.}$

C.8.3 Limit state variables

This section contains the expressions of state limit indicators adopted in the application. The expressions are those indicated in §2.5, adapted to the present case. In particular, the local response quantities considered are, for the structural members, the flexural distortion θ for the columns, and the interstory drift Δ for the non-structural components (the infills).
To take account of the state of biaxial deformation and of the different deformation capacities in the two planes of bending of the columns (see §4.2), it has been adopted the biaxial demand/capacity ratio given by the expression:

$$y_{j,SL} = \sqrt{\left(\frac{\theta_{j,12}}{\theta_{SL,j,12}}\right)^2 + \left(\frac{\theta_{j,13}}{\theta_{SL,j,13}}\right)^2} \qquad \text{(C.21)}$$

in which $\theta_{j,12}$ and $\theta_{j,13}$ are the total flexural distortions (obtained by combination of the modal contributions as indicated in §C.7.1.2) in the two planes of bending 1-2 and 1-3, and the corresponding capacities are, for the SLD:

$$\theta_{SLD} = \theta_y \qquad \text{(C.22)}$$

and for the SLS:

$$\theta_{SLS} = \theta_f \quad \text{o} \quad \theta_V \tag{C.23}$$

where the flexural or the shear limit apply according to the criterion specified in §C.8.2 .
For the SLC, one must distinguish the case of the model with degradation from that of the model without degradation. In the first case the mode of collapse due to loss of vertical bearing capacity as a result of a shear failure is not modeled and, therefore, is checked later using the (biaxial) ratio between the distortion demand and the corresponding cyclic capacity provided by the model of Zhu et al (2007), shown in §4.4.4.3 :

$$\theta_{SLC,a} = \theta_{a,Zhu} \tag{C.24}$$

In the case of the model without degradation one must instead define a local biaxial D/C ratio $y_{SLC,fV}$ that expresses the exceedance of the maximum available ductility and the beginning of the unmodelled degradation equal to $\theta_{SLC,fV} = \theta_{f,Zhu}$ or $\theta_{SLC,fV} = \theta_{V,Zhu}$ according to the criteria specified in §C.8.2.
The attainment of the state limit of damage is quantified by the variable (see Eq.2.5):

$$Y_{SLD} = \max\left(\max_{pilastri} y_{SLD}; \max_{NS} \frac{\Delta_i}{\Delta_{Ci}} \right) \tag{C.25}$$

in which the capacity of the infills in terms of inter-floor sliding is 0.006.
The attainment of the state limit of severe damage is quantified by the variable (see Eq.2.7):

$$Y_{SLS} = \alpha_S \frac{1}{N_S} \sum_S c\left(y_{SLS}\right) + \left(1-\alpha_S\right) \frac{1}{N_{NS}} \sum_{NS} c\left(\frac{\Delta}{\Delta_C}\right) \tag{C.26}$$

in which it is assumed the value α_S = 0.3, and the cost functions have the following expressions[35]:

$$c\left(y_{SLS}\right) = \min\left(1; \frac{y_{SLS}}{0.5}\right) \quad c\left(\frac{\Delta}{\Delta_C}\right) = \min\left(1; \frac{\Delta}{0.01}\right) \tag{C.27}$$

which vary linearly between 0 and 1, respectively for y_{SLS} between 0 and 0.5 (ie the conventional cost repair equals that of replacing already at 50% of the ultimate strain, shear or bending), and for Δ between 0 and 1%.
Reaching the limit state of collapse it is quantified in the model *with degradation* through the variable (see Eq.2.10):

$$Y_{SLC} = \max\left[1.2 - \frac{dS/d\theta_{\max}}{\left(dS/d\theta_{\max}\right)_0}; \max_{pilastri} y_{j,SLC,a} \right] \tag{C.28}$$

In the model *without degradation* the variable used is (see Eq.2.8):

[35] The value adopted for the α_S is relatively high and corresponds to the characteristics of the school building considered, in which the economic value of the content and of the installations is reduced.

$$Y_{SLC} = \max_{pilastri} y_{j,SLC,fV} \tag{C.29}$$

where the D/C relations are calculated with reference only to the columns. This variable defines the collapse in conservative terms as the exhaustion of ductility available from the first column. The capacities used are those provided by the cyclic model of Zhu *et al* (2007).

C.9 Results

This section describes and comments on the results for the three models analyzed, respectively entitled:

- Model A: model *without degradation*
- Model B: model *with degradation*, without infills (first branch of the logic tree)
- Model C: model *with degradation* and infills (second branch of the logic tree)

The results for the models B and C are combined with the technique of the logic tree to obtain the final estimate of the risk in the case of the model with degradation.

C.9.1 Model A

The modelling without degradation represents the current state of the art, as noted in §C.1. For this case it has been chosen not to consider modelling alternatives to be-weighted with the technique of the logic tree and therefore the point 6 of the procedure illustrated in §C.3 is carried out only once.

The process started by sampling $N = 30$ structures (§C.6.2), associated with the 30 recordings selected, and carrying out for each one a modal analysis. In all cases three modes of vibration proved to be sufficient. For each of them both the positive and negative pushover analyses have been carried out. Fig. C-21 reports summarized results of these analyses, showing the 30 curves for the two signs (60 analyses) relative to the three modes, starting from left to right.

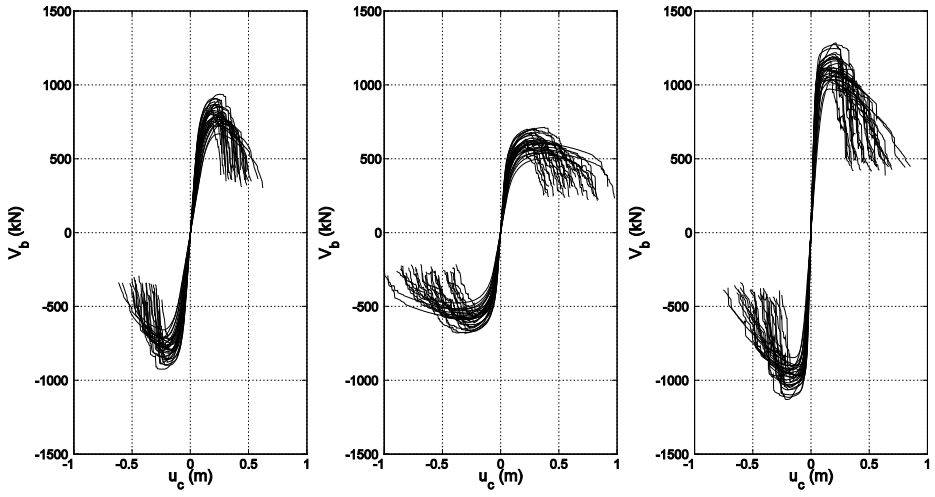

Fig. C -21 Model A: Dispersion in the capacity curves for the three significant modes.

The figure allows to evaluate the effect of the uncertainties modeled (§C.6.2) on the response of the structure. In particular, one observes how the effect is increasing passing from the initial stiffness, to the peak resistance, to the ultimate deformability.
In this case the negative stiffness in the post-peak branch is due solely to the geometric nonlinearity.
Fig. C-22 shows in greater detail the curves of the three modal pushover analyses, for two of the 30 models. The figure shows also the trilinear approximations and the factors *L*relative to the two orthogonal directions in plan (§C.7.1), proportional to the weight that each component of the motion has in the dynamic analysis of the corresponding oscillator.

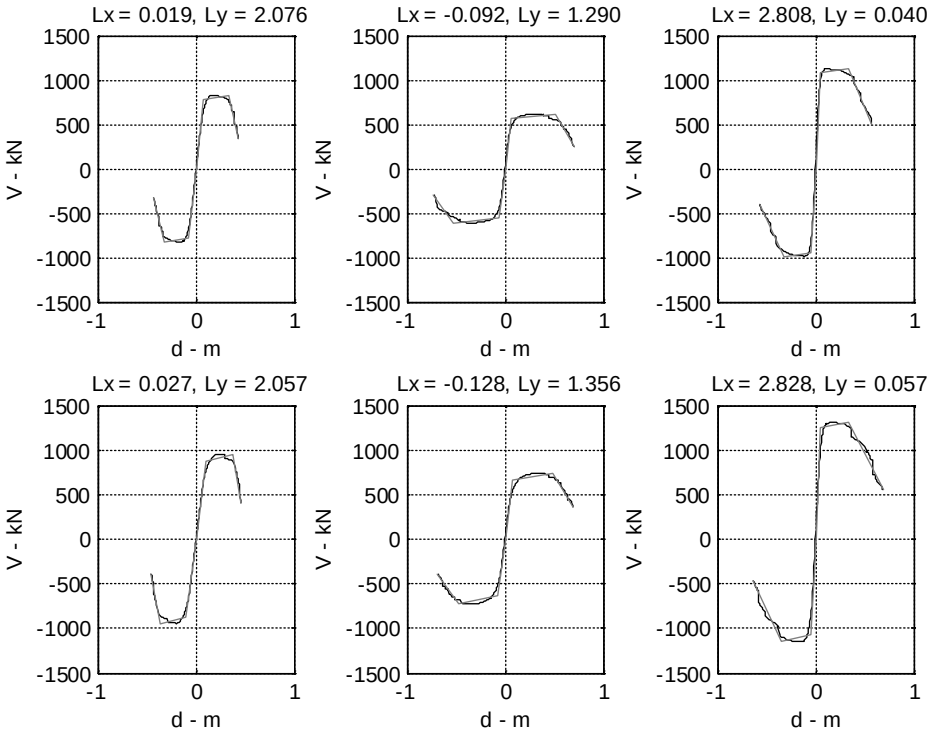

Fig. C -22 Model A: Details of the capacity curves and the corresponding tri-linear approximations for the three significant modes (left to right) and for two of the 30 models sampled (top and bottom).

Further details of the pushover analysis, with the deformations of the structure and the indication of the level of inelastic behaviour, as well as on the dynamic analysis of the single oscillator, are reported for brevity with reference only to model B in §C.9.3.
The Fig. C-23 shows the IDA curves of the structure (obtained by a combination of the IDA modal curves, as indicated in §C.7.1.2) for the 30 models analyzed. On every curve there are three points that indicate the global intensity-response pairs corresponding, for each model and corresponding record, the limit states of damage (green), severe damage (blue) and collapse (red). The relationship between the intensity of the earthquake and the limit state variables is shown in detail in Fig. C-24, in which the points that mark the attainment of the state limit are obviously aligned along the vertical axis at the unit value of the corresponding variable. In the figure there are also shown the values of the mean and standard deviation of the logarithm of the intensity $S_{Y=1}$, i.e., the parameters of the fragility curve.

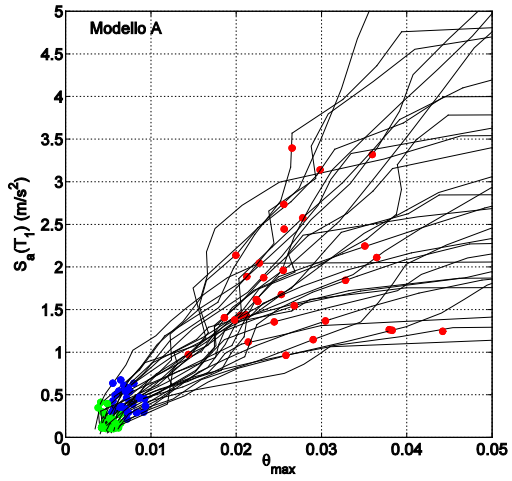

Fig. C-23 Model A: IDA curves of the structure (combination of the modal curves, see Fig. C-16).

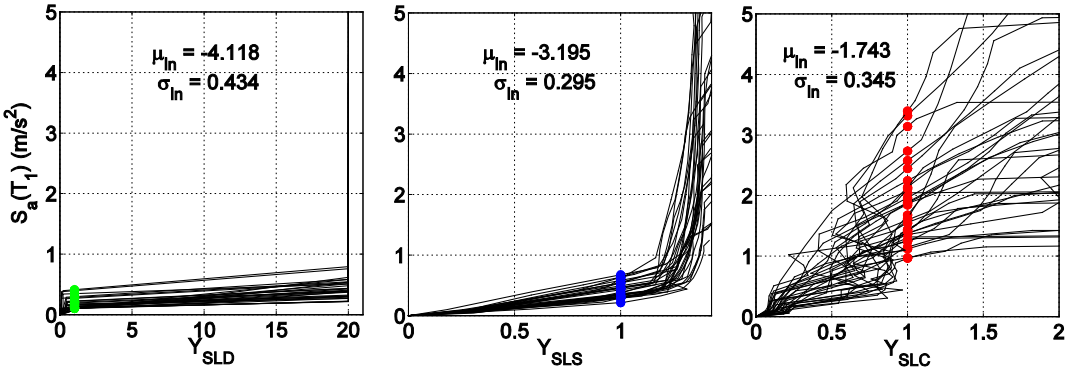

Fig. C-24 Model A: Details of the IDA curves in terms of limit state variables.

The fragility curves relative to the three limit states are shown in Fig. C-25. These curves, integrated with the site hazard in terms of the spectral ordinate close to the average period of the 30 models, lead to the average annual frequencies of exceeding the three limit states.

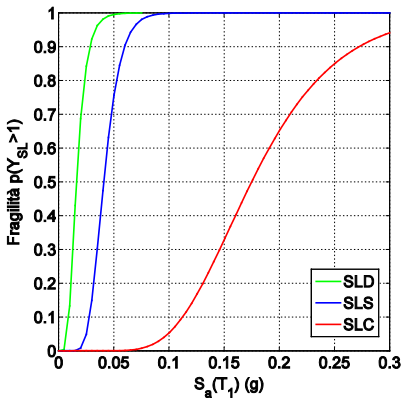

Fig. C-25 Model A: Fragility curves for the three limit states.

C.9.2 Models with degradation (models B and C)

This modelling considers two alternatives, with equal weights in the logic tree. The presentation of the results follows the methods used for model A.
For each of the two branches of the logical tree the process starts by sampling as previously $N = 30$ structures. Also in this case the results of the three vibration modes proved to be sufficient. The Fig. C-26 and C-27 show, respectively for the model B and C, the 30 curves for the two signs (60 analyses) relative to the three modes. One observes how the introduction of the infills increases the resistance (the maximum in the scale of the shear at the base is equal to 1500 kN in model B, and equal to 2000 kN in model C). Given the peripherical and sufficiently regular disposition of the infills in plan, the increase in stiffness is proportionally greater for the torsional mode that passes from the second mode in model B to the third mode in model C.
Also in this case the effect of the uncertainties is increasing, in passing from the initial stiffness, to the peak resistance, to the ultimate deformability.

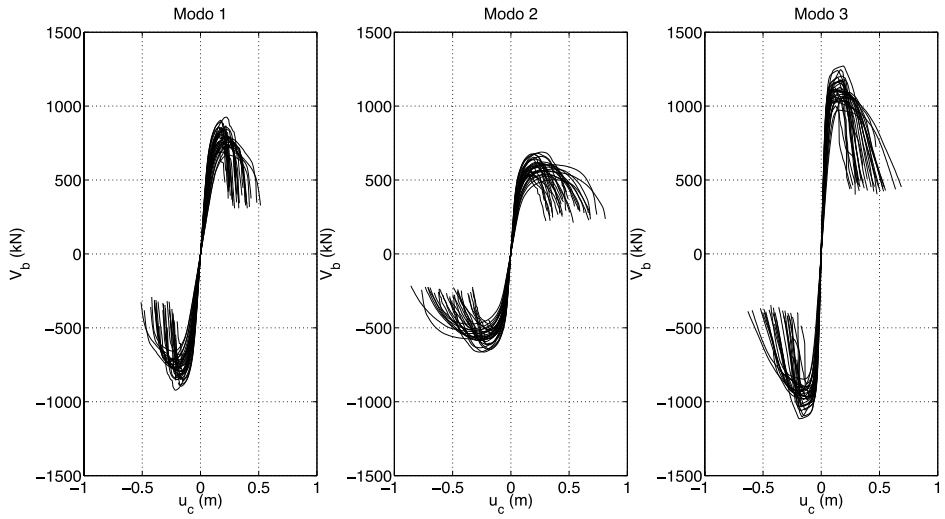

Fig. C-26 Model B: Dispersion in capacity curves for the three significant modes.

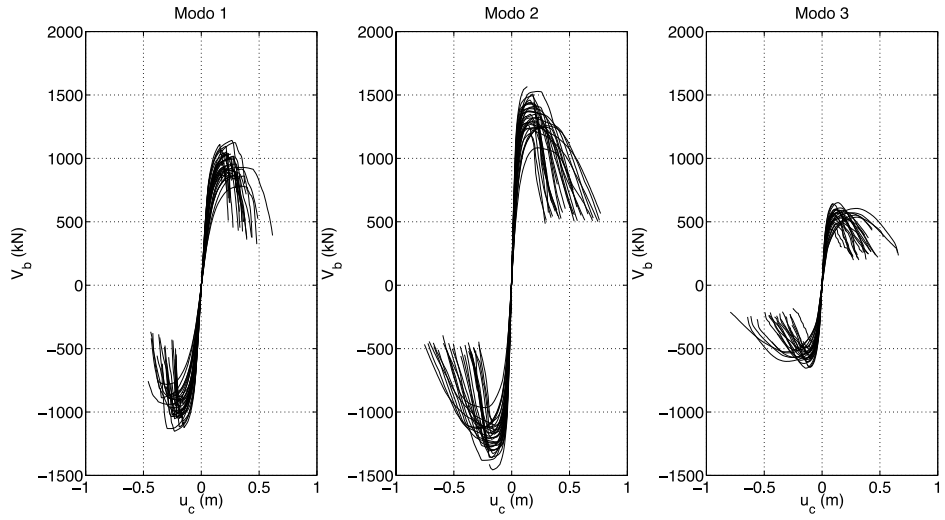

Fig. C-27 Model C: Dispersion in capacity curves for the three significant modes.

The Fig. C-28 shows the IDA curves of the structure for the 30 models analyzed, for branch B (above) and branch C (below) of the logic tree. As before, the three dots indicate the attainment of the limit state of damage (green), severe damage (blue) and collapse (red). The most obvious effects of the introduction of the infills is the increased intensity at collapse, with maximum values (the highest ordinates of the red points), which rise from less than 3 m/s^2 to more than 4.5 m/s^2, and an increase in the dispersion of these values. It is also noted that, in particular in case B, there is an overlap between the sets of corresponding points in different limit states: within each analysis of course the points are always in the correct sequence.

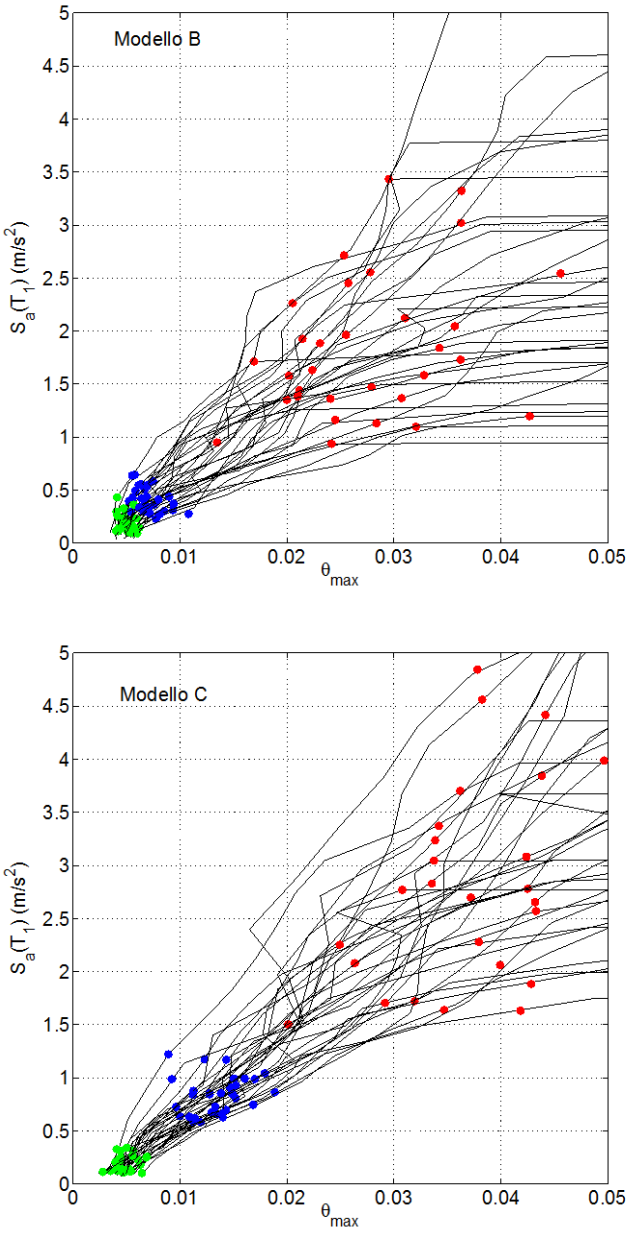

Fig. C-28 Models B (above) and C (below): IDA curves of the structure (combination of modal curves, see Fig. C-16).

The relationship between the intensity of the earthquake and the variables of SL is shown in detail for both branches in the Fig. C-29 , in which are also shown the values of the mean and standard deviation of the logarithm of the intensity $S_{Y=1}$.

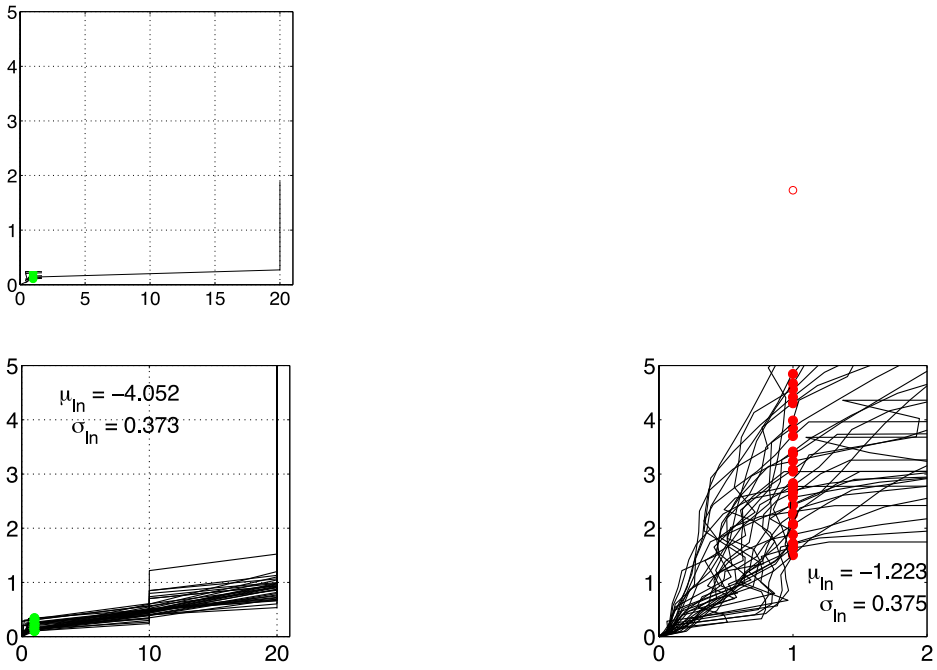

Fig. C-29 Models B (above) and C (below): Details of IDA curves in terms of the limit state variables.

The fragility curves relating to the three limit states are shown at the top in Fig. C-30 for model B and in Fig. C-31 for the model C. These curves, integrated with the site hazard in terms of the spectral ordinate close to the average period of the 30 models, lead to the average annual frequencies of exceeding the three limit states.

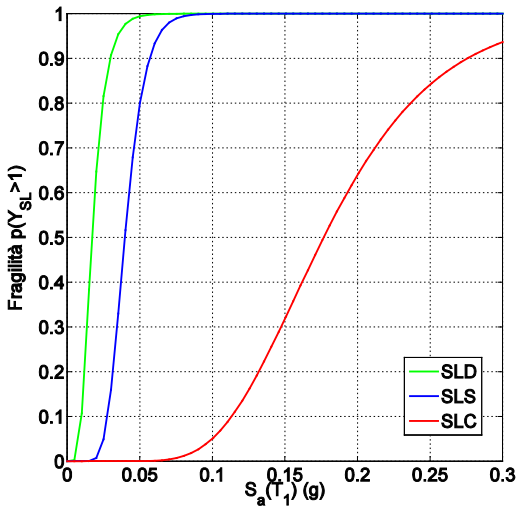

Fig. C-30 Model B: Fragility curves for the three SL.

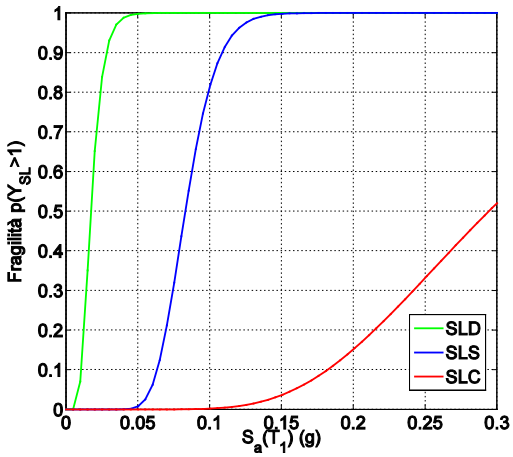

Fig. C-31 Model C: Fragility curves for the three SL.

C.9.3 Further details of the analysis (model B)

The Fig. C-32 illustrates the analysis of pushover of one of the 30 models in the positive direction of mode 3, of the type already shown in Fig. C-15 and Fig. C-22 . On the capacity curve, shown in the upper left, there are indicated three characteristic points: the yield strength, the peak (maximum ductility) and an intermediate point on the branch with negative stiffness.

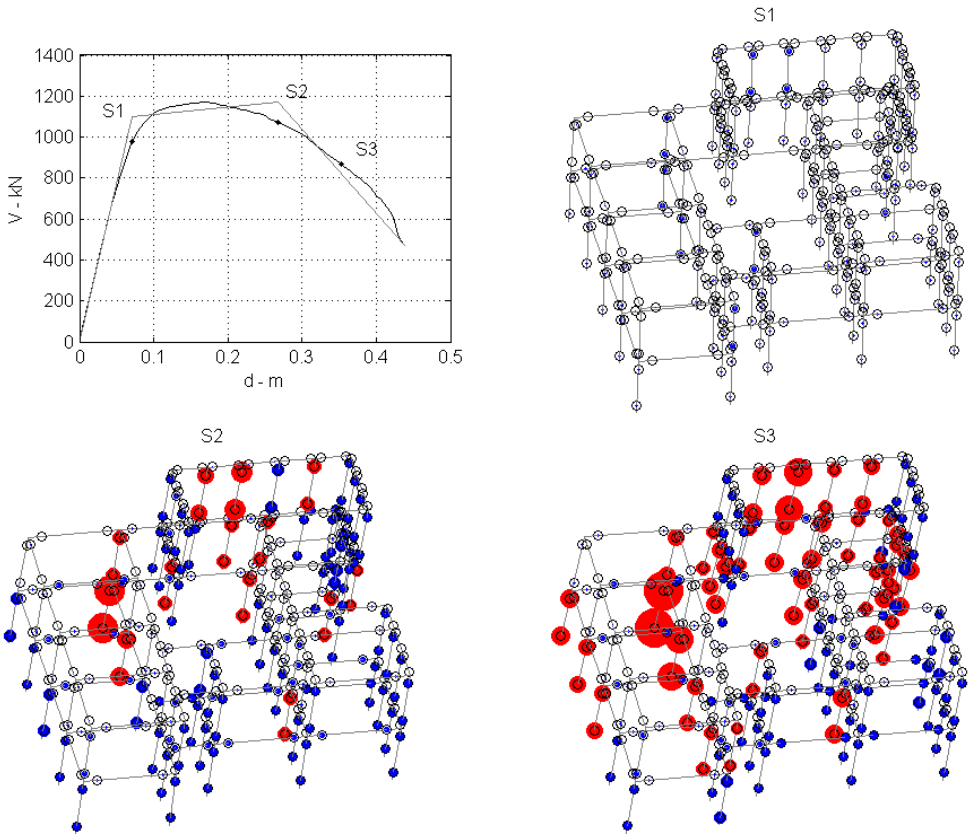

Fig. C-32 Capacity curve and deformations corresponding to the three points: yield strength, peak and intermediate on the branch of degradation.

The corresponding deformed shapes of the building are shown in the other three diagrams, in which there is also highlighted the level of deformation in the plastic hinges, following the convention already adopted in (Haselton and Deierlein, 2007). The areas of potential plastic hinge formation are indicated with empty black circles at the ends of the elements. The level of deformation is represented with another circle, of blue color, the diameter of which increases with the bidirectional quantity:

$$y_j = \sqrt{\left(\frac{\theta_{j,12}}{\theta_{picco,j,12}}\right)^2 + \left(\frac{\theta_{j,13}}{\theta_{picco,j,13}}\right)^2} \qquad \text{(C.30)}$$

where the peak flexural distortion θ (maximum ductility) is equal to θ_f or θ_V depending on the mode of failure of the element. When $y_j = 1$, the diameter of the circle is equal to that of the empty circle. Upon further growth of the deformation the diameter increases and the color changes to red (which then signals the descending branch of the constitutive link).

One notes how, in particular at the state S3 on the descending branch, the diameter of the red circles in some elements is very high, even amounting to more than three times that of the black circle. This is possible since the mode of axial collapse ($\theta > \theta_a$) is not modeled, and then the analysis continues with redistribution of the shear to the element to the adjacent elements (the fact that the results in the points that follow are fictitious, because the element would lose its vertical bearing, is not a problem as such a mode of collapse is detected later using the state variable limit, Eq. C.28).

Fig. C-33 shows, for the sake of illustration, some details of the incremental dynamic analysis of one of the equivalent oscillators. In particular, the time histories of the displacement *D* for three different intensities of excitation are shown at the top, while the bottom shows the corresponding force-deformation cycles.

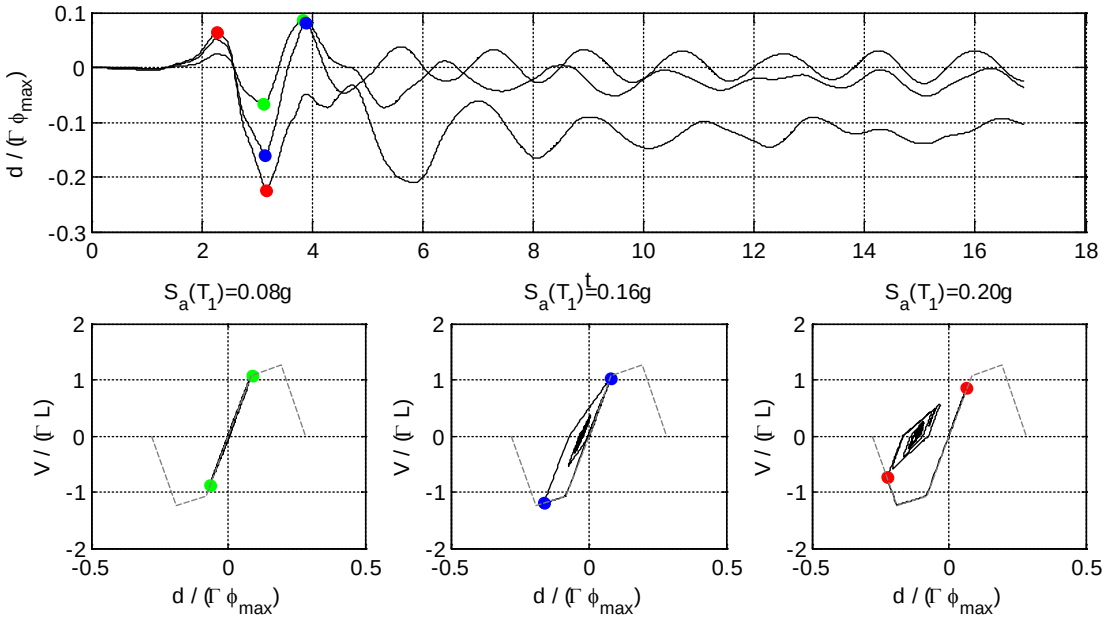

Fig. C-33 Example of cyclic degrading response of the equivalent oscillator (structure and signal n ° 1): time histories of the displacement response for three different intensities (top), the force-deflection cycles for the lower intensity (below, left), average (below, center) and for the higher intensity (down, right).

C.10 Conclusions

The results of the analysis are condensed in Table C-9 . The aspect that comes out with most evidence is the low sensitivity of the results with respect to the modeling.

Table C-9. The results of the three models compared.

	A (no deg.)	B (degradation / no infills)	C (degradation / infills)	Degradation (combined)
T_1 (s)	1:52	1:52	1.16	-
λ_{SLD}	0.0315	0.0304	0.0383	0.0343
λ_{SLS}	0.0127	0.0131	0.0078	0.0104
λ_{SLC}	0001**19**	0001**17**	0.0009	0.0010

This Technical Document has been prepared by a Task Group whose members are:

Coordinator:
PINTO Prof. Paolo Emilio University of Roma “La Sapienza”

Study Group:

CATTARI Prof . Serena [b)] University of Genova
FRANCHIN Prof . Paolo [a)] University of Roma “La Sapienza”
IERVOLINO Prof. Iunio [c)] University of Napoli “Federico II”
LAGOMARSINO Prof. Sergio [b)] University of Genova
PINTO Prof. Paolo Emilio [a)] University of Roma “La Sapienza”

BAZZURRO Prof.Paolo [d)] University Institute of Advanced Studies, Pavia
MAGENES Prof. Guido [d)] University of Pavia
PAOLUCCI Prof.Roberto [d)] Polytechnical Institute of Milano

a) for chapters 1, 2 and 4 and Appendices A and C
b) for section 2.6.4 , chapter 3 and Appendices A.1.1.1, A.5 and B
c) for the Appendix A.4
d) for final review at following public inquiry

This technical document has been produced with the assistance of the Italian Department of Civil Protection within the Executive Project DPC-Reluis 2010-2013.

The Italian version of this Technical Document has been approved in a preliminary version on October 10th 2013 and in the final version on May 14th 2014, at the conclusion of the public inquiry, with the changes made to it, by the "CNR Advisory Committee on Technical Recommendations for Construction", whose members are:

ANGOTTI Prof. Franco	- University of Firenze
ASCIONE Prof. Luigi	- University of Salerno
AURICCHIO Prof. Ferdinando	- University of Pavia
BARATTA Prof. Alessandro	- University "Federico II" – Napoli
COSENZA Prof. Edoardo	- University "Federico II" – Napoli
MACERI Prof. Franco, *Chairman*	- University "Tor Vergata" – Roma
MANCINI Prof. Giuseppe	- Polytechnical Institute of Torino
MAZZOLANI Prof. Federico Massimo	- University "Federico II" – Napoli
PINTO Prof. Paolo Emilio	- University "La Sapienza" – Roma
POGGI Prof. Carlo	- Polytechnical Institute of Milano
ROYER CARFAGNI Prof. Gianni	- University of Parma
SAVOIA Prof. Marco	- University of Bologna
SCARPELLI Prof. Giuseppe	- Polytechnical University of Marche
SOLARI Prof. Giovanni	- University of Genova
URBANO Prof. Carlo	- Polytechnical Institute of Milano
VINCI Arch. Roberto	- National Research Council
ZANON Prof. Paolo	- University of Trento

The present English translation has been approved on June 16th 2016, by the "Advisory Committee on Technical Recommendations for Construction" of the National Research Council of Italy, in its new composition:

ANGOTTI Prof. Franco	- University of Firenze
ASCIONE Prof. Luigi	- University of Salerno
AURICCHIO Prof. Ferdinando	- University of Pavia
BARATTA Prof. Alessandro	- University "Federico II" – Napoli
COSENZA Prof. Edoardo	- University "Federico II" – Napoli
DI PRISCO Prof. Marco	- Polytechnical Institute of Milano
LAGOMARSINO Prof. Sergio	- University of Genova
MACERI Prof. Franco, *Chairman*	- University "Tor Vergata" – Roma
MANCINI Prof. Giuseppe	- Polytechnical Institute of Torino
MAZZOLANI Prof. Federico Massimo	- University "Federico II" – Napoli
OCCHIUZZI Prof. Antonio	- National Research Council
PINTO Prof. Paolo Emilio	- University "La Sapienza" – Roma
POGGI Prof. Carlo	- Polytechnical Institute of Milano
PROTA Prof. Andrea	- University "Federico II" – Napoli
ROYER CARFAGNI Prof. Gianni	- University of Parma
SAVOIA Prof. Marco	- University of Bologna
SCARPELLI Prof. Giuseppe	- Polytechnical University of Marche
SOLARI Prof. Giovanni	- University of Genova
URBANO Prof. Carlo	- Polytechnical Institute of Milano
ZANON Prof. Paolo	- University of Trento